CHEMICAL REVIEWS

Review

pubs.acs.org/CR

Diradicals

Manabu Abe*

Department of Chemistry, Graduate School of Science, Hiroshima University (HIRODAI), 1-3-1 Kagamiyama, Higashi-Hiroshima, Hiroshima 739-8526, Japan

Institute for Molecular Science (IMS), Okazaki, Aichi 444-8787, Japan

JST-CREST, 5 Sanbancho, Chiyodaku, Tokyo 102-0075, Japan

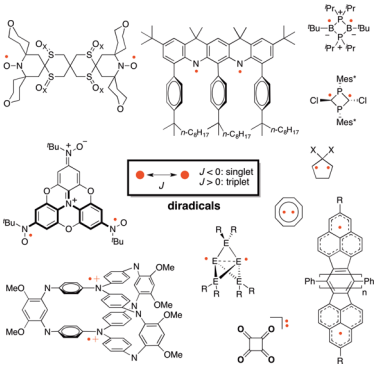

CONTENTS

1. INTRODUCTION

Open-shell molecules such as radicals, carbenes, and electronically excited-state molecules exhibit high energies, and thus, in general, they are quite reactive.[1] The short-lived species play crucial roles in molecular transformations and also in materials science. In the last century, scientists carried out pioneering studies on methods to detect and characterize these short-lived intermediates. Quantum chemical calculations allowed scientists not only to understand the three-dimensional structures

Special Issue: 2013 Reactive Intermediates

Received: January 31, 2013
Published: July 24, 2013

   dx.doi.org/10.1021/cr400056a | *Chem. Rev.* 2013, 113, 7011−7088

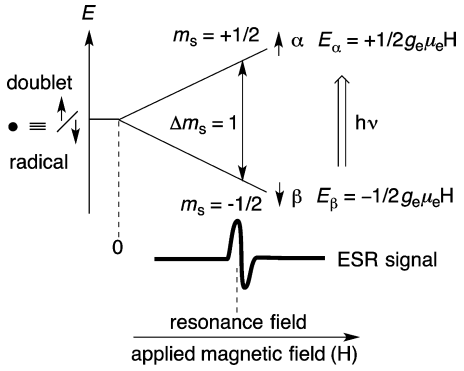

Figure 1. Zeeman effect on unpaired electrons and ESR spectrum for the simplest system (i.e., free electrons).

and electronic properties of these species, but also to design new molecules with novel properties. Experimental techniques such as laser flash photolysis (LFP) and low-temperature matrix isolation methods provided opportunities for the direct detection of short-lived species using spectroscopic techniques such as electron spin resonance (ESR) spectroscopy, electronic absorption and emission spectroscopy, and IR spectroscopy. These fundamental research studies made great contributions to the significant development in the fields of mechanistic chemistry, synthetic chemistry, materials chemistry, and biological chemistry.

Since the end of the last century, significant developments in the chemistry of open-shell molecules have been achieved. Most of the developments originate in the preparation of long-lived open-shell molecules.[2] The creative design of ligands and substituents have made it possible to increase the lifetimes of reactive molecules or even isolate inherently high-energy molecules. The unique character of heteroatoms has also provided opportunities to isolate exotic compounds. In this review article, diradicals among the open-shell molecules were chosen as the focus, and their chemistry is summarized. The technical term "biradical(s)" is also used in the literature with the same meaning as diradical(s). However, use of a single name throughout an article is more straightforward. Thus, the term diradical is first defined, and then, recent developments in their chemistry are summarized and discussed.

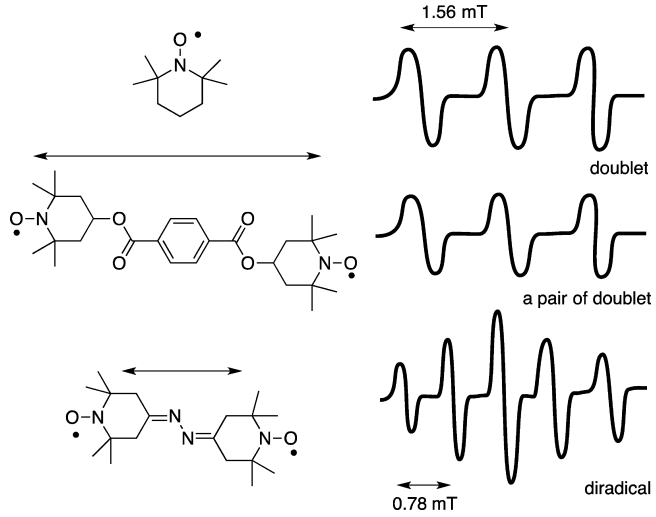

Figure 3. ESR spectra of bis(nitroxide)s with different exchange interactions (J).

1.1. What are Diradicals?[3−5]

Molecules containing an unpaired electron are called monoradicals, free radicals, or simply radicals. Every electron has a magnetic moment and a spin quantum number of $S = {}^1/_2$, with magnetic components $m_s = +{}^1/_2$ and $m_s = -{}^1/_2$. When an external magnetic field (H) is applied in a direction, the electron's magnetic moment aligns itself either parallel ($m_s = -{}^1/_2$, β spin) or antiparallel ($m_s = +{}^1/_2$, α spin) to the field (Figure 1). The spin multiplicity ($2S + 1$) of monoradicals is doublet (2); thus, monoradicals are also called doublet species.

Each electron's magnetic moment has a specific energy due to the Zeeman effect in the presence of an external magnetic field (H). These energies (E_α and E_β) are given by the equation of $E = m_s g_e \mu_e H$, where g_e is the electron's so-called g factor (g_e = 2.0023 for the free electron), μ_e is the Bohr magnetron (9.274078×10^{-24} J T^{-1}), and H is the strength of the applied magnetic field. Thus, the Zeeman energy difference between the lower and upper states ($\Delta E = E_\alpha - E_\beta$) is given by $\Delta E = g_e \mu_e H$. Electron spin resonance (ESR) occurs when the frequency (ν) is adjusted to the energy of $\Delta E = E_\alpha - E_\beta = g_e \mu_e H = h\nu$.

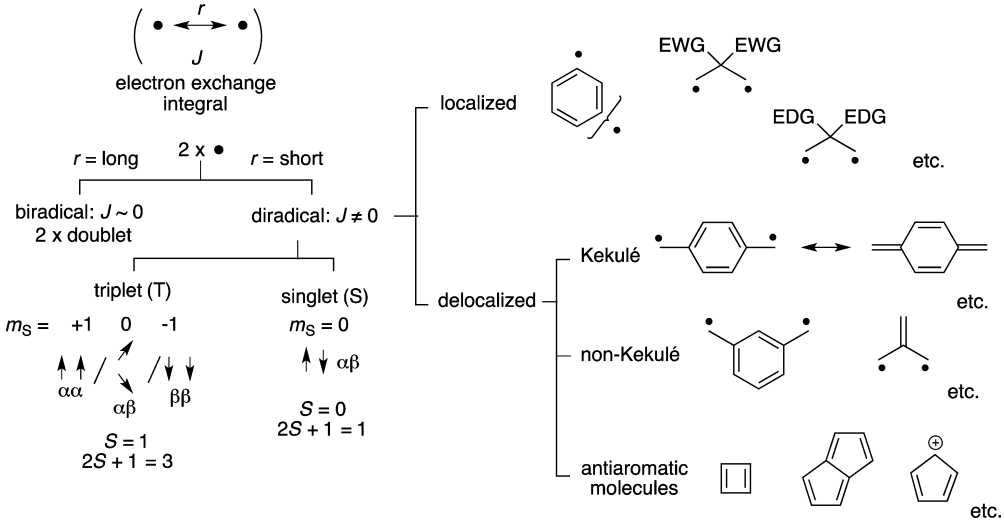

Figure 2. What are diradicals?

dx.doi.org/10.1021/cr400056a | Chem. Rev. 2013, 113, 7011−7088

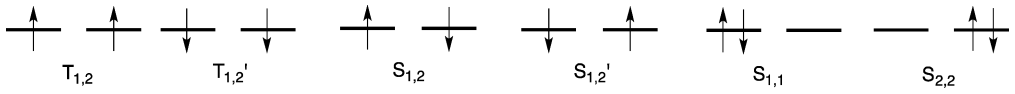

Figure 4. Possible electronic configurations for triplet and singlet states.

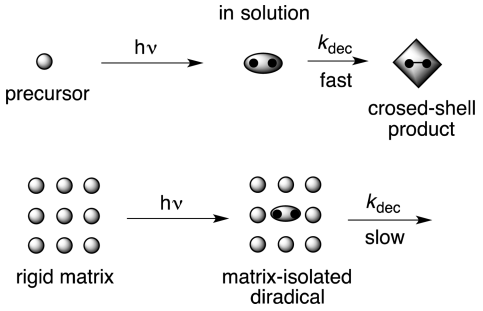

Figure 5. Generation and detection of diradicals in a cryogenic matrix.

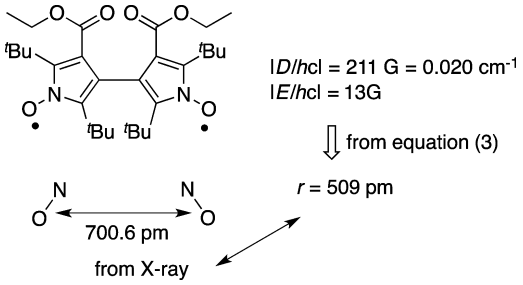

Figure 7. Example of the inadequate estimation of a radical−radical distance in delocalized diradicals using the point-dipole approximation.

When there are two unpaired electrons (radicals) in a molecule, the term diradical or biradical refers to the molecule. According to the *IUPAC Compendium of Chemical Terminology*, the so-called Gold Book,[6] biradical is a technical term for molecules in which the two electrons act independently or nearly independently.[6] Thus, biradicals are most easily understood as two doublets in a molecule. In other words, the electron exchange interaction (J) between the two unpaired electrons is negligible or nearly negligible for biradicals because of the long distance (r) between the two electrons (Figure 2). When the magnitude of the dipole−dipole interaction in a molecule is large enough to produce two spin states, namely, singlet (S, $S = 0$, spin multiplicity = 1) and triplet (T, $S = 1$, spin multiplicity = 3), the molecular species with the two unpaired electrons is referred to as a diradical.[7] The electron

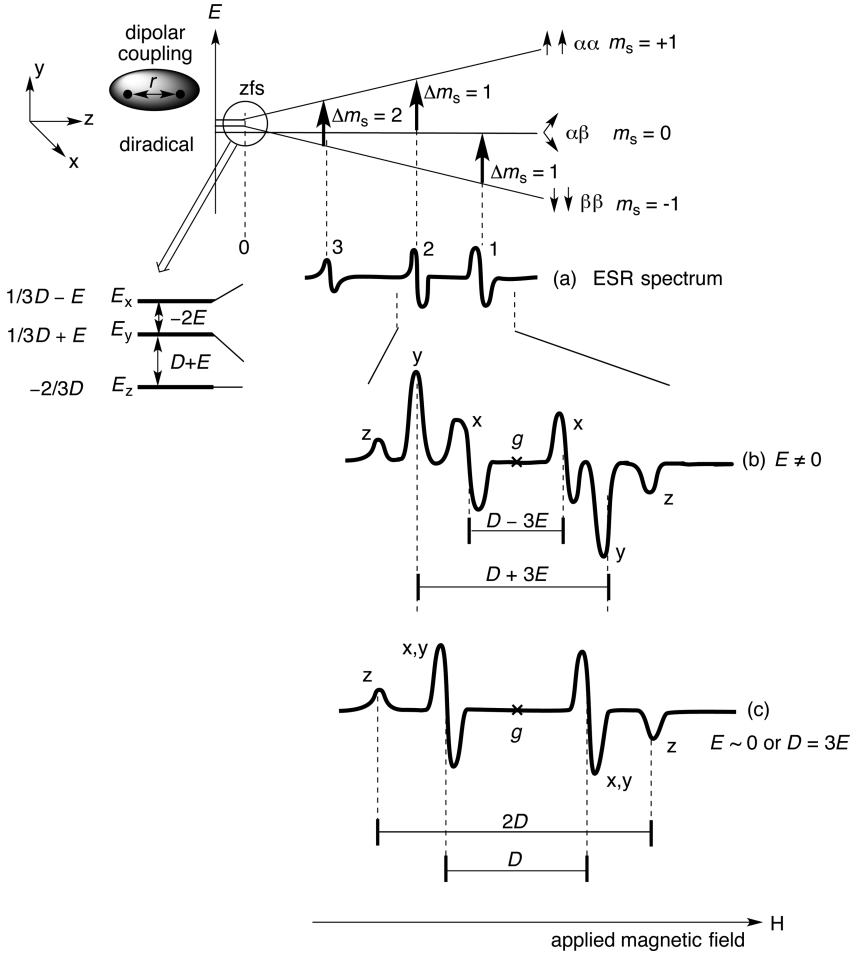

Figure 6. Typical ESR spectra of triplet diradicals in the solid state.

dx.doi.org/10.1021/cr400056a | *Chem. Rev.* 2013, 113, 7011−7088

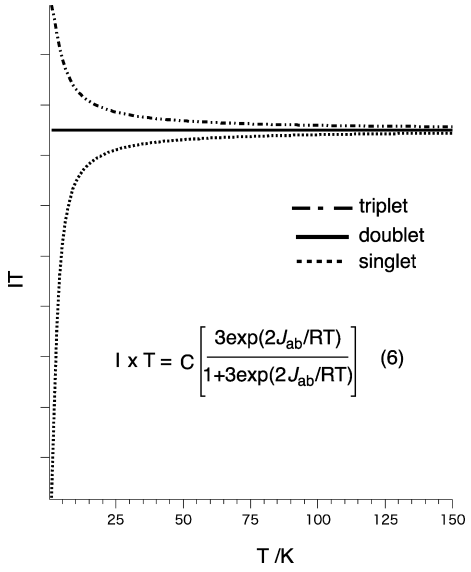

Figure 8. Typical temperature- (T-) dependent changes of ESR signal intensities (I) for triplet- and singlet-ground-state diradicals.

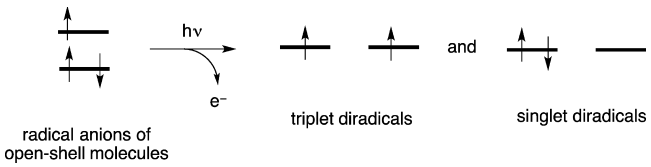

Figure 9. Photodeatachement of radical anions to generate the triplet and singlet diradicals.

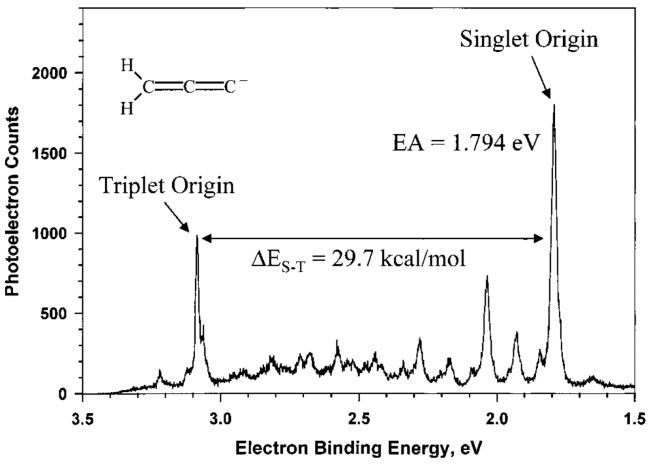

Figure 10. Photoelectron spectrum of the negative anion of propadienylidene ($CH_2C{=}C{:}$). Reprinted with permission from ref 30. Copyright 1995 American Chemical Society.

exchange interaction is largely dependent on the distance between the two spins.

The distance-dependent change of the electron exchange interaction (J), that is, the through-space interaction between the two spins, can be visualized by the electron spin resonance (ESR) spectroscopic analysis using stable radicals (Figure 3). For example, when the two nitroxides ($R_2N{-}O^{\bullet}$) in a molecule are isolated or separated from each other at a sufficient distance, three-line signals are typically derived from the coupling of the electron with nitrogen nucleus (^{14}N), $2I$ (= 1 for ^{14}N) + 1 = 3 (triplet), appear in the ESR spectrum. The hyperfine coupling constant (A_N = 1.56 mT) should be just the same as that of the corresponding monoradical. Thus, there is a negligible interaction between the two spins. When the electron exchange interaction is large enough ($J \gg A_N$, $J/A_N > 5$) with a short distance, a five-line signal, $2 \times 2I + 1 = 5$, will appear in the ESR spectrum. The species are then defined as diradicals.[8−10] Diradicals can be categorized as localized and delocalized diradicals (Figure 2). Delocalized diradicals are further divided into Kekulé and non-Kekulé molecules. Antiaromatic molecules can be classified as delocalized diradicals.

The terminology of singlet and triplet states in diradicals is derived from the number of energy level in diradicals under an external magnetic field (Figure 2). Singlet diradicals (S) are ESR-silent species, because the magnetic quantum number (m_s) is zero, $S = 0$. Thus, only one energy level, spin multiplicity = $2S + 1 = 1$, exists even in the presence of a strong magnetic field. When three different energy levels arise in the presence of a strong magnetic field, the ESR-active species are called triplet species with $S = 1$, namely, $\alpha\alpha$ ($m_s = +1$), $\alpha\beta$ ($m_s = 0$), and $\beta\beta$ ($m_s = -1$) (Figure 2). The spin multiplicity is calculated to be 3 ($= 2S + 1$). Typical ESR spectra for triplet diradicals are shown later in Figure 6.

Questions quickly arise: (1) Which spin state, singlet or triplet, is lower in energy? (2) How can one distinguish between the two spin states experimentally? In the following section, these fundamental questions are answered.

1.2. Which Spin-State Is Lower in Energy, Singlet or Triplet?

When two electrons occupy two nonbonding molecular orbitals (NBMOs), the six electronic configurations $T_{1,2}$, $T_{1,2}'$, $S_{1,2}$, $S_{1,2}'$, $S_{1,1}$, and $S_{2,2}$ shown in Figure 4 are possible to describe the diradicals. The first two electronic configurations are triplets, and the other four configurations are singlets. Thus, the relative energies of the two spin states determine the ground-state spin multiplicity. When the two-nonbonding molecular orbitals are energetically degenerate, the molecules are called diradicals. The term "diradicaloids" (diradical-like, or molecules with diradical character) is used for molecules in which the two molecular orbitals are nearly degenerate.[11]

1.2.1. For Diradicals. The most energetically stable electronic configuration of atoms can be predicted according to Hund's rule.[12] When electrons are added to atomic orbitals with the same energy, the electrons have to first half-fill every orbitals of equal energy with unpaired spins to avoid electron−electron repulsion. Thus, when filling two energetically equivalent orbitals with two electrons, the triplet electronic configuration is more stable in energy than the singlet configuration. In general, Hund's rule for determining the ground-state spin multiplicity can apply to molecular diradicals. Thus, the order of energetic stability of the six electronic configurations must be $T_{1,2} = T_{1,2}' > S_{1,2} = S_{1,2}' \gg S_{1,1}$, $S_{2,2}$ in the absence of an external magnetic field. Triplet should be the ground-state spin multiplicity for diradicals. The singlet−triplet energy gap (ΔE_{ST}) can be calculated from the electron exchange interaction (J), with $\Delta E_{ST} = E_S - E_T = 2J$. A negative (positive) J value indicate singlet (triplet) ground state.

The magnitude of the electron exchange interaction (J) caused by electron−electron repulsion is proportional to the value of the overlap integral between the two molecular orbitals. When the overlap of the two orbitals is quite small or

dx.doi.org/10.1021/cr400056a | Chem. Rev. 2013, 113, 7011−7088

negligible, Hund's rule might not apply to molecular diradicals. Typical examples of the violation of Hund's rule can be found in delocalized non-Kekulé molecules such as tetramethyleneethane (TME), which is a disjoint non-Kekulé molecule (vide infra, section 3.4). The effect of spin polarization should also be considered for the electronic energy of two spin states in diradicals such as twisted ethylene molecules.

1.2.2. For Diradicaloids (Diradical-like Molecules). Undoubtedly, the triplet state is the ground-state spin multiplicity for diradicals in which a large overlap integral exists between the two energetically degenerate molecular orbitals that are occupied by two electrons. The electron−electron exchange interaction (J) dominates the energy preference of triplet states. Which spin state, singlet or triplet, is the ground state for diradicaloids[11] in which the two molecular orbitals occupied by two electrons are nearly degenerate in energy? In this review article, diradicaloids are defined as a subset of diradicals. Thus, the recent developments in diradicaloid chemistry are also included in this review article.

When the two molecular orbitals are energetically degenerate, the electronic configuration $S_{1,1}$ (= $S_{2,2}$) should be energetically much less stable than the electronic configuration $S_{1,2}$ (= $S_{1,2}'$) because of the severe electron−electron repulsion in $S_{1,1}$ and $S_{2,2}$ (Figure 4). Thus, the contributions of these configurations are negligible in singlet diradicals. When the two molecular orbitals are energetically separated by an energy gap, the energetic preference (B) of the singlet state derived from the contribution of the electronic configuration $S_{1,1}$ should be considered. In other words, when the energetic stabilization is larger than the electron−electron repulsion interaction (K), $B > K$, the singlet should be the ground-state spin multiplicity. The energetic stabilization is proportional to the energy gap between the two molecular orbitals occupied by two electrons. As the energy spacing increases, the singlet is more stabilized.

The energy gap between the two orbitals that are occupied by two electrons is determined by through-space (TS) and through-bond (TB) interactions. The energy difference between nonbonding molecular orbitals that are occupied by two electrons and the singlet−triplet energy gaps provide valuable insights regarding the balance of through-bond and through-space components of the interaction. The details of the interactions that affect the energy difference are discussed for each of the diradicals mentioned below. The diradical character of diradicaloids can be estimated from the natural orbital occupation number of the lowest unoccupied molecular orbital (LUMO), which can be obtained by complete-active-space multiconfiguration self-consistent-field (CASSCF) calculations.[13] How can one determine and predict the ground-state spin multiplicity of diradicals and the energy gap between the singlet and triplet states?

The magnitude of the singlet−triplet energy gap ($\Delta E_{ST} = E_S - E_T$) provides direct information on the extent of the interaction between the two radical orbitals. An accurate singlet−triplet energy spacing is essential for understanding the diradical character. However, in general, it is not easy to determine the energy gap experimentally because of the high reactivity of diradicals. For large molecules, the energy gaps are hard to calculate accurately by ab initio quantum chemical calculations. In the following sections, the most reliable computational methods and experimental procedures available at this point for quantitatively determining the singlet−triplet energy spacing are introduced.

1.2.3. Computational Methods. The electronic configuration of triplet states can be described in one way (Figure 4), because the energy of $T_{1,2}$ is equal to the energy of $T_{1,2}'$ in the absence of an external magnetic field. Thus, the triplet states can generally be calculated accurately by methods with conventional unrestricted wave functions such as unrestricted Hartree−Fock (UHF) and unrestricted density functional theory (UDFT). However, the singlet diradicals cannot be described using single-reference HF and post-HF methods, because the electronic configurations of the singlet states of diradicals include $S_{1,2}$, $S_{1,1}$, and $S_{2,2}$. Thus, multireference (MR) approaches that can treat the entire electronic configurations of singlet diradicals are needed for their proper quantum mechanical descriptions.

Accurate experimental studies on singlet−triplet energy gaps provide the only solid benchmarks for computational studies. The singlet−triplet energy gaps for benzynes (dehydrobenzens) determined by Wenthold, Squires, and Lineberger have been used for the benchmarks of computations.[14] Schaefer and Cramer reported that multireference coupled-cluster calculations, namely, Mk-CCSD(T), with the cc-PVTZ basis set are the minimum needed to obtain accurate singlet−triplet splittings for *ortho*-, *meta*-, and *para*-benzyne.[15] In addition, the complete-active-space self-consistent-field second-order perturbation theory (CASPT2) method is also reliable in reproducing the energies of singlet diradicals. Multireference ab initio methods accurately reproduce the experimentally determined singlet−triplet energy gaps and are excellent methodologies for predicting the reactivities and structures of singlet diradicals. However, the computational costs are quite high, and thus, it is sometimes quite difficult to use these methodologies for large molecules. Carpenter and co-workers recently reported that the broken-symmetry (BS)-(U)CCSD-(T)/cc-pVTZ//BS-(U)CCSD/cc-pVDZ level of theory reproduces well the computational results of the multireference MkCCSD(T)/cc-PVDZ method for the chemistry of spiropentane including the reactivity of 2-spiropropane-1,3-diyl.[16]

Density functional (DFT) calculations are computationally very efficient compared to multireference ab initio methods. However, as mentioned previously, DFT cannot properly describe the electronic configurations of open-shell singlet state of diradicals; thus, singlet−triplet energy spacings (ΔE_{ST}) calculated by DFT include large uncertainties. The broken-symmetry (BS) formalism proposed by Noodleman and Yamaguchi is one possible way to describe the singlet diradicals as a compromise method.[17,18] The BS solution is not the pure eigenstate of the singlet diradical, but the BS state is a mixed state of the singlet and triplet states. To evaluate the reliable magnetic exchange constant ($J_{ab} = \Delta E_{ST}/2$), the singlet-state energy values need to be refined, as developed by Yamaguchi and co-workers, to eliminate the spin contamination (eq 1).[18] Since their discovery, BS methods have been utilized as convenient and practical procedures for estimating the effective electron exchange integrals (J_{ab}), that is, the singlet−triplet energy spacings, of diradicals. Because the BS method admixes the singlet state with the triplet state, a spin correction (SC) is necessary to accurately obtain the J_{ab} value (i.e., the singlet−triplet energy spacing); see eq 2. The spin contamination can be determined from the calculated values of $\langle S^2 \rangle = \langle S(S+1) \rangle$. For triplet-state diradicals, the $\langle S^2 \rangle$ value should be 2; on the other hand, the $\langle S^2 \rangle$ value for the pure singlet state should be 1 using the BS method. Thus, when the $\langle S^2 \rangle$ values are calculated to be significantly less than 1 using the BS method, a large

dx.doi.org/10.1021/cr400056a | *Chem. Rev.* 2013, 113, 7011−7088

contribution of the closed-shell electronic configuration $S_{1,1}$ (= $S_{2,2}$) is included in the singlet diradicals. Smaller $\langle S^2 \rangle$ values of less than 1 are a sign of a singlet ground state.

$$J_{ab} = \frac{E_{BS} - E_T}{\langle S^2 \rangle_T - \langle S^2 \rangle_{BS}} \quad (1)$$

$$\Delta E_{ST}^{SC} = E_S^{SC} - E_T = \Delta E_{ST} \frac{\langle S^2 \rangle_T}{\langle S^2 \rangle_T - \langle S^2 \rangle_{BS}} \quad (2)$$

The use of an approximate spin projection (AP) method was recently developed by Kitagawa and co-workers to improve the computational results, that is, to reduce the remaining spin contamination of the singlet energy.[19] Ess et al. reported that the spin-projected singlet−triplet energy gap calculated at the M06-2x/6-31G(d,p) level of theory well reproduces the experimental singlet−triplet energy gaps of benzyne.[20] Conventional DFT methods such as B3LYP/cc-PVTZ provide a large error in the energy and structure of the relatively simple *meta*-benzyne. However, a pure generalized gradient approximation (GGA) functional, such as BLYP/cc-PVTZ, was found to give structures in close agreement with those calculated by ab initio computations (section 2.5). The DFT method might be the minimum necessary for predicting the IR spectra for singlet diradicals.

1.2.4. Experimental Methods. As mentioned in the preceding section, the quantum chemical calculations developed recently predict and reproduce well the experimentally determined singlet−triplet energy spacing and reactivity of open-shell species. An interplay between computations and experiments is necessary to further improve the methodologies and bring new ideas to the treatment of such fascinating molecules. In experiments, two methods are well-known to determine the singlet−triplet energy spacing. The first is magnetic susceptibility measurements including ESR spectroscopic analysis, by which the structure of triplet diradicals can be analyzed. The second is the use of negative-ion photoelectron spectroscopy (NIPES). The structural analysis of open-shell molecules and their reactivity can be also investigated using low-temperature matrix-isolated IR spectroscopic analysis and time-resolved IR and UV−vis spectroscopic analyses.[21] However, the singlet−triplet energy spacing, which is one of the most important quantities in diradical chemistry, is difficult to analyze by these methods. In this review, the two methods of ESR and NIPES are introduced next to determine the singlet−triplet energy gaps for reactive open-shell molecules.

Electron Spin Resonance (ESR) Spectroscopy.[22] Triplet states are the only ESR-active species in diradicals. The Zeeman effect does not apply for singlet diradicals, because the spin quantum number of singlet states is zero. Thus, the ESR spectroscopic analysis is a very useful method for distinguishing between the two spin states, singlet and triplet. Because diradicals are, in general, reactive species, the species are normally generated under cryogenic matrix isolation conditions. In a rigid medium and under low-temperature conditions (typically in an organic glass, <100 K), the bimolecular and intramolecular chemistry of reactive intermediates are suppressed (Figure 5).

The doublet species (i.e., monoradicals) are also ESR-active (Figure 1). How can one distinguish between the triplet and doublet species? The simplest energy-level diagram for a doublet species in an external magnetic field is shown in Figure 1. By varying the static field H, one can change the energy difference between the α and β electron spin states, which are degenerate in the absence of the external magnetic field. The resonance absorption occurs when the frequency (ν) is adjusted to the energy difference of $\Delta E = g_e \mu_e H = h\nu$. When a nuclear spin is connected to an atom that has an unpaired electron, so-called hyperfine splitting A occurs, giving rise to complex ESR signals. For example, methyl radical ($^{\bullet}CH_3$) shows an ESR signal of a quartet of lines with A_H = 2.3 mT due to the hyperfine coupling of the electron with the three protons. The ESR signal of a doublet species is sometimes complex, but only one resonance absorption can be observed, because the two energy levels of doublet species are degenerate in the absence of an external magnetic field.

In contrast to the single resonance signal of a doublet species, three resonance absorptions are typically observed for triplet states in a rigid solid state (Figure 6a). Two of them, resonance signals 1 and 2, correspond to the allowed transitions with Δm_s = 1 from $m_s = -1$ to $m_s = 0$ and from $m_s = 0$ to $m_s = +1$. The third signal, resonance signal 3, which appears at about half-field with respect to the Δm_s = 1 transition, corresponds to the formally forbidden transition of Δm_s = 2, that is, from $m_s = -1$ to $m_s = +1$. The three resonance signals clearly indicate that the three energy levels are not energetically degenerate even in the absence of an external magnetic field. If the three energy levels were degenerate at zero magnetic field, only two resonance signals including the forbidden transition would appear in triplet diradicals. Thus, a dipolar coupling of the two electronic spins in triplet diradicals produces an internal magnetic field to split the energy level into three levels at zero magnetic fields.

This energy splitting is called zero-field splitting (zfs). As exemplified in Figure 6, the relative energies of the three levels are described by the two zfs parameters D and E. The two zero-field splitting parameters are feasibly determined from triplet ESR signals (Figure 6b,c). In real triplet ESR signals, the two allowed transitions are expected to appear as six lines because of the three magnetic axes of x, y, and z (Figure 6b). Because the zero-field splitting is derived from the dipole−dipole interaction, the parameter D is related to the distance r between the two unpaired electrons and can thus be used to calculate the average distance r between the two unpaired electrons by the point−dipole approximation (eq 3), where g is the g value of the triplet diradicals (~2.0) D is in gauss (G), and r is in angstroms,[23] The average spin−spin distance r (in angstroms) can also be explained by the relative intensity between the signal of the allowed transition $|\Delta m_s = 1|$ and that of the forbidden transition $|\Delta m_s = 2|$ (eq 4), where ν is the resonance frequency in gigahertz and F = 19.5 for organic radicals.

$$D = 1.39 \times 10^4 (g/r^3) \quad (3)$$

$$|\Delta m_s = 2|/|\Delta m_s = 1| = F/r^6 (9.1/\nu)^2 \quad (4)$$

The calculated distances based on the experimentally determined D values and the relative intensities of $|\Delta m_s = 2|$/$|\Delta m_s = 1|$ were reported to be consistent with each other. A spin−spin distance of less than ~10 Å can be determined by the combination of the two values. The intensity of the forbidden half-field transition is proportional to r^{-6} (eq 4). When the distance between the two spins if greater than ca. 10 Å, the signal intensity of the forbidden resonance is assumed to become extremely weak or to vanish. In other words, the resonance signal of Δm_s = 2 is absent when the D value is small, say, D < 25 G. The observation of the forbidden signal is strong

dx.doi.org/10.1021/cr400056a | *Chem. Rev.* 2013, 113, 7011−7088

evidence of triplet diradicals. The zero-field splitting parameter E relates the symmetry of two electrons in triplet diradicals. In a structure with 3-fold or higher symmetry, the two triplet sublevels of E_x and E_y are degenerate; thus, the ESR signal of the allowed transitions 2 and 3 appear like in Figure 6c.

It is also known that, at short distances or in delocalized systems, the use of the point-dipole approximation (eq 3) is inadequate for relating the D value to the intercenter distance.[24] For example, the distance calculated from the point-dipole approximation with a D value of 211 G was determined to be 509 pm, which is significantly shorter than the X-ray-determined distance of 700.6 pm for the midpoints of the two N−O bonds in bis(nitroxide) diradical **1** (Figure 7).[25]

As mentioned in relation to Figure 6, the detection of the forbidden transition is strong evidence for the generation of triplet diradicals in solid state. However, the intensity is largely dependent on the distance between the two unpaired electrons (eq 4). When the two spins have a large separation, the D value should be small, and the half-field transition ($\Delta m_s = 2$) might not be detected. Thus, it is quite difficult to distinguish between triplet and doublet signals using continuous-wave (cw) ESR spectroscopic analysis when the D values are small. However, measurement of the two-dimensional electron spin transient nutation (2D-ESTN) using a pulsed ESR spectrometer is a powerful tool for determining the spin multiplicity of high-spin molecules. The nutation frequency, ω_{NT}, is dependent on the spin-quantum number S (eq 5), where ω_1 stands for the strength of the magnetic field of the microwave irradiation field. The 2D-ESTN method is highly useful for discriminating among high-spin species in mixed-spin systems.[26]

$$\omega_{NT}\ (\mathrm{Hz}) = [S(S+1) - m_s(m_s - 1)]^{1/2}\omega_1 \qquad (5)$$

The intensity (I) of the triplet ESR signal depends on temperature (T), because the triplet states are thermally equilibrated with the singlet states. For such a ferromagnetic (triplet) and antiferromagnetic (singlet) system, a plot of IT versus T (in kelvin) should deviate from linearity, whereas that for a paramagnetic (i.e., doublet) species should be linear (Figure 8, eq 6). Because the intensity of the allowed ESR signals is normally sensitive to a saturation effect especially at low temperatures, it is better to use the forbidden transition signals ($\Delta m_s = 2$) for the $IT-T$ plots. Typical plots for the spin-state-dependent change are shown in Figure 8. The plot for triplet-ground-state diradicals deviates upward from a linear fit as temperature decreases. The temperature effect on the ESR intensity for the singlet-ground-state diradicals behaves in the opposite way to that for the triplet plot. The temperature effect on the IT values cannot be observed for paramagnetic doublet species. The singlet−triplet energy spacing ($2J_{ab}$) can be obtained by simulating the experimentally obtained plot using the Bleaney and Bowers equation (eq 6 in Figure 8), where C is the Curie constant and J_{ab} is the exchange integral, that is, $J_{ab} < 0$ (singlet ground state), $J_{ab} > 0$ (triplet ground state).[27] When diradicals are stable at high temperatures above room temperature, this equation is a quite powerful method for determining singlet−triplet energy gaps. For highly reactive diradicals, singlet−triplet energy gaps of less than 1 kcal mol^{-1} can possibly be determined for singlet-ground-state diradicals using this equation. For triplet-ground-state molecules, this equation is useful for cases in which the energy gap is less than 0.1 kcal mol^{-1}.

Negative-Ion Photoelectron Spectroscopy (NIPES).[28,29] Negative-ion photoelectron spectroscopy (NIPES) is a very useful method for measuring the physical properties of reactive intermediates. In gas-phase experiments, a beam of mass-selected negative ions (R^-) is intersected with an intense laser beam, resulting in photodetachement of an electron to produce neutral reactive intermediates. A plot of the number of photodetached electrons as a function of electron binding energy provides the electron affinity and electronic state term energies for the neutral intermediate. The electron affinity is of importance in calculating the dissociation energy of the R−H bond. Furthermore, accurate values of vibrational frequencies for the isolated molecule can be determined. A combined study with quantum chemical calculations provides important information on the structure and electronic configuration of the reactive intermediates.

The photoelectron spectrum of the negative anion of an open-shell molecule provides useful information on the singlet−triplet energy gap. The typical photodetachement process of an electron is depicted in Figure 9. The doublet radical anion yields both singlet and triplet states of the neutral open-shell molecules in the photoelectron spectrum; thus, the singlet−triplet energy splitting can be measured directly. A typical example for propadienylidene ($CH_2C{=}C{:}$) is shown in Figure 10, from which the singlet−triplet energy gap ($\Delta E_{ST} = E_S - E_T$) of the vinylydene carbene was determined to be −29.7 kcal mol^{-1}.[30]

Recent developments of diradical chemistry mainly during the past decade are summarized in the following sections.

2. LOCALIZED DIRADICALS

Localized diradicals are key intermediates in processes involving the homolytic bond-cleavage and -formation reactions of cyclic

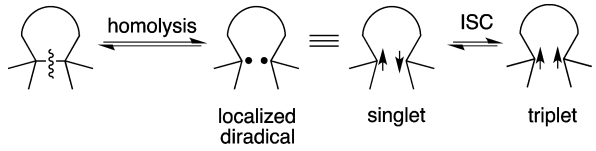

Figure 11. Generation of localized diradicals in homolysis.

Table 1. Values of Zero-Field Splitting Parameters D and E for Localized Diradicals

diradical	R	|D/hcl /cm^{-1}	|E/hcl /cm^{-1}	reference
 **1**	H	0.084	0.002	44
	Ph	0.045	0.001	41
 **2**	X	ΔD		
	NO_2	0.0414 +0.90		
	CN	0.0449 +0.55		
p-XC_6H_4	NH_2	0.0474 +0.30	~0.000	48
	Cl	0.0495 +0.09		
	H	0.0506 0.00		
	OMe	0.0510 -0.04		
	OH	0.0509 -0.05		
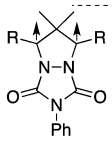 **3**	Me	0.068	0.0058	43
	Ph	0.048	0.001	
 **4**	Me	0.084	0.005	
	Ph	0.060	0.002	46,47
	CH_2=CH	0.050	0.001	

dx.doi.org/10.1021/cr400056a | *Chem. Rev.* 2013, 113, 7011−7088

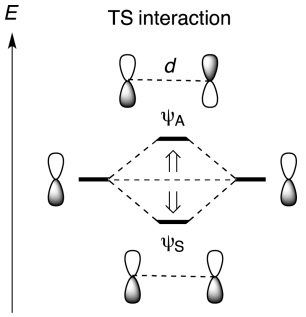

Figure 12. Through-space (TS) interaction between the two p orbitals.

Scheme 1. Generation of Kinetically Stabilized Cyclopentane-1,3-diyls (DR1) and Cyclobutane-1,3-diyls (DR2) in the Denitrogenation of Azoalkanes

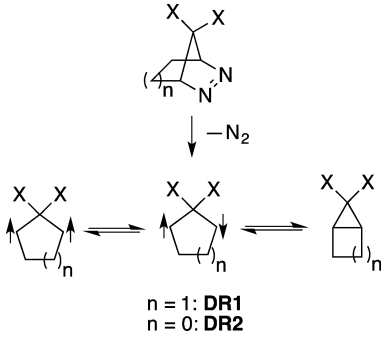

compounds (Figure 11). The singlet state (↑↓) and triplet state (↑↑) are in equilibrium with one another through the intersystem crossing (ISC) process.[31−33] Since the 1960s, the chemistry of localized triplet diradicals has been well investigated not only as reactive intermediates but also in materials chemistry, because triplet diradicals have long enough lifetimes to allow the diradicals to be detected using time-resolved spectroscopic analysis at ambient temperature and ESR spectroscopic analysis under low-temperature matrix conditions.[34−39] The paramagnetic character of triplet diradicals makes them potential building blocks for organic magnets and other materials with novel properties. Thus, the chemistry of localized triplet diradicals is very rich, and the high-spin property has attracted continuous interest in many fields of materials chemistry.[40] Typical examples of localized triplet-ground-state diradicals are listed in Table 1, along with the zero-field splitting parameters D and E.[41−47] The substituent-dependent changes of the D parameter in triplet diradicals **2** were used for the radical stabilization parameters (ΔD) for benzylic radicals.[48]

In contrast to the rich chemistry of localized triplet diradicals, the chemistry of localized singlet diradicals has been less studied, especially experimentally. The singlet state of localized diradicals had been recognized as putative (undetectable) intermediates, because the intramolecular radical−radical coupling reactions are assumed to be barrierless processes (Figure 11). To observe singlet diradicals directly and investigate their chemistry experimentally, the generation of diradicals with a singlet ground state is indispensable, because only the ground-state spin multiplicity can be detected at low temperatures such as that of liquid helium. Thus, the main topics of research on localized diradicals in the past decade were the generation of singlet-ground-state diradicals, their detection, and their isolation.[49]

First, the basic properties that determine the ground-state spin multiplicity in localized 1,3-diradicals are described. As mentioned in the Introduction, the ground-state spin multiplicity and singlet−triplet energy spacing in diradicals are determined by two factors: (1) the energy gap between the two nonbonding molecular orbitals (NBMOs, ψ_A and ψ_S) that are occupied by two electrons and (2) the exchange repulsion energy. The energy gap between the two NBMOs is determined by the through-space (TS) and through-bond (TB) interactions. When the energy difference between the two NBMOs is sufficiently large, for example, greater than ∼1.2 eV,[50] the singlet is expected to be the ground-state spin multiplicity. When the energy gap is small or zero, the ground-state spin multiplicity is determined by the magnitude of the exchange repulsion.

The through-space (TS) interaction between the two radical p orbitals gives rise to an energy gap between the two NBMOs (ψ_S and ψ_A), so that the paired electrons preferentially occupy the energetically lowered bonding orbital ψ_S (Figure 12). Thus, the singlet state should be the ground-state spin multiplicity for spatially oriented diradicals. The singlet preference should be independent of the distance (d) between the two radicals. However, as mentioned previously, triplet ground states are known for the localized 1,3-diradicals **1**−**4** (Table 1). Why do these 1,3-diradicals with relatively short distances (∼200 pm) between the two spins have triplet ground states? Another important orbital interaction, namely, the through-bond (TB)

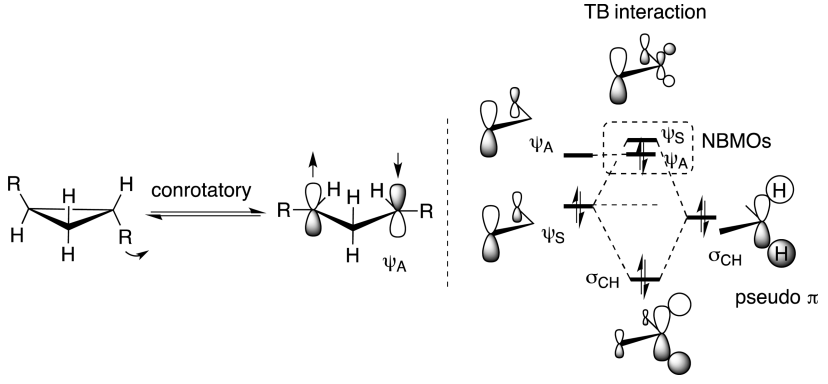

Figure 13. Energetically favored conrotatory processes for the thermal isomerization reactions of cyclopropane derivatives. Through-bond (TB) interaction on the energy level of the symmetric nonbonded orbital (ψ_S). Most stable electronic configuration of propane-1,3-diyl.

dx.doi.org/10.1021/cr400056a | Chem. Rev. 2013, 113, 7011−7088

DR1

	a	b	c	d	e
X	H	F	OH	SiH_3	
ΔE_{ST}	+1.3[a]	-12.7[a]	-6.7[a]	-4.1[a]	-12.2[a]
	+1.2[b]	-11.2[c]	—	-5.8[c]	—
HOMO	ψ_A	ψ_S	ψ_S	ψ_A	ψ_S
	Type-2	**Type-1**	**Type-1**	**Type-2**	**Type-1**

[a] at the UB3LYP/6-31+G(d,p), ref. 53
[b] at the CISD level of theory, ref. 54
[c] at the CASPT2 level of thoery, ref. 55,57

DR2

	a	b	c	d	e	f	g	h	i
X	H	F	OH	SiH_3	F	OH	SiH_3	F	OH
Y	H	F	OH	SiH_3	H	H	H	SiH_3	SiH_3
ΔE_{ST}	+2.7	-21.7	-13.3	-7.4	-6.5	-2.2	-2.1	+2.6	+2.5
HOMO	ψ_A	ψ_S	ψ_S	ψ_A	ψ_S	ψ_S	ψ_A	ψ_S	ψ_A
	Type-2	**Type-1**	**Type-1**	**Type-2**	**Type-1**	**Type-1**	**Type-2**	**Type-1**	**Type-2**

at the UB3LYP/6-31+G(d,p), ref. 50

Figure 14. Effects of substituents X and Y on the ground-state spin multiplicities in **DR1** and **DR2**.

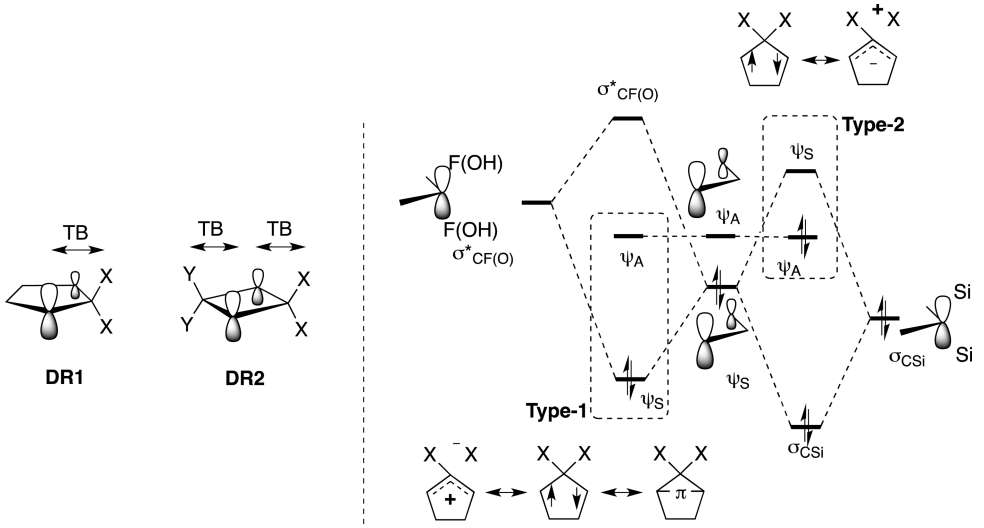

Figure 15. Through-bond (TB) interactions in **DR1** and **DR2**: Type-1 versus type-2 interactions and the most stable electronic configurations of type-1 and type-2 diradicals.

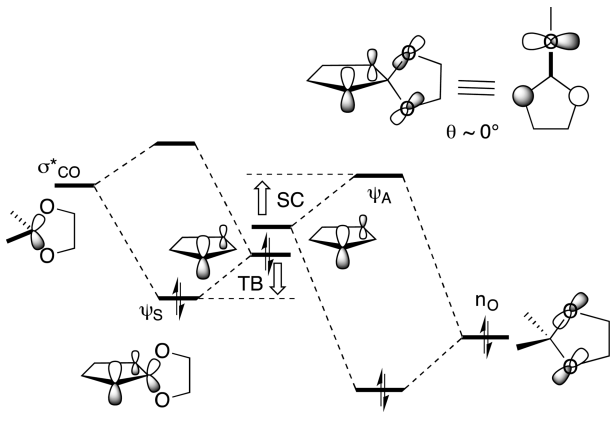

Figure 16. Effects of the through-bond (TB) interaction on the energy level of ψ_S and of spiroconjugation (SC) on the energy level of ψ_A.

interaction, explains well the triplet ground state for localized 1,3-diradicals.

In 1968, Hoffmann predicted that the conrotatory ring-opening and -closing modes are energetically favored processes during the thermal isomerization reactions of cyclopropane derivatives, because the two electrons selectively occupy the antisymmetric nonbonding molecular orbital (ψ_A) (Figure 13).[51,52] The pseudo-π interaction (TB interaction) explains the unusual electronic configuration. Thus, the interaction of the ψ_S orbital with the high-lying σ_{CH} orbital destabilizes the ψ_S orbital to energetically locate ψ_A below ψ_S. The resulting small energy gap between the two NBMOs explains the triplet ground states of the parents cyclopentane-1,3-diyl and cyclobutane-1,3-diyl. Thus, the balance between TS and TB interactions plays an important role in determining the ground-state spin multiplicity of localized 1,3-diradicals. Theoretical study suggests that the energy level of the ψ_S orbital can be changed by the TB interaction (pseudo-π interaction).

dx.doi.org/10.1021/cr400056a | *Chem. Rev.* 2013, 113, 7011−7088

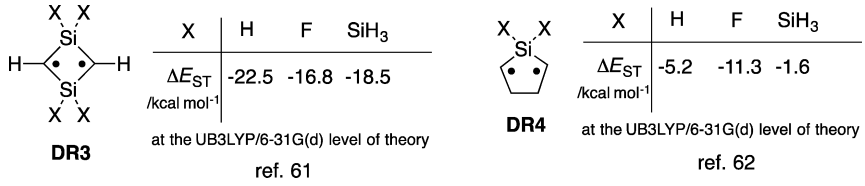

Figure 17. Effects of silicon atoms on the ground-state spin multiplicities of **DR3** and **DR4** and their energy gaps (ΔE_{ST}).

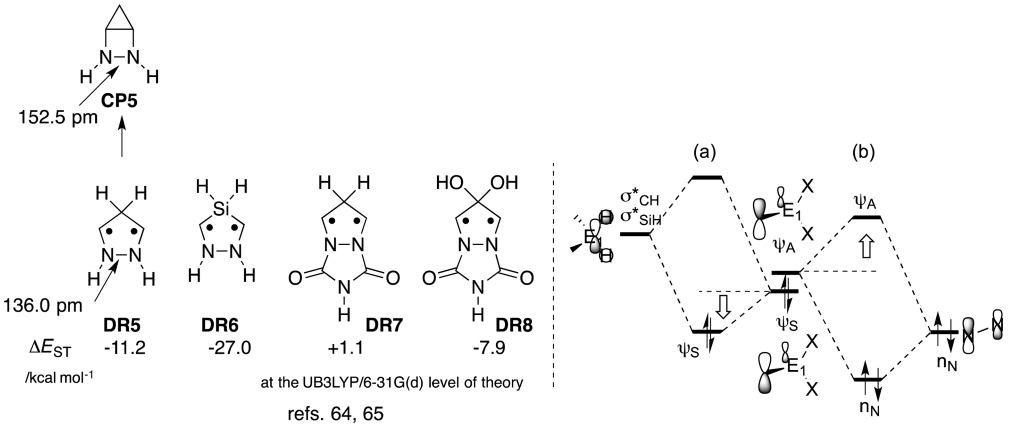

Figure 18. Effects of nitrogen and silicon atoms on singlet–triplet energy spacing.

Scheme 2. Generation and Reactivity of Singlet Diradicals 9 in the Denitrogenation of Azoalkanes AZ9

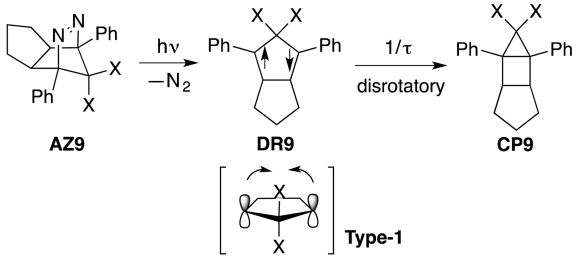

DR9a: X = F, λ_{max} = 530 nm, τ_{298} = 80 ns in pentane
DR9b: X = OEt, λ_{max} = 570 nm, τ_{298} = 520 ns in hexane
DR9c: X = OH, λ_{cald} = 625 nm at the TD-UB3LYP/6-31+G* level of theory

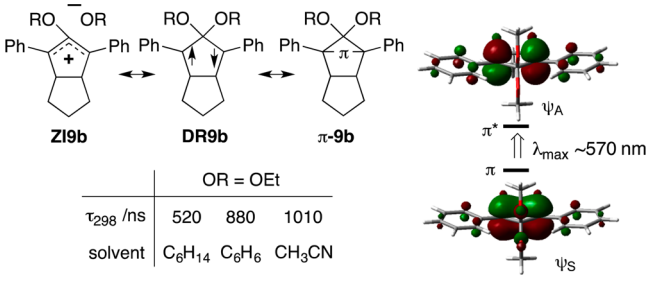

Figure 19. Resonance structures of singlet diradical **9b**.

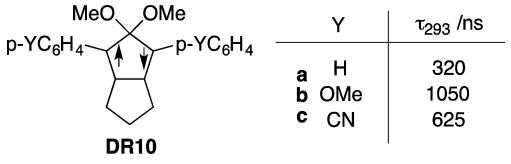

Figure 20. Effect of substituent Y on the lifetimes of singlet diradicals **DR10**, indicating the zwitterionic (ZI) character of singlet 2,2-dialkoxypropane-1,3-diyls.

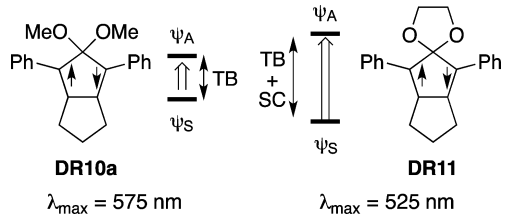

Figure 21. Effect of spiroconjugation (SC) on the energy gap between ψ_S and ψ_A.

2.1. Cyclobutane-1,3-diyls and Cyclopentane-1,3-diyls[53]

Singlet cyclopentane-1,3-diyls **DR1** (n = 1) and cyclobutane-1,3-diyls **DR2** (n = 0), which are promising intermediates in the thermal cycloreversion reaction of strained bicyclo[2.1.0]-pentanes (n = 1) and bicyclo[1.1.0]butanes (n = 0), are good candidates for studying singlet diradical chemistry. The diradicals are kinetically stabilized to have longer lifetimes than the flexible open-chain singlet diradicals (Scheme 1). The 1,3-diradicals in cyclic systems can be cleanly generated from the corresponding cyclic azoalkanes using photochemical denitrogenation. The generation and isolation of the diradicals might be possible under low-temperature matrix conditions. The isolation of singlet diradicals at low temperatures will make it possible to thoroughly study the molecular and electronic structures using UV–vis, emission, and IR spectroscopic analyses. Furthermore, the reactivity, including the lifetime, of the diradicals can be studied using laser flash photolysis techniques, which is now a conventional method for detecting photochemically generated intermediates.

2.1.1. Effect of the Substituent at C2 on the Ground-State Spin Multiplicity.[50] Computational studies on the effects of substituents X and Y at the C2 position on the ground-state spin multiplicity of cyclopentane-1,3-diyls **DR1** and cyclobutane-1,3-diyls **DR2** are summarized in Figure 14. Conrad et al. computationally reproduced the triplet ground state of the parent cyclopentane-1,3-diyl **DR1a** (X = H).[54] In

dx.doi.org/10.1021/cr400056a | Chem. Rev. 2013, 113, 7011–7088

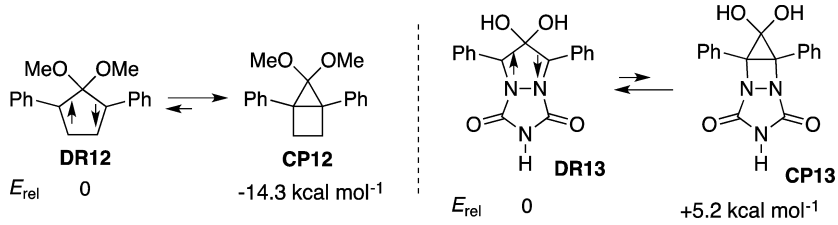

Figure 22. Effect of nitrogen atoms on the equilibrium constant between the singlet diradicals **DR12** and **DR13** with π-bonding character and the corresponding σ-bonding compounds **CP12** and **CP13**.

Scheme 3. Generation of Singlet 4,4-Dialkoxy-1,2-diazacyclopentane-3,5-diyl

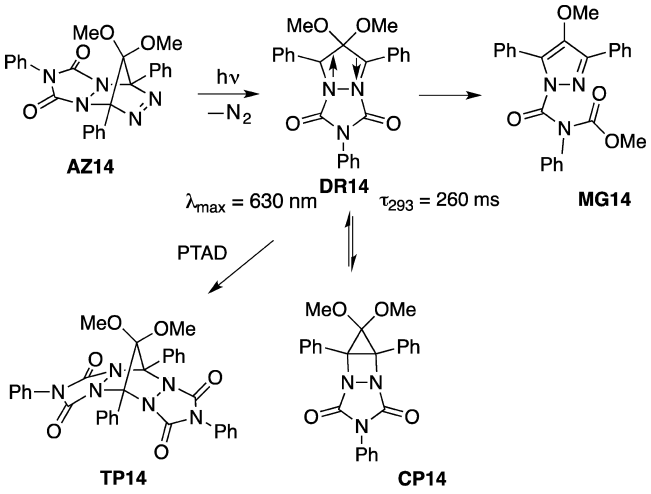

1994, Getty et al. predicted the singlet ground state of 2,2-difluorocyclopentane-1,3-diyl (**DR1b**: X = F, $\Delta E_{ST} = E_S - E_T$ = −11.2 kcal mol^{-1}).[55] The pioneering study of the substituent effect prompted an investigation of the effect of the electronegative alkoxy group (X = OR) on the ground-state spin multiplicity by both computations and experiments.[53] Many derivatives can be designed and synthesized by simply changing the substituents (R) on the oxygen atom. The parent 2,2-dihydroxycyclopentane-1,3-diyl (**DR1c**, X = OH) was found to be a singlet-ground-state molecule with a singlet−triplet energy gap ($\Delta E_{ST} = E_S - E_T$) of −6.7 kcal mol^{-1}.[56] The singlet state was also calculated to be the ground-state spin multiplicity for 2,2-disilylcyclopentane-1,3-diyl **DR1d** (X = SiH_3), in which the electron-donating silyl groups are substituted at the C2 position.[57] The notable substituent effects on the ground-state spin multiplicity are explained by the TB interaction (Figure 15). For diradicals substituted with electron-withdrawing groups (X = F or OR), as shown in Figure 15, the type-1 TB interaction of the symmetric NBMO ψ_S with the low-lying π^*_{CF} or π^*_{CO} orbital stabilizes ψ_S to increase the energy gap with ψ_A. Thus, the singlet was calculated to be the ground-state spin multiplicity. The smaller $|\Delta E_{ST}|$ value for 2,2-dihydroxycyclopentane-1,3-diyl **DR1c** compared to **DR1b** (X = F) can be explained by the weaker electronegativity of the oxygen atom compared to the fluorine atom. Thus, the hyperconjugative electron delocalization of the p-π AOs to π^*_{CX} plays an important role in stabilizing the singlet state. CASSCF(2/2) calculations for the singlet 2,2-dihydroxycyclopentane-1,3-diyl **DR1c** revealed that 81% of the two electrons selectively occupy the ψ_S. Type-1 singlet diradicals with electron-withdrawing groups (EWGs) as substituents have the symmetric ψ_S as the highest occupied molecular orbital (HOMO) and the antisymmetric ψ_A as the lowest unoccupied molecular orbital (LUMO). Thus, π-single-bonding (−π−) character was proposed to be included in singlet-state molecules with the hyperconjugative resonance structure of zwitterions (C^+X^-) .

For the silyl-substituted diradical **DR1d** (X = SiH_3), the type-2 TB interaction of ψ_S with the high-lying occupied σ_{CSi} destabilizes ψ_S to energetically locate ψ_A below ψ_S (Figure 15). Thus, the hyperconjugative electron delocalization of σ_{CSi} to the p-π AOs plays an important role in stabilizing the singlet state. CASSCF calculations clarified that the antisymmetric NBMO ψ_A of the disilyl-substituted diradical **DR1d** was occupied by 72% of the two electrons.[57b] In contrast to the type-1 electronic configuration, for type-2 singlet diradicals, the HOMO is ψ_A, and the LUMO is ψ_S. The singlet-state molecule has the hyperconjugative resonance character of zwitterions (C^-X^+). Thus, the singlet diradicals can be categorized as type-1 and type-2 on the basis of the most stable electronic configuration of the singlet state (Figure 14). The two types of

Scheme 4. Generation of Singlet 1,5-Diaza-3-silapentane-2,4-diyls

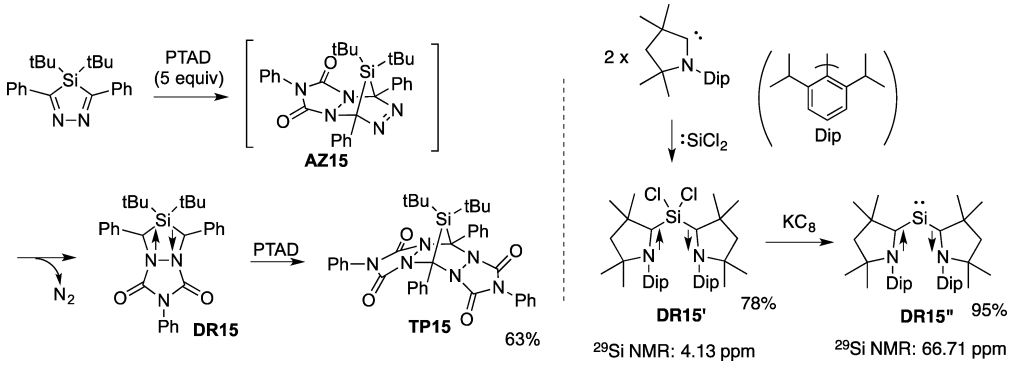

dx.doi.org/10.1021/cr400056a | Chem. Rev. 2013, 113, 7011−7088

Scheme 5. Generation of Type-2 Singlet Diradicals DR18 and DR19 and Their Reactivities

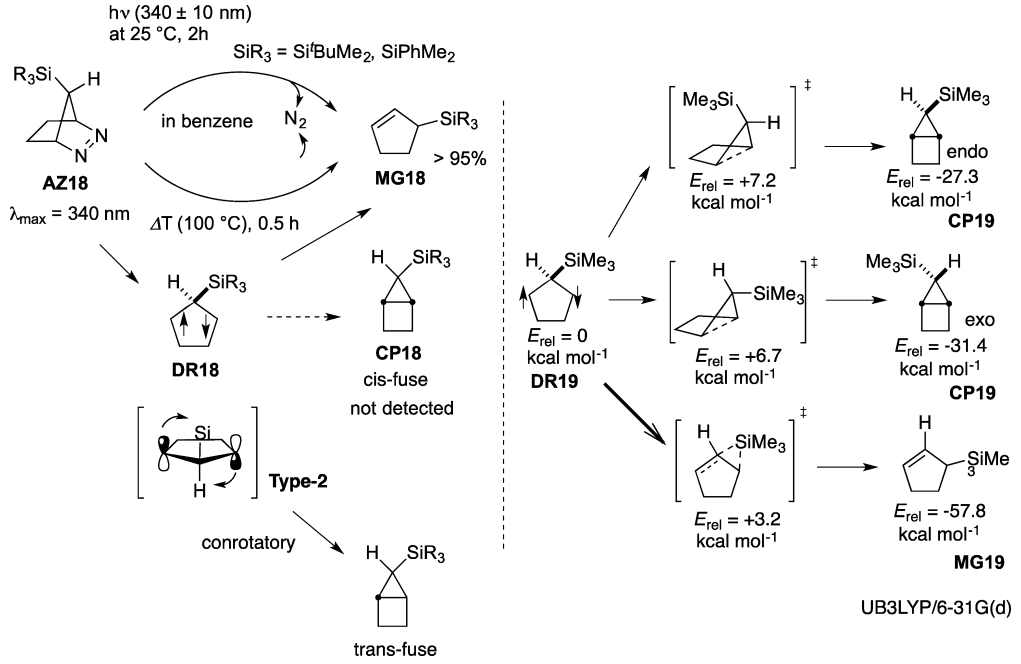

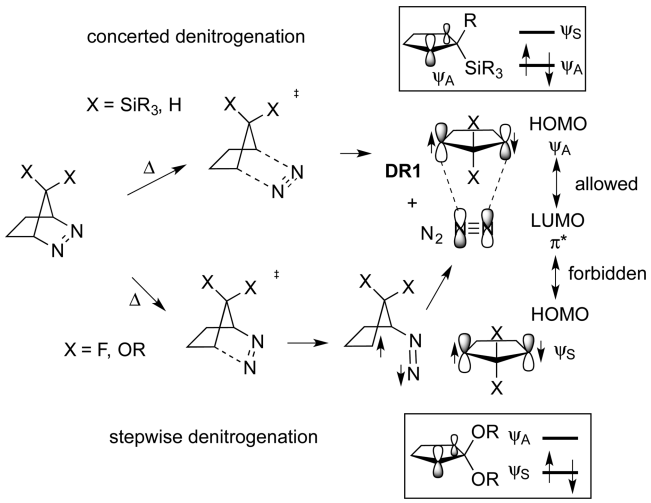

Figure 23. Substituent effect on the thermal denitrogenation mechanism of 1,2-diazabicyclo[2.2.1]heptenes.

singlet diradicals in heterocyclic systems were reported by Schoeller et al.; see ref 100 in section 2.2.

As shown in Figure 14, the singlet−triplet energy gaps for cyclobutane-1,3-diyls **DR2a−d** were found to be nearly twice as large as those for **DR1a−d**.[58] The substituent effect of nearly a factor of 2 can be explained by the two sets of TB interactions for **DR2** (Figure 15). For the mixed-substituent cases **DR2e−g** (X ≠ Y), smaller singlet−triplet energy gaps were found. The triplet ground state was found for diradicals **DR2h** and **DR2i**, in which the TB interaction induced by the electron-withdrawing group is canceled by the TB interaction induced by the electron-donating group.

As shown in Figure 14, the singlet−triplet energy spacing (ΔE_{ST} = −12.2 kcal mol^{-1}) of the ethylene ketal-substituted 1,3-diradical **DR1e** [X = $-O(CH_2)_2O-$] was found to be nearly the same as that calculated for 2,2-difluorocyclopentane-1,3-diyl **DR1b** (ΔE_{ST} = −12.7 kcal mol^{-1}) and much larger than that of 2,2-dihydroxycyclopentane-1,3-diyl **DR1c** (ΔE_{ST} = −6.7 kcal mol^{-1}).[59] The significant effect of the ethylene ketal substituent on the singlet−triplet energy spacing cannot be explained by only the TB interaction depicted in Figure 15. The notable effect of the lone-pair direction on the singlet−triplet energy spacing is explained by spiroconjugation (SC),[60] Figure 16. The spiroconjugation of the n orbital (n_O) of oxygen with the antisymmetric NBMO energetically destabilizes the antisymmetric NBMO (ψ_A), which leads to an increase in the energy gap between the two NBMOs. Thus, in addition to the through-bond (TB) interaction of ψ_S with σ^*_{CO}, spiroconjugation (SC) plays a crucial role in increasing the energy gap.

2.1.2. Effect of Heteroatoms on the Ground-State Spin Multiplicity. *Silicon Atoms.* Ma et al.[61] and our group[62] reported an effect of silicon atoms on the ground-state spin multiplicity in 1,3-diradicals (Figure 17). For example, 2,4-disilacyclobutane-1,3-diyls **DR3** were found to have singlet ground states and large singlet−triplet energy gaps. The singlet-ground-state preference can be explained by the low-lying σ^*_{SiX},[63] which interacts with the ψ_S orbital to increase the energy gap between the two NBMOs. The parent 2-silacyclopentane-1,3-diyl **DR4** with X = H was calculated to have a singlet ground state and a singlet−triplet energy spacing of −5.2 kcal mol^{-1}. The singlet ground state is also explained by the low-lying σ^*_{SiX}. Thus, electron-withdrawing substituents such as fluorine amd oxygen atoms (X = F, OR) are not always needed to make type-1 singlet diradicals, namely, HOMO = ψ_S and LUMO = ψ_A.

Nitrogen Atoms. Nitrogen atoms in cyclopentane-1,3-diyls were also found to significantly affect the ground-state spin multiplicity (Figure 18). The orbital interaction of the n orbital (n_N) on the nitrogen atoms with the antisymmetric combination of the p-π AOs (ψ_A) destabilizes the energy of ψ_A (Figure 18b).[64] Thus, a large singlet−triplet energy gap of −11.2 kcal mol^{-1} was found for the parent 1,2-diazacyclopentane-3,5-diyl **DR5** without any electron-withdrawing substituents at the C2 position. A larger singlet−triplet energy gap of ΔE_{ST} = −27.0 kcal mol^{-1} was calculated for 1,2-diaza-4-

dx.doi.org/10.1021/cr400056a | Chem. Rev. 2013, 113, 7011−7088

Scheme 6. Generation of DR20 Using a Mechanochemical Method (Namely, Ultrasonic Irradiation)

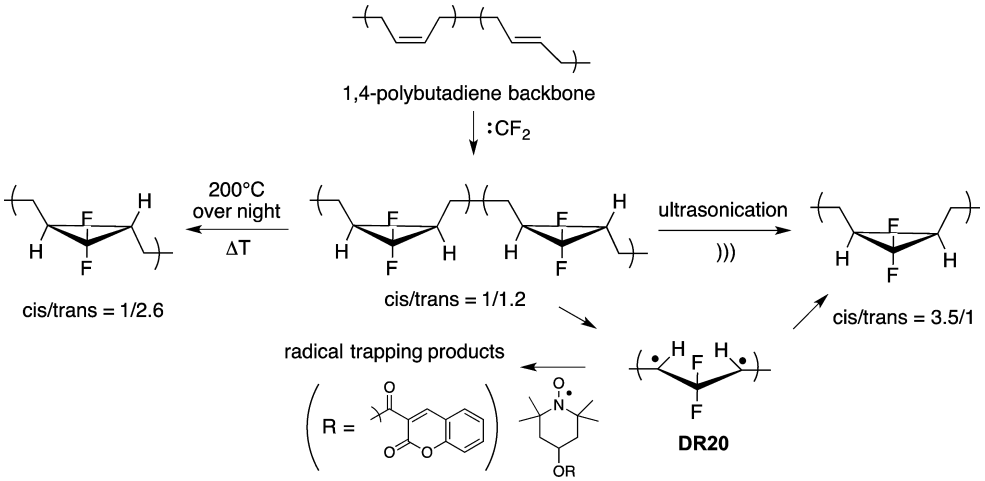

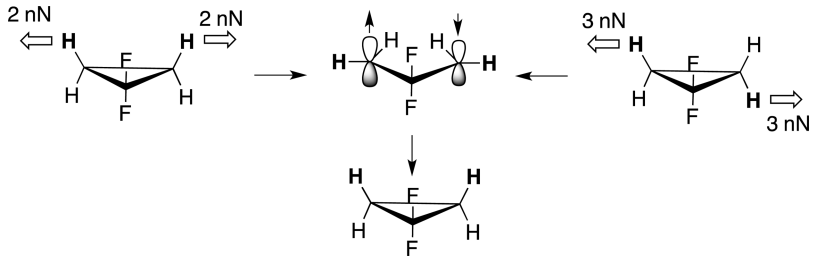

Figure 24. Molecular dynamics (MD) simulations of the mechanochemically induced ring-opening reaction and the generation of a diradical intermediate.

Scheme 7. Generation, Isolation, and Reactivity of B_2P_2 Singlet Diradical

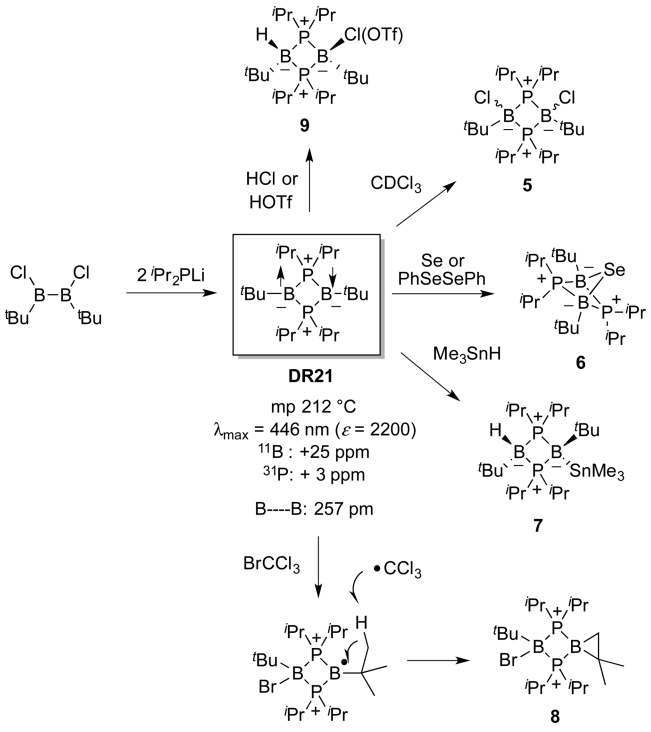

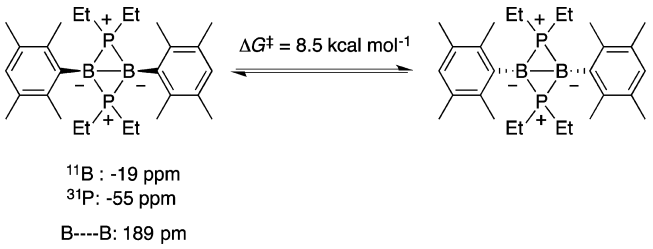

Figure 25. Thermal cycloreversion reaction of a bicyclo[1.1.0]butane derivative.

silacyclopentane-3,5-diyl **DR6**, in which the carbon atom was replaced by the more electropositive silicon atom.[65] The effect of the nitrogen atom, namely, electron delocalization of the lone-pair electrons of the nitrogen atom to the p-π AOs, was confirmed by the fact that the N1−N2 bond length of 136.0 pm in the singlet diradical **DR5** was calculated to be significantly shorter than the N−N bond length of 152.5 pm in the corresponding ring-closed compound, 2,3-diazabicyclo[2.1.0]-pentane **CP5**.

The nitrogen-atom effect on lowering the energy of the singlet state was further confirmed by computations on the ground-state spin multiplicity of diradical **DR7** with the electron-withdrawing carbamate group on the nitrogen atoms (Figure 18).[65] Thus, the triplet ground state with ΔE_{ST} = +1.1 kcal mol^{-1} was found for the parent 1,2-diazacyclopentane-3,5-diyl diradical **DR7** (Figure 18). Indeed, Arnold et al. reported the triplet ground state for 1,2-diaza-4,4-dimethylcyclopentane-3,5-diyl diradicals **3** in Table 1.[43] The singlet state was calculated to be the ground-state spin multiplicity for diradical **DR8**, in which electron-withdrawing OH substituents exist between the p-π AOs.

2.1.3. Generation of Type-1 Singlet Cyclopentane-1,3-diyls. Adam et al. observed the localized singlet 1,3-diradical

dx.doi.org/10.1021/cr400056a | Chem. Rev. 2013, 113, 7011−7088

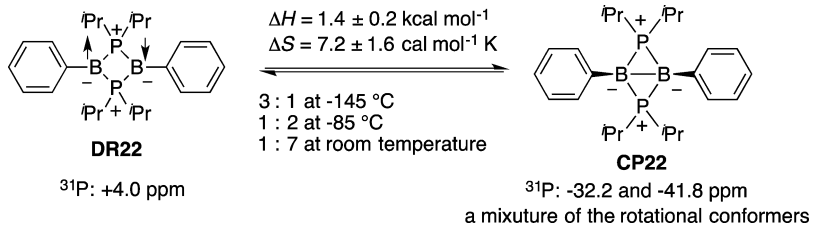

Figure 26. Observation of the thermal equilibration between **DR22** and **CP22**.

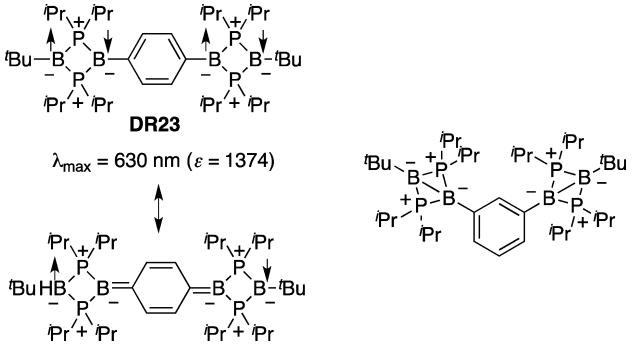

Figure 27. Catenation of two singlet diradicals through *para*-phenylene and *meta*-phenylene units.

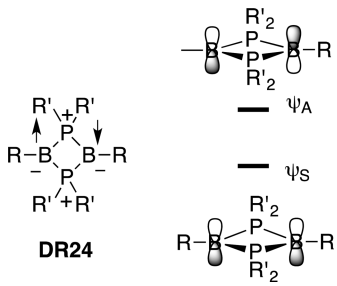

Figure 28. Effects of substituents R and R′ on the diradical character of **DR24**.

DR9a (X = F), which is categorized as a type-1 singlet diradical using a nanosecond laser flash photolysis technique (Scheme 2).[66] Diradical **DR9a** was generated by the denitrogenation of the corresponding azoalkane **AZ9a**. **DR9a** was found to persist at liquid-nitrogen temperatures and absorb light in the visible region, with $\lambda_{max} \approx 530$ nm. The lifetime was determined to be ~80 ns at 298 K in *n*-pentane. The temperature dependence of the rate of disappearance of the diradical was measured, giving the activation parameters $E_a = 7.8$ kcal mol^{-1} and log $A = 12.8$, which are very different from those obtained for the disappearance of the triplet cyclopentane-1,3-diyl **1** (R = Ph), $E_a = 2.6$ kcal mol^{-1} and log $A = 6.7$. At 77 K, the singlet diradical exhibited no ESR signal, which clearly indicates that the singlet state is located energetically well below the triplet state. Indeed, a large energy spacing of 7.4 kcal mol^{-1} was calculated for the 2,2-difluoro-1,3-diphenylcyclopentane-1,3-diyl **DR9a**.[67]

In 2000, the singlet diradical **DR9b** (OR = OEt, $\tau = 520$ ns in *n*-hexane at 293 K, $E_a = 7.6$ kcal mol^{-1}, log $A = 12.0$), which is much longer-lived than **DR9a**, was reported.[56] The assignment of a singlet spin multiplicity to **DR9b** was supported by the following observations: (1) First-order decay kinetics with a high log *A* value was found for the quantitative formation of the ring-closed product **CP9b** (OR = OEt). (2) A strong absorption maximum [$\lambda_{max} = 570$ nm in 2-methyltetrahydrofuran (MTHF) at 77 K, ~3500 M^{-1} cm^{-1}] was observed in the visible region, and the absorption spectrum was similar to that calculated ($\lambda_{calcd} = 625$ nm at TD-UB3LYP/6-31+G*) for the singlet state of 2,2-dihydroxy-substituted diradical **DR9c** (OR = OH). The absorption maximum of the corresponding triplet state was calculated to be 345 nm at the same level of theory. (3) The molecule was EPR-silent at 77 K. (4) The lifetime was insensitive to the presence of molecular oxygen, and the quenching rate constant, $k_{O2} \approx 3 \times 10^6$ M^{-1} s^{-1}, was determined to be significantly lower than that of the triplet, ~3×10^9 M^{-1} s^{-1}.

The breakthrough in the generation of long-lived localized singlet diradicals made it possible to investigate thoroughly the reactivity of localized singlet diradicals in experiments. First, the effect of solvent on the lifetime of the singlet diradical **DR9b** (OR = OEt) was examined to reveal the character of singlet 2,2-dialkoxy-1,3-diradicals (Figure 19). The lifetime was found to increase with increasing solvent polarity: 520 ns in *n*-hexane < 880 ns in benzene < 1010 ns in acetonitrile.[56] The solvent effect on the lifetime indicates that the type-1 singlet state has the character of zwitterion **ZI9b** (OR = OEt), namely, the hyperconjugative resonance structure of singlet diradicals.

This zwitterionic character was further supported by examining the electronic substituent effect on the lifetimes of singlet diradicals **DR10** (Figure 20). The lifetime ($\tau = 1050$ ns in benzene at 293 K) of the singlet diradical **DR10b** with the electron-donating methoxy group (Y = OMe) at the para position of the phenyl ring was found to be longer than those of the parent diradical **DR10a** (Y = H) and the electron-withdrawing-group-substituted diradical **DR10c** (Y = CN, τ =

Scheme 8. Generation of Al_2P_2 Type-1 Singlet Diradical DR25

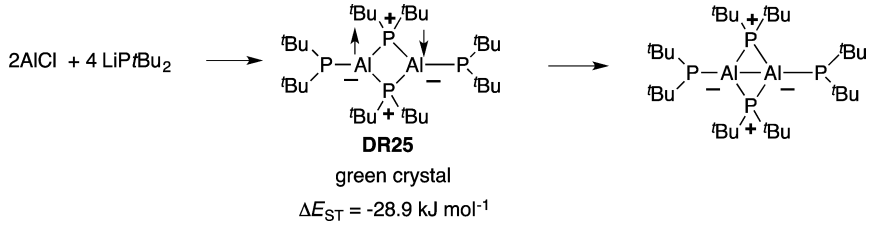

dx.doi.org/10.1021/cr400056a | Chem. Rev. 2013, 113, 7011−7088

Scheme 9. Preparation of Ge−Ge π-Single-Bonded Species DR26

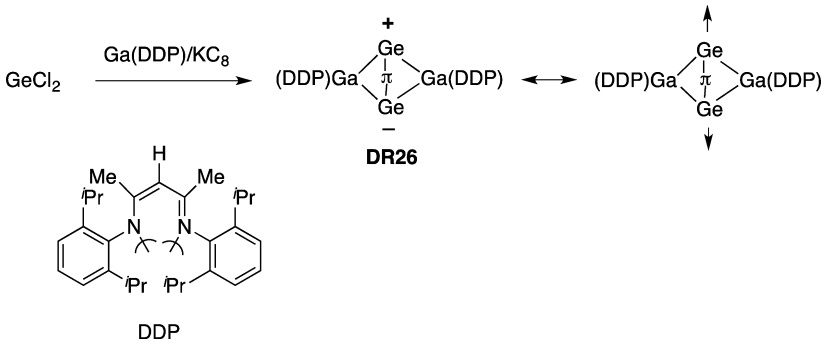

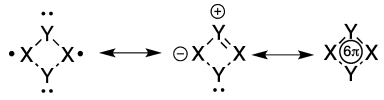

Figure 29. Electronic structure of X_2Y_2.

625 ns in benzene at 293 K).[68] The substituent effect was explained by the stabilization of the allylic cation in the hyperconjugative resonance structure.[69] The radical character of the singlet diradical was also proposed to be significant, because the lifetime of **DR10c** (Y = CN) was found to be longer than that of the parent diradical **DR10a** (Y = H). The stabilization effect of the *para*-cyano group on the benzyl-type radical was suggested to be responsible for the longer lifetime of **DR10c**, because the effects of substituents on the stabilization of benzyl radical are in the order CN (σ_C• = 0.47) > OMe (σ_C• = 0.27) > H (σ_C• = 0.00).[70] The strong absorption band around 570 nm was assigned to the HOMO(π)−LUMO(π*) excitation in the π single bond between the two radical sites.

As mentioned in section 2.1.1, Effect of the Substituent at C2 on the Ground-State Spin Multiplicity, the singlet−triplet

Scheme 10. Synthesis of C_2P_2 Diradicals and Their Chemistry

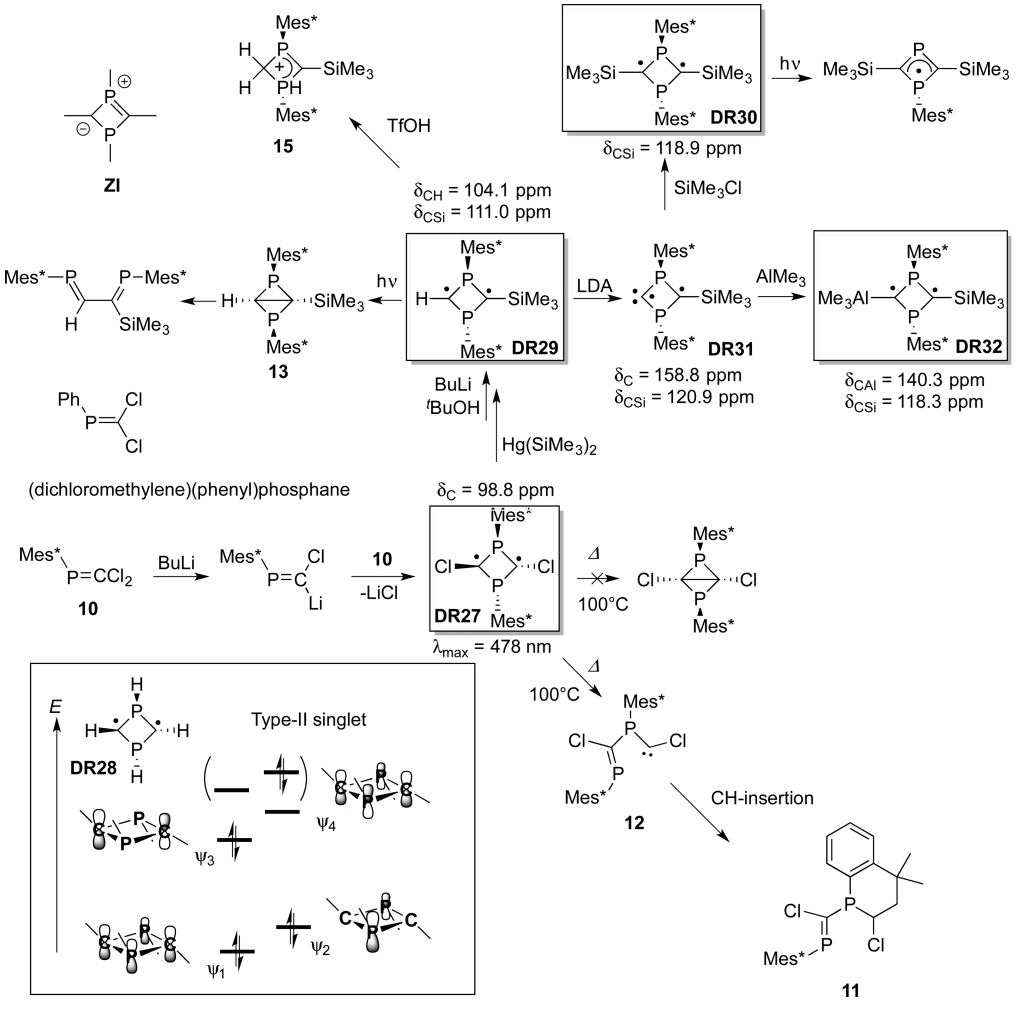

dx.doi.org/10.1021/cr400056a | Chem. Rev. 2013, 113, 7011−7088

Scheme 11. Reactivity of Amino-Substituted Diradical

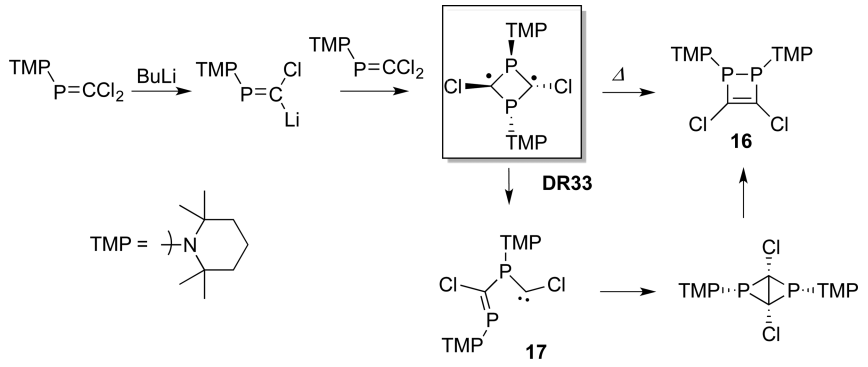

Scheme 12. Chemistry of C_2P_2 Diradical DR35

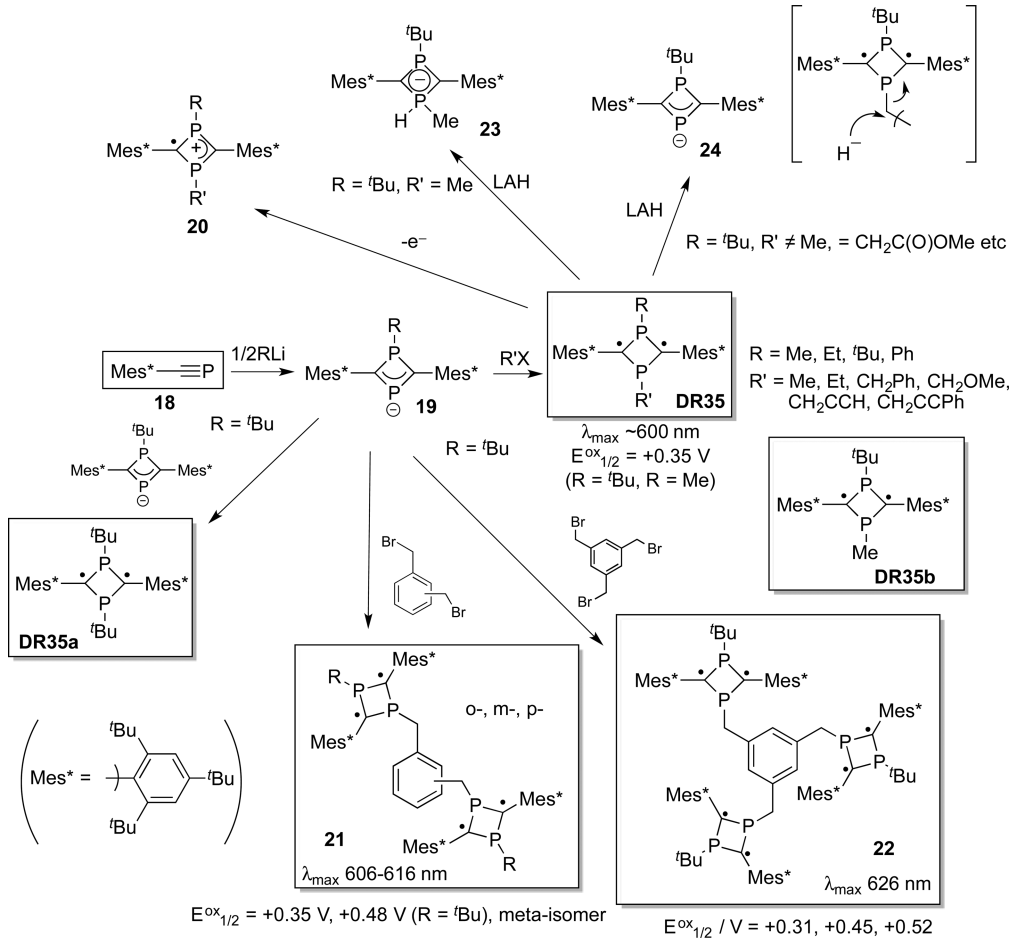

energy spacing of 2,2-ethylene ketal-substituted 1,3-diradical was found to be much larger than that of 2,2-dihydroxycyclopentane-1,3-diyl (Figure 14). The notable effect was explained by spiroconjugation (SC), which increases the energy gap between ψ_S and ψ_A (Figure 16). Indeed, an absorption maximum of λ_{calcd} = 585 nm was calculated for the ethylene ketal-substituted diradical **DR11** (Figure 21). The absorption maximum was predicted to be blue-shifted in comparison with that of the dihydroxy-substituted diradical **DR9c** (OR = OH, λ_{calcd} = 625 nm) at the TD-UB3LYP/6-31+G(d) level. The effect of spiroconjugation (SC) on the singlet−triplet energy spacing was confirmed by measuring the absorption spectrum of the 2,2-ethylene ketal-substituted diradical **DR11**.[71] The diradical **DR11** was generated by the photodenitrogenation reaction of the corresponding azoalkane at 80 K in an MTHF matrix. The absorption spectrum was compared with that of the 2,2-dimethoxy-substituted singlet 1,3-diyl **DR10a** generated under similar conditions. The absorption maximum of **DR11** was observed at λ_{max} = 525 nm, which is significantly blue-shifted in comparison with that of **DR10a** at λ_{max} = 575 nm (Figure 21). The experimental results support that spiroconjugation (SC) increases the energy spacing between the two nonbonding molecular orbitals and, thus, the singlet−triplet energy spacing.

The kinetic stabilization and reactivity of the π-single-bonded species **DR9b** were investigated in detail by generating a series

dx.doi.org/10.1021/cr400056a | *Chem. Rev.* 2013, 113, 7011−7088

Scheme 13. Ge_2N_2 and Ge_2NO Diradicals

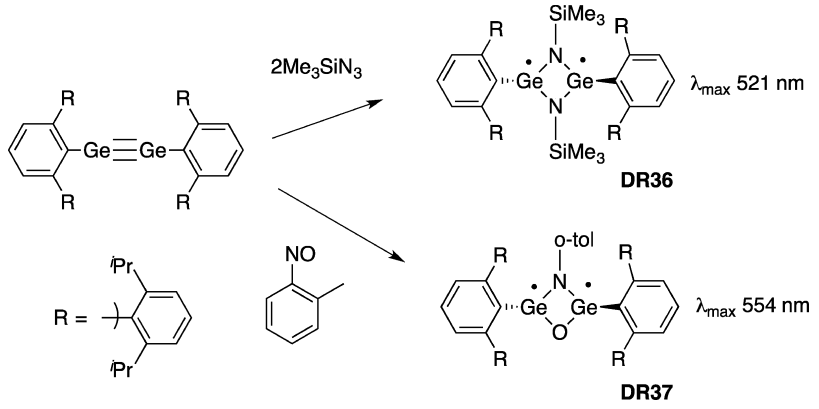

Scheme 14. Sn_2N_2 Diradicals

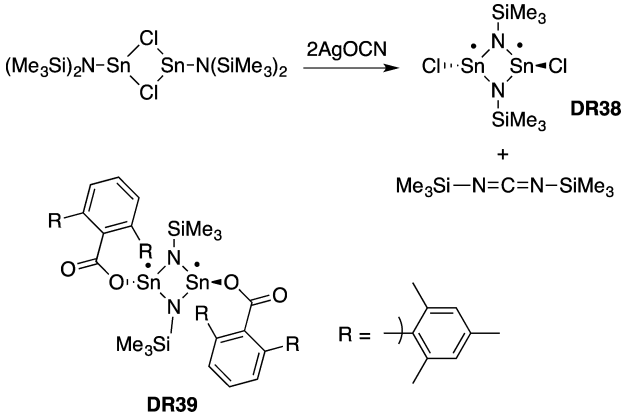

Scheme 15. P_2N_2 Diradical

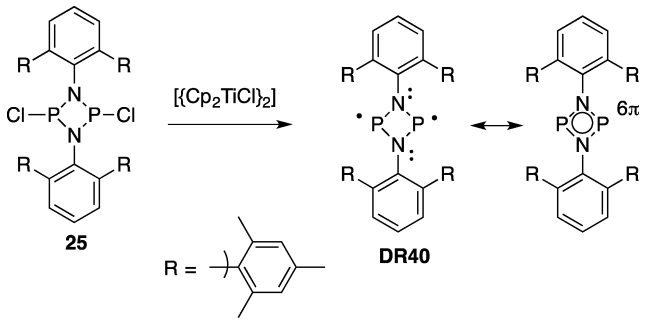

Scheme 16. Synthesis of As_2N_2 Singlet Diradical DR41 and Its Reactivity

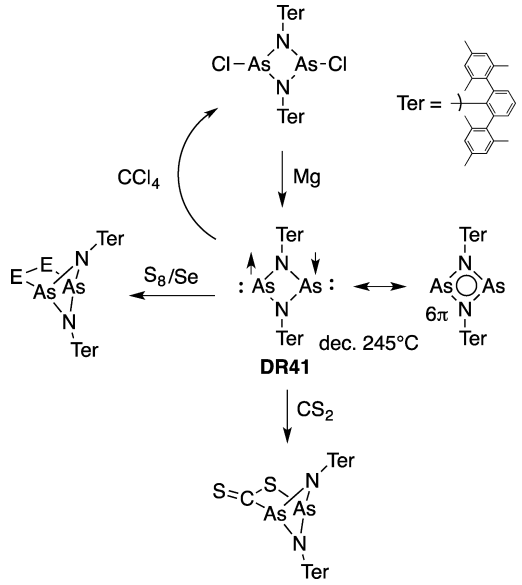

of singlet 2,2-dialkoxy-1,3-diphenyloctahydropentalene-1,3-diyls (**DR9b**).[72] The lifetime at 293 K in benzene was found to increase with increasing carbon chain length of the alkoxy groups: 292 ns (OR = OCH_3) < 880 ns (OR = OC_2H_5) < 1899 ns (OR = OC_3H_7) ≈ 2292 ns (OR = OC_6H_{13}) ≈ 2146 ns (OR = $OC_{10}H_{21}$). Activation parameters determined for the first-order decay process revealed that the enthalpy factor plays a crucial role in determining the energy barrier of the ring-closing reaction, that is, from the π-bonding to the σ-bonding compounds (Scheme 2). Computational studies using density functional theory (DFT) provided more insight into the structures of the singlet species with π-single-bonded character and the transition states for the ring-closing reaction, clarifying the role of the alkoxy group in the lifetime and stereoselectivity of the ring-closing reaction.

In general, the ring-closed (σ-bonded) compounds, namely, bicyclo[2.1.0]pentane derivatives **CP**, are energetically much more stable than the singlet 2,2-dialkoxy-1,3-diphenylcyclopentane-1,3-diyls, which exhibit π-single-bonding character (Figure 22). Indeed, the singlet diradicals **DR9b**, **DR19**, and **DR11** quantitatively produced the ring-closed compounds **CP** by the disrotatory ring-closing mode (Scheme 2). In accordance with the experimental observations, the model ring-closed compound **CP12** was calculated to be more stable than the singlet diradical **DR12** by ca. 14 kcal mol^{-1} at the (U)B3LYP/6-31G(d) level of theory (Figure 22). In contrast, the singlet cyclopentane-1,3-diyl diradical **DR13** was calculated to be more stable than the corresponding ring-closed compound at the (U)B3LYP/6-31G(d) level of theory (Figure 22). Although the UB3LYP method is known to overestimate the stability of the singlet diradicals, the computations clearly suggest that diradical **DR13** is a longer-lived species than singlet diradical **DR12** (Figure 22).

The effects of the nitrogen atoms on the ground-state spin multiplicity and the reactivity of the singlet diradicals were confirmed by the photochemical denitrogenation of the azoalkane **AZ14** (Scheme 3). The photodenitrogenation of azoalkane **AZ14** produced the alkoxy-group migration product

dx.doi.org/10.1021/cr400056a | Chem. Rev. 2013, 113, 7011−7088

Scheme 17. Synthesis of Si_2N_2 Diradical and Its Reactivity

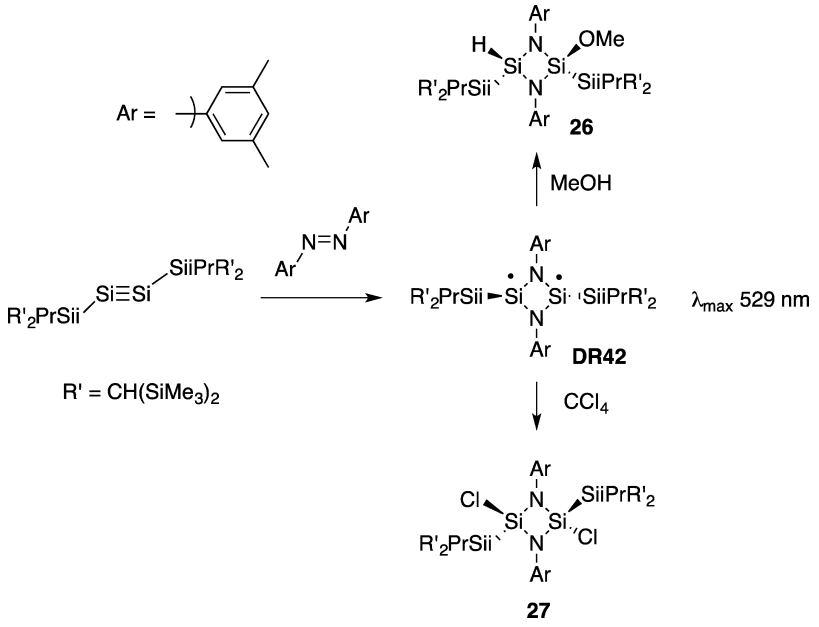

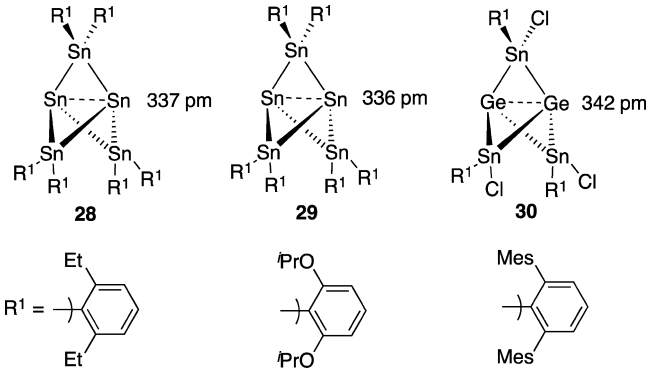

Figure 30. Heavy-atom [1.1.1]propellane derivatives **28**–**30**.

MG14 in 70% isolated yield (Scheme 3).[64] No trace amount of the intramolecular ring-closure compound **CP14** was detected in the photolysate. The singlet diradical **DR14** was cleanly observed at λ_{max} = 630 nm at 77 K in an MTHF glass matrix for the photodenitrogenation of **AZ14**. A green-colored species was found to be stable up to 140 K and ESR-silent. The ground state of **DR14** was calculated to be a singlet, ΔE_{ST} = −3.9 kcal mol^{-1}. Thus, the species at λ_{max} = 630 nm was assigned to the singlet state of diradical **DR14**. The bleaching of the green-colored species **DR14** was observed upon the addition of 4-phenyl-1,2,4-triazole-3,5-dione (PTAD) at 130 K to give the PTAD-trapping product **TP14** in 42% yield. The lifetime of the singlet diradical was found to be extremely long, at ca. 260 ms at 293 K, which was determined by the laser flash photolysis technique in dry toluene solution.[73]

1,2-Diaza-4-silacyclopentane-3,5-diyl diradical **DR15** was trapped by PTAD during the synthesis of **AZ15** from the 1,2,4-diazasilole to give the PTAD adduct **TP15** in 63% yield (Scheme 4).[74] The results indicate that the thermal denitrogenation from **AZ15** is faster than the cycloaddition reaction of PTAD with the diazasilole. Although the singlet diradical **DR15** was not observed directly, the formation of the PTAD adduct **TP15** suggests that the singlet diradical has a sufficient lifetime to allow the diradical to react intermolecularly with PTAD. Very recently, Mondal et al. reported the isolation of 1,5-diaza-3-silapentane-2,4-diyl **DR15′** and **DR15″** in 78% and 95% yields, respectively.[75] The ^{29}Si NMR spectrum of **DR15″** has a singlet at δ = 66.71 ppm, which was found to be downfield of that of **DR15′** (δ = 4.13 ppm); see Scheme 4.

Abe et al. designed kinetically stabilized type-1 diradicals **DR16** and **DR17**. The bond-formation reaction between the radical sites was assumed to be quite slow because of the stretching effect derived from the substituents.[76]

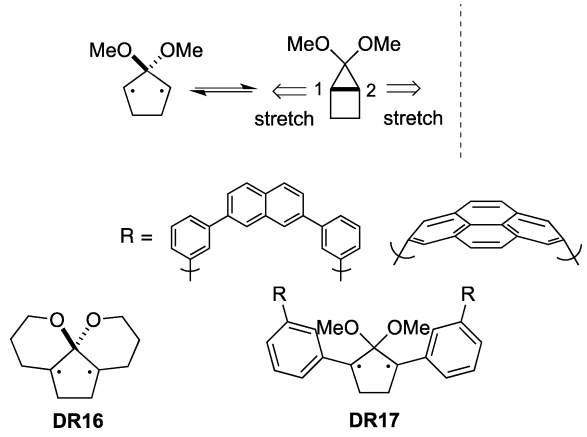

2.1.4. Generation of Type-2 Singlet Diradicals. The generation and reactivity of localized singlet diradicals **DR18** with the type-2 electronic configuration were investigated in the photochemical ($h\nu \approx$ 340 nm) and thermal (100 °C) denitrogenation reactions of the silyl-substituted azoalkanes **AZ18** (Scheme 5).[77] Two electrons selectively occupy the antisymmetric ψ_A orbital in the type-2 diradical. The conrotatory ring-closing mode was required from the type-2 electronic configuration to give the trans-fused ring-closing products **CP18**. However, the trans-fused compounds are too strain to form. In fact, the silyl-migrated products 3-silylcyclopentenes **MG18** were isolated in quantitative yields. The intramolecular cyclization products **CP18**, bicyclo[2.1.0]-pentane derivatives, were reported to be stable at temperatures

dx.doi.org/10.1021/cr400056a | Chem. Rev. 2013, 113, 7011–7088

Scheme 18. Synthesis of Heavy-Atom [1.1.1]Propellane Derivatives 31 and Their Reactivity

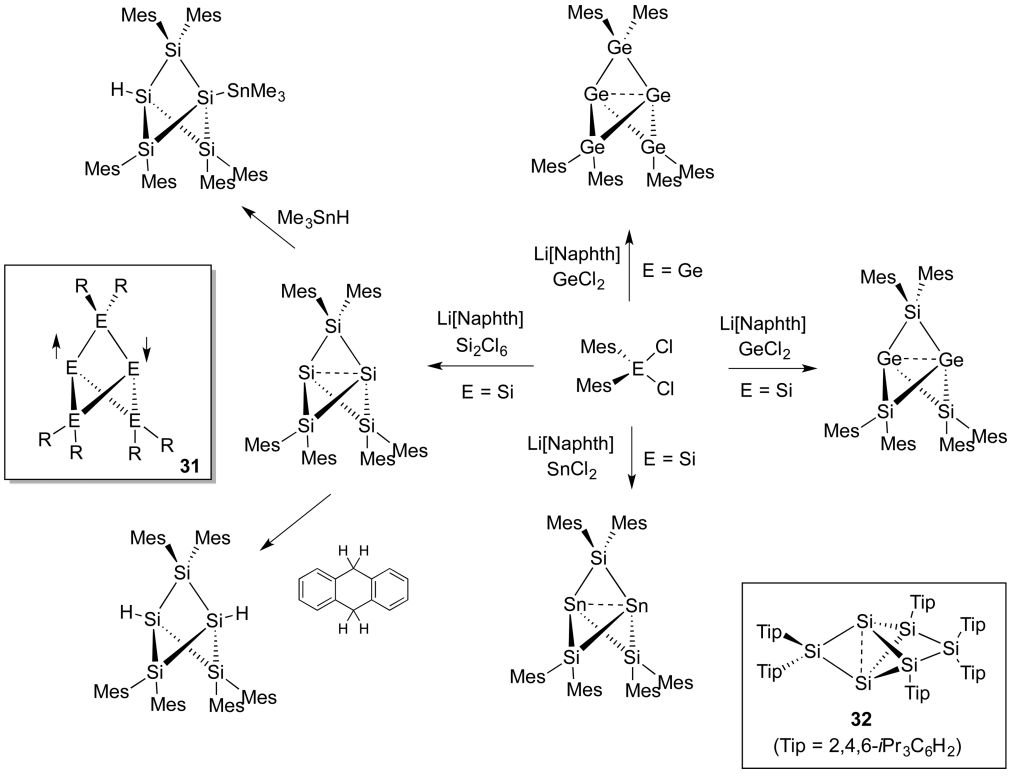

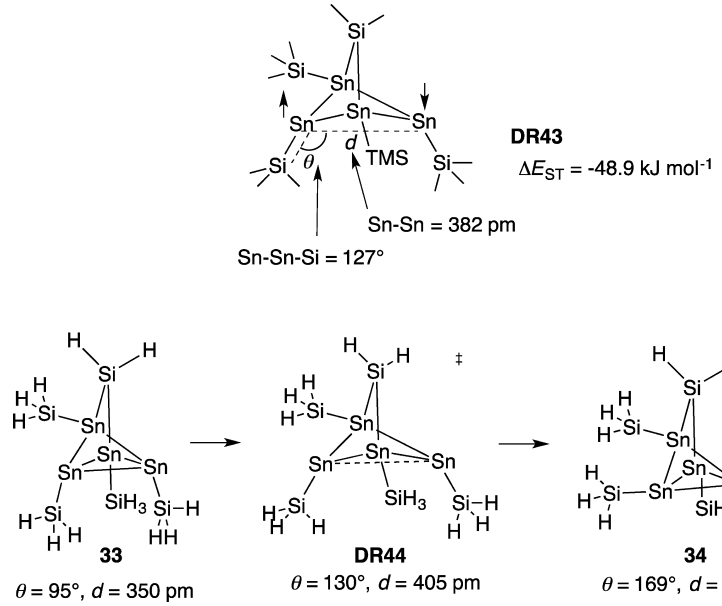

Figure 31. Sn−Sn diradical in the bicyclo[1.1.1]pentane structure.

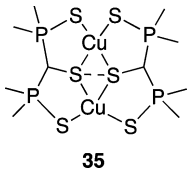

35

Figure 32. Diradical character of the binuclear Cu(I) complex $\{Cu_2[(SPh_2P)_2CSSC(PPh_2S)_2]\}$ **35**.

below 150 °C.[78] The type-2 electronic configuration of diradical **DR18** explains why the ring-closed compound **CP18** was not formed in the denitrogenation reaction.

The reactivity of the type-2 singlet diradical 2-silylcyclopentane-1,3-diyl **DR19** (SiR_3 = trimethylsilane) was computed at the UB3LYP/6-31G(d) level of theory (Scheme 5). In contrast to the barrierless process of the disrotatory ring-closing mode of the type-1 diradicals, such as 2,2-dihydroxycyclopentane-1,3-diyl **DR1c**, significant energy barriers of ∼7 kcal mol^{-1} were calculated for the formation of both the endo- and exo-configured bicyclo[2.1.0]pentanes **CP19** from the type-2

dx.doi.org/10.1021/cr400056a | Chem. Rev. 2013, 113, 7011−7088

Scheme 19. Diradical Intermediate DR45 in the Cope Rearrangement of 1,5-Hexadiene

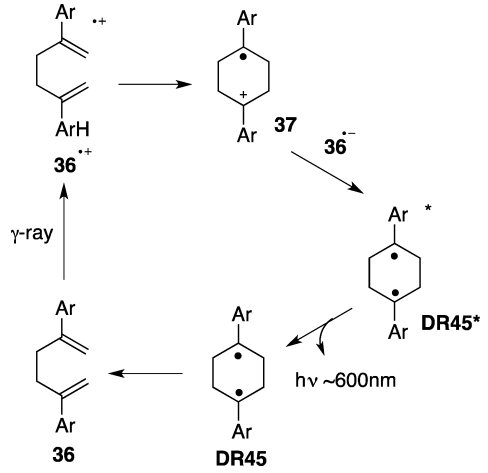

Scheme 20. Cope Rearrangement of 38

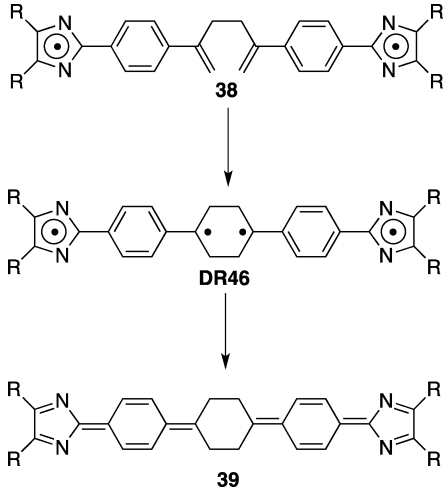

Scheme 21. Mechanochemical Generation of Diradical DR47 in Polymer 40

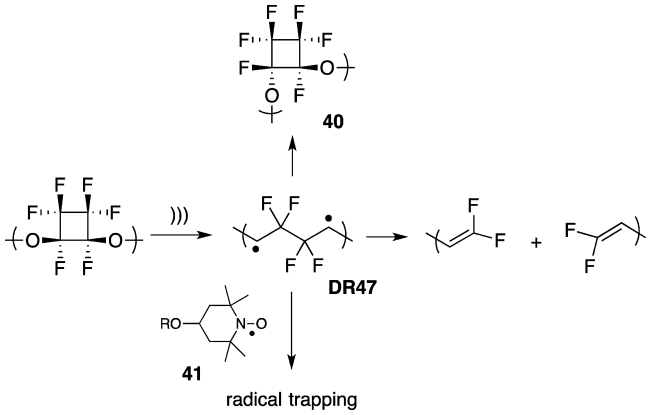

Scheme 22. 1,4-Diradical Character in DR48

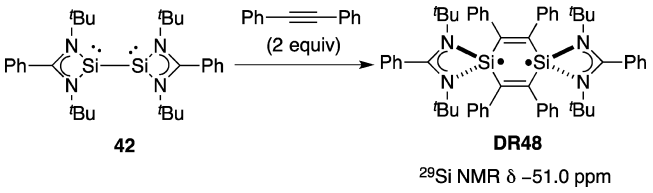

Scheme 23. Ge−Ge Diradical DR49 from Digermyne 43

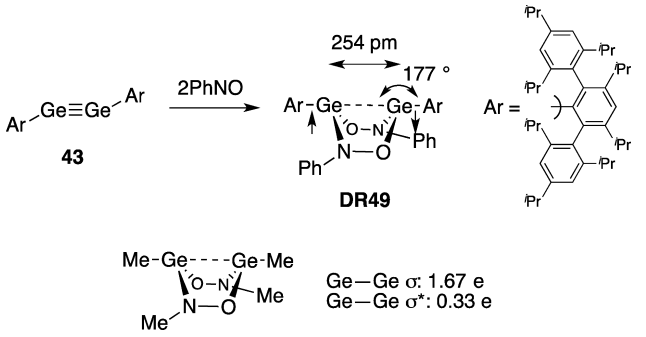

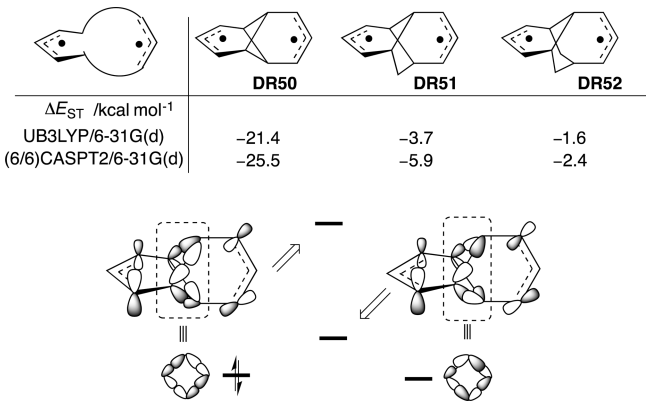

Figure 33. Through-bond effect in twisted diradicals on the singlet−triplet energy gap.

Scheme 24. Generation of σ,π Diradicals in the Myers−Saito Reaction and Schmittel Cyclization of Hepta-1,2,4-trien-6-yne

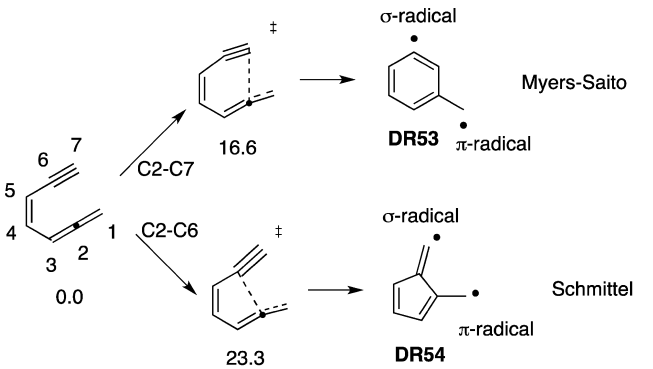

singlet diradical **DR19**. The transition state for the concerted silyl-migration pathway from the singlet 2-silylcyclopentane-1,3-diyl was found in a suprafacial manner to give the silylcyclopentene derivative **MG19**. The energy barrier of the migration step was calculated to be ~3 kcal mol^{-1} at the same level of theory, which was lower than those of the ring-closing reactions.

As discussed previously, the most stable electronic configuration of localized singlet diradicals, type-1 versus

dx.doi.org/10.1021/cr400056a | Chem. Rev. 2013, 113, 7011−7088

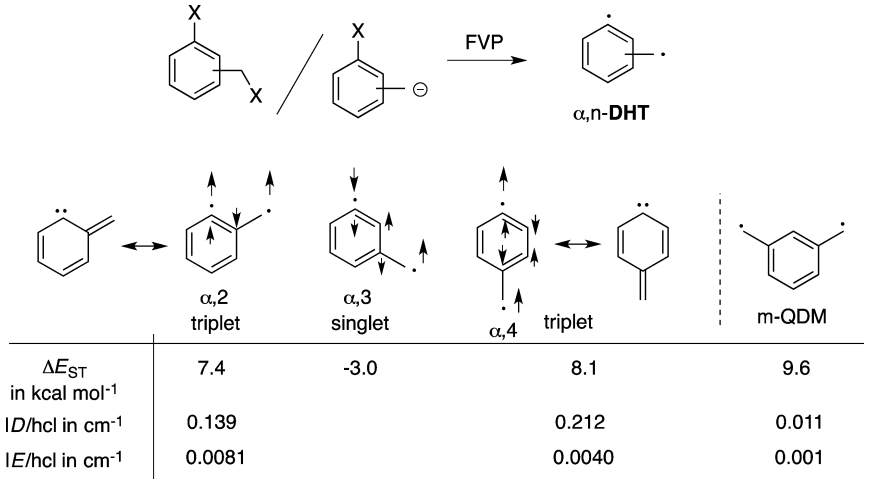

	α,2 triplet	α,3 singlet	α,4 triplet	m-QDM
ΔE_{ST} in kcal mol^{-1}	7.4	-3.0	8.1	9.6
$\|D/hc\|$ in cm^{-1}	0.139		0.212	0.011
$\|E/hc\|$ in cm^{-1}	0.0081		0.0040	0.001

Figure 34. Ground-state spin multiplicity of *α,n*-dehydrotoluenes (DHTs) and ESR zero-field splitting parameters for *α*,2- and *α*,4-DHT.

Scheme 25. Generation of *α,n*-DHT in the Photochemical Elimination of Chlorobenzyltrimethylsilanes

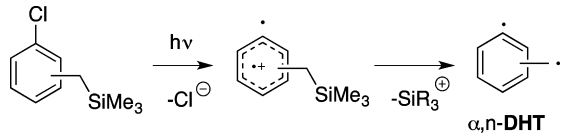

Scheme 26. Schmittel Cyclization and the Substituent Effect on the Reactivity of the Diradical DR55

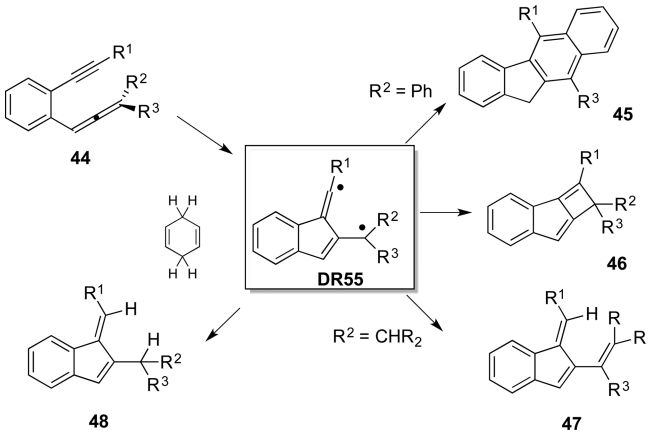

type-2, plays a crucial role in determining their chemistry. In 2005, the thermal denitrogenation mechanism of the precursor azoalkanes, namely, 2,3-diazabicyclo[2.2.1]hept-2-ene (DBH) derivatives, was found to be largely influenced by the most stable electronic configuration of the 1,3-diyls (eq 7,

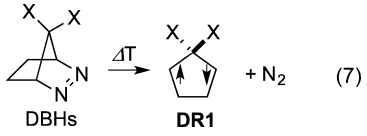

(7)

Figure 23).[79] Thus, when the HOMO of the lowest singlet state of the resulting diradicals is antisymmetric NBMO (ψ_A), that is, for the type-2 configuration, the concerted denitrogenation is a symmetry-allowed process, because the phase of the HOMO matches with the π^* phase of the nitrogen molecule (Figure 23).[80] However, when the HOMO is the symmetric NBMO (ψ_S), that is, for the type-1 configuration, the concerted denitrogenation was predicted to be a symmetry-forbidden process, because the two phases do not match each other. Thus, the concerted denitrogenation would be the preferred denitrogenation mechanism for the electron-donating-silyl-group-substituted azoalkane (X = SiR_3). In contrast, the stepwise denitrogenation was found to be the preferred mechanism in the thermal denitrogenation of the electron-withdrawing-group-substituted azoalkanes (X = F, OR). The

Scheme 27. Photochemical Schmittel Reaction of 49

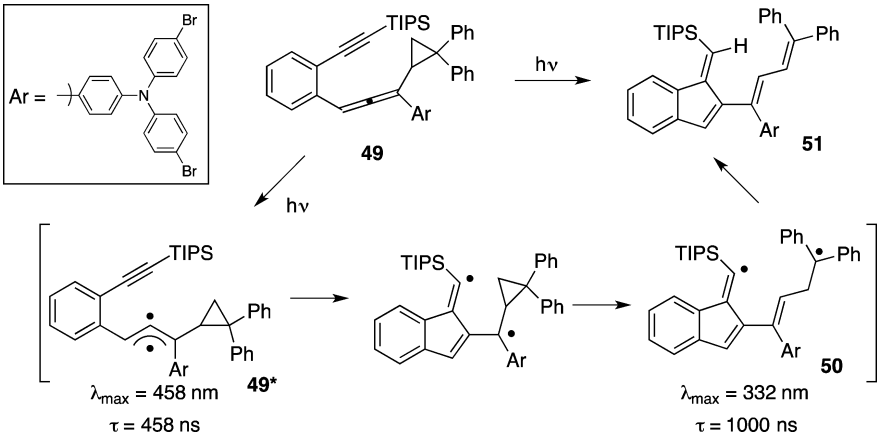

dx.doi.org/10.1021/cr400056a | *Chem. Rev.* 2013, 113, 7011−7088

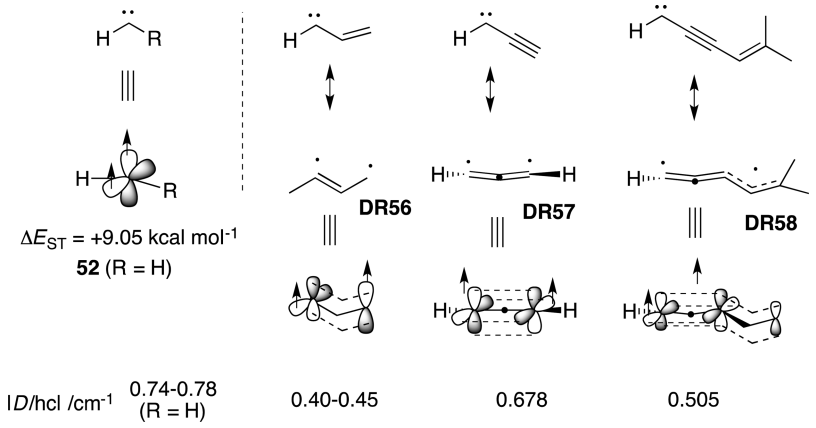

Figure 35. σ,π-Diradical character in vinylmethylenes, propargylenes, and penta-1,2,4-triene-1,3-diyls.

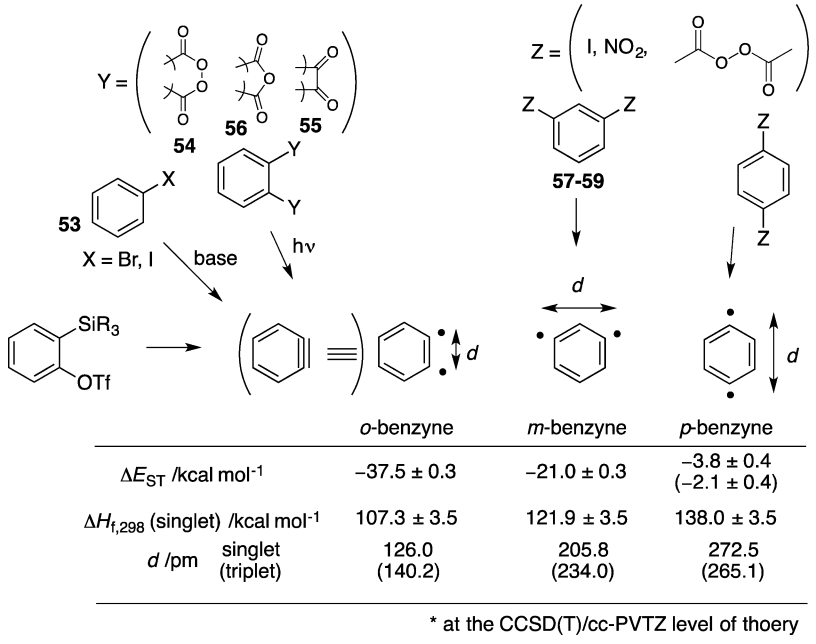

	o-benzyne	*m*-benzyne	*p*-benzyne
ΔE_{ST} /kcal mol^{-1}	−37.5 ± 0.3	−21.0 ± 0.3	−3.8 ± 0.4 (−2.1 ± 0.4)
$\Delta H_{f,298}$ (singlet) /kcal mol^{-1}	107.3 ± 3.5	121.9 ± 3.5	138.0 ± 3.5
d /pm singlet (triplet)	126.0 (140.2)	205.8 (234.0)	272.5 (265.1)

* at the CCSD(T)/cc-PVTZ level of thoery

Figure 36. Ground-state spin multiplicity of benzynes and their structural features.

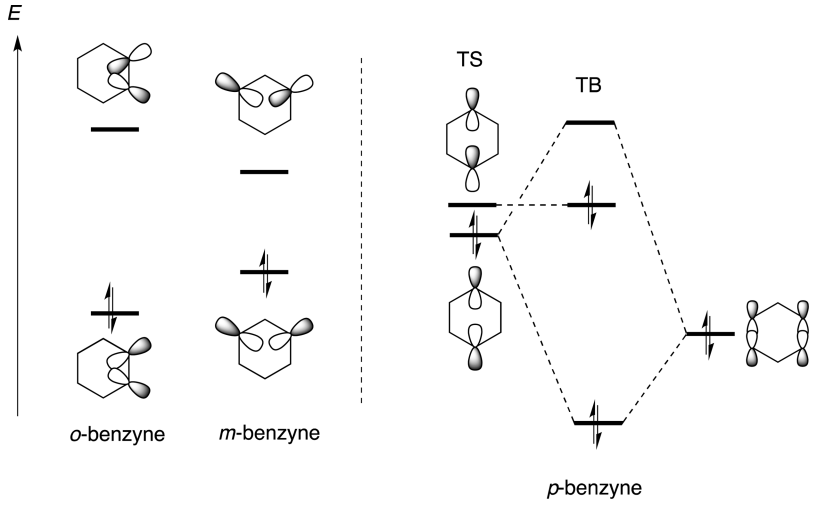

Figure 37. Through-space and through-bond interactions in *o*-, *m*-, and *p*-benzyne.

substituent effect was confirmed by the combination of quantum chemical calculations and experimental studies.[81,82]

Mechanochemically Generated 1,3-Diradicals.[83−85] Chemistry includes bond-breaking and -formation processes.

dx.doi.org/10.1021/cr400056a | *Chem. Rev.* 2013, 113, 7011−7088

Scheme 28. Generation of *p*-Benzyne Derivatives in Masamune–Bergman Cyclization

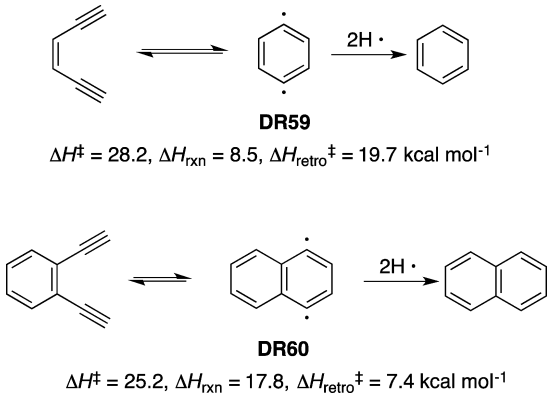

In general, the processes are triggered by heat, light, oxidation, and reduction. Recently, mechanochemical[86] polymer extension derived from ultrasonication [denoted by ")))"] was reported to induce bond-breaking processes, generating diradical species. Lenhardt et al. reported that an unusual cis/trans ratio was observed in the isomerization reaction of the *gem*-difluorocyclopropane ring system in 1,4-polybutadiene (PB) polymer (Scheme 6).[87] The trans isomer is more stable in energy than the cis isomer. Thus, the thermal isomerization induced by heating the polymer at 200° overnight gave a cis/trans ratio of 1:2.6. However, a cis/trans ratio of 3.5/1 was obtained in the ultrasonication of the PB polymer (209 kD) after 60 min at 6–9 °C. The isomerization reaction was found to be largely dependent on the molecular weight of the polymer. An 8.2-kD PB polymer with the difluorocyclopropane moiety was below the critical molecular weight necessary for the mechanochemically induced cis–trans isomerization. The diradical intermediate **DR20** generated by the mechanochemically induced tension was proposed for the selective formation of the cis isomer through the disrotatory ring-closing reaction. The diradical intermediate was trapped by a 2,2,6,6-tetramethylpiperidin-1-oxyl (TEMPO) derivative. The disrotatory ring-closing and -opening modes are the energetically favored processes, because the singlet 2,2-difluorocyclopropane-1,3-diyl has a type-1 electronic configuration.

Molecular dynamics simulations supported the mechanochemically induced ring-opening reaction and the generation of the diradical intermediate (Figure 24). Upon application of a 2 nN force to cis attachment points, 6 of 20 trajectories opened in the disrotatory mode to form the diradical, which is the symmetry-allowed process. A larger 3 nN applied force was required to observe ring opening within the 1-ps simulation window for the trans isomer case.

2.2. 1,3-Diradicals in Heterocyclic Four-Membered Ring Systems

2.2.1. Type-1 Diradicals (B_2P_2).[88] Type-1 localized singlet 1,3-diradicals are recognized only as short-lived intermediates or transition states for the cycloreversion reaction of bicyclic ring compounds such as bicyclo[1.1.0]butanes and bicyclo[2.1.0]pentanes, because the two electrons preferentially occupy the bonding π orbital (Figure 15). Scheschkewitz et al. designed the isolable localized B_2P_2 singlet diradical **DR21** (Scheme 7), which was dictated by taking advantage of several factors to kinetically stabilize the singlet diradical: (1) a substantial ring strain in the bicyclo[1.1.0]butane structure, (2) the low-lying σ orbital of P^+R_4, (3) a weak B–B σ bond due to electrostatic repulsion, and (4) the bulky substituents ^{i}Pr and ^{t}Bu (Scheme 7).[89] The singlet diradical was synthesized in the reaction of 1,2-dichloro-1,2-di(*tert*-butyl)diborane with 2 equiv of lithium di(isopropyl)phosphide. After workup and recrystallization from a toluene solution at room temperature, **DR21** was isolated in 68% yield as air-sensitive but highly thermally stable yellow crystals (mp. 212 °C). X-ray diffraction analysis revealed that the B_2P_2 ring is perfectly planar, and the B–B distance was found to be 257 pm. The long B–B distance indicates that there is no σ-bonded interaction between the boron atoms. The relatively low-field ^{11}B and ^{31}P NMR chemical shifts (δ_B = +25 ppm and δ_P = +3 ppm) clearly

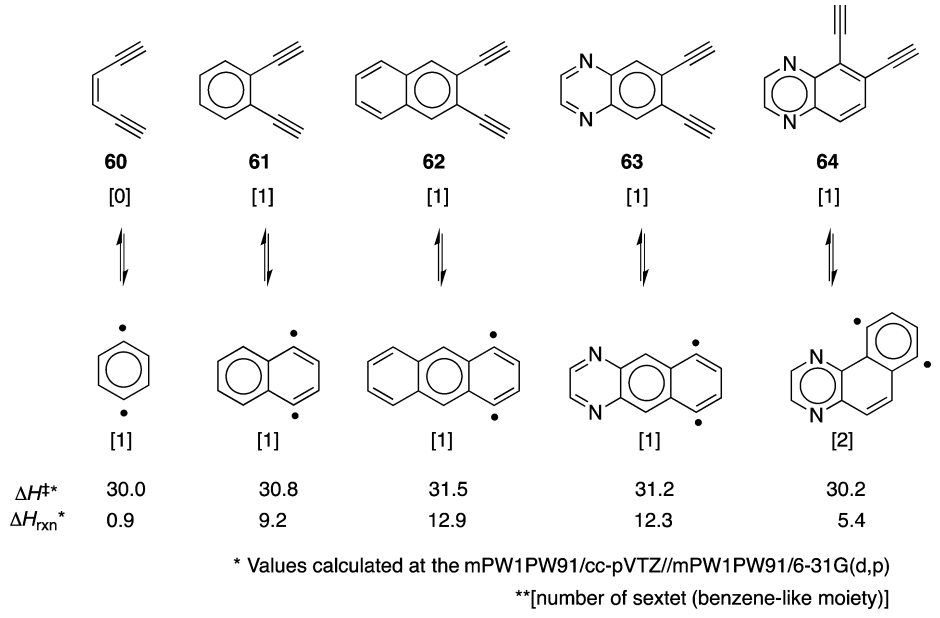

Figure 38. Computed activation enthalpies ($\Delta H^{\ddagger}$, kcal mol^{-1}) and endothermicities (ΔH_{rxn}, kcal mol^{-1}) for the C1–C6 cyclization of 1,2-diethynylbenzene derivatives.

dx.doi.org/10.1021/cr400056a | *Chem. Rev.* 2013, 113, 7011–7088

Scheme 29. Radical Trapping Reaction Using Phenyl *tert*-Butyl Nitrone (PBN) in the Masamune–Bergman Cyclization Reaction

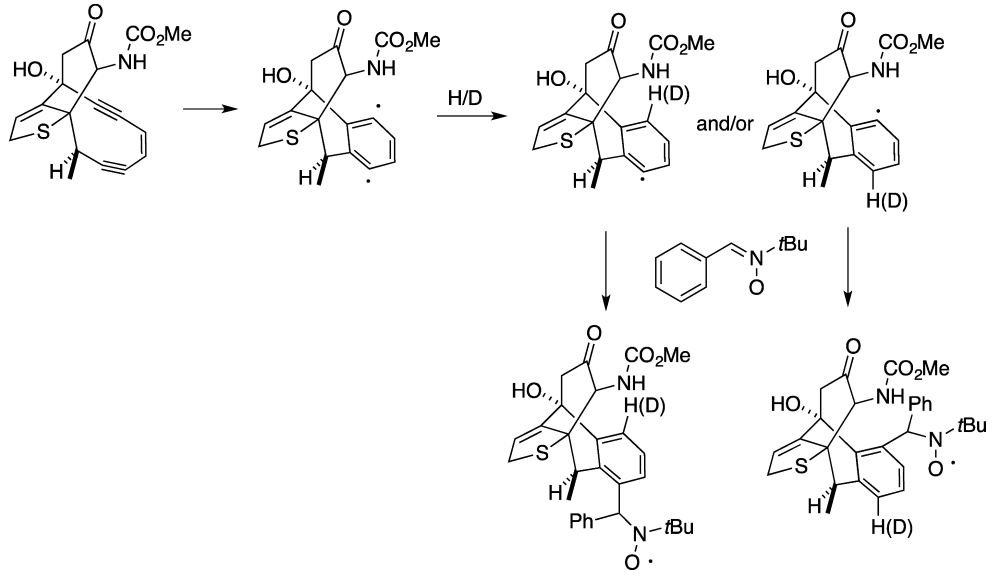

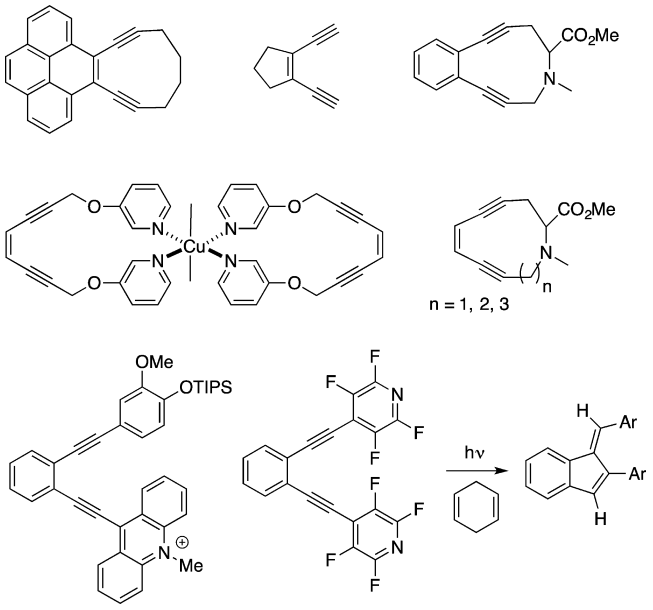

Figure 39. Examples of Masamune–Bergman cyclizations.

indicate the absence of four-coordinate B centers and three-membered rings. The electronic absorption was observed in the visible region at λ_{max} = 446 nm (ε = 2200), which suggests an interaction between the two radical sites. A computational study of the parent B_2P_2 diradical at the UB3LYP/6-311++g(d,p) level of theory revealed that the singlet–triplet energy gap is 17.2 kcal mol^{-1} and the planar singlet state is the transition state for the cycloreversion reaction. Thus, the substituents of ^{t}Bu and ^{i}Pr on B and P atoms were indispensable in kinetically stabilizing the type-1 singlet diradical.

The radical-type reactivity of the B_2P_2 diradical was confirmed by reaction with $CDCl_3$, Se, PhSeSePh, and Me_3Sn–H (Scheme 7).[90] In the reaction with $CDCl_3$ at room temperature, the 2,4-dichloro adduct **5** was isolated with an approximate cis/trans ratio of 3/1. The [1.1.1]bicyclic structure (asterane) of adduct **6** was obtained in 70% isolated yield in the reaction with elemental selenium (Se) at room temperature in toluene. Interestingly, bridged structure **6** was also formed in the reaction with PhSeSePh, although the mechanism is not clear for the formation of the asterane derivative. A spontaneous and clean reaction was observed with trimethyltin hydride to selectively give the trans-configured adduct **7**. The trans geometry of **7** was unambiguously deduced by X-ray analysis. A stepwise rather than concerted mechanism was proposed for the formation of **7**. When a bulky radical trapping agent such as $BrCCl_3$ was used for the reaction, compound **8** was obtained together with the trans-1,3-dibromo-substituted compound in 56% yield. The formation of **8** most probably results from a stepwise reaction: (1) the singlet

Scheme 30. Phototriggered Cycloaromatization in the Photolysis of 63

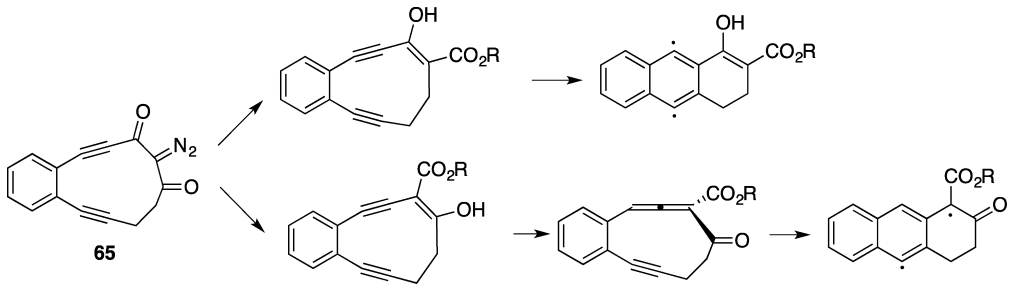

dx.doi.org/10.1021/cr400056a | *Chem. Rev.* 2013, 113, 7011–7088

Scheme 31. Facile Cyclization Reaction for the Methoxy-Substituted Substrate 66

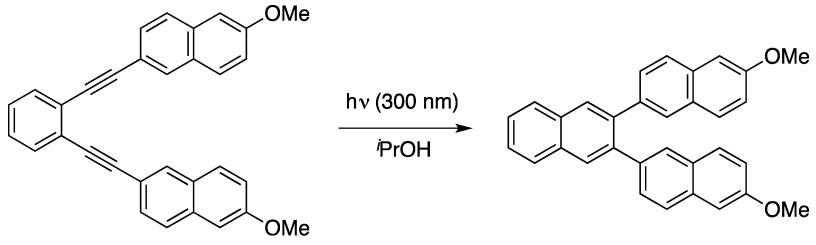

66

Scheme 32. Polyaromatization Using the Masamune–Bergman Cyclization of 67

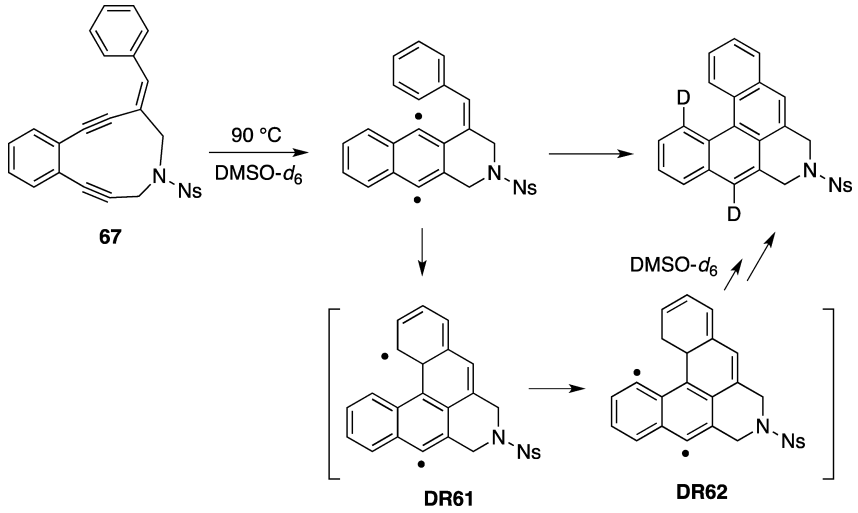

67 DR61 DR62

Scheme 33. Memory of Chirality in the Cascade Rearrangements of Enediynes

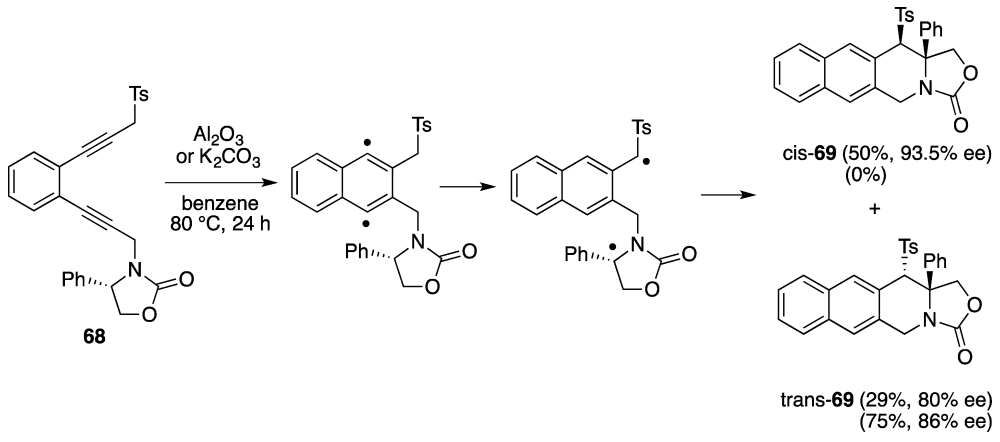

68

Scheme 34. Synthesis of 2,3-Dihydrobenzo[*f*]isoindoles Using Masamune–Bergman Cyclization

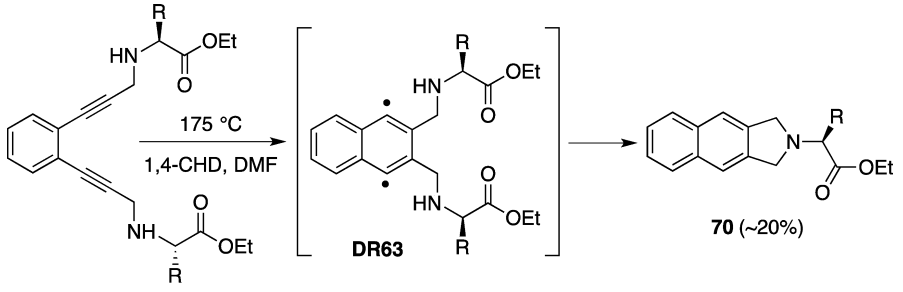

R = CH_3, $CH(CH_3)_2$, $CH_2CH(CH_3)_2$

dx.doi.org/10.1021/cr400056a | *Chem. Rev.* 2013, 113, 7011–7088

Scheme 35. Myers–Saito (MS) Cyclization versus Garratt–Braverman (GB) Cyclization in Diallene

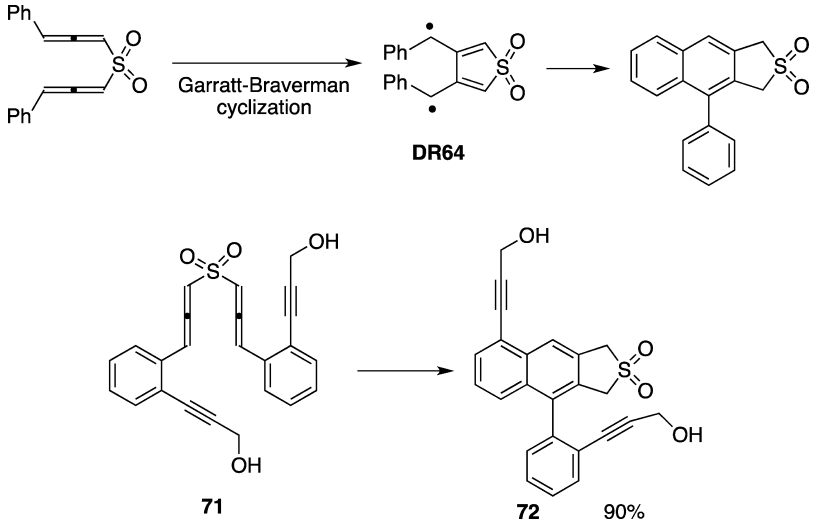

Scheme 36. Photoinduced Masamune–Bergman Cyclization

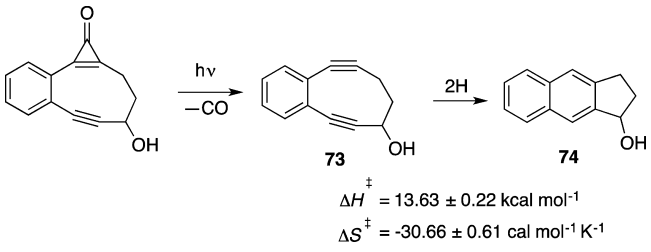

Scheme 38. Ruthenium-Induced Masamune–Bergman Cyclization of 76

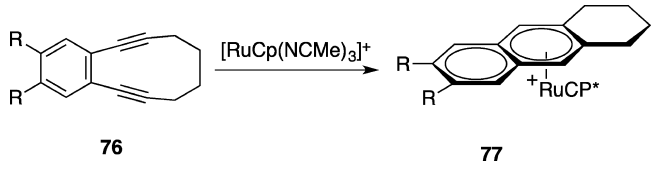

diradical abstracts a bromine atom from the bromotrichloromethane, and (2) the disproportionation of the resulting radical pair gives **8** and chloroform. HCl and HOTf were also found to add readily to B_2P_2 singlet diradical **DR21**.[91] The reaction proceeds in a concerted or stepwise manner, but always with complete stereo- and regioselectivity.

The importance of steric hindrance in stabilizing the type-1 diradical was confirmed by the B–B σ-bonding formation reaction in the sterically less-hindered ethyl-group-substituted case, B–B = 183 pm (Figure 25). ^{11}B and ^{31}P NMR signals were observed for the ring-closed compounds at ca. −12 and −55 ppm, respectively, which are quite different from the chemical shifts observed for the singlet diradical **DR21**.[92] The energy barrier ($\Delta G^{\ddagger}$) of the cycloreversion process was determined to be 8.5 kcal mol^{-1}.

When the substituents on P are ^{i}Pr groups and those on B are Ph groups, the two bond-stretching isomers, i.e. singlet diradical **DR22** and the bicyclic form **CP22**, were observed by variable-temperature NMR spectroscopy (Figure 26).[93] From the van't Hoff plot of the temperature-dependent change of the two isomer ratios, the enthalpy and entropy differences between the two isomers were determined to ΔH = 1.4 ± 0.2 kcal mol^{-1} (the single diradicals form is enthalpically more stable than the bicyclic form) and ΔS = 7.2 ± 1.6 cal mol^{-1} K. Thus, it was concluded that the order of stability of the bond-stretch isomers **DR22** and **CP22** is largely entropy-driven.

The catenation of the singlet diradicals, through the *para*-phenylene and *meta*-phenylene, was found to lead to antiferromagnetic low-spin polymers in which the half-filled electron bands conferred the capability of metallic conduction without doping.[94,95] The catenation of the singlet diradical through the *para*-phenylene unit successfully produced the bis(singlet diradical) **DR23** (Figure 27). From the X-ray analysis data, a small quinoidal character in the singlet state of the tetraradical was confirmed. The weak communication between the two diradical units was proposed to be due to the weakness of the B–C double bonds. The absorption maxima of **DR23** was observed at 630 nm with ε = 1374, which was a much longer wavelength than observed for the monosinglet

Scheme 37. Fragmentation and Rearrangement from the Diradical Intermediate in Masamune–Bergman Cyclization

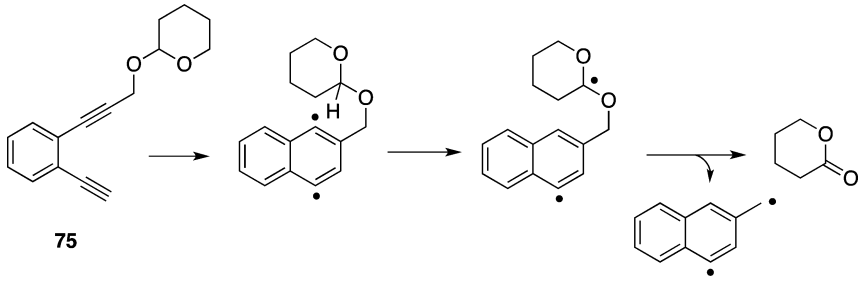

dx.doi.org/10.1021/cr400056a | Chem. Rev. 2013, 113, 7011–7088

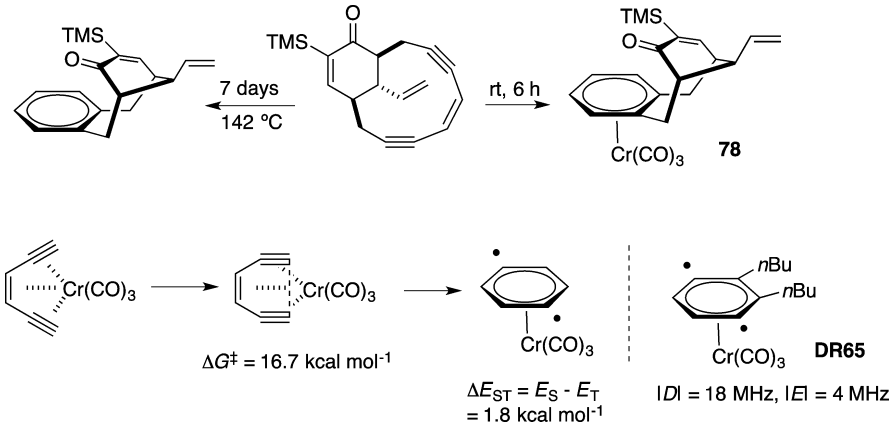

Figure 40. Masamune–Bergman cyclization triggered by chromium tricarbonyl complex.

Scheme 39. Thermal Cyclization of Allene-Yne Derivatives

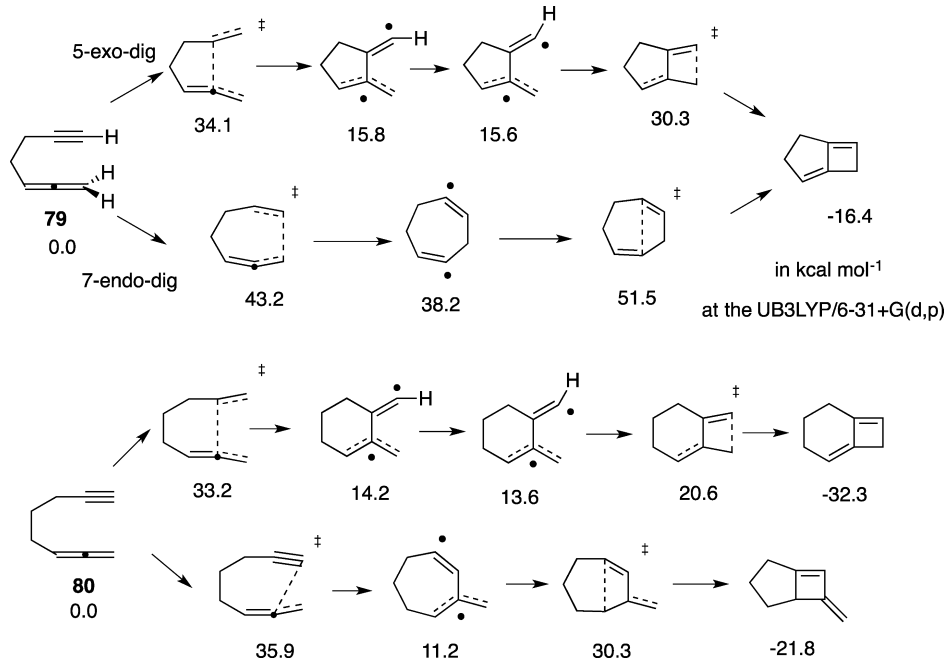

Scheme 40. Intramolecular Trapping Reaction of the Diradical Intermediate in the Thermal Cyclization Reaction of 81

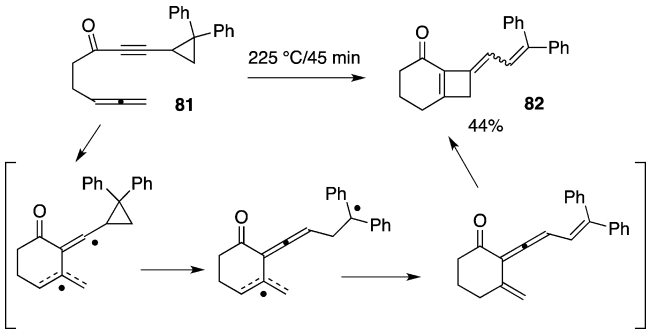

diradical **DR21**. In contrast to the open-shell singlet diradical structures with the *para*-phenylene unit, closed-shell structures, namely, two bicyclic[1.1.0] structures, were found for the *meta*-phenyl unit. The steric repulsion in the open-shell structure was responsible for the ring-closing structure. Computational studies by Bell et al. suggest that the stability of the *para*-tetraradical can be rationalized by its moderate extent of radical character.[96]

Seiertstad et al. reported that the diradical character of **DR24** could be engineered by the substituents R and R′ at the B and P atoms, respectively (Figure 28). For example, silyl substitution at the phosphorus atom decreased the energy gap between the two nonbonding molecular orbitals (ψ_S and ψ_A). Thus, the occupation numbers in ψ_S and ψ_A were found to be 1.61 and 0.39 at the GVB(2,2)/6-31G(d) level of theory, increasing the diradical character with decreasing singlet–triplet energy gap from 18.7 kcal mol^{-1} (R = R′ = H) to 5.8 kcal mol^{-1} (R = SiH_3, R′ = H).[97] Cheng and Hu,[98] Saettel and Wiest,[99] Schoeller et al.,[100] and Jung and Head-Gordon[101] also investigated the electronic nature of the type-1 singlet diradical **DR21** using quantum chemical calculations.

Al_2P_2 Diradical. In 2009, Henke et al. isolated Al_2P_2 type-1 singlet diradical **DR25** as a green crystal in the reaction of AlCl and LiP^tBu (Scheme 8).[102] The singlet–triplet energy gap was calculated to be 28.9 kJ mol^{-1}, with a preference for the singlet

dx.doi.org/10.1021/cr400056a | *Chem. Rev.* 2013, 113, 7011–7088

Scheme 41. Generation of *ortho*-Caboryne and *meta*-Carboryne in the Photolysis of Lithiolated Iodocarboranes

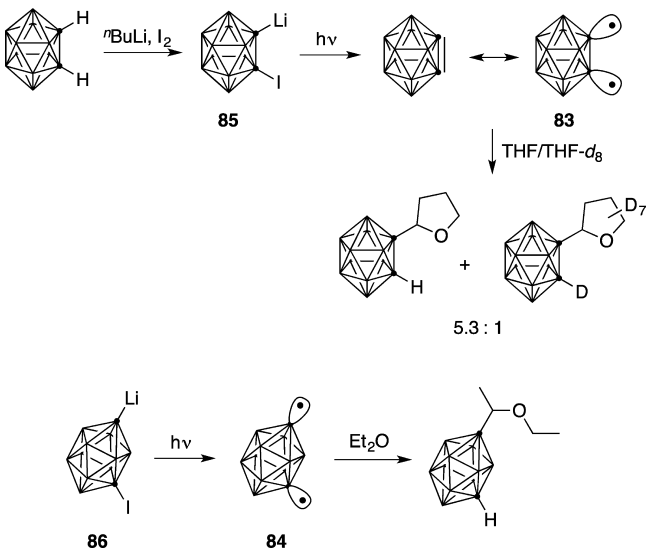

state. A long Al−Al bond distance of 350.8 pm was determined on the basis of X-ray crystallographic analysis.

Ge_2Ga_2 Diradical. Doddi et al. very recently reported the synthesis of an unusual molecule **DR26** with a Ge−Ge π-single bond in the reduction of $GeCl_2$ with Ga(DDP)/KC_8 (Scheme 9).[103] The Ge−Ge bond distance was determined to 287.14 pm, which is much longer than a typical Ge−Ge σ bond. The computational study of the model compound clearly indicated the existence of a π-single-bonding system.

2.2.2. Type-2 Diradicals in Heterocycles. The electronic structure of four-membered heterocycles X_2Y_2 with six π electrons, such as the S_2N_2 molecule, has been discussed in the literature (Figure 29).[104−106] In principle, the molecules exhibit diradical character, zwitterionic character, and 6π aromaticity. The singlet state was found to be the ground-state spin multiplicity for the S_2N_2 molecule. A relatively large LUMO occupation number of 0.12 e^- was calculated for S_2N_2, indicating that the molecule has a diradical character.

C_2P_2 Diradicals. In 1995, Niecke et al. found the formation of C_2P_2 diradical **DR27** in the reaction of phosphane **10** with butyllithium in a mole ratio of 2:1 (Scheme 10).[107] X-ray crystallographic analysis of the deep red crystal (λ_{max} = 478 nm) clarified the planar four-membered ring of the C_2P_2 unit, in which the substituents at the radical carbon and phosphorus

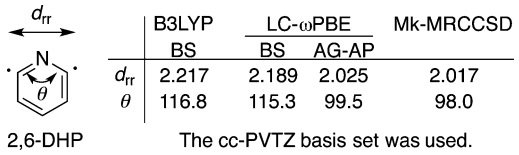

	B3LYP	LC-ωPBE		Mk-MRCCSD
	BS	BS	AG-AP	
d_{rr}	2.217	2.189	2.025	2.017
θ	116.8	115.3	99.5	98.0

The cc-PVTZ basis set was used.

Figure 42. Comparison of the 2,6-DHP optimized geometry obtained by the multireference CCSD method with that calculated from the analytical gradients (AGs) with approximate spin projection (AP) by density functional theory.

atoms both adopt a trans configuration. The ring carbons were detected at the chemical shift of 98.8 ppm in the ^{13}C NMR spectrum, which is strongly deshielded. Quantum chemical calculations for the parent diradical $C_2(H_2)P_2(H_2)$ **DR28** were performed to understand the electronic structure of the C_2P_2 diradical. A multiconfigurational self-consistent-field (MCSCF) optimization of the geometry indicated a singlet ground state with C_i symmetry. The singlet−triplet energy spacing was computed to be 7.4 kcal mol^{-1}. Configuration interaction (CI) calculations clarified that the occupation number in ψ_3 (HOMO) was 1.6 electrons. Thus, the diradical was categorized as type-2. As expected from the electronic configuration, the thermolysis (Δ) of **DR27** did not produce any ring-closing product, but rather produced the ring-opened product **11** through the formation of carbene **12**.

The photochemical reaction ($h\nu$) of the silyl-substituted diradical **DR29**, which was prepared by the reaction of **DR27** with $Hg(SiMe_3)_2$, produced the ring-closing product **13**.[108] The structure was confirmed by X-ray crystallographic analysis. During the ring-closing reaction in solution, a significant upfield shift was detected at the ring carbon atoms from 111.0 and 104.1 to 28.3 ppm in the ^{13}C NMR spectrum. The thermal ring-opening reaction of **13** was observed to afford the 1,4-diphosphabutadiene. In contrast to the formation of the bicyclo[1.1.0] system of the monosilyl-substituted diradical **DR29**, the elimination of the Mes* group at the phosphorus atom was observed in the photolysis of the bis(silyl)-substituted diradical **DR30**. A severe steric repulsion between the two silyl groups was suggested to prevent the ring-closing reaction.

1,3-Diphosphacyclobutane-2,4-diyl-2-ylidenide **DR31** was prepared in the deprotonation reaction with lithium diisopropyl amide (LDA). The compound spontaneously reacted with $AlMe_3$ to give the diradical **DR32**.[109] The ring carbon atoms appeared at 118.3 and 140.3 ppm in the ^{13}C NMR spectrum.

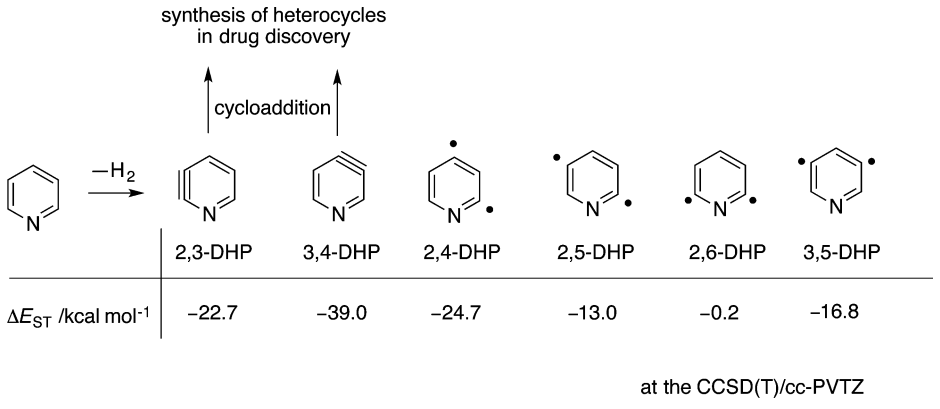

Figure 41. Singlet−triplet energy spacing of didehydropyridines (DHPs).

dx.doi.org/10.1021/cr400056a | *Chem. Rev.* 2013, 113, 7011−7088

Because C_2P_2 is an electron-rich diradical, protonation by TfOH was possible and gave the protonated compound **15**.[110] The planar structure of the cation was confirmed by X-ray crystallographic analysis. The ^{13}C NMR signals of the ring carbon atoms of **15** appeared at 75.8 and 123.3 ppm. The position of protonation suggests the contribution of zwitterion **ZI** in the diradical formula.[111]

Amino-substituted diradical **DR33** was found to be very reactive, giving the rearranged compound **16** (Scheme 11). The diradical was detected only by magic-angle-spinning (MAS) NMR spectroscopic analysis. Computations at the MCSCF-(10,10)/6-31G(d) level revealed that the isomerization from **DR33** to **16** is a two-step process through carbene intermediate **17**. The rate-determining step was found to be the ring-opening reaction of diradical **DR33**, with an energy barrier of 105.5 kJ mol^{-1}.[112]

Very recently, Schoeller and Niecke reported the closed-shell character of diradicals **DR34** and the effects of substituents on the singlet−triplet energy gap for C_2P_2 diradicals. The amino-substituted diradicals on the phosphorus atoms were predicted to be the triplet ground state with an energy gap of ∼2−4 kcal mol^{-1}.[113]

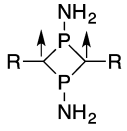

DR34

R = Ph, Cl, NH_2

Yoshifuji and co-workers prepared the type-2 singlet diradical **DR35** from the phosphaalkyne and investigated its chemistry (Scheme 12).[114−118] To do so, they reacted 0.5 equiv of *tert*-butyl lithium with the kinetically stabilized phosphaalkyne **18** to generate the corresponding anion **19**. The resulting anion was quenched with alkyl iodide or alkyl bromide (R−X) to afford a variety of types of singlet diradicals **DR35**. The symmetric C_2P_2 diradical **DR35a** (R = R′ = ^{t}Bu) was formed in the dimer interaction of the anion **19**. The diradical was reported to be air-stable and not moisture-sensitive. The planar structure of the C_2P_2 ring was confirmed by X-ray crystallographic analysis. The radical carbon was observed at δ_C = 111.3 ppm for compound **DR35b** (R = ^{t}Bu, R′ = Me). The absorption maximum was observed at 612 nm, indicating a small HOMO−LUMO energy gap of ∼2 eV. A reversible oxidation peak was observed at +0.35 V (versus Ag/Ag^+), and an irreversible oxidation peak was observed at +1.56 V. In contrast to the thermal and photochemical reactivity of Schoeller and Niecke's diradical, the thermolysis of **DR35a** produced the starting compound phosphaalkyne, and **DR35b** was unreacted under irradiation conditions.

The one-electron oxidation of **DR35b** using a blue solution of tris(4-bromophenyl)ammoniumyl hexachloroantimonate produced an ESR-active compound with absorptions at 510, 625, 732, and 846 nm. The green-colored compound was assigned to the radical cation **20**. Two or three stable C_2P_2 diradical units were concatenated to construct multiradical derivatives **21** and **22**.[119] The UV−vis and cyclic voltammetry (CV) measurements of multiradicals **21** and **22** indicate a nonconjugative covalent interaction between the diradical units.

Compound **DR35b** (R = ^{t}Bu, R′ = Me) was allowed to react with lithium aluminum hydride (LAH) to give anion **23**, in which the hydride is attached to the less-hindered phosphorus atom.[120] However, with the substituent R′ = $CH_2C(O)OMe$, the elimination of substituent R′ was observed to give the anion **24**.[121−123] An S_N2-like mechanism was proposed for the formation of the anion, because R′−H compounds were isolated from the reduction reactions.

Ge_2XY Diradicals. Cui et al. reported the formation of Ge_2N_2 diradical **DR36** in the reaction of a Ge−Ge triple-bonded compound with excess trimethylsilyl azide (Scheme 13).[124] The compound **DR36**, with a dark violet color, was found to be extremely air- and moisture-sensitive and rapidly changed to a white powder once exposed to the atmosphere. The structure was confirmed by X-ray crystallographic analysis. The geometry at the nitrogen was found to be trigonal-planar (sum of interligand angles = 359.97°) and that of germanium was pyramidal (sum of interligand angles = 322.10°). The singlet−triplet energy gap was calculated to be 17.5 kcal mol^{-1} with the singlet ground state. The UV−vis spectrum showed a strong absorption maximum at λ_{max} = 521 nm, which corresponds to a HOMO−LUMO energy gap of 54.88 kcal mol^{-1}.

The formation of Ge_2NO diradical **DR37** was also found in the reaction of the Ge−Ge triple bond with a nitrosobenzene derivative.[125] A purple black crystal with λ_{max} = 554 nm was obtained as a pure form. X-ray crystallographic analysis indicated that the coordination geometries at the Ge and N atoms were pyramidal and trigonal-planar, respectively. A HOMO−LUMO energy gap of 55.3 kcal mol^{-1} was computed at the UB3LYP/6-31G(d) level of theory.

Sn_2N_2 Diradical. Cox et al. isolated colorless and ESR-silent crystals of Sn_2N_2 compound **DR38** from the reaction of dimeric $Sn(Cl)N(SiMe_3)_2$ with AgOCN (Scheme 14).[126] ^{119}Sn NMR spectroscopy showed that compound **DR38** was the major tin-containing product in the reaction. They attributed the driving force of the reaction to the oxophilicity of silicon atoms. The singlet state was found to be favored by 57 kJ mol^{-1} over the triplet state. A derivative of 1,3-diaza-2,4-diistannacyclobutane-diyl **DR39** was also isolated by Dickie et al.[127]

P_2N_2 Diradical. P_2N_2 diradical **DR40** was prepared in the reduction of 1,3-diphospha-2,4-diazane **25** using $[\{Cp_2TiCl\}_2]$ as the reducing agent (Scheme 15).[128] The diradical **DR40** was crystallized as orange crystals from toluene in the monoclinic space group *C*2/*c*. In this compound the phenyl rings on the amino nitrogen are twisted with respect to each other. Computations of the electronic structure support the diradical character of compound **DR40** with a type-2 electronic configuration. Natural atomic orbital analysis suggests six delocalized π electrons in the heterocyclic system. The singlet was calculated to be lower in energy than the triplet state at the UDFT level of theory. CASSCF calculations clarified that the antisymmetric NBMO is occupied by 1.7 electrons.

As_2N_2 Diradical. Demeshko et al. also succeeded in synthesizing As_2N_2 diradical **DR41** in 92% yield in the reaction of 3 equiv of activated Mg with 1,3-dichloro-2,4-diterphenyl-1,3-diarsa-2,4-diazane (Scheme 16).[129] The As_2N_2 diradical exists as extremely air- and water-sensitive but highly thermally stable purple crystals (dec 245 °C). X-ray diffraction analysis revealed the perfect planar four-membered ring structure of **DR41**. The bond length of As−N was found to be ∼186 pm, which is slightly shorter than expected for normal As−N single bonds (192 pm). The As−As distance was found to be 288.39 pm, which indicates that there was only a very small transannular As···As interaction. The diradical **DR41** was reported to be ESR-silent. The existence of a singlet ground state was confirmed by temperature-dependent magnetic

dx.doi.org/10.1021/cr400056a | *Chem. Rev.* 2013, 113, 7011−7088

measurements, diplaying exclusively diamagnetic behavior between 295 and 2 K. DFT calculations of the electronic structure revealed that **DR41** is a singlet ground state with six delocalized π electrons. The NICS(0) value (where NICS is nucleus-independent chemical shift) was computed to be −6 ppm, which supports the aromaticity of the singlet diradical **DR41**. The singlet state was found to be 19.3 kcal mol^{-1} lower in energy than the triplet state at the UB3LYP/6-311+G(d,p)//6-31G(d,p) level. The radical character was examined in reactions with CCl_4, elemental sulfur and selenium, and CS_2 (Scheme 16).

Si_2N_2 Diradical. Takeuchi et al. succeeded in isolating the singlet ground state of Si_2N_2 diradical **DR42** from the reaction of disilyne with 1 equiv of azobenzene in tetrahydrofuran (THF) at room temperature (Scheme 17).[130] The diradical has a dark purple color with λ_{max} = 529 nm. According to computations, the electronic absorption corresponds to the HOMO (ψ_A) to LUMO (ψ_S) excitation. The singlet−triplet energy spacing was calculated to be 12.8 kcal mol^{-1}. Compound **DR42** was reacted with MeOH at room temperature to give the cis-configured MeOH adduct **26**. In contrast, the trans-addition reaction was found in the reaction with CCl_4 to give **27**. A similar diradical reactivity was found by Nied et al.[131]

2.2.3. 1,3-Diradical Character in [1.1.1]Propellane Structures.[132] In 1989, Sita and co-workers first reported the formation of pentastanna[1.1.1]propellane **28** by heating $Sn_3R^1{}_6$ (Figure 30).[133] The purple-colored sample was isolated and analyzed by X-ray crystallography to reveal a bridgehead Sn−Sn distance of 337 pm, which is ca. 20% longer than a normal Sn−Sn single bond. Derivatives **29** and **30** were synthesized by Drost et al.[134] and Richards et al.,[135] respectively. The bridgehead Sn−Sn and Ge−Ge bond lengths were determined to be 336 and 342 pm, respectively.

Nied et al. improved the synthetic procedure of heavy-atom [1.1.1]propellane derivatives **31** (Scheme 18).[136] The singlet diradical character for propellanes **31** was confirmed by the computation of the occupation number in the LUMOs at the (6,4)CASSCF level of theory. A LUMO occupation number of ~0.1 electron was found for all of the derivatives. The reactivity toward radical-trapping agents supports the diradical character of the heavy-atom propellanes. Very recently, Ito et al. reported the synthesis of a stable spirobis(pentagerma[1.1.1]-propellane).[137]

Stable derivative **32** of Si_6H_6 was synthesized by Abersfelder et al.[138] The longest wavelength of **32** was observed at 473 nm. The corresponding Si_5Mes_6 was found at 396 nm by Nied et al.[136] The red shift was attributed to the degeneracy of the HOMO and LUMO.

Sn−Sn Singlet Diradical. In 2011, Schrenk et al. isolated Sn−Sn singlet diradical **DR43** (Figure 31). The bond distance between the Sn atoms was found to be 382 pm using X-ray crystallographic analysis.[139] The Sn−Sn distance was considered to be too long for a single bond, which should be around 280 pm. DFT computations for **DR43** showed a singlet−triplet energy spacing of 48.9 kJ mol^{-1} with a singlet ground state. CASSCF calculations support the singlet diradical character of the compound. The occupation number in the HOMO was found to be 1.7 for the parent structure **DR44**, in which all of the substituents on Si and Sn are hydrogen atoms. According to the calculations for the parent compound **DR44**, the structure with an angle (θ) of 130° was found to be nearly the transition state for the two bond-stretching isomers "long" **33** and "short" **34**.[140]

Konu et al. reported that a diradical character of a dinuclear copper(I) complex **35** in a strained system (Figure 32).[141]

2.3. 1,4-Diradicals

Cyclohexane-1,4-diyls **DR45** have been proposed as hypothetical diradical intermediates for the Cope rearrangement of 1,5-hexadienes **36** (Scheme 19). Namai et al. confirmed the existence of the singlet diradical **DR45** using the thermoluminescence in the charge recombination of radical ion pairs of **37** and **36**, which were generated by γ irradiation at 77 K in a methylcyclohexane (MCH) glassy matrix.[142]

Compound **38**, in which the two lophyl radical moieties are attached, was designed for a mechanistic probe for the Cope rearrangement. The promising intermediate tetraradical **DR46** was assumed to be trapped intramolecularly using the lophyl radicals to produce the corresponding quinoidal structure **39** (Scheme 20).[143]

A mechanochemical ring-opening reaction of perfluorocyclobutane polymer **40** was also found to give the diradical intermediate **DR47** that was trapped by TEMPO derivative **41** (Scheme 21).[144] The diradical finally produced a pair of difluoroethylene derivatives. The molecular weight degradation of the sonochemical reaction of **40** was largely dependent on the molecular weight of the polymer. Polymers over 20 kDa in molecular weight were found to efficiently produce the degradation product.

Compound **DR48**, with singlet 1,4-diradical character, was isolated in the reaction of **42** with 2 equiv of diphenylacethylene, and the structure was characterized by X-ray crystallographic analysis (Scheme 22).[145] The singlet diradical **DR48** was reported to be a highly air-sensitive and moisture-sensitive dark red solid.

Ge−Ge singlet diradical character in the bicyclo[2.2.0]-hexane structure **DR49** was found by Wang et al. and Power (Scheme 23).[146,147] The singlet diradical was formed in the digermyne ArGeGeAr **43** with 2 equiv of nitrosobenzene. X-ray crystallographic analysis gave a bond length of 254 pm for Ge−Ge, and an Ar−Ge−Ge angle of 177°. The structure was assigned to the long-bond isomer for the bicyclo[2.2.0]-structure. Natural bond orbital (NBO) analysis for the model compound clarified the diradical character of **DR49**. Only 0.33 electron was calculated to be in the σ^* orbital of the Ge−Ge bond. The singlet diradical character of heavy alkynes and alkenes such as Si═Si and Ge═Ge was proposed experimentally and computationally.[148]

In 2010, Lovitt et al. found that a strong through-bond interaction determines the singlet−triplet energy spacing of diradicals **DR50**−**DR52**, in which the two allyl radicals are located perpendicularly (Figure 33).[149] When the two allyl radials are connected in the four-membered ring system as in **DR50**, a large singlet−triplet energy spacing of ~25 kcal mol^{-1} with singlet preference was found, whereas much smaller singlet−triplet energy gaps were found for the five-membered (**DR51**) and six-membered (**DR52**) systems. The two sets of through-bond (TB) interactions, which make the energy spacing between the nonbonding orbitals large, explained the larger singlet−triplet energy gap for the diradical **DR50** with the four-membered ring system than for the other two cases.

2.4. σ,π Diradicals

σ,π Diradicals are an interesting family of heterosymmetric diradicals, in which one of the unpaired electrons is located at

dx.doi.org/10.1021/cr400056a | *Chem. Rev.* 2013, 113, 7011−7088

the allylic position (π radical) and another unpaired electron is a σ radical at the vinyl carbons. α,3-Dehydrotoluene **DR53**, the intermediate of the Myers−Saito reaction,[150,151] has attracted much attention because of the DNA cleaving activity of its derivatives (Scheme 24). The Schmittel diradical **DR54**[152] is important for the cyclization reaction of substrates in which a bulky substituent is located at the C7 position (vide infra). In 2010, Sakai and Nishitani calculated the mode of cyclization reactions at the multireference MRMP2/6-311+G(d,p)//CASCF(10,10)/6-31G(d) level of theory. Actually, the Myers−Saito reaction ($\Delta E^{\ddagger}$ = 16.6 kcal mol^{-1}) was found to be energetically favored over the Schmittel cyclization reaction ($\Delta E^{\ddagger}$ = 23.3 kcal mol^{-1}) by ca. 7 kcal mol^{-1}.[153]

***α,n*-Dehydrotoluenes (DHTs).** Wenthold et al. determined the absolute heats of formation for the three α,*n*-DHT molecules from measurements of the collision-induced dissociation (CID) threshold energies for the dissociations of chloride, bromide, and iodide ions from the corresponding *o*-, *m*-, and *p*-halobenzyl anions in the gas phase.[154] The 298 K heats of formation of all three derivatives were determined to be 103 ± 3 kcal mol^{-1}. According to multiconfigurational self-consistent field (MCSCF) calculations, α,2 and α,4 derivatives are triplet-ground-state molecules with singlet−triplet energy gaps of 7.4 and 8.1 kcal mol^{-1}, respectively (Figure 34). The triplet ground states of the two species were experimentally confirmed by Neuhaus et al. by the low-temperature matrix isolation technique.[155] They did not observe any ESR signals for the α,3 derivative at 5 K in an Ar matrix. This observation is also consistent with the singlet ground state predicted by MCSCF calculations, in which the energy gap was estimated to be 3 kcal mol^{-1}. The ground-state spin multiplicity can be well understood by the spin polarization effect as depicted in the structures.

The values of the ESR zero-field splitting (zfs) parameter $|D/hc|$ for the α,2 and α,4 isomers were determined to be 0.139 and 0.212 cm^{-1}, respectively, with corresponding relatively large $|E/hc|$ values of 0.0081 and 0.004 cm^{-1}, respectively. These values are much larger than those for *meta*-quinodimethane (*m*-QDM),[156−158] for which the $|D/hc|$ and $|E/hc|$ values were determined to be 0.011 and 0.0010 cm^{-1}, respectively (vide infra). The larger zfs values of the α,*n*-DHTs compared to *m*-QDM are explained by the resonance structures of carbene.

Despite the simple structures of α,*n*-DHTs, their generation was rather difficult. Protti et al. reported that all of the isomers could be generated by the photochemical elimination of the electrofugal group (SiR_3) and the nucleofugal group (Cl) in a protic solvent such as methanol (Scheme 25).[159]

Schmittel Diradicals. In 1995, Cinar et al. found that the C2−C6 cyclization reaction from ene-allenes with a bulky substituent at the alkyne terminus affords the σ,π diradicals **DR55** (Scheme 26). Because of this finding, the so-called Schmittel cyclization has attracted much attention in the field of mechanistic study, as well as for synthetic purposes. The benzofulvene diradicals **DR55** generated in the thermal cyclization of ene-allenes **44** are known to undergo intramolecular reactions to give the products **45**−**47** (Scheme 26).[160] The effect of intermediacy and nonstatistical dynamics on the product selectivity have been discussed on the basis of experimental observations as well as theoretical studies.[161] The evidence for the generation of diradicals **DR55** was supported by the formation of **48** in radical-trapping experiments in the presence of 1,4-cyclohexadiene.

The diradical intermediate in the photoinduced Schmittel reaction was confirmed by the direct observation of the intermediary diradical using laser-flash-photolysis (LFP) experiments and the ultrafast radical clock reaction of the ring-opening of the diphenylcyclopropane moiety. Bücher et al. reported the detection of the excited state of enyne-allene **49** (λ_{max} = 458 nm, τ = 458 ns) and the intermediary diradical **50** (λ_{max} = 332 nm, τ = 1000 ns) in the photochemical cyclization reaction of **49** (Scheme 27). The diradical intermediate was intramolecularly trapped to give the final product **51**.[162]

***σ,π*-Diradical Character in Vinylmethylenes, Propargylenes, and Penta-1,2,4-triene-1,3-diyls.** Methylene **52** with R = H is a triplet-ground-state one-center diradical with ΔE_{ST} = 9.05 kcal mol^{-1} (Figure 35).[163] When the hydrogen atom is substituted by a vinyl or acetylenyl group (R = C_2H_3 or C_2H), the corresponding resonance structures are 1,3-diradicals **DR56**−**DR58**. For propynylidene **DR57**, studies using isotope labeling, IR spectroscopy, and ESR spectroscopy and ab initio calculations are all consistent with a C_2 structure for triplet propynylidene. As judged by the small $|D/hc|$ value, the vinyl carbene is best described in the structure of 1,3-diradical **DR56**.[164−167] Very recently, a carbene composed of vinyl and ethynyl units was also reported to be best described in the structure of 1,3-diyl **DR58**. Multireference ab initio calculations reproduced well the values of zfs parameters *D* and *E*. The calculations revealed that spin polarization significantly affects the magnitude of the *D* values.[168]

2.5. Didehydrobenzenes (Benzynes)

Since the finding of *o*-benzyne, the chemistry of benzynes including *m*-benzyne and *p*-benzyne has become quite rich in the fields of both mechanistic and synthetic organic chemistry.[169−172] In 2010, quantum chemical calculations and experiments on benzyne chemistry were summarized in excellent review articles written by several experts, including Wentrup,[173] Wenthold,[174] Winker and Sander,[175] and Sato and Niino.[176] The basic topics of benzyne chemistry, including ground-state spin multiplicity, thermochemistry, structural feature, and typical reactions are also described in this review article, as well as benzyne chemistry reported since 2010.

The ground states of the benzynes are all singlets, with ΔE_{ST} = −37.5 ± 0.3 kcal mol^{-1} for *o*-benzyne, −21.0 ± 0.3 kcal mol^{-1} for *m*-benzyne, and −3.8 ± 0.4 (or −2.1 ± 0.4) kcal mol^{-1} for *p*-benzyne, which were all determined by NIPES (Figure 36).[177] For *p*-benzyne, two values were assumed to be possible, as the origin of the triplet state was not observed because of overlapping with the singlet state. By modeling the shape of the spectroscopic band, Wenthold et al. assigned the singlet−triplet energy spacing as −3.8 ± 0.4 kcal mol^{-1}. However, it was noted that a value of −2.1 ± 0.4 kcal mol^{-1} was also possible. The experimental results were reproduced well by multireference calculations such as CASPT2 and CASRS3. According to the quantum chemical calculations, the distances (*d*) between the two carbon atoms in the singlet states of *o*-benzyne and *m*-benzyne are shorter than those of the triplet states, whereas the carbon−carbon distance of singlet *p*-benzyne was calculated to be longer than that of the triplet state at the CCSD(T)/cc-PVTZ level of theory.

The singlet ground states of all of the benzyne derivatives can be explained by the through-space (TS) and through-bond (TB) interactions between the two radical orbitals (Figure 37). The magnitudes of the TS interactions should be in the order *o*-benzyne > *m*-benzyne, and *p*-benzyne, because the distance

dx.doi.org/10.1021/cr400056a | Chem. Rev. 2013, 113, 7011−7088

between the two interacting radical orbitals increases in the same order of magnitude. Thus, the singlet preference of *o*-benzyne is greatest. The two electrons selectively occupy the bonding orbital for *o*-benzyne and *m*-benzyne; thus, the bond lengths between the radical sites in the singlet states were found to be shorter than those in the triplet states. In contrast to the most stable electronic configurations of *o*- and *m*-benzyne, the two electrons selectively occupy the antibonding molecular orbital in the singlet state of *p*-benzyne. The longer C−C bond of the triplet state compared to the singlet state can be explained by the opposite electronic configuration of the singlet state of *p*-benzyne.

Recently, spin-flip (SF) time-dependent density functional theory was applied to calculate the singlet−triplet energy spacing of benzynes. Singlet−triplet energy gaps of −41.7, −22.3, and −3.50 kcal mol^{-1} were calculated for *o*-benzyne, *m*-benzyne, and *p*-benzyne, respectively.[178] The values were found to be consistent with the experimental results, as well as values calculated by high-level ab initio methods.

o-Benzyne can be generated from the treatment of halobenzene derivatives **53** with base. The photolyses of peroxide **54**, diketone **55**, and anhydride **56** are also known for the formation of *o*-benzyne derivatives. *m*-Benzyne can be generated by the pyrolysis of peroxide **57**, dinitro-substituted compound **58**, and diiodide **59** and detected under low-temperature matrix conditions. *p*-Benzyne can be generated by the conventional Masamune−Bergman cyclization and elimination reactions.

***para*-Benzynes.** *p*-Benzynes are the most well-known isomers among benzyne derivatives, because these singlet-ground-state diradicals are intermediates of the Masamune−Bergman[179,180] (C1−C6) cyclization of enediynes (Scheme 28). Kinetic studies by Roth and co-workers on **DR59** and 1,2-diethynylbenzene **DR60** revealed a slightly lower activation enthalpy ($\Delta H^{\ddagger}$) with a significantly increased reaction enthalpy (ΔH_{rxn}) for the cycloaromatization reaction, which resulted in a reduced barrier ($\Delta H_{retro}^{\ddagger}$) of the retro-ring-opening reaction of **DR60**.[181] Perrin and Reyes-Rodriguez recently reported nucleophilic addition reactions toward π-benzyne derivatives and summarized the electrophilic reactivity.[182]

At the mPW1PW91/cc-pVTZ//mPW1PW91/6-31G(d,p) level of theory, Spence et al. computationally found that extending benzannelation from 1,2-diethynylbenzene in a linear fashion with respect to the enediyne core increases the C1−C6 cyclization endothermicity (ΔH_{rxn}) from 0.9 kcal mol^{-1} (for **60**) to 12.9 kcal mol^{-1} (for **62**), whereas extending benzannelation in an angular orientation from the enediyne core reduces the cyclization endothermicity (ΔH_{rxn}) from 12.3 kcal mol^{-1} (for **62**) to 5.4 kcal mol^{-1} (for **64**) (Figure 38).[183] The activation energy ($\Delta H^{\ddagger}$) for the cyclization reaction was not largely affected by the number of aromatic rings or the substitution pattern. The energetic trends can be explained by Clar's rule, whereby arenediynes that produce new aromatic sextets lead to more favorable cyclization endothermicity because of increased gains in aromatic stabilization energy.

The huge amount of interest in the transformation reaction was driven by the discovery of the enediyne family of natural antitumor agents, such as esperamicine and calicheamicin.[184,185] The intermediacy of the diradical species in the cycloaromatization reaction was recently confirmed using the phenyl *tert*-butyl nitrone (PBN) as a spin-trapping agent (Scheme 29). The highly reactive species abstracts a hydrogen atom from double-stranded DNA. The hydrogen-abstraction process leads to DNA cleavage and causes cells to undergo apoptosis.[186] Thus, enediynes are used as anticancer agents.

Bergman cyclization of the parent enediyne occurs only at elevated temperatures. Triggers are needed to enhance the rate constant to efficiently produce *p*-benzyne diradical. Molecular design and reaction conditions that accelerate the Masamune−Bergman cyclization reaction have been developed in the past decade (Figure 39).[187] The most important molecular design is the fixation of the enediyne moiety in a cyclic system. The molecular strain caused by the macrocyclic ring and the entropy factor are assumed to decrease the energy barrier for the ring-closing reaction. Nicolaou et al. noted that the reaction temperature varies with the distance between the enediyne alkyne termini.[188] A distance of less than 3.25 Å is required to obtain a reasonable rate constant at room temperature.

Bergman cyclization triggered by photolysis is also used to generate *p*-benzyne diradicals. The advantage of photochemical generation is illustrated by the emergence of photodynamic therapy for cancer. Recently, Popik and co-workers developed two methods for the phototriggered cycloaromatization in which 10-membered-ring enediynes and ene-allenes were generated by the in situ photolysis of α-diazo-β-diketone **65** (Scheme 30).[189−191] Breiner et al. found the C1−C5 cyclization mode by introducing a highly electron-deficient substituent at the terminal carbon of the enediyne.[192] They also found intramolecular hydrogen abstraction to produce more stable radicals. Korovina et al. identified the effect of the methoxy group at the C6 position of the naphthyl group on the photochemical Bergman cyclization reaction of **66** (Scheme 31).[193]

In 2011, Roy et al. reported the preparation of polycyclic aromatics using the Masamune−Bergman cyclization of **67** (Scheme 32).[194] A deuterium-labeling study suggested that the polycyclization products were formed through diradicals **DR61** and **DR62**.

Nechab et al. reported a memory of chirality in the cascade rearrangements of enediynes, the Bergman cyclization reaction.[195] For example, the rearrangement of (*S*)-**68** under benzene reflux conditions led to a mixture of cis and trans diastereomers **69** in 50% and 29% yields, respectively, in the presence of Al_2O_3 (Scheme 33). The enantiomeric excess (ee) of cis-**69** was found to be 93.5%, whereas the ee of trans-**69** was reported to be 80%. When the reaction was carried out in the presence of K_2CO_3, only trans isomer **69** was formed in 86% ee and 75% yield.

Masamune−Bergman cyclization was used for the synthesis of 2,3-dihydrobenzo[*f*]isoindoles (Scheme 34). The initial formation of 1,4-diradicals **DR63** and H-atom abstraction from 1,4-cyclohexadiene (1,4-CHD) was followed by S_N2 substitution leading to product **70**. The mechanism was supported by a computational study of the energetically favored formation of the diradical **DR63**.[196]

Basak et al. investigated a competitive reaction mode of the two types of cyclization, Myers−Saito (MS) versus Garratt−Braverman (GB) (Scheme 35).[197] According to their computational study at the B3LYP/6-31G(d) level of theory, both reactions are feasible. However, the diradical intermediate **DR64** from the GB cyclization reaction was calculated to be lower in energy than the diradical derived from the Myers−Saito reaction. Thus, GB cyclization was computed to be thermodynamically favored over the MS reaction. Indeed, the thermal cyclization reaction of **71** was found to selectively produce the GB cyclization product **72** in 90% yield.

Pandithavidana et al. designed a phototriggered Bergman cyclization reaction of a nine-membered ring cyclic enediyne (Scheme 36).[198] Decarbonylation from the cyclopropenone moiety produced the nine-membered enediyne **73** to give the Bergman cyclization product **74**. The activation parameters were determined to $\Delta H^{\ddagger}$ = 13.63 ± 0.22 kcal mol^{-1} and $\Delta S^{\ddagger}$ = −30.66 ± 0.61 cal mol^{-1} K^{-1}.

A variety of fragmentations and rearrangements were observed in the Bergman reaction of enediyne **75**, which contains an acetal ring mimicking the carbohydrate moiety of esperamicine and calchiamicine families (Scheme 37).[199]

O'Connor and co-workers were the first to find that the cycloaromatization of an enediyne **76** was triggered by ruthenium metal (Scheme 38).[200] The cyclization reaction occurred smoothly to give the ruthenium arene complex **77** at room temperature. Ylijoki et al. reported that a chromium tricarbonyl complex also triggered the Masamune−Bergman cyclization to give the chromium complex **78** stereoselectively (Figure 40).[201] Without the metal, they found that the cyclization reaction requires a temperature of 140 °C. The transition-state energy of the metal-mediated cyclization reaction was calculated to be 16.7 kcal mol^{-1} at the B3LYP/6-31G(d) level of theory. Interesting, the metal-coordinated *p*-benzyne diradical was calculated to be a triplet ground state with the singlet−triplet energy spacing of 1.8 kcal mol^{-1}. Indeed, a typical triplet ESR signal with $|D|$ = 18 MHz and $|E|$ = 4 MHz was observed during the chromium-mediated cyclization reaction in THF. The ESR signals were assigned to **DR65**. Although the molecule is highly symmetric, the *E* value was found to be very large. The hyperfine coupling with the two protons on the phenyl ring at the half-field area (Δm_s = 2) is strong evidence for the triplet structure. The triplet ground state can be explained by the electron-withdrawing character of the chromium metal on the phenyl ring. Clark and Davidson reported that the singlet−triplet energy spacing decreases when electron-withdrawing substituents are introduced.[202]

Siebert et al. report a combined computational and experimental study on the intervention of the diradical during the thermal [2 + 2] cyclization reaction of allene-yne derivative **79** (Scheme 39).[203] The 5-exo-dig mode of intramolecular cyclization was found to be energetically more favored than the 7-endo-dig mode of cyclization at the UB3LYP/6-31G+(d,p) level of theory. The exocyclization was also calculated to be the energetically favored pathway for the allene-yne **80**. The intervention of the diradical intermediates was experimentally confirmed by the thermal cyclization reaction of allene-yne **81** (Scheme 40), in which the diphenyl-substituted cyclopropane ring was introduced for the radical trapping reaction. The ring-opened product **82** was isolated in 44% yield.

Carborynes. In 2011, Wang et al. reported the generation of *ortho*-caboryne **83** and *meta*-carboryne **84** in the photolysis of lithiolated iodocarboranes **85** and **86** (Scheme 41).[204] The observed isotope effect, k_H/k_D = 5.3, on the C−H insertion reaction to the ethers indicated that the hydrogen abstraction by the carborynes is the rate-determining step in the insertion reaction.

Hetarynes. Didehydropyridines (DHPs) are reactive diradical intermediates and consist of six possible isomers: 2,3-DHP, 3,4-DHP, 2,4-DHP, 2,5-DHP, 2,6-DHP, and 3,5-DHP (Figure 41). All of the derivatives are also the singlet-ground-state molecules.[205] Rau and Wenthold reported the absolute enthalpies of formation of 2,3-DHP, 2,4-DHP, and 3,4-DHP determined by using energy-resolved collision-induced dissociation of the deprotonated 2- and 3-chloropyridines.[206] The enthalpy of formation of 3,4-DHP was measured to be 121 ± 3 kcal mol^{-1} by using the chloride dissociation energy for the deprotonated 3-chloropyridine. The enthalpies of formation of 2,3-DHP and 2,4-DHP were both found to be 130 ± 3 kcal mol^{-1}. The computational studies clarified that the nitrogen in the pyridine ring does not have any effect on the stability of the aryne triple bond in 3,4-DHP, destabilizes the aryne triple bond in 2,3-DHP, and stabilizes the 1,3-interaction in 2,4-DHP. Natural bond order calculations showed that the effects on 2,3-DHP and 2,4-DHP resulted from polarization of the electrons caused by the interaction with the lone pair on nitrogen. The polarization in 2,4-DHP is stabilized because it creates a 1,2-interaction between the nitrogen and dehydrocarbons. The energetic destabilization in 2,3-DHP is likely due to the electron repulsion between the nitrogen lone pair and the electrons of the in-plane π bond.

Similarly to the reactivity of *o*-benzynes, the isomers of 2,3-DHP and 3,4-DHP were found to be useful reactive intermediates for the synthesis of polyfunctionalized pyridine derivatives, which are important in drug discovery.[207]

Recently, Saito and Thiel reported the superior method of analytical gradients (AGs) with approximate spin projection (AP) for geometry optimizations for large open-shell singlet diradicals (Figure 42). For example, they tested the AG−AP method for optimizing the geometry of the singlet state of 2,6-pyridyne (2,6-DHP).[208] A previous study showed that the geometry obtained from BS-UDFT calculations differed significantly from that obtained by multireference (MR) ab initio calculations. The optimized geometry by the AG−AP method with LC-PBE level of theory was found to be consistent with that optimized with a state-specific multi-reference coupled-cluster singles and doubles approach (Mk-MRCCSD). Ess et al. recently reported the fractional-spin density functional theory for calculating singlet−triplet energy gaps for diradicals such as trimethylenemethane (TMM) and polyacenes.[209]

3. DELOCALIZED DIRADICALS

3.1. Triplet Diradicals in Antiaromatic Compounds[210]

In 1972, Baird proposed an "aromaticity" (or special stabilization in energy) for the lowest triplet state of 4*n*π

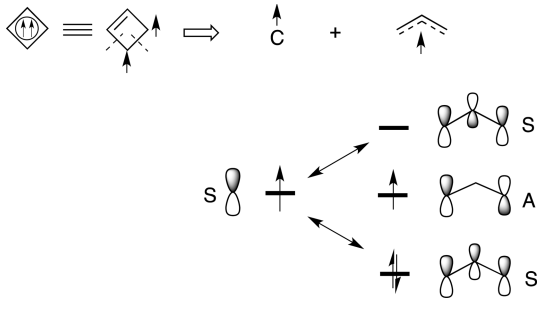

Figure 43. Baird's aromaticity in the triplet state of 4*n*π annulenes.

annulenes.[211] 4*n*π annulenes are antiaromatic compounds by Hückel's definition. Baird explained the special energetic stabilization of the triplet state of cyclobutadiene using perturbation molecular orbital theory, as follows: The triplet state of cyclobutadiene can be decomposed into the triplet pair

dx.doi.org/10.1021/cr400056a | *Chem. Rev.* 2013, 113, 7011−7088

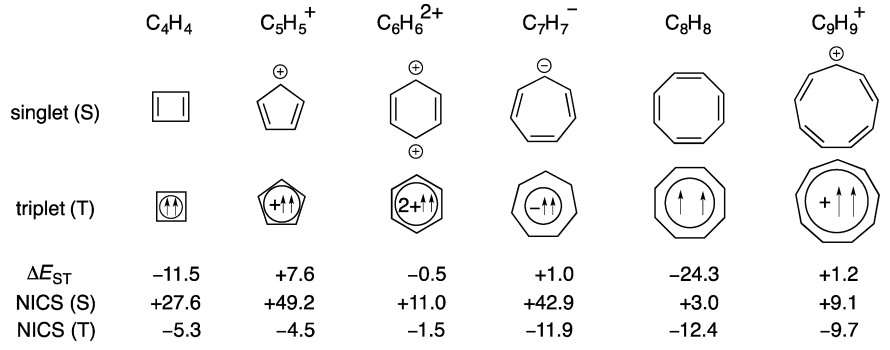

Figure 44. Aromatic characters of the triplet states of Hückel antiaromatic compounds at the CCSD(T)/cc-pVDZ//B3LYP/6-311+G(d,p).

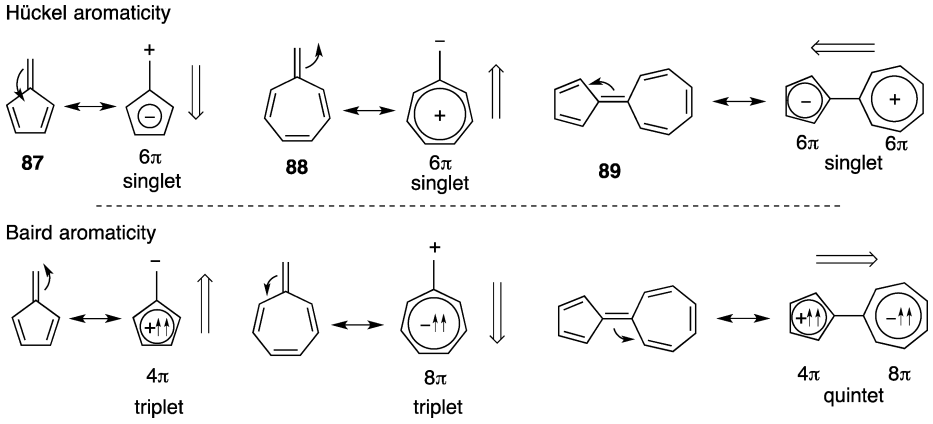

Figure 45. Spin-state-dependent change of aromaticity: Hückel aromaticity in the singlet state versus Baird aromaticity in the triplet state.

Table 2. Singlet−Triplet Energy Gaps in Hückel Antiaromatic Compounds

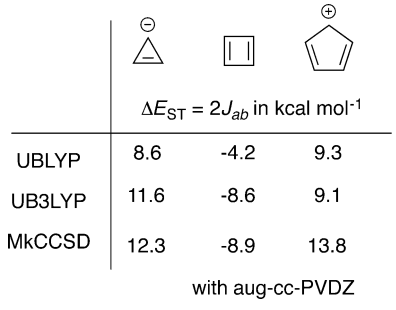

of odd electrons, namely, C• and allylic radical (Figure 43). The singly occupied molecular orbital (SOMO) can interact with the LUMO and HOMO of the allylic radical, because the three molecular orbitals have the same symmetry.

Schleyer and co-workers confirmed the concept by calculating the nucleus-independent chemical shift (NICS)[212] values of Hückel antiaromatic compounds C_4H_4, $C_5H_5^+$, $C_6H_6^{2+}$, $C_7H_7^-$, C_8H_8, and $C_9H_9^+$ (Figure 44).[213] The bond alternation, singlet−triplet energy spacing, and NICS values for the $4n\pi$ annulenes were computed at the CCSD(T)/cc-pVDZ//B3LYP/6-311+G(d,p) level of theory. For comparison, acyclic reference compounds such as butadiene and pentadienyl cation were also calculated. The triplet states of the

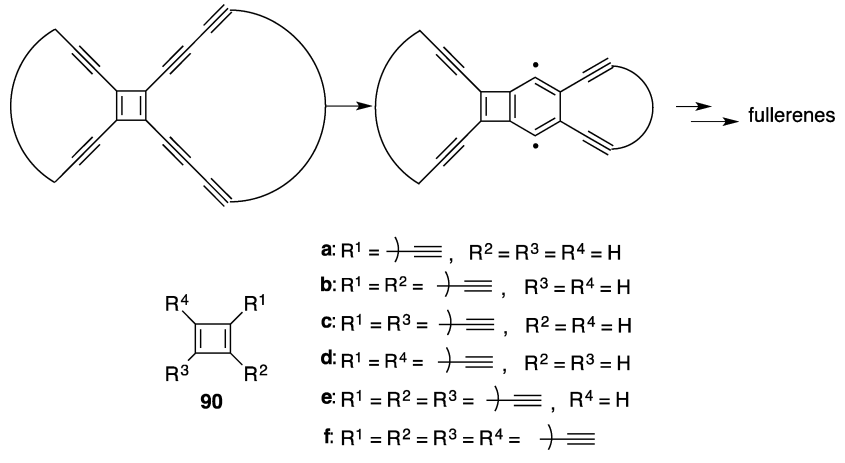

Figure 46. Ethynyl-substituted cyclobutadienes for large ordered carbon systems.

dx.doi.org/10.1021/cr400056a | Chem. Rev. 2013, 113, 7011−7088

$(CO)_n$	CO	$(CO)_2$	$(CO)_3$	$(CO)_4$	$(CO)_5$	$(CO)_6$
ΔE_{ST} /kcal mol^{-1}	-139[a]	10.3[b]	-26.5[b]	2.4[b] (1.5)[a]	-27.0[b]	-27.8[b]

[a]experimental value; [b] at (U)CCSD(T)/6-311+G(2df)

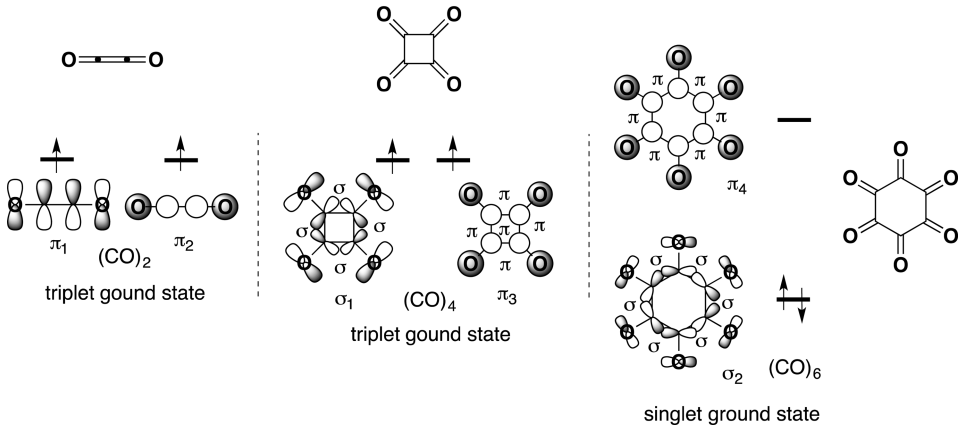

Figure 47. Singlet−triplet energy differences (kcal mol^{-1}) in $(CO)_n$ and two orbitals that are occupied by two electrons.

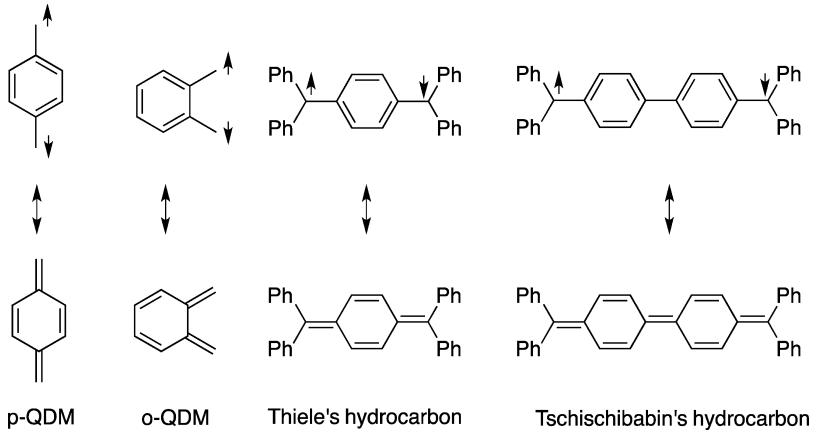

Figure 48. Typical examples of Kekulé-type delocalized diradicals.

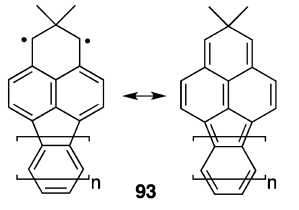

n	ground state	ΔE_{ST}*
1	closed-shell singlet	-2.6
2	triplet	1.8

93

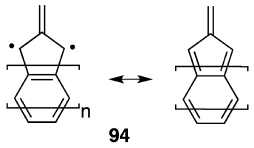

n	ground state	ΔE_{ST}*
1	closed-shell singlet	-15.2
2	closed-shell singlet	-2.5
3	triplet	3.0
4	triplet	4.4

94

* in kcal mol^{-1}, calculated at the RASPT2/6-31G(d) level of theory

Figure 49. Effects of the number (n) of aromatic rings on the ground-state spin multiplicity in **93** and **94**.

reference compounds were calculated to be energetically higher than the singlet states by 57.0 and 47.1 kcal mol^{-1}, respectively. Significant stabilization of the triplet energies was found for C_4H_4 (ΔE_{ST} = −11.5 kcal mol^{-1}) and $C_5H_5^+$ (ΔE_{ST} = +7.6 kcal mol^{-1}). The singlet−triplet energy gaps, ΔE_{ST}, for other antiaromatic $4n\pi$ annulenes $C_6H_6^{2+}$, $C_7H_7^-$, C_8H_8, and $C_9H_9^+$ were also calculated to be very small, at −0.5, +1.0, −24.3, and +1.2, respectively. The small energy gaps and the negative NICS values for the triplet state of the $4n\pi$ annulenes clarify the special energetic stability of their triplet state, indicating the aromatic character of their triplet states. The relatively large singlet−triplet energy gaps for C_4H_4 (ΔE_{ST} = −11.5 kcal mol^{-1}) and C_8H_8 (ΔE_{ST} = −24.3 kcal mol^{-1}) with singlet ground states are rationalized by the Jahn−Teller distortion in the singlet states.

The directions of the dipole moment of the singlet states of pentafulvene **87** and heptafulvene **88** can be depicted by the arrows in the structures in Figure 45. The direction can be explained by the large contribution of the zwitterionic resonance structures. The direction of the arrows is due to the $(4n\pi + 2)$ aromatic stabilization in the cyclic ring systems, namely, Hückel aromaticity. Thus, the dipole moment of pentaheptafulvalene **89** is from the seven-membered ring to the five-membered ring. The dipole moment was calculated to be

dx.doi.org/10.1021/cr400056a | *Chem. Rev.* 2013, 113, 7011−7088

Scheme 42. Synthesis and X-ray Crystallographic Analysis of *o*-QDM Derivative 95

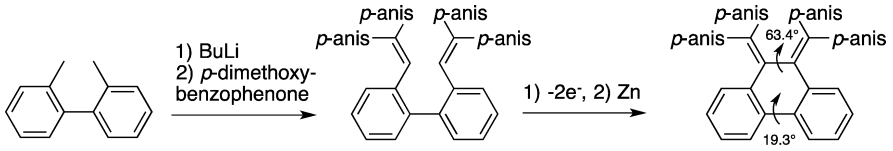

Scheme 43. Formation of *o*-Quinodimethane Structure 96 in the Reaction of Naphthalene-1,4-dione with the Germanium−Carbon Double Bond

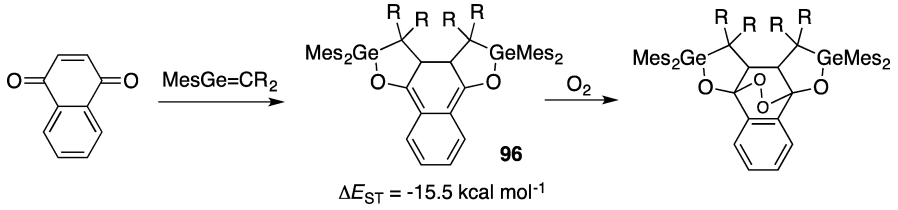

Scheme 44. Synthesis of Air-Stable *o*-Benzoquinodimethane Derivative 97

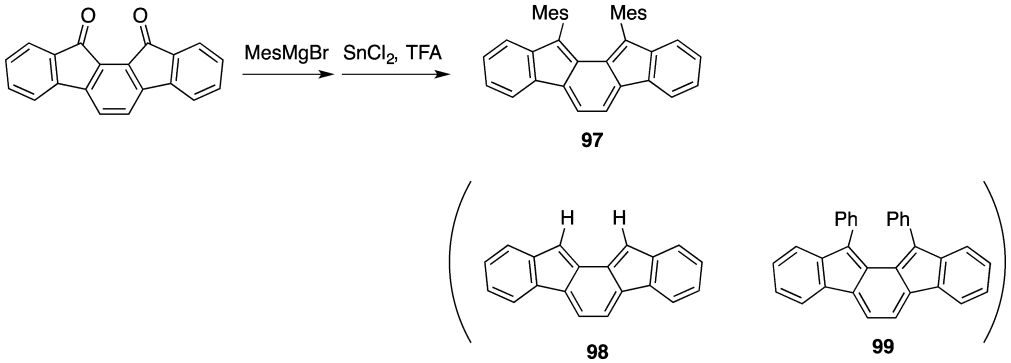

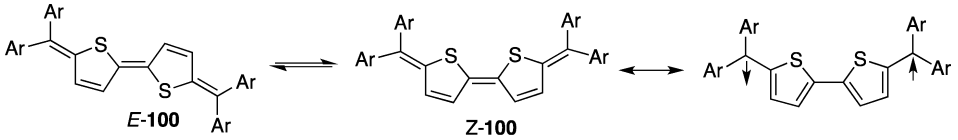

b: *E*/*Z* = 3/7 in toluene, 1/8 in DMSO

a: Ar = Ph, E_1^{redox}= 1.93 V; E_2^{redox}= 2.42 V
b: Ar = Thienyl, E_1^{redox}= 1.61 V; E_2^{redox}= 1.86 V
c: 5-MeSthienyl, E_1^{redox}= 1.46 V; E_2^{redox}= 1.63 V
d: bis-thienyl, E_1^{redox}= 1.22 V; E_2^{redox}= 1.36 V
Tschischibabin's hydrocarbon, E_1^{redox}= 1.51 V; E_2^{redox}= 2.06 V

Figure 50. Synthesis of stable 5,5′-bis(diarylmethylene)-5,5′-dihydro-2,2′-bithiophenes **100** as a mixture of *Z* and *E* isomers with highly amphoteric multistage redox properties.

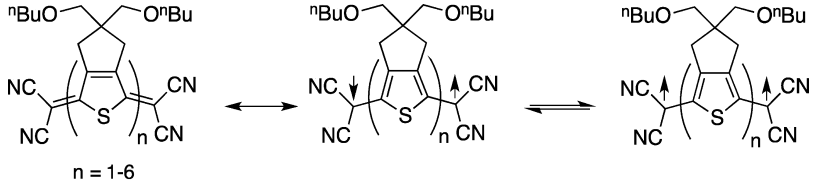

Figure 51. Character of quinoidal oligothiophenes **101** (n = 1−6).

38 D at the OLYP/TZ2p level of theory. In contrast to the singlet state of the fulvenes, the direction of the dipole moment of the triplet state of the fulvenes was found to be just the opposite of that of the corresponding singlet state, because the $4n\pi$-electron system is aromatic for the triplet state.[214] The chameleon behaviors of fulvenes and fuvalenes are explained by differences in the numbers of π electrons in their singlet states (Hückel aromaticity) and triplet states (Baird aromaticity).

dx.doi.org/10.1021/cr400056a | *Chem. Rev.* 2013, 113, 7011−7088

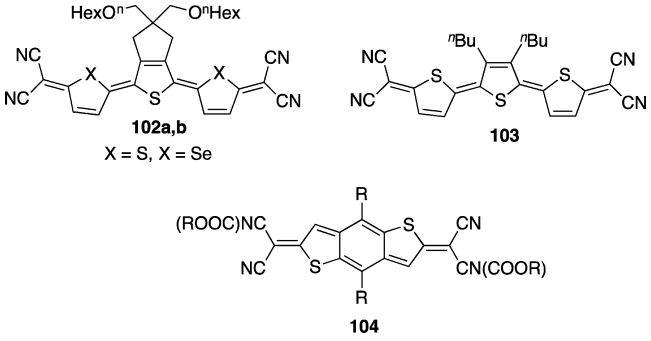

Figure 52. Quinoidal oligothiophene derivatives have a small HOMO−LUMO energy spacing.

First-principles calculations of the effective exchange integral (J) in the Heisenberg model for antiaromatic diradicals were performed by both the symmetry-adapted multireference (MkCCSD) and the single-reference broken-symmetry (BS) DFT methods. An approximate spin-projection (AP) scheme was applied to the BS solutions. As shown in Table 2, the BS-UDFT method well reproduced the singlet−triplet energy gaps of the three selected antiaromatic diradicals. More examples were tested in the original work.[215]

Because of their unique optical and electric properties, graphene, fullerenes, and carbon nanotubes have attracted much attention in the area of materials science.[216] Ethynyl-substituted cyclobutadienes have recently become important as starting compounds for large ordered carbon systems (Figure 46). The substituent effect of the ethynyl group on the singlet−triplet energy gap in cyclobutadienes **90** was independently computed by the McMahon group[217] and the Slipchenko group[218] in 2012. The ethynyl substitutions were found to provide enthalpy stabilization for both the singlet and triplet states of the cyclobutadiene ring system. According to computational studies at the coupled-cluster singles and doubles (CCSD) level of theory, the singlet state was stabilized by ca. 3 kcal mol^{-1} by the introduction of one ethynyl group, and the triplet state was found to be stabilized by 4 kcal mol^{-1} per ethylnyl group. Thus, the singlet−triplet energy spacing was calculated to decrease with increasing number of ethynyl groups, from −11.5 (**90a**) to approximately −7.0 kcal mol^{-1} (**90f**) at the CCSD(T)/cc-PVTZ//CCSD/cc-PVDZ level of theory. Conventional DFT methods such as the B3LYP/6-31G(d) level of theory could not reproduce the CCSD computational results. The equation of spin-flip coupled-cluster single and double excitations method was found to accurately describe the diradical states.

3.2. Oxocarbons $(CO)_n$[219]

The ground-state spin multiplicity of $(CO)_n$ was reported to be largely dependent on the value of n (Figure 47).[220] Thus, triplet ground states were found for $(CO)_2$[221] and $(CO)_4$,[222] whereas CO, $(CO)_3$, $(CO)_5$, and $(CO)_6$ are singlet-ground-state molecules.[223]

The two molecular orbitals, π_1 and π_2, that are occupied by two electrons are energetically degenerate for $(CO)_2$. These orbitals are nondisjoint, so Hund's rule applies to $(CO)_2$. Thus, the triplet state should be the ground-state spin multiplicity, although a Lewis structure can be drawn for $(CO)_2$. The degeneracy in energy of the two orbitals, π_1 and π_2, is reasonable, because these orbitals are both in π-bonding systems.

Surprisingly, the two orbitals σ_1 and π_3, which are occupied by two electrons, are nearly degenerate for $(CO)_4$, although σ-bonding interactions are more stable in energy than π-bonding interactions. The stabilization in energy of the π_3 orbital is explained by the cross-ring π overlaps between the 2p AOs on C1 (C2) and C3 (C4). The cross-ring π overlaps in $(CO)_6$ are smaller than those in $(CO)_4$, because the distances between the two carbons in $(CO)_6$ longer than those in $(CO)_4$. Thus, the singlet is the ground-state spin multiplicity in $(CO)_6$.

3.3. Kekulé-Type Delocalized Diradicals

Typical examples of Kekulé-type delocalized diradicals are *para*- and *ortho*-quinodimethanes (QDMs), Thiele's hydrocarbon, and Tschitschibabin's hydrocarbons (Figure 48). These hydrocarbons have inherently diradical character, because the open-shell singlet diradical structure appears in the canonical form. Thus, the singlet state of the diradicals is known to be the ground-state spin multiplicity with an energy splitting of 8−30 kcal mol^{-1}. A significant contribution of the diradical character in the hydrocarbons can be expected because of the formation of aromatic rings in the diradical form. The diradical character of Tschitschibabin's hydrocarbon should be larger than that of Thiele's hydrocarbon, because two aromatic rings appear in the diradical form. The inherent diradical contribution in Kekulé hydrocarbons makes these compounds quite reactive, especially to molecular oxygen.

Since the identification of graphene, polycyclic hydrocarbons (PAHs), in which Kekulé-hydrocarbon units exist, have attracted much attention in the fields of both structural organic chemistry and materials science.[224] The π-extended derivatives of Kekulé hydrocarbons are regarded as good model compounds for understanding the fundamental properties of graphene.[225] The π-extended derivatives exhibit low energy gaps between the HOMO and LUMO. Thus, the diradical character of π-extended Kekulé molecules is expected to be higher than that os the parent Kekulé molecules such as *p*-QDM. Such π-extended Kekulé molecules play a vital role in

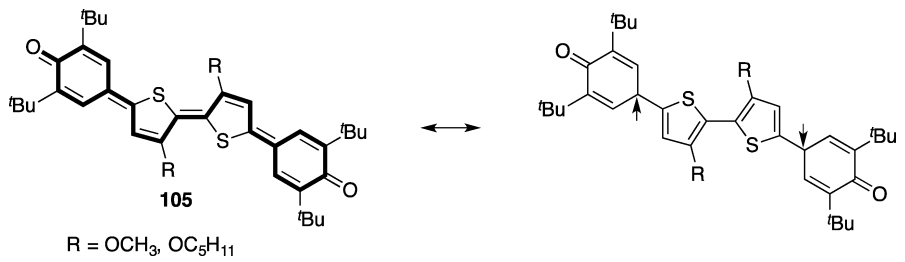

Figure 53. Substituent R effects on quinoidal versus diradical character in **105**.

dx.doi.org/10.1021/cr400056a | *Chem. Rev.* 2013, 113, 7011−7088

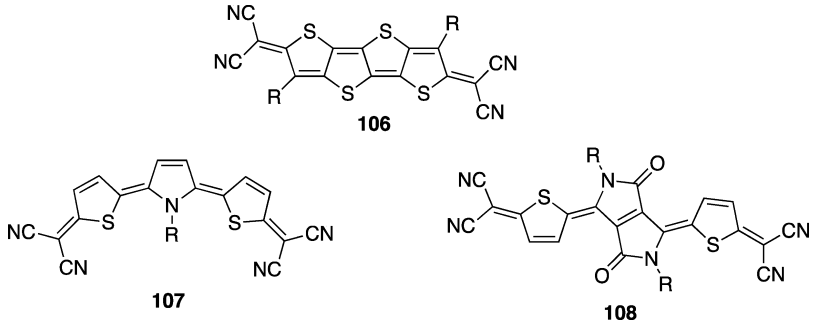

Figure 54. Quinoidal compounds **106**−**108** with FET properties.

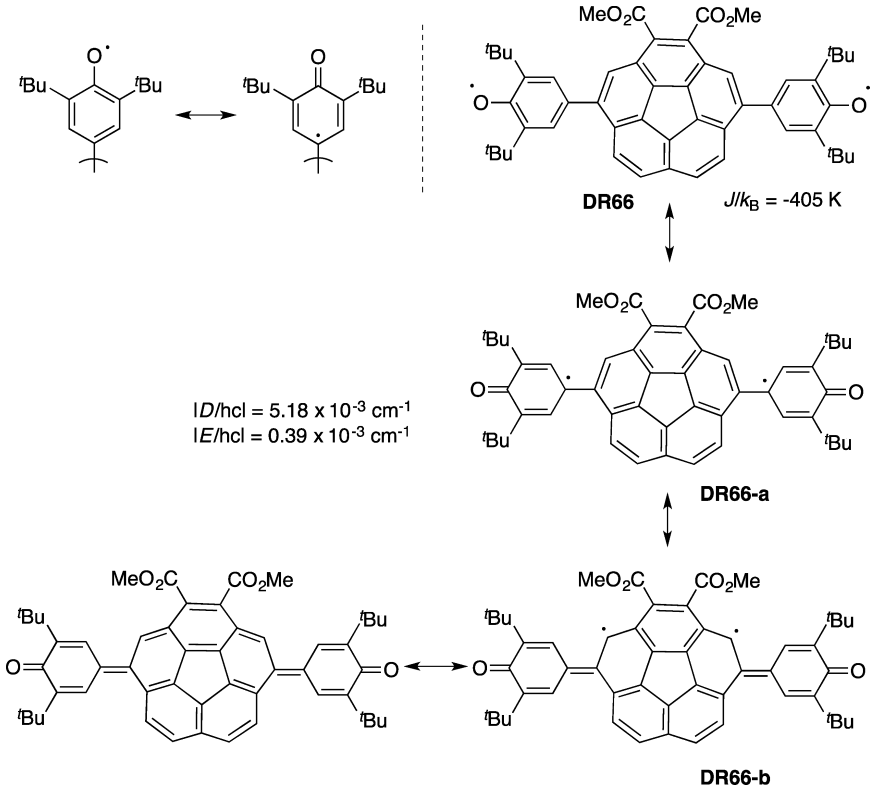

Figure 55. Stable diradicals with a corannulene unit.

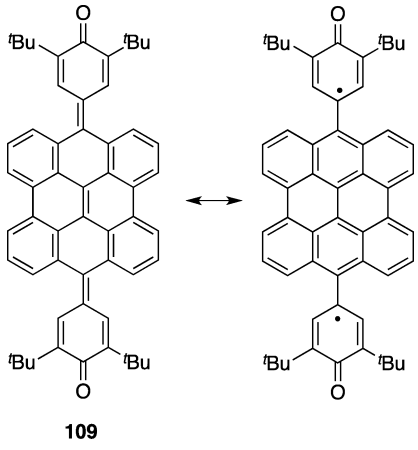

Figure 56. Synthesis and isolation of quinoidal bisanthene **109** with 2,6-*tert*-butylphenoxyl units.

understanding the properties of graphenes. Many applications, such as near-infrared dyes, organic field-effect transistor (OFETs), and nonlinear optical materials, are possible for molecules with low HOMO−LUMO energy gaps, including Kekulé molecules with diradical character. However, Kekulé hydrocarbons are inherently quite reactive because of the contribution of the diradical character. The stabilization of Kekulé molecules is necessary to understand their performance as functional organic molecules. In the next section, recent developments in stabilizing Kekulé molecules are introduced.

***o*-Quinodimethane (*o*-QDM).** The parent *o*-QDM is stable only below −150 °C.[226] The extension of the π conjugation is one of the most promising strategies for isolating unstable Kekulé molecules. Tetraphenyl substitution, however, was not successful in isolating *o*-quinodimethane derivative **91**.[227] Introduction of the naphthyl ring also was not successful in isolat ing molecule **92**.

McMasters and Wirz[228] and Snyder[229] reported that the triplet-ground-state spin multiplicity can be switched by introducing an aromatic ring adjacent to the diradical moiety

dx.doi.org/10.1021/cr400056a | *Chem. Rev.* 2013, 113, 7011−7088

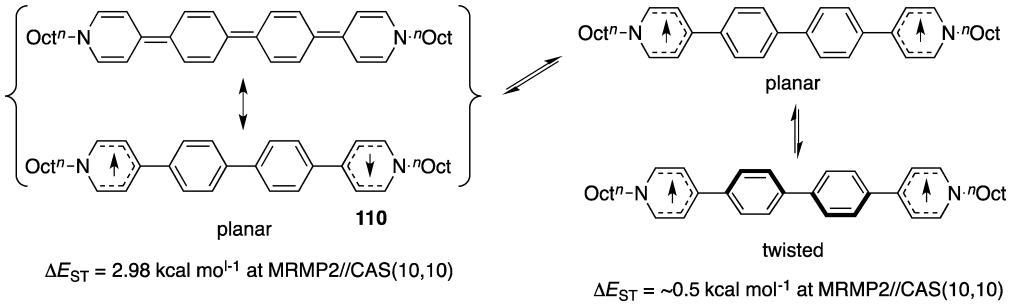

Figure 57. Synthesis of extended viologen derivative **110**.

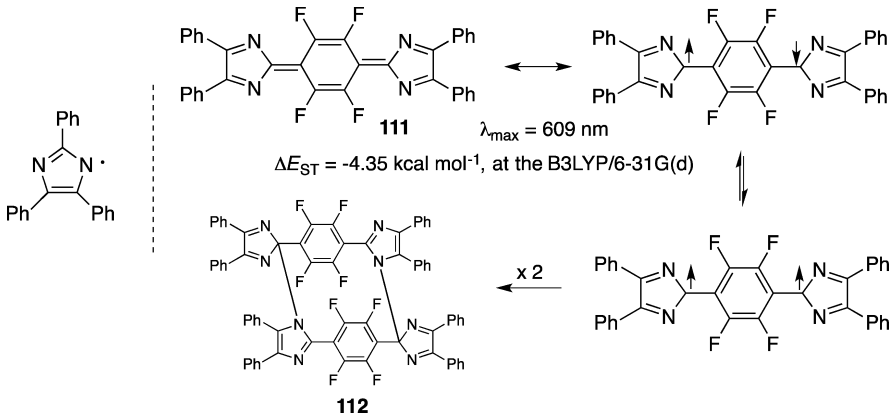

Figure 58. Kekulé hydrocarbon with an imidazolyl radical moiety.

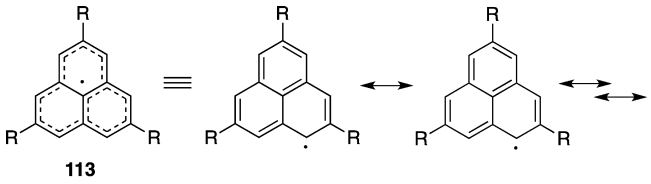

Figure 59. Phenalenyl radical, a persistent radical.

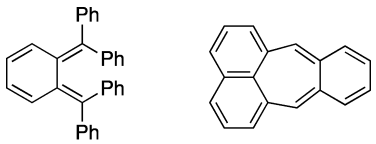

(Figure 49). For example, 1,8-naphthoquinodimethane- (1,8-NQDM-) based diradical **93** (n = 1) was found to be the closed-shell singlet ground state, because the energy penalty of one missing π bond (65 kcal mol^{-1}) cannot be compensated by destroying one benzene ring (21 kcal mol^{-1}) and one naphthalene ring (33 kcal mol^{-1}). However, when one additional benzene ring was introduced into the 1,8-NQDM moiety (n = 2), the triplet state was found to be the ground-state spin multiplicity. In the latter case, the energetic penalty of one missing bond was not able to destroy two benzene rings and one naphthalene ring.

A similar switch of the ground-state spin multiplicity was reported for the annulated trimethylenemethane (TMM) derivatives **94**. For n = 1 with a benzene ring, the closed-shell quinoidal structure was calculated to be more stable than the open-shell triplet state by 15.2 kcal mol^{-1}. For n = 2 with a naphthalene ring, the closed-shell singlet state was still found to be the ground state. However, when the anthracene ring (42 kcal mol^{-1}) was introduced (n = 3), the open-shell triplet state was calculated to be the ground-state spin multiplicity at the RASPT2/6-31G(d) level of theory. The resonance energy of the triplet diradical in TMM is known to be 24 kcal mol^{-1}. Thus, the energetic penalty of one missing π bond was compensated by introducing the anthracene ring.

In 2004, Iwashita et al. reported the first synthesis and X-ray crystallographic analysis of *o*-QDM derivative **95** (Scheme 42).[230] The quinodimethane structure was prepared from 2,2′-bitolyl according to the scheme. X-ray crystallographic analysis clarified a large torsion angle of 63.4° for $Ar_2C{=}C{-}C{=}CAr_2$ and 19.3° for the biphenyl unit. The stable feature of the *o*-quinodimethane structure is attributed to the highly twisted conformation, which decreases the resonace between the double-bond moieties and, thus, the contribution of the open-shell diradical character.

Ghereg et al. found the formation of *o*-quinodimethane structure **96** in the reaction of naphthalene-1,4-dione with a germanium−carbon double bond (Scheme 43).[231] X-ray analysis clarified the bond alternation of the quinoidal structure. The *o*-quinodimethane is highly reactive to moisture and molecular oxygen. Thus, the endoperoxide was formed in the spontaneous reaction with molecular oxygen. The singlet−triplet energy spacing was calculated to be −15.5 kcal mol^{-1} (singlet ground state) at the RI-BP86/SVP level of theory. The energy splitting was found to be slightly lower than that of the parent *o*-QDM at the same level of theory, ΔE_{ST} = −20.5 kcal mol^{-1}.

Shimizu and Tobe succeeded in synthesizing the air-stable *o*-benzoquinodimethane derivative **97** (Scheme 44).[232] The parent compound **98** and phenyl-substituted derivative **99** are reactive with molecular oxygen to give the corresponding

dx.doi.org/10.1021/cr400056a | *Chem. Rev.* 2013, 113, 7011−7088

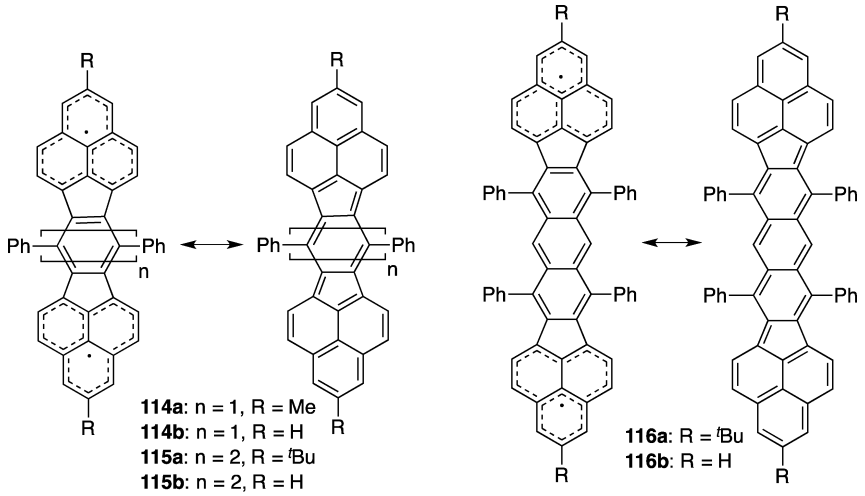

	DR/%	ΔE_{ST}/kJ mol^{-1} SQUID	ΔE_{ST}/kJ mol^{-1} B3LYP/6-31G(d)	H-L gap /eV UV	H-L gap /eV CV	zfs /mT |D|	zfs /mT |E|
114a	30	-20	-30 (**114b**)	1.64	1.20	9.6	< 0.2
115a	50	-16	-19 (**115b**)	1.43	1.04	nd	nd
116a	68	nd	-12 (**116b**)	1.26	0.98	nd	nd

Figure 60. Series of Kekulé hydrocarbons **114**–**116** with phenalenyl-ring units and their physical properties.

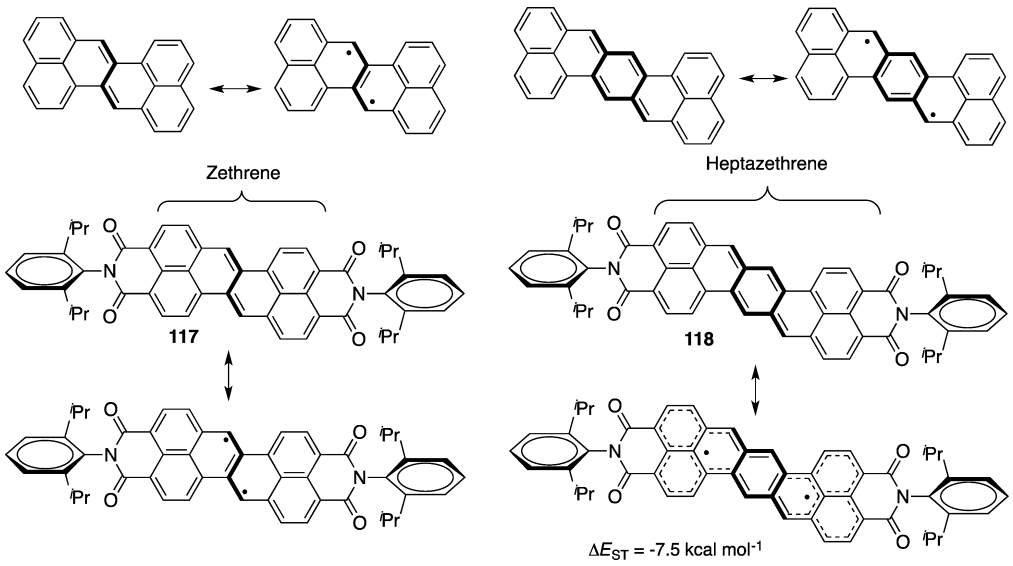

Figure 61. Stable Kekulé hydrocarbons with low HOMO–LUMO energy gaps.

peroxides. Detailed analysis of the electrochemical properties was difficult because of the intrinsic instability of the *o*-quinodimethane structure. Kinetic stabilization using the mesityl group (= 2,4,6-trimethylphenyl), which retards the oxidation reaction at the two benzyl carbons, was found to be effective in isolating the air-stable *o*-quinodimethane. The stability under air conditions allowed the oxidation and reduction potentials to be measured, from which the HOMO–LUMO energy gap was estimated to be 2.10 eV.

***p*-Quinodimethane Derivatives.** Thiele's and Tschitschibabin's hydrocarbons have both been isolated and analyzed by X-ray crystallography. However, the compounds are inherently reactive, so the analyses had to be performed at approximately −160 °C. Indeed, the quinoidal structure with bond alternation was confirmed by the analysis.[233] Quinoidal hydrocarbons present an interesting motif for compounds with a small HOMO–LUMO energy gap. A significant effort to stabilize and isolate such quinoidal molecules has been made in the past decade. In principle, two approaches have been reported: (1) use of a smaller aromatic stabilization energy and (2) thermodynamic stabilization of the radical moiety.

Kawase et al. chose the first strategy. They reported the synthesis of stable 5,5′-bis(diarylmethylene)-5,5′-dihydro-2,2′-bithiophenes **100** as a mixture of *Z* and *E* isomers with highly amphoteric multistage redox properties (Figure 50).[234] For example, tetrakis(bisthienyl) compound **100d** gave a remarkably small redox potential energy between the first oxidation potential and the first reduction potential, E_1^{redox} = 1.22 V. The

dx.doi.org/10.1021/cr400056a | *Chem. Rev.* 2013, 113, 7011–7088

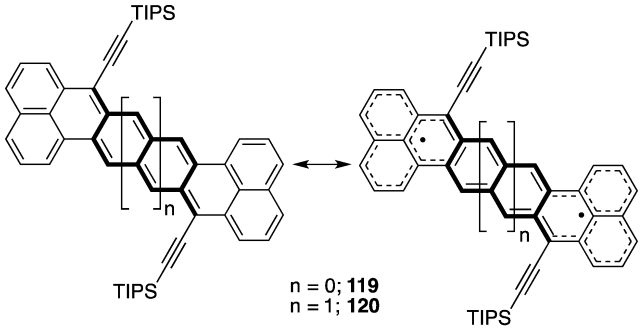

n	ΔE_{ST} /kcal mol^{-1}	TPA /GM	ΔE_1^{redox} /V
0	nd (-8.1)*	920	1.65
1	-3.9 (-4.4)*	1200	1.32

* exp. (calcd at CAM-B3LYP)

Figure 62. New family of stable Kekulé hydrocarbons with a zethrene structure.

redox potential for Tschitschibabin's hydrocarbon was reported to be 1.51 V. The low contribution of the diradical form is due to the low aromatic stability of the thiophene ring.

The introduction of the dicyanomethylidene at the terminal carbon, which stabilizes the radical character and increases the electron-accepting ability, provided representative examples as organic field-effect transistor (OFET) operations. OFETs are attracting much interest because of their use as low-cost materials. Takahashi et al. found that the quinoidal oligothiophenes **101** (n = 1–6) displayed very interesting properties (Figure 51).[235] The unrestricted singlet state of the hexamer was found to be more stable than the closed-shell singlet state, which clearly indicates a small HOMO–LUMO energy spacing and a small singlet–triplet energy gap, 0.84 eV and $\lambda_{max} \approx 1012$ nm. Indeed, the hexamer was found to be the ESR-active species. Quinoidal oligothiophene derivatives are proposed to be candidates for organic spintronics.[236] Electron-withdrawing-group-substituted quinoidal origothiophenes were actually found to exhibit a property of n-type semiconductors. The electron mobility of these oligothiophene derivatives was determined to be largely dependent on the structure.

Although quinoidal oligothiophene derivatives have a small HOMO–LUMO energy spacing, the compounds are not suitable as organic semiconductors because of the steric hindrance of the butoxymethyl-substituted core units, which prevents intermolecular interactions in the solid state. Handa et al. designed new compounds **102**, in which the high-solubility hexyloxy methyl group was introduced only at the central thiophene unit (Figure 52).[237,238] Owing to the high solubility of compound **102** (2×10^{-2} mol L^{-1} in chloroform), thin-film fabrication of **102a** was achieved using the conventional spin-coating method. The UV–vis spectrum, X-ray diffraction (XRD) pattern, and electron mobility were dramatically changed upon annealing. The absorption maximum was shifted from 650 to 1000 nm after the sample had been annealed at 150 °C. The electron mobility increased from 1.4×10^{-4} cm^2 V^{-1} s^{-1} (room temperature) to 0.16 cm^2 V^{-1} s^{-1}(150 °C) with $I_{on}/I_{off} = 10^3$. The XRD pattern showed the formation of a crystalline domain in the film after annealing. The electron mobility was close to the value of 0.2 cm^2 V^{-1} s^{-1} for quinoidal oligothiophene derivative **103**, which was prepared by Chesterfields et al.[239] Suzuki et al. developed new types of quinoidal core **104** with the zigzag orientation of the thiophene moiety.[240] When the sulfur atoms at both ends were replaced by selenium atoms, an ambipolar transport character of the materials was discovered. Thus, the n-channel FET response was determined to be 1.6×10^{-2} cm^2 V^{-1} s^{-1}, with $I_{on}/I_{off} = 10^3$, which is 1 order of magnitude smaller than that of **102**. The p-channel FET response was found to be 7.0×10^{-3} cm^2 V^{-1} s^{-1}.

Canesi et al. found that the ground-state electronic character (quinoidal versus diradical) of bithiophenes **105** can be controlled by the substituents on the thiophene ring system (Figure 53).[241] According to NMR, UV–vis, and Raman spectroscopic analyses and quantum chemical calculations, the electron-donating substituents of the alkoxy groups strongly affect the electronic structure and the ground-state energy and stability of bithiophenes **105**. Thus, for R = H, the open-shell singlet diradical character (S^2 = 0.67) was found to be the ground state at the B3LYP/6-31G(d) level of theory, which was found to be more stable in energy than the closed-shell quinoidal structure by ca. 1 kcal mol^{-1}. Upon introducing alkoxy groups onto the thiophene ring (R = OCH_3/OC_5H_{11}), the closed-shell quinoidal structure was found to largely contribute to the ground-state electronic structure (S^2 = 0.00). The quinoidal structure was also confirmed by spectroscopic analyses.

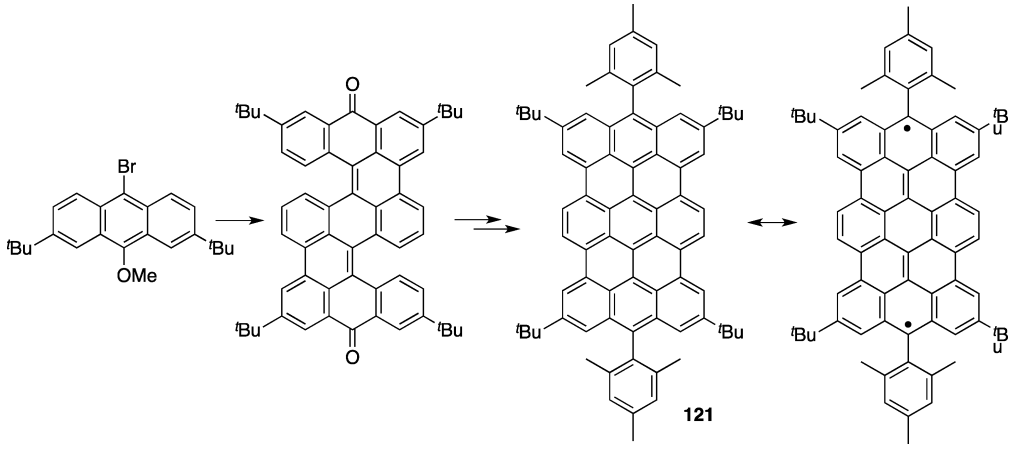

Figure 63. Teranthracene derivative **121** with an open-shell singlet diradical character.

dx.doi.org/10.1021/cr400056a | Chem. Rev. 2013, 113, 7011–7088

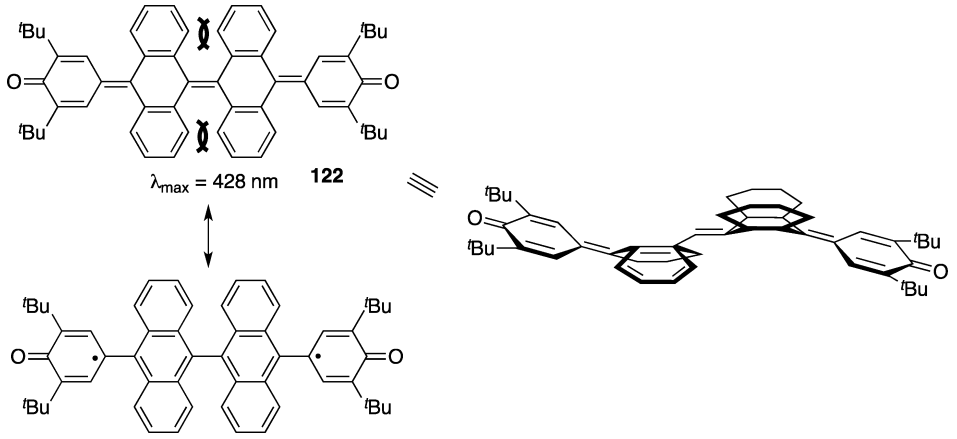

Figure 64. Double-saddle-like structure of Tschitschibabin's hydrocarbon **122**.

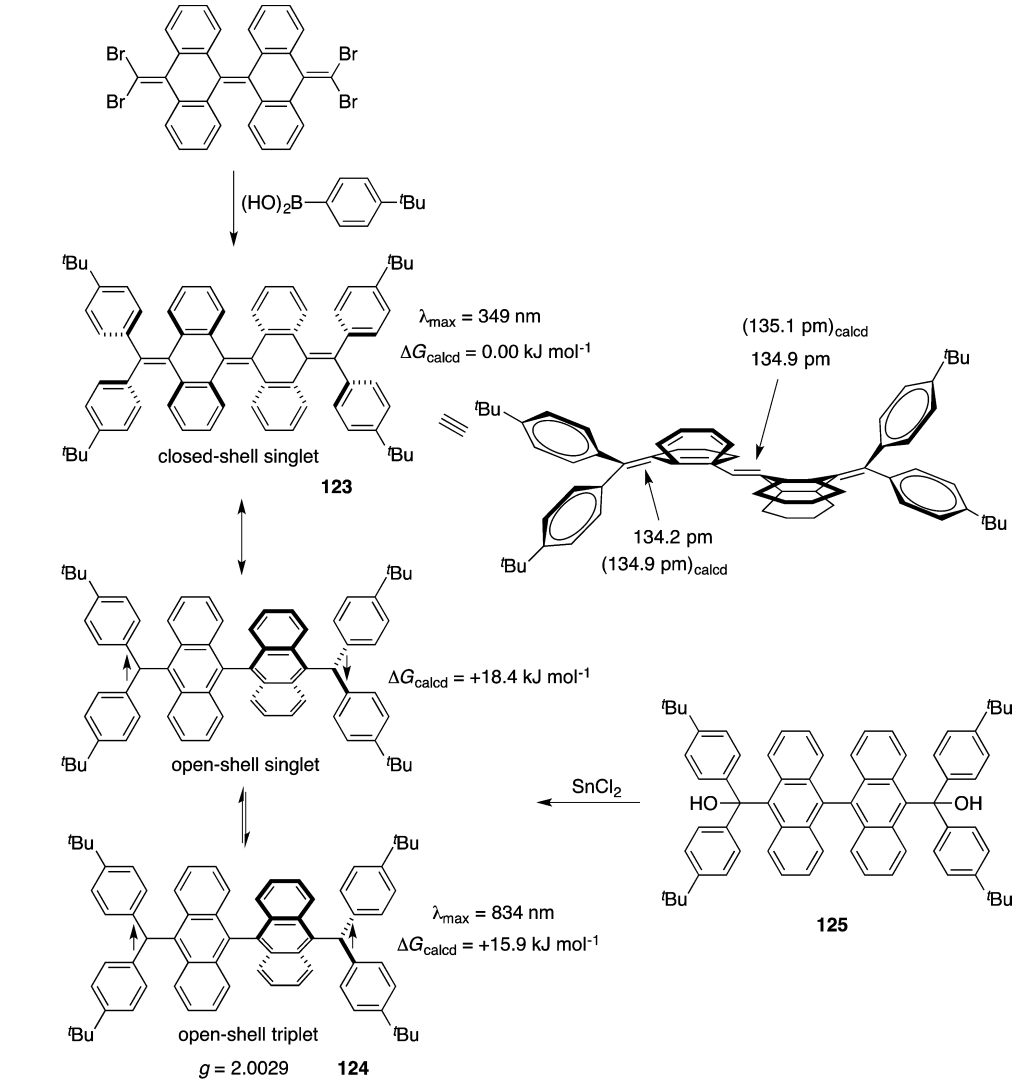

Figure 65. Thermal equilibration of the closed-shell singlet **123** with the open-shell triplet **124**.

Wu et al. recently developed quinoidal compounds **106**–**108** (Figure 54). The vapor-processed FET response of compound **106a** (R = 2-ethylhexyl) was found to be up to 0.55 $cm^2\ V^{-1}\ s^{-1}$ with $I_{on}/I_{off} = 10^{6.2}$.[242] The FET response of compound **106b**

dx.doi.org/10.1021/cr400056a | Chem. Rev. 2013, 113, 7011–7088

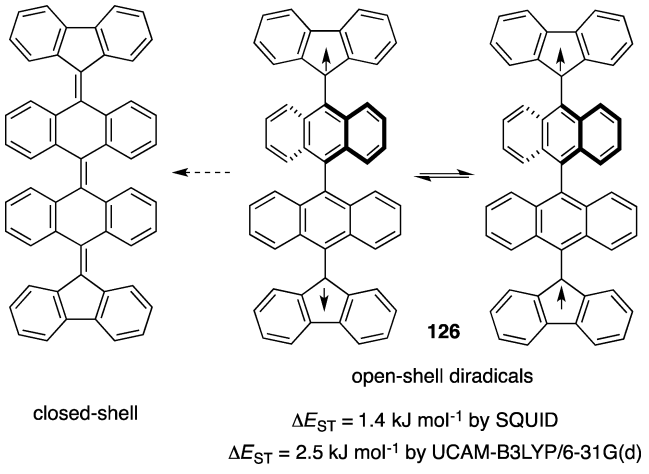

Figure 66. Open-shell diradical character of Tschitschibabin's hydrocarbon **126** with a triplet ground state.

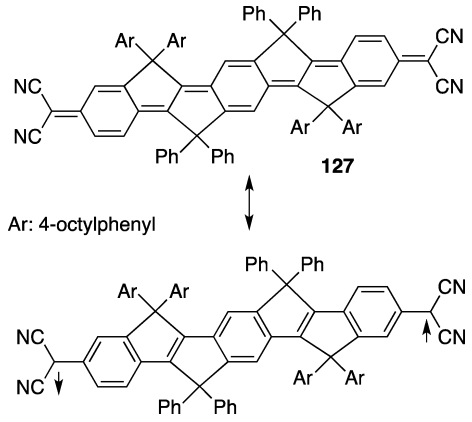

Figure 67. Synthesis of the air- and heat-stable planar tri-*p*-quinodimethane **127** with a distinct diradical character.

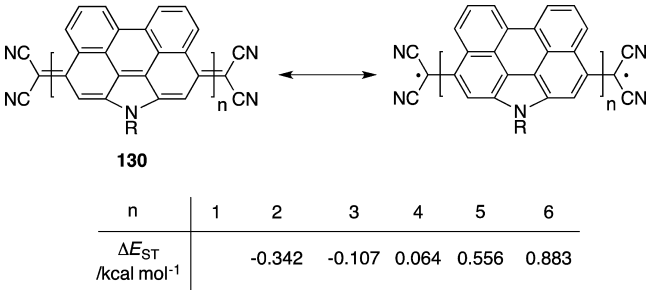

Figure 69. Singlet−triplet energy difference (ΔE_{ST}, kcal mol^{-1}) in tetracyano-oligo(*N*-annulated perylene)quinodimethanes **130**.

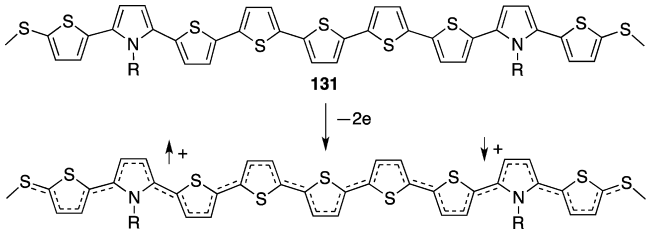

Figure 70. Singlet diradical character of π-conjugated oligomer dications **131**.

(R = 2-hexyldecyl) with high solubility was determined to be up to 0.35 cm^2 V^{-1} s^{-1} with I_{on}/I_{off} = 10^5−10^6 by the solution process in air.[243] For **107**, the solution process was used for the preparation of the device. The electron mobilities for n-type materials **107** and **108** were found to be 0.9 and 0.014 cm^2 V^{-1} s^{-1}, respectively.[244]

The diradicals and the polyenic character of the quinoidal oligothiophenes were confirmed by the presence of a low-lying double excitation state that is responsible for the weak features observed in the near-IR absorption region at the CASPT2/CASSCF computational level.[245]

Thermodynamic stabilization of the diradical resonance form is another strategy for isolating Kekulé hydrocarbons. 2,6-*tert*-

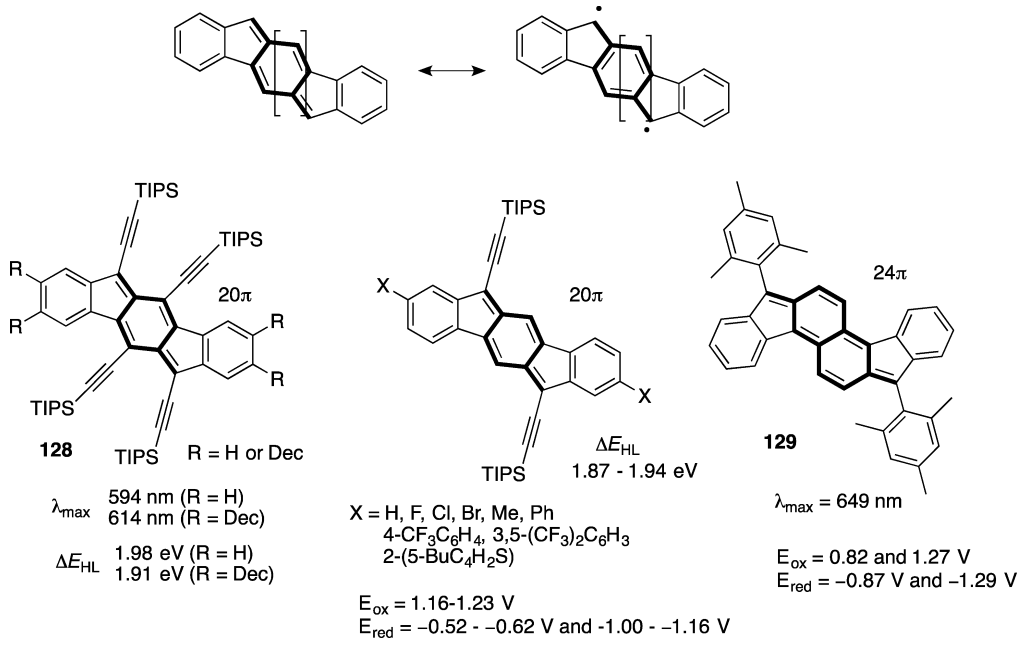

Figure 68. Synthesized indeno[1,2,-*b*]fluorene structures.

dx.doi.org/10.1021/cr400056a | *Chem. Rev.* 2013, 113, 7011−7088

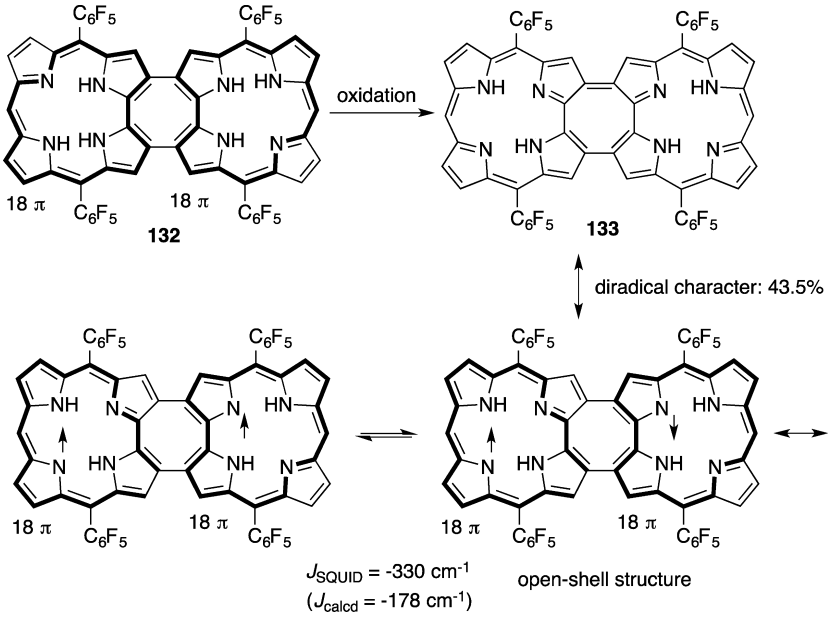

Figure 71. Singlet diradical character of a doubly linked corrole dimer.

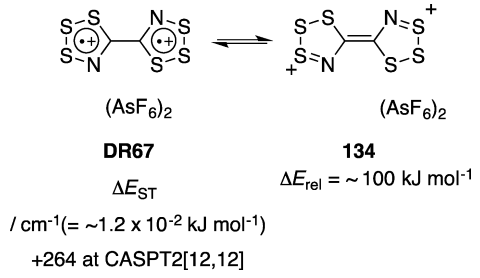

Figure 72. 1,2,3,5-Trithiazole diradical **DR67**.

Butylphenoxyl radical is one of the stable radicals.[246,247] The highly stable character is assumed to be derived from the kinetic protection provided by the *tert*-butyl groups and the highly delocalized character of the oxyl radicals.[248] Tschitschibabin-type structures and thiophene-cored structures were synthesized in the 1990s.[249] After the successful isolation of those quinoidal structures, in 2010, Ueda et al. succeeded in introducing two 2,6-*tert*-butylphenoxyl units into the corannulene unit (Figure 55).[250] From temperature-dependent magnetic susceptibility measurements, the singlet ground state of the diradical **DR66** was found with an energy gap of $2J/k_B = -810$ K. From the ESR spectrum of the thermally equilibrated triplet state, the D and E values were determined to be 5.18×10^{-3} cm^{-1} and 0.39×10^{-3} cm^{-1}, respectively. The relatively large D value, from which the spin−spin distance was estimated to be ∼8 Å, indicates that the contributions of resonance structures **DR66a** and **DR66b** are high. Indeed, the C−O distance was found to be 1.28 Å, which is longer than the C−O single bond of phenol (138 pm) and close to the C−O bond distance of the quinone structure.

Zhang et al. succeeded in synthesizing and isolating quinoidal bisanthene **109** with 2,6-*tert*-butylphenoxyl units (Figure 56).[251] The Kekulé hydrocarbon exhibited sharp NMR signals even at a high temperature of 100 °C, indicating that the contribution of diradical character is quite small in compound **109**. A solution of **109** in dichloromethane displays a dark green color, and absorption bands between 500 and 800 nm with a peak at 690 nm were observed. Clear amphoteric multistage redox behavior was observed for compound **109**: two reversible one-electron oxidation waves at $E_{ox} = 0.22$ and

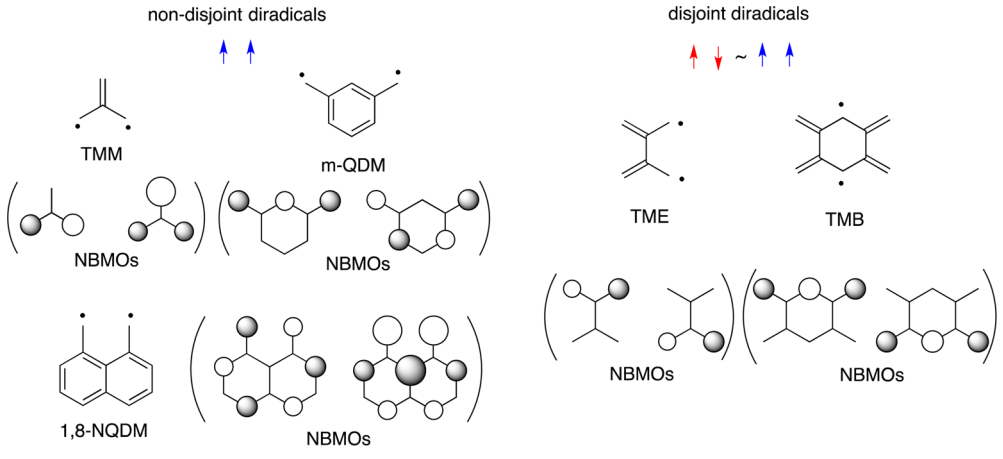

Figure 73. Non-Kekulé delocalized molecules.

dx.doi.org/10.1021/cr400056a | *Chem. Rev.* 2013, 113, 7011−7088

Scheme 45. Flash Vacuum Pyrolysis (FVP) of 135 at 450−500 °C for the Generation of *m*-QDM and Its Photochemical Reactivity

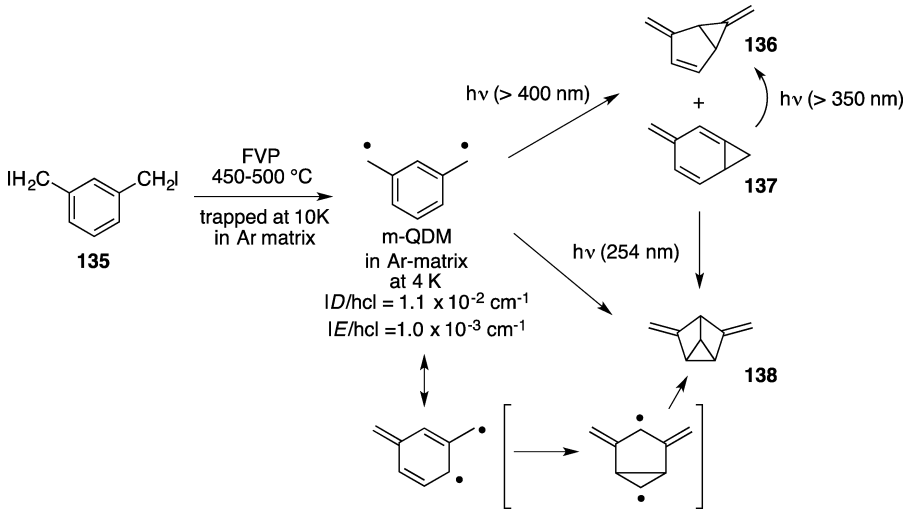

Scheme 46. Flash Vacuum Pyrolysis of 1,3,5-Tris(iodomethyl)benzene 140 for the Generation of Triradical 139

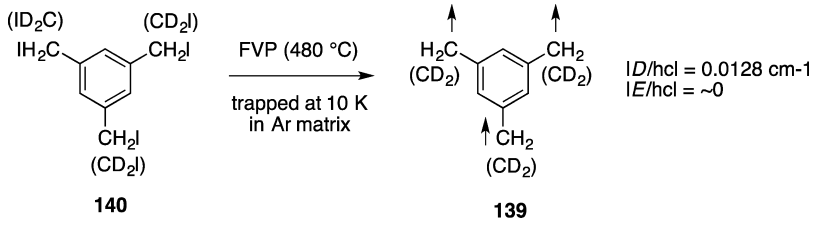

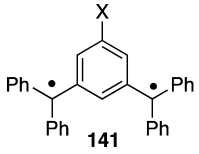

X	H	NMe_2	OH	Me	CF_3	COOH	CO	CN
J /cm^{-1}	602	517	581	585	615	607	617	617

Figure 74. Effect of substituent X on the exchange coupling constant (J /cm^{-1}).

Scheme 47. Generation of Trimethylenemethane (TMM) Derivative DR68

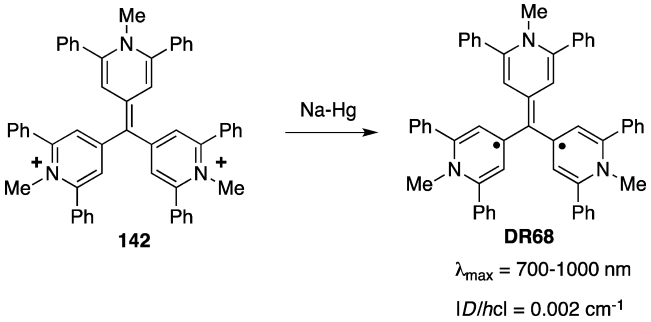

0.71 V vs AgCl/Ag$^+$ and two reversible one-electron reduction waves at E_{red} = −1.42 and 1.86 V vs AgCl/Ag$^+$. Thus, compound **109** also has a small HOMO−LUMO energy spacing, ΔE_{onset}^{redox} = 1.64 eV.

Extended viologen derivative **110** was first synthesized by Porter et al. in 2005 (Figure 57).[252] From the X-ray crystal structure, the central C—C bond length (1.438 Å) was found to be greater than that in the neutral methyl viologen (C═C, 1.363 Å), as well as that in the phenyl viologen dications (C—C, 1.485 Å). Thus, the viologen has the character of an open-shell singlet diradical, which can be drawn as a resonance structure. In the NMR spectrum, although clear signals corresponding to the methyl protons and some CH_2 protons of the *n*-octyl group were observed, a broad resonance signal was observed around 6.4 ppm. The vinyl protons on the quinoidal carbons could not be identified. The broad signal suggests the presence of unpaired electrons on the ring systems. However, ESR signals were not observed because of the singlet-ground-state spin multiplicity. Casado and co-workers succeeded in observing the rapid thermal singlet-to-triplet intersystem crossing in the viologen derivative using Raman spectroscopy.[253,254] The singlet−triplet energy gap in the planar form was calculated to be −2.98 kcal mol^{-1} at the MRMP2//CAS(10,10) level of theory. The twisted structure was found to be the most stable triplet structure, with an energy calculated to be ∼0.5 kcal mol^{-1} less than that of the planar singlet quinoidal structure.

The stability of the imidazolyl radical moiety was utilized to prepare Kekulé hydrocarbon **111** (Figure 58). The singlet state was calculated to be more stable than the triplet state by 4.35 kcal mol^{-1} at the B3LYP/6-31G(d) level of theory. Interestingly, the Kekulé hydrocarbon with a blue-purple color thermally dimerized to the colorless dimer **112**.[255] Thus, a photochromic color change was observed upon irradiation. Upon irradiation with 360-nm light, the colorless

dx.doi.org/10.1021/cr400056a | *Chem. Rev.* 2013, 113, 7011−7088

Scheme 48. Thermoluminescence (TL) from the Radical Ion Pair of Arylated Methylenecyclopropanes 143

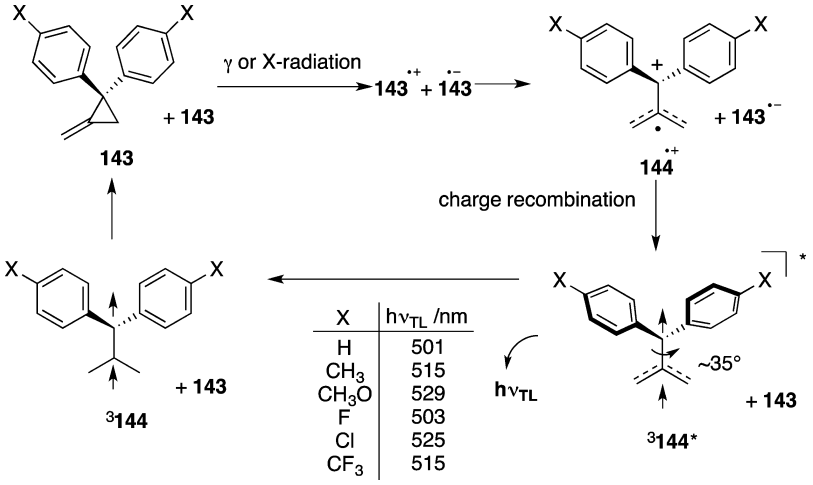

Scheme 49. Generation of Tetramethyleneethane (TME) Derivative DR69 in the Photoinduced Electron-Transfer Reaction of Distyrylfuran Derivative 145

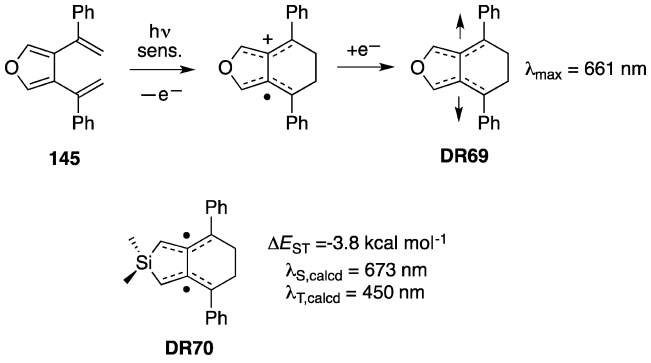

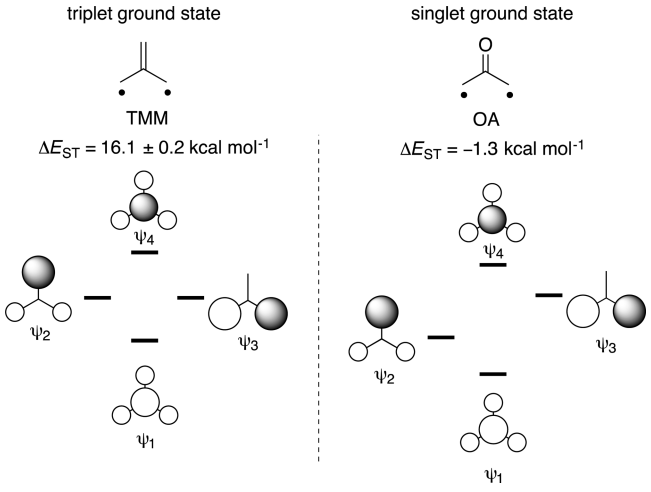

Figure 75. Trimethylenemethane (TMM) versus oxyallyl (OA).

Table 3. Computed Singlet−Triplet Energy Gaps ($\Delta E_{ST} = E_S - E_T$) in TMM and OA

	ΔEST = 2J in kcal mol-1	
exp.	16.1	-1.3
UBLYP	15.8	-3.5
UB3LYP	21.6	1.2
MkCCSD	15.8	-1.6

with acc-PVDZ

Scheme 50. Generation of DR71 in the Photochemical Decarbonylation Reaction of the Cyclobutane-1,3-diyl Derivative 146

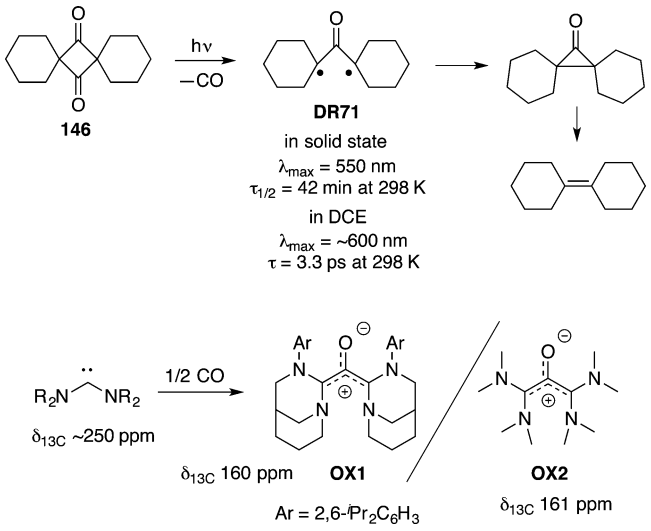

benzene solution quickly became blue-purple with a concomitant increase in the 609-nm signal.

Phenalenyl **113** is the smallest open-shell graphene, in which the unpaired electron is highly delocalized on the aromatic ring system (Figure 59). Haddon proposed the potential use of phenalenyl as a component for a molecular-based conductor, because of its small HOMO−LUMO energy spacing, ~1.6 eV.[256] Such a characteristic feature has been widely utilized for exploring new conjugated electronic systems such as amphoteric redox species. The parent phenalenyl is intermolecularly reactive to give the dimer. The tri-*tert*-butyl-substituted phenalenyl was synthesized and isolated as a stable radical.[257,258] The isolation of the phenalenyl opened up a new field of chemistry.

Kubo and co-workers prepared the series of Kekulé hydrocarbons **114−116** with phenalenyl-ring units (Figure

dx.doi.org/10.1021/cr400056a | Chem. Rev. 2013, 113, 7011−7088

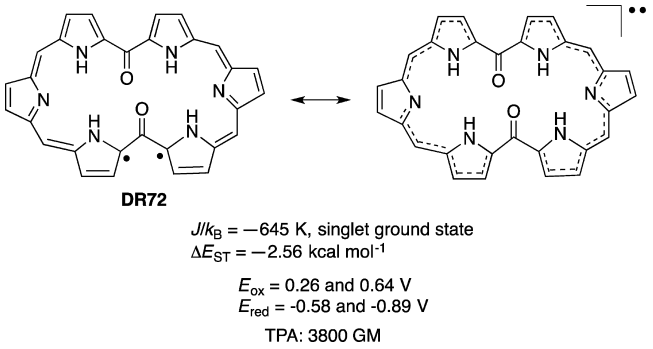

Figure 76. Singlet ground state of deketohexaphyrin **DR72**.

Scheme 51. Detection of 1,4-Dioxy Diradical DR73, an Oxygen Analogue of TME, in the Decomposition Reaction of 1,2-Dioxetanedione 147

Table 4. Electron Affinities (EAs) of Benzoquinone Derivatives

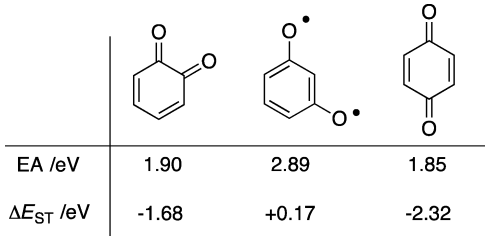

60).[259−266] The two phenalenyl units are connected to benzene (n = 1), naphthalene (n = 2), and anthracene linkers. The aromaticity of the linkers increases with the number of benzene rings, as indicated by the homodesmic stabilization energy (HSE), from which aromaticity can be quantitatively evaluated: benzene (HSE = 89.9 kJ mol^{-1}), naphthalene (HSE = 137.2 kJ mol^{-1}), anthracene (HSE = 173.4 kJ mol^{-1}). With increasing aromaticity of the linker, the percentage diradical character (DR) increased from 30%, to 50%, and to 68%. The diradical character was determined by natural orbital occupation number (NOON) analysis, that is, by determining the occupation number of the LUMO of the diradicals. The HOMO−LUMO energy gaps (in electronvolts) for **112**−**114** were determined by UV−vis electronic absorption spectroscopy (and cyclic voltammetry analyses), being to be 1.64 (1.20), 1.43 (1.04), and 1.26 (0.98), respectively. All of these Kekulé hydrocarbons are singlet-ground-state molecules. Their singlet−triplet energy spacings were calculated to be 30, 19, and 12 kJ mol^{-1}, respectively, at the UB3LYP/6-31G(d) level of theory.

When the R group is hydrogen (R = H), superimposed phenalenyl overlaps were observed for all of these Kekulé hydrocarbons. The distance of the phenalenyl ring was determined to be ∼3.1 Å, which is significantly shorter than the van der Waals radius of the carbon atom (3.4 Å). The intermolecular interaction is indispensable for electron movement. An OFET of **112b** exhibited ambipolar transport with balanced hole and electron mobility on the order of 10^{-3} cm^2 V^{-2} s^{-1}. Polarized reflection measurements clearly indicated that a balanced intra- and intermolecular covalent interaction was found for **114**. In contrast, the intermolecular covalent interaction was much stronger than the intramolecular interaction in **114b**. This observation is quite reasonable, because the diradical character in **114a** is much higher than that in **112a**.

Kekulé hydrocarbons with small HOMO−LUMO energy gaps and large contributions of diradical character provide unique properties for optoelectronic devices,[267] singlet fission,[268] and nonlinear optical properties,[269] as well as for spintronics.[270,271] For example, a large two-photon-absorption

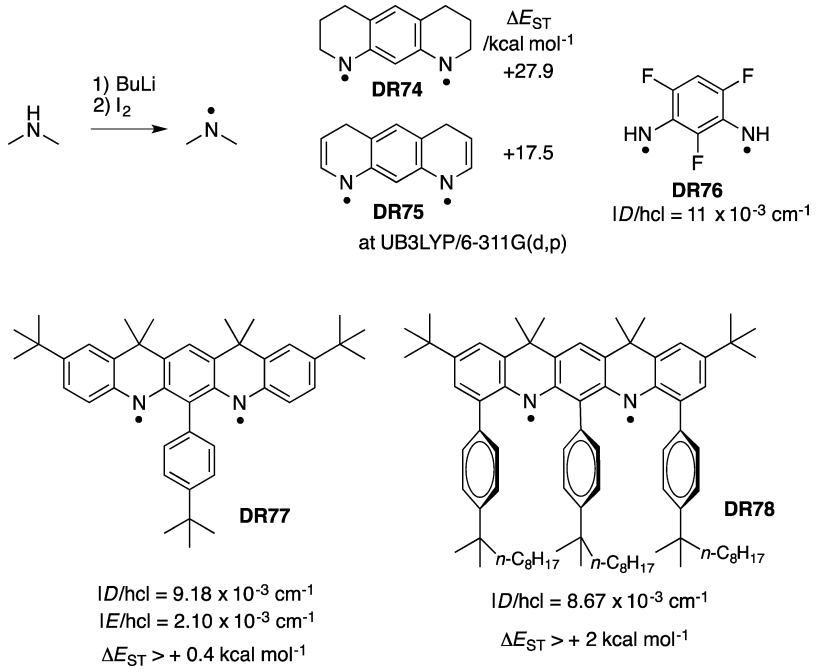

Figure 77. Generation of nitrogen-centered radicals and diradicals.

dx.doi.org/10.1021/cr400056a | Chem. Rev. 2013, 113, 7011−7088

Scheme 52. Generation and Isolation of *p*- and *m*-Disilaquinodimethanes DR80 and DR81 in the Reductive Dehalogenation of the Corresponding Bis(halosilyl)benzenes

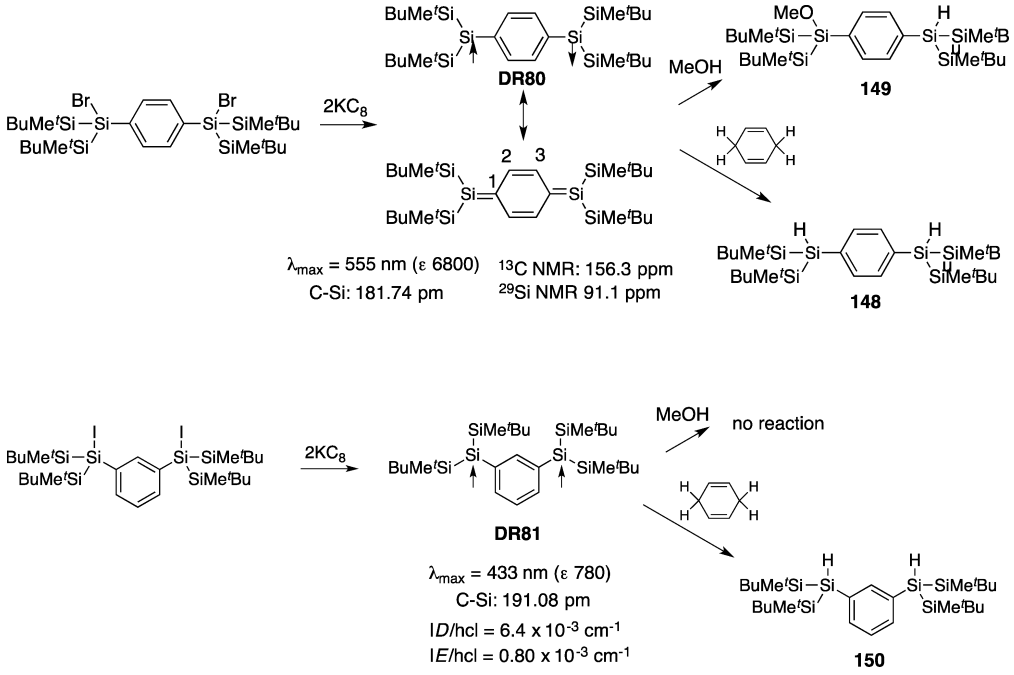

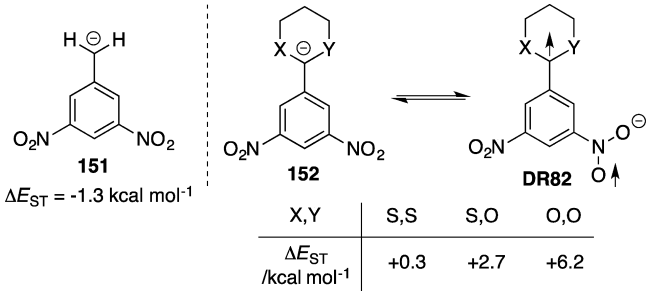

Figure 78. Diradical character of benzyl anions with strong π-electron-withdrawing groups at the meta positions.

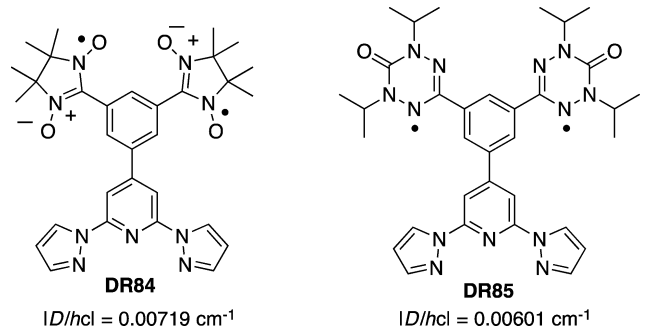

Figure 79. Nitronyl nitroxide- and oxoverdazyl-based meta-substituted diradicals **DR84** and **DR85**.

(TPA) cross section of 890 GM at 1500 nm was found for Kekulé hydrocarbon **114a**.

Wu and co-workers focused on zethrene and its homologue, heptazathrene, to construct stable Kekulé hydrocarbons with small HOMO−LUMO energy gaps (Figure 61).[272−274] The name of "zethrene" was derived from the Z-shaped molecular structure. First, the smallest-sized compound, **117**, was prepared from the acetylene derivative. This molecule had no or negligible diradical character but rather exhibited a normal closed-shell character. However, the homologue **118** with heptazethrene actually showed an open-shell character with a

Scheme 53. Generation of Cation 154 with Diradical Character in the Photolysis of 155

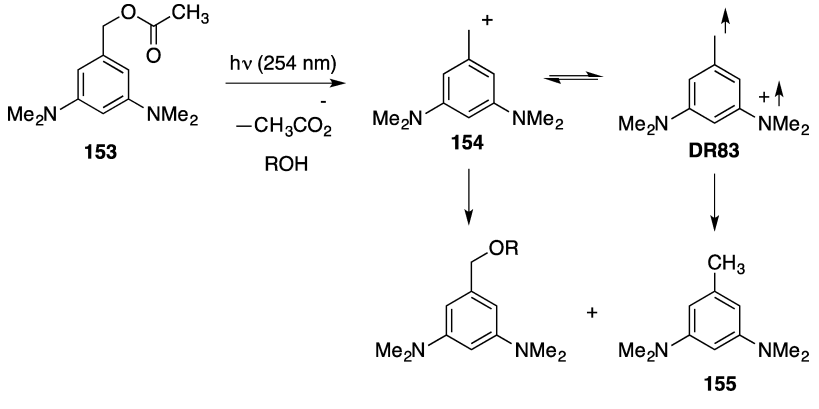

dx.doi.org/10.1021/cr400056a | Chem. Rev. 2013, 113, 7011−7088

Scheme 54. Heteroatom Analogue of Trimethylenemethane (TMM) DR86

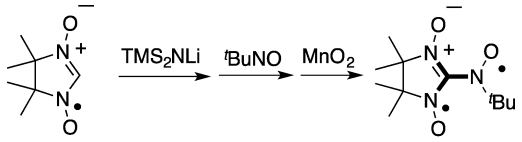

DR86

small HOMO−LUMO energy gap of 0.99 eV. The open-shell singlet diradical ($\langle S^2 \rangle$ = 1.017) was calculated to be more stable in energy than the triplet state and the closed-shell molecule by 7.5 and 5.8 kcal mol^{-1}, respectively, at the CAM-B3LYP level of theory. Because of the relatively large singlet−triplet energy gap, ESR signals were not observed. Thus, the spin−spin interaction was not directly measured.

A new family of stable Kekulé hydrocarbons with the zethrene structure was synthesized from easily available compounds (Figure 62). Compound **119**, with a heptazethrene unit, showed well-resolved NMR and absorption spectra (λ_{max} = 634 nm). The well-resolved NMR spectrum suggested the closed-shell character of **119**. The higher analogue **120** was found to have a blue-to-green color with absorption spectrum maxima at 795, 719, 668, and 613 nm. In contrast to the well-resolved NMR signal of **119**, the shape of the NMR signals around the central aromatic ring in **120** was largely dependent on the temperature. Thus, the aromatic protons became sharp below 0 °C. The effect of temperature on the NMR spectrum is typical for open-shell singlet-ground-state molecules. The broadening is due to the thermally accessible triple state. The singlet−triplet energy spacing of **120** was determined to −3.9 kcal mol^{-1} by superconducting quantum interference device (SQUID) measurements of a powder sample at 5−380 K. The singlet−triplet energy spacing was calculated to be −4.4 kcal mol^{-1} at the CAM-B3LYP level of theory. Thus, the DFT method reproduced the experimental value well. According to DFT computations, the singlet−triplet energy spacing of **119** was determined to be −8.1 kcal mol^{-1}. The thermal equilibration between the singlet diradical and triplet diradical of **120** was confirmed by Raman spectroscopic analysis. The magnitude of the two-photon-absorption (TPA) cross section was found to be 920 and 1200 GM at 1250 nm. Small HOMO−LUMO energy gaps were found in electrochemical measurements of compounds **119** and **120**. Compound **119** showed two reversible oxidations with half-wave potentials ($E_{ox}^{1/2}$) at 0.17 and 0.69 V and two reversible reductive waves with half-wave potentials ($E_{red}^{1/2}$) at −1.48 and −1.86.

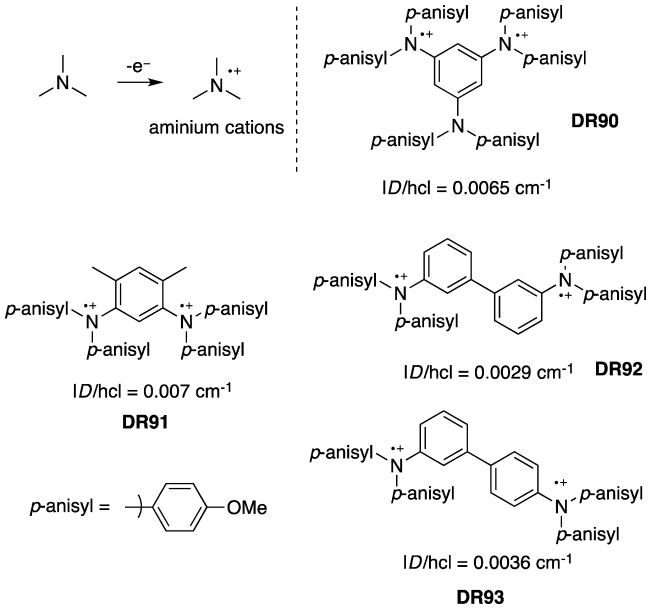

Figure 80. Generation of stable aminium radical cations by electrochemical and/or chemical oxidation.

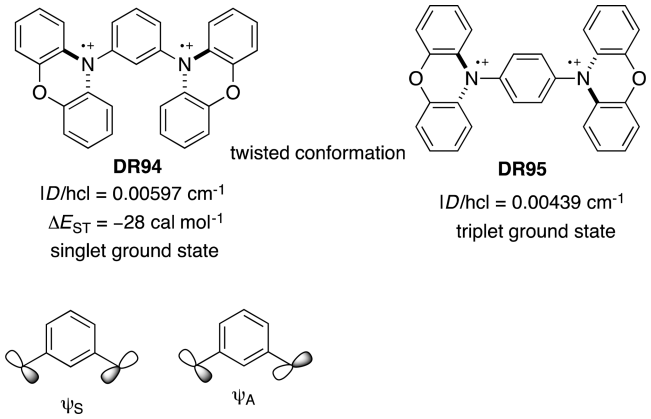

Figure 81. Conformational effects on the ground-state spin multiplicity in diradical dications **DR94** (singlet) and **DR95** (triplet).

Compound **120** showed three reversible oxidation waves at 0.02, 0.22, and 0.61 V and three reversible reductive waves at −1.30, −1.56, and −1.82 V. The first electrochemical energy gap (ΔE_1^{redox}) was determined to be 1.65 and 1.32 eV for **119** and **120**, respectively.

Scheme 55. Preparation of Nitroxide-Substituted Nitronyl Nitroxide DR87 and Iminonitroxide DR88 from 2-Methyl-2-nitrosopropane

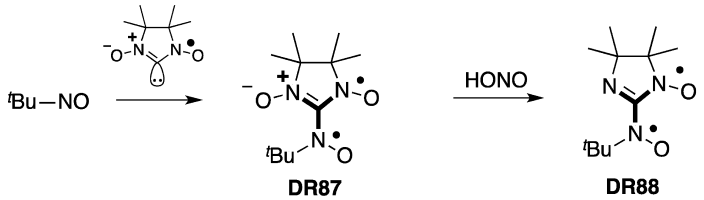

DR87
|D/hcl| = 0.0250 cm^{-1}
|E/hcl| = 0.0016 cm^{-1}
J/k_B = +390 K
$\Delta E_{ST} = 2J/k_B$ = +1.56 kcal mol^{-1}

DR88
|D/hcl| = 0.0639 cm^{-1}
|E/hcl| = 0.0050 cm^{-1}
J/k_B = +550 K
$\Delta E_{ST} = 2J/k_B$ = +2.20 kcal mol^{-1}

dx.doi.org/10.1021/cr400056a | Chem. Rev. 2013, 113, 7011−7088

DR96

D = ~0.0145 cm^{-1}, E ~ 0

ΔE_{ST} = −320 cal mol^{-1}

DR97

D = ~0.0276 cm^{-1}, E ~ 0.0016 cm^{-1}

ΔE_{ST} = 10 cal mol^{-1}

Figure 82. Singlet ground state of the diradical dication of 1,4-bis(hydrazino)benzene **DR96** and triplet ground state of **DR97**.

Teranthracene derivative **121** with open-shell singlet diradical character was synthesized by Konishi et al. (Figure 63).[275] The compound was prepared in four steps from the anthranyl bromide. X-ray crystallographic analysis of compound **121** revealed that the two mesityl-groups kinetically stabilized the radical sites, and thus, the compound was found to be relatively stable. Compound **121** was reported to decompose with a half-life of 3 days upon exposure to air under room light at room temperature. CASSCF(2/2)-level computations clarified that the parent teranthracene has a diradical character of 0.42. Isolated compound **121** was found to be an open-shell singlet-ground-state molecule with a singlet−triplet energy gap of 16 kcal mol^{-1}, which was determined by SQUID measurements. The cyclic voltammogram of compound **121** showed four reversible redox waves, including E_2^{ox} = +0.09 V, E_1^{ox} = −0.35 V, E_1^{red} = −1.40 V, and E_2^{red} = −1.76 V (all vs Fc/Fc$^+$). Thus, the HOMO−LUMO energy gap was determined to be 1.05 eV. The electronic absorption spectrum exhibited a low-energy band at 1054 nm, from which the HOMO−LUMO energy gap was determined to be 1.18 eV. The high diradical character is due to the small HOMO−LUMO energy spacing.

Zhang et al. proposed a new strategy using benzannulation of the central biphenyl unit of Tschitschibabin's hydrocarbon to stabilize and isolate Kekulé hydrocarbons (Figure 64).[276] They first introduced the anthracene structure into quinoidal hydrocarbon **122**. The NMR signals of compound **122** were quite sharp at high temperature, indicating that the compound is a closed-shell singlet species. Because of the highly congested units of the bianthracene, the central two anthracene rings are not planar; thus, a double-saddle-like structure was found by calculations.

For the hydrocarbon system, Zeng et al. and Sun and Wu reported the synthesis of a closed-shell singlet compound and an open-shell diradical (Figure 65).[277,278] Closed-shell singlet species **123** was prepared from a 4-fold Suzuki−Miyaura coupling reaction of the tetrabromide. All of the NMR signals were observed to be sharp, and the electronic absorption maximum was observed at 349 nm, which is typical for closed-shell molecules. Indeed, the closed-shell structure was confirmed by X-ray crystallographic analysis. The double-saddle-like structure was reproduced well by computational optimization at the UCAM-B3LYP/6-31G(d) level of theory. Open-shell diradical **124** was generated by the $SnCl_2$-reduction of the diol **125**. The freshly generated species from the diol displayed a broad absorption spectrum with λ_{max} = 834 nm and a strong ESR signal at g = 2.0029. Thus, the species was assigned to the triplet state of the open-shell diradical **124**. An almost-perpendicular conformation of the central two anthraces moiety was found computationally at the UCAM-B3LYP/6-31G(d) level of theory. The first-order decay process to the closed-shell compound was monitored for the open-shell diradical, and the activation parameters were determined to be 38.5 ± 5.1 kJ mol^{-1} and −189.5 ± 0.6 J mol^{-1} for $\Delta H^{‡}$ and $\Delta S^{‡}$, respectively. According to UDFT calculations, the open-shell singlet diradical is located above the closed-shell compound and the triplet diradical by 18.4 and 2.5 kJ mol^{-1}, respectively.

In contrast to the stability of closed-shell compound **123**, the fluorenyl derivative was isolated as an open-shell diradical. The compound did not show any NMR signals at room temperature or even at −100 °C, indicating the presence of a considerable paramagnetic species (Figure 66). Actually, a strong ESR signal was observed for compound **126**. From SQUID measurements at 5−380 K, the singlet−triplet energy gap was determined to be 1.4 kJ mol^{-1}. The triplet is the ground-state spin multiplicity. The experimental finding was reproduced by UCAM-B3LYP calculations, from which the energy gap was found to be 2.5 kJ mol^{-1}. The triplet state was calculated to be lower in energy than the singlet state.

Zhu et al. reported the synthesis of air- and heat-stable planar tri-*p*-quinodimethane **127** with a distinct diradical character (Figure 67).[279] The tri-*p*-quinodimethane was prepared from the bisacetylene and obtained as a green solid. Compound **127** showed ^{13}C NMR signals only from the sp^3 carbon atoms and *n*-octyl groups. The ^{1}H NMR signals showed temperature-dependent broadening, suggesting the open-shell character of compound **127**. The ESR signal of **127** at 340 K in the solid state exhibited a signal at g = 2.003 with a typical triplet signal. From the D value, the distance between the two spins was estimated to be 15 Å. The singlet state was found to be the ground-state spin multiplicity, with an energy gap of 2.12 kcal mol^{-1}, which was determined by SQUID measurements. BS-UB3LYP calculations suggested that the open-shell singlet state is more stable than the closed-shell singlet state by 5.21 kcal mol^{-1}. The open-shell singlet molecule has a very narrow band gap of ca. 1 eV, which was determined by UV−vis and CV measurements.

Haley and co-workers synthesized indeno[1,2,-*b*]fluorene structure **128**, a 6−5−6−5−6 fused ring system, and an antiaromatic 20π ring system.[280−282] The structure inherently has diradical character because of the *para*-quinoidal structure (Figure 68). Tetraalkynyl-substituted indeno[1,2-*b*]fluorenes

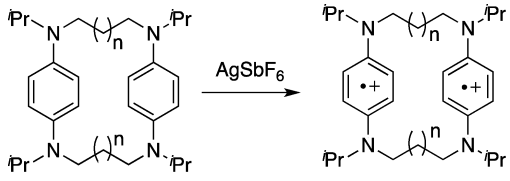

DR98

n = 1: ΔE_{ST} = −70 cal mol^{-1}, = −25 cm^{-1} = −36 K

|D/hc| = 0.0065 cm^{-1}

|E/hc| = 0.00 cm^{-1}

n = 3: ΔE_{ST} = −50 cal mol^{-1}, = −17 cm^{-1} = −25 K

Figure 83. Singlet ground state of diradical dications **DR98**.

dx.doi.org/10.1021/cr400056a | *Chem. Rev.* 2013, 113, 7011−7088

Scheme 56. Synthesis of the Triplet Ground State of Air-Stable Diradical DR99

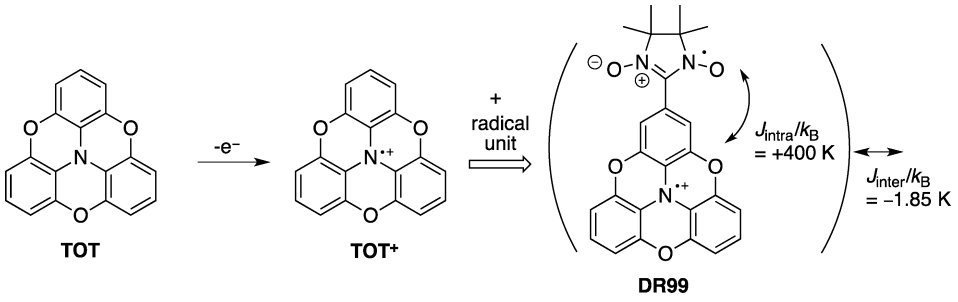

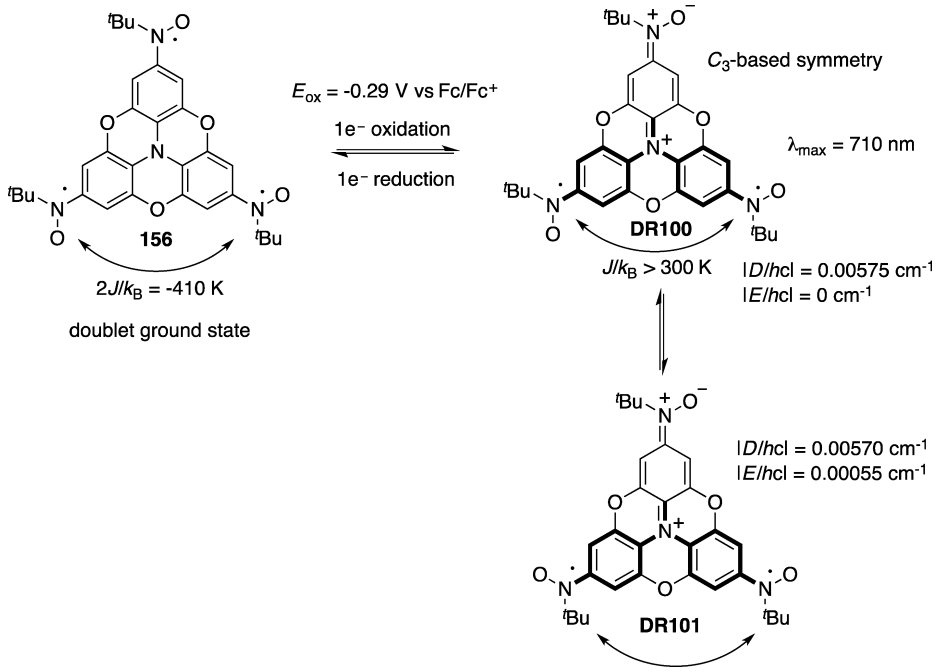

Figure 84. Change in spin state from the doublet species to the triplet state upon oxidation.

Scheme 57. Generation of a Dication from the Double-Layered Triphenylamine (TPA) Linked by Three *meta*-Phenylenediamine Pillars

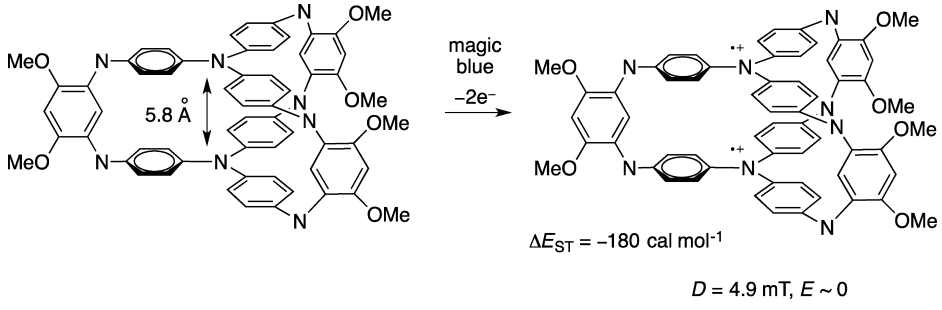

and a variety of their derivatives were synthesized using the $SnCl_2$ reduction of the corresponding alcohols. X-ray crystallographic analyses confirmed the existence of the antiaromatic 20π ring systems. The absorption maxima were observed in the visible region around 600 nm. The HOMO−LUMO energy gaps were determined to be around 1.9 eV by CV measurements. The compounds were found to be nonemissive. Antiaromatic 24π ring system **129** was also synthesized using a method similar to that used for the 20π-electron system, and the open-shell character was investigated using NMR measurements and quantum chemical calculations. The deep-blue solution of **129** with λ_{max} = 649 nm exhibited no line broadening even at 160 °C, and the ESR spectrum of the powder sample showed no triplet signals. An $\langle S^2 \rangle$ value of 0.0001 was obtained from calculations on the open-shell singlet state at the UB3LYP level of theory. The triplet state was calculated to be 16.1 kcal mol^{-1} higher in energy than the singlet state. Cyclic voltammetry for **129** exhibited redox amphoterism with two reversible reductions and two oxidations. The first reduction half-potential was found to be −0.87 V and the second was −1.29 V, whereas the first

dx.doi.org/10.1021/cr400056a | *Chem. Rev.* 2013, 113, 7011−7088

oxidation half-potential was 0.82 V, and the second was 1.27 V. The LUMO energy of **129** was estimated at −3.77 eV from CV.

The singlet−triplet energy differences (ΔE_{ST} in kcal mol^{-1}) in tetracyano-oligo-(*N*-annulated perylene)-quinodimethanes **130** were reported to be largely dependent on the value of *n* (Figure 69).[283] SQUID measurements on the compounds with *n* = 2−6 at 5−300 K revealed the ground-state spin multiplicity. The singlet ground state was found for *n* = 2 and 3 with ΔE_{ST} = −0.342 and −0.107, respectively, whereas the triplet ground state was reported for *n* = 4−6 with ΔE_{ST} = 0.064, 0.556, and 0.883, respectively.

A singlet diradical character of π-conjugated oligomer dications **131** composed of thiophene and pyrrole was reported by Nishinaga et al.[284] Absorption peaks was observed in the near-IR region at 965 and 1093 nm (Figure 70).

In 2006, Hiroto et al. found the singlet diradical character of a doubly linked corrole dimer (Figure 71).[285] The DDQ (2,3-dichloro-5,6-dicyano-*p*-benzoquinone) oxidation of the precursor corrole dimer **132** produced **133** quantitatively. The ^{1}H NMR spectrum of the bis(zinc) complex was found to be very broad even at −90 °C. An ESR signal was obtained at room temperature at *g* = 2.0053, indicating the existence of an unpaired electron. From the temperature-dependent change of the magnetic susceptibility of the oxidation product, the singlet state was found to be the ground-state spin multiplicity with an energy gap of *J* = −330 cm^{-1}. The singlet ground state was reproduced by DFT calculations at the BS-B3LYP/631TZVP level of theory, from which the singlet state was located 178 cm^{-1} below the triplet state. Cyclic voltammetry of **132** exhibited two reversible oxidation potentials at 0.20 and 0.38 V and two reversible and one irreversible reduction potentials at −0.19, −034, and −1.9 V, respectively. The gap between the first oxidation and reduction potential (ΔE_1^{redox}) was found to be only 0.40 V, suggesting a small HOMO−LUMO energy spacing.[286]

In 2010, Passmore and co-workers reported the synthesis of stable main-group diradical **DR67** (Figure 72).[287] X-ray crystallographic analysis revealed that the trans-planar geometry of **DR67** is stabilized by inter-ring $Sd^+\cdots Nd^-$ electrostatic interactions. The C−C single bond (1.462 Å) joines the 7p rings. The experimentally found structure is in good agreement with that predicted at the [12,12]CASSCF/6-311G(d) level of theory. The calculated geometries of the triplet and open-shell singlet states are almost identical, implying very weak or even negligible interaction between the unpaired electrons. The triplet was calculated to be the ground-state spin multiplicity (ΔE_{ST} = +264 cm^{-1}) at the [12,12]CASPT2 level of theory. For quinoidal structure **134**, the closed-shell singlet state was found to be less stable than the open-shell singlet state by ca. 100 kJ mol^{-1}. The valuable temperature magnetic studies gave an energy difference between the open-shell singlet and triplet states of less than ±2 cm^{-1}.

3.4. Non-Kekulé Delocalized Diradicals[288−290]

Non-Kekulé delocalized molecules are defined as molecules that are fully conjugated but have Kekulé structures that contain at least two atoms that are not π-bonded. Typical examples of non-Kekulé diradicals are *meta*-quinodimethane (*m*-QDM), trimethylenemethanes (TMMs), 1,8-naphthoquinodimethane (NQDM), tetramethylenemethane (TME), and tetramethylenebenzene (TMB) (Figure 73). Davidson and Borden showed that, when the degenerate nonbonding molecular orbitals (NBMOs) are disjoint (i.e., have no atoms in common), there is no strong spin-state preference.[291] However, when the orbitals are nondisjoint, the triplet state experiences less electron repulsion than the singlet state, leading to a triplet ground state. Thus, the first three non-Kekulé molecules are categorized as nondisjoint-type diradicals, which generally have a triplet ground state. The last two molecules belong to the disjoint type of diradicals, which generally have a singlet ground state.

***m*-QDM Derivatives.** *meta*-Quinodimethane (*m*-QDM), *m*-xylylene, is the parent molecule of high-spin polyradical systems with *meta*-phenylene coupling units. The photochemical generation of *m*-xylylene using UV light has frequently been used for detecting inherently reactive species under low-temperature matrix conditions. However, *m*-xylylene itself is a highly photolabile species, which makes the species difficult to generate and detect feasibly. In 2008, Neuhaus et al. accomplished the clean generation and detection of *m*-xylylene from 1,3-bis(iodomethyl)benzene **135** using flash vacuum pyrolysis (FVP) at 450−500 °C and the subsequent trapping of the species in argon at 10 K (Scheme 45).[292] Irradiation of the matrix-isolated *m*-xylylene with visible light (>400 nm) resulted in a decrease of the IR bands to give the two new compounds, which were assigned as **136** and **137** on the basis of a comparison of the IR spectra with those calculated at the B3LYP/6-311G(d,p) level. Irradiation at a slightly shorter wavelength resulted in rearrangement from **137** to **136**. Short-wavelength UV irradiation (254 nm) led to the formation of 3,5-dimethylene-tricyclohexane **138**.

In 2010, the FVP method was successfully applied to generate 1,3,5-trimethylenebenzene **139**. The triradical was isolated using flash vacuum pyrolysis of 1,3,5-tris(iodomethyl)-benzene or deuterated derivative **140** with subsequent trapping of the products in argon at 10 K (Scheme 46).[293] The structural assignment was confirmed by comparison of the IR spectrum with those calculated at various levels of theory. Weak electronic absorption signals were found at 367 and 254.9 nm at 10 K under argon matrix conditions. Further evidence for the formation of the triradical was obtained by measuring the ESR spectrum. A five-line ESR spectrum centered at 3427 G was obtained. At 5 K, the spectrum was found to persist for days without any change. A half-field signal at 1708 G and a very weak signal at 1130 G corresponding to a $\Delta m_s = \pm 3$ transition appeared together with the main signals at *g* = 2. The simulation of a quartet state ($S = {}^3/_2$) with zero-field-splitting parameters $|D/hc|$ = 0.0128 cm^{-1} and $|E/hc|$ = 0 cm^{-1} was found to give the best agreement with the experimental spectrum.

The effect of substituent X on the exchange coupling constant (*J*, cm^{-1}) was investigated for the Schlenk diradical **141** at the broken-symmetry (BS)-UB3LYP/6-311++G(d,p) level of theory (Figure 74).[294] The diradicals were predicted to be ferromagnetically coupled (*J* > 0), in agreement with the experimental finding by Rajca and co-workers. Substituents with +M and +I effects decrease the singlet−triplet energy gap, whereas those with −I and −M effects increase the *J* value, where +M represents mesomerically electron-donating substituents (X = NMe_2, OH), +I represents inductively electron-donating substituents (X = CH_3), −M represents mesomerically electron-withdrawing substituents (X = CN, CHO, COOH), and −I represents inductively electron-withdrawing substituents (X = CF_3). The calculated results were explained in terms of the influence of the functional groups on the spin density of the coupler.

dx.doi.org/10.1021/cr400056a | *Chem. Rev.* 2013, 113, 7011−7088

TMM Derivatives. The trimethylenemethane (TMM) derivative **DR68**, in which the parent TMM is π-extended, was synthesized by the alkali-metal reduction of the isolated corresponding dication **142** (Scheme 47).[295] The frozen-glass X-band cw-ESR spectrum of diradical **DR68** gave unresolved fine structure because of the small zero-field-splitting parameter of $|D/hc| = 0.002$ cm^{-1}. Pulsed ESR two-dimensional electron spin transient nutation spectroscopy revealed that the triplet state of the diradical **DR68** was generated in the reduction of **142**.

Ikeda and co-workers found thermoluminescence (TL) from the radical ion pair of arylated methylenecyclopropanes **143** (Scheme 48).[296−298] The ring opening of the radical cation of the methylenecyclopropane to the trimethylenemethane radical cation **144** was found to be the key for the thermoluminescence from the triplet excited state of TMM derivatives **144**. The wavelength ($h\nu_{TL}$) of the thermoluminescence was found to be substituent- (X-) dependent. The effect of the substituent on the wavelength was correlated with the radical stabilizing parameter ($\sigma^{\bullet}$) for benzyl radicals.

TME Derivatives. In 2008, the generation of tetramethyleneethane (TME)[49] derivative **DR69** was reported in the photoinduced electron-transfer reaction of distyrylfuran derivative **145** (Scheme 49). The singlet-ground-state diradical **DR69** was observed at $\lambda_{max} = 661$ nm.[299] DFT computational predictions of the ground-state spin multiplicity and electronic properties, including excitation energies, were obtained for silole-fused TME diradical **DR70**.[300] The singlet state was found to be the ground-state spin multiplicity with an energy difference of 3.8 kcal mol^{-1}. A blue shift of the wavelength of electronic transition in the triplet state, $\lambda_{calcd} = 450$ nm, was calculated in comparison with the wavelength of the singlet state, $\lambda_{calcd} = 673$ nm.

Oxyallyls (OAs). Trimethylenemethane (TMM) derivatives have been the subject of many theoretical and experimental studies. The nondisjoint diradicals are triplet-ground-state molecules, for example, the singlet−triplet energy spacing was found to be 16.1 kcal mol^{-1} for the parent TMM, because nonbonding molecular orbitals ψ_2 and ψ_3 are degenerate (Figure 75). The long-lived character of the triplet state makes it possible to detect the species using conventional spectroscopic methods such as ESR spectroscopy. In contrast to the well-investigated chemistry of TMMs, the oxygen analogues, oxyallyls (OAs), which have been postulated as intermediates in the ring-opening of cyclopropanone, Favorskii rearrangement, and prostaglandin biosynthesis, have only recently been directly detected and isolated.

Ichino et al. succeeded in measuring the photoelectron spectrum of the OA radical anion.[301] The spectroscopic analysis determined a singlet−triplet energy spacing of 1.3 kcal mol^{-1} with a singlet ground state. The singlet ground state can be explained by the energetic stabilization of the ψ_2 orbital due to the electronegative character of oxygen atoms (Figure 75). CASPT2/CASCF(4/4) calculations confirmed the experimental findings and revealed that the planar structure of the singlet OA has a very shallow energy minimum, which vanished when zero-point corrections were considered.[302,303] Thus, OA is considered to be a transition state for the disrotatory ring-closing reaction. Lopez et al. used natural orbital functional (NOF) theory to investigate TMM derivatives.[304]

Singlet−triplet energy gaps determined by experiments are very important benchmarks for assessing computational methods. The singlet−triplet energy gaps for TMM and OA were calculated by the multireference CCSD and broken-symmetry (BS) DFT methods. As shown in Table 3, the low-cost computational method at the UBLYP/cc-pVDZ level qualitatively reproduced the experimentally obtained energy differences. Mukherjee's state-specific multireference coupled-cluster singles and doubles (MkMRCCSD) method was found to quantitatively reproduce the experimentally determined energy differences.[305]

The kinetically stabilized OA derivative **DR71** was generated and detected in the Norrish type-1 reaction, a photochemical decarbonylation reaction, of the cyclobutane-1,3-diyl derivative **146** (Scheme 50). Thus, the photochemical decarbonylation reaction in the crystalline solid state resulted in the formation of a deep-blue-colored transient species with $\lambda_{max} = 550$ nm and a half-life of 42 min at 298 K.[306,307] The lifetime of **DR71** was determined to be 3.3 ps in dichoroethane (DCE) solution at room temperature. The clean formation of OA was achieved because of the ring strain of the cyclobutane-1,3-dione structure. Very recently, isolable oxyallyls **OX1**[309] and **OX22**[310] were reported by in the reaction of CO with 2 equiv of Bertrand- or Alder-type carbenes $(R_2N)_2C$: (Scheme 50).

Koide et al. and Ishida et al. isolated and characterized the singlet-ground-state deketohexaphyrin **DR72** (Figure 76).[308,311] The temperature effect on the magnetic susceptibility of **DR72** indicated a singlet ground state with an energy gap of $J/k_B = -645$ K ($\Delta E_{ST} = -2.56$ kcal mol^{-1}). Cyclic voltammetry of **DR72** revealed two reversible oxidation and reduction potentials at 0.26 and 0.64 V and at −0.58 and −0.89 V (vs Fc/Fc$^+$), respectively. The small gap between the first oxidation and reduction potentials was determined to be 0.84 V. Open-aperture Z-scan measurements revealed that the two-photon-absorption (TPA) cross section of **DR72** was 3800 GM. The large TPA cross section supports the singlet diradical character of **DR72**, because it has been well-established that molecules having diradical character exhibit an enhanced third-order nonlinear optical response (see section 5).

1,4-Dioxy diradical **DR73**, which is an oxygen analogue of TME, was detected in the decomposition reaction of 1,2-dioxetanedione **147** (Scheme 51).[312] A typical triplet ESR spectrum was observed at 130 K in THF. From the simulation of the triplet signals, the zero-field-splitting parameters were determined to be $|D/hc| = 0.041$ cm^{-1} and $E/D = 0.1$.

Heteroatom-Centered Non-Kekulé Molecules. Benzoquinones are biologically important molecules because of their presence in all organisms as proton-coupled electron-transfer agents. The electron affinities (EAs) and electronic structures are important in the molecular functions. Fu et al. succeeded in determining experimental EA values for all three benzoquinone isomers using photodetachment photoelectron spectroscopy (PES) (Table 4).[313] The EAs of *o*- and *p*-benzoquinone were determined to be 1.90 and 1.85 eV with singlet−triplet energy gaps of −1.68 and −2.32 eV, respectively. For the meta isomer, the spectrum was found to be distinctly different from those of the ortho and para isomers, with no clear band gap and a much higher EA value of 2.89 eV. The singlet−triplet energy gap was determined to be around 0.17 eV, with a triplet ground state.

Nitrogen-centered (aminyl) radicals are typically short-lived and have been detected as intermediates in a variety of chemical and biological processes. Their generation can be achieved by the deprotonation of amines, followed by oxidation by iodine (Figure 77). Aminyl diradicals, in which the aminyl radicals are connected through *m*-phenylene, are predicted by computa-

dx.doi.org/10.1021/cr400056a | Chem. Rev. 2013, 113, 7011−7088

tional studies to have a strong preference for a triplet ground state. Amiri and Schreiner reported the strong triplet preference of diradicals **DR74** and **DR75**.[314] As found for the carbon-centered *m*-QDM diradicals, a nitrogen-centered diradical with a large singlet−triplet energy spacing might be relevant to the design of magnetic materials and devices. In 1989, Haider first detected aminyl diradical **DR76** at 77 K in the generation of dinitrene.[315] The zero-field-splitting parameter $|D/hc|$ was determined to be 0.011 cm^{-1}.

In 2007 and 2010, Rajca and co-workers reported the isolation of triplet-ground-state aminyl diradicals **DR77** using the planar diamine platform **DR78**.[316,317] Double deprotonation of the diamines, followed by oxidation of the resultant dianions with iodine, was found to afford the diradicals. From the solid-state ESR spectrum, the zero-field-splitting parameter D was determined to be 9.18×10^{-3} cm^{-1} for **DR77** and 8.67×10^{-3} cm^{-1} for **DR78**, and the singlet−triplet energy spacings were determined to be greater than 0.4 and 2.0 kcal mol^{-1}, respectively.

In 2011, triplet-ground-state aza-*m*-xylylene diradical **DR79** with a large singlet−triplet energy gap of ∼10 kcal mol^{-1} was synthesized and characterized by Rajca et al.[318] The zero-field-splitting parameters were determined to be 1.75×10^{-2} cm^{-1} and 3.60×10^{-3} cm^{-1} for $|D/hc|$ and $|E/hc|$, respectively.

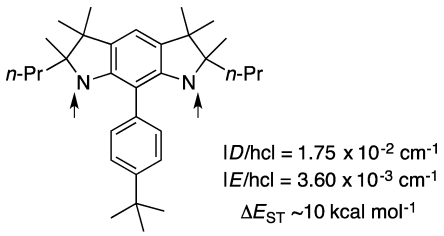

DR79

In 2011, *p*- and *m*-disilaquinodimethanes **DR80** and **DR81** were synthesized by the reductive dehalogenation of the corresponding bis(halosilyl)benzenes and isolated and structurally characterized (Scheme 52).[319] The longest-wavelength absorption of the para isomer **DR80** (λ_{max} = 555 nm, ε = 6800) was red-shifted compared with that of the meta isomer **DR81** (λ_{max} = 433 nm, ε = 780). The Si−C1 bond distance in **DR80** (181.74 pm) was found be shorter than typical single bonds (187.9 pm), and the C−C bond alternation characteristic of the cyclohexa-1,4-diene system was observed (i.e., C1−C2 = 142.3 pm, C2−C3 = 137.0 pm). Thus, the quinoidal structure was reasonably assigned to **DR80**. The singlet diradical character was assessed by hydrogen abstraction from cyclohexadiene to give the hydrogen-abstraction product **148**. The para isomer with closed-shell character was also found to react with methanol to give adduct **149**. In contrast to the reactivity of the para isomer, meta isomer **DR81** did not react with MeOH. The hydrogen-abstraction product **150** was formed in the reaction with cyclohexadiene. Thus, the meta isomer showed typical reactivity of open-shell molecules. Indeed, a typical triplet-state EPR spectrum was observed for meta isomer **DR81** at 80 K in 3-methylpentane. The zero-field-splitting parameters D and E were determined from the signals in the region of $\Delta m_s = \pm 1$ to be $|D/hc| = 6.4 \times 10^{-3}$ cm^{-1} and $|E/hc| = 0.80 \times 10^{-3}$ cm^{-1}, from which the radical−radical distance was estimated to be 589 pm.

Perrotta et al. reported a new family of *m*-xylyrenes. The benzyl anions with strong π-electron-withdrawing groups at the meta positions have diradical characters or triplet electronic states (Figure 78).[320] Although benzylic anion **151** with dinitro groups at both of the meta positions was predicted to have a singlet ground state at the UB3LYP/6-31+G(d,p) level of theory, the ketal-substitued diradical **DR82**, which contains the more-electron-donating ketal anions, and anion **152** were predicted to have triplet ground states because of the nondisjoint character of diradical **DR82**. ^{1}H NMR and ESR experiments showed that **DR82a** (X, Y = S, S) is actually paramagnetic.

Photochemical heterolysis of 3,5-bis(dimethylamino)benzyl ester **153** was found to generate cation **154** equilibrated with triplet diradical **DR83** (Scheme 53).[321] The formation of reduction product **155** provided evidence for diradical character with a small singlet−triplet energy gap.

Meta-substituted diradicals **DR84** and **DR85**, based on nitronyl nitroxide and oxoverdazyl, respectively, were prepared by Hui et al. (Figure 79).[322] The D value ($|D/hc|$ = 0.00719 cm^{-1}) for compound **DR84** was found to be larger than that for diradical **DR85** ($|D/hc|$ = 0.00601 cm^{-1}). Cryogenic ESR measurements of the two diradicals showed Curie magnetic behavior of the $\Delta m_s = \pm 2$ signal intensities down to 4.2 K. The results indicated that both of the diradicals are triplet-ground-state molecules or have very small singlet−triplet energy gaps.

Heteroatom analogue of trimethylenemethane (TMM) **DR86** was prepared and characterized by Tretyakov et al. (Scheme 54).[323] From the Bleaney−Bowers plot, a triplet ground state was found with an intramolecular exchange coupling of J/k_B = 400 K.

Before Tretyakov et al.'s report, Suzuki et al. reported that the nitroxide-substituted nitronyl nitroxide **DR87** (= **DR86**) and iminonitroxide **DR88**, which includes the TMM skeleton, were prepared by the nucleophilic addition of 2-lithio(nitronyl nitroxide) to 2-methyl-2-nitrosopropane, followed by oxidation by lead(IV) dioxide (Scheme 55).[324] Triplet ground states for both diradicals were determined by measuring the temperature dependence of the paramagnetic susceptibility. Thus, triplet ground states and large singlet−triplet energy gaps of +1.56 and +2.20 kcal mol^{-1} were determined for diradical **DR87** and **DR88**, respectively.

In 2012, Zhang et al. reported the synthesis and characterization of a derivative of 2,4-diimino-1,3-disilacyclobutanediyl **DR89**.[325] Although the parent 2,4-dimethylene-1,3-cyclobutanediyl (DMCB) is known to be a triplet-ground-state molecules, a singlet ground state was found for diradical **DR89**, with ΔE_{ST} = −30.1 kcal mol^{-1}, at the B3PW91/6-31G(d) level of theory.

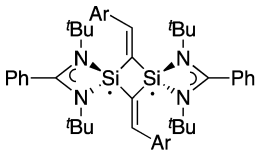

DR89

ΔE_{ST} = −30.1 kcal mol^{-1}
at the B3PW91/6-31G(d)

3.5. Aminium-Radical-Cation-Based Diradicals

Research on magnetic materials to find new magnetic properties that can be utilized for information storage and computer logic production has attracted much attention. Most magnetic materials are inorganic metals and alloys because of the stability and high-spin character at one atom. Organic

dx.doi.org/10.1021/cr400056a | Chem. Rev. 2013, 113, 7011−7088

materials are soft and well-designed. The instability of organic compounds is always pointed out as a disadvantage for use of these materials. Recently, however, air-stable organic radicals have been developed, and their magnetic characteristics have been well-studied. In this section, recent developments in the intramolecular and intermolecular magnetic properties of aminium-radical-cation-based diradicals are summarized.

Aminium radical cations that can be feasibly generated by electrochemical and/or chemical oxidation are well-known for their exceptional stability (Figure 80). In the 1990s, the electron−electron dipolar interaction was investigated in molecules that contain two aminium radical-cation units. As found in a family of delocalized non-Kekulé-type molecules, the ground-state spin multiplicity of bis(amino)-substituted radical cations was investigated by a combination of computational and experimental methods. Stickley and Blackstock designed high-spin molecules using the aminium radical-cation unit.[326] They found that the diradical dication of 1,3,5-tris(di-*p*-anisylamino)-benzene **DR90** is a triplet-ground-state molecule. Sato et al. reported that the dication of 1,3-bis(di-*p*-anisylamino)benzene **DR91** is also a triplet-ground-state molecule with a zfs *D* value of 0.007 cm^{-1}.[327] However, the dications of the biphenyl-linked isomeric diamines **DR92** and **DR93** were found to be singlet-ground-state molecules.[328]

An effect of conformation on ground-state spin multiplicity was typically found for the diradical dications of bis-(phenothiazine)benzene-substituted *meta*-phenylene diamine **DR94** (Figure 81). The phenothiazine group is easily oxidized to give radical cations with long lifetimes, because the phenothiazine group is 16-π-electron system. Triplet diradical ESR spectra were observed for diradicals **DR94** and **DR95**, with *D* values of 0.00597 and 0.00439 cm^{-1}, respectively.[329] The temperature-dependent change of the triplet signals clearly suggests that the ground state of diradical **DR94** is not the triplet state, but rather the singlet state with an energy gap of 28 cal mol^{-1}. On the other hand, a triplet ground state with a small singlet−triplet energy spacing was found for *para*-phenylene-substituted diradical **DR95**.[330] A conformational effect was first found for bis(*tert*-butyl nitroxide)-substituted *m*-phenylenes. Later, conformational-dependent changes in the ground-state spin multiplicity were investigated computationally by Fang et al.[331] The through-bond interaction was found to selectively destabilize the antisymmetric combination of the nonbonding molecular orbital (ψ_A) in the twisted conformation of *m*-QDM.

Nelsen and co-workers reported a singlet ground state for the diradical dication of 1,4-bis(hydrazino)benzene **DR96** (Figure 82).[332] They observed clear triplet ESR signals at 77 K in a 1:1:1 mixture of acetonitrile, butyronitrile, and methylene chloride. The temperature-dependent change of the bis(radical cation) triplet ESR intensities clarified the singlet ground state of **DR96** with a singlet−triplet energy gap of 0.32 kcal mol^{-1}. The singlet ground state was reasonably explained by the quinoidal contribution of the *para*-phenylene diradicals. Sakurai et al. designed a high-spin molecule, TMM derivative **DR97**, in which the aminium radical cation was connected with nitronyl nitroxide.[333] The oxidation of the precursor with I_2 cleanly produced the radical cation with typical triplet ESR signals, with $D = 0.0276$ cm^{-1} and $E = 0.0016$ cm^{-1}. The triplet ground state was determined by variable-temperature analysis of the triplet signals below 100 K.

ESR studies in rigid glass for the dication of dimeric compounds **DR98** indicated singlet ground states with small singlet−triplet energy gaps of around 50−70 cal mol^{-1} (Figure 83).[334]

Kuratsu and co-workers synthesized air-stable radical cation **DR99** based on the structure of trioxytriphenylamine (TOT) (Scheme 56).[335] The trioxy-substituted amine has a low oxidation potential and is well stabilized by the electron delocalization. The structure of TOT^+ was used as a platform for making the stable diradical. A strong intramolecular ferromagnetic interaction with $J/k_B = +400$ K was reported for the diradical **DR99** with a nitronyl nitroxide (NN).[336] A weak intermolecular antiferromagnetic interaction of $J/k_B = -1.85$ K was found in the solid state.

Triradical **156** was found to have a doublet ground state with $2J/k_B = -410$ K and to exhibit a reversible one-electron oxidation wave at $E_{ox} = -0.29$ V vs Fc/Fc^+ (Figure 84).[337] The UV−vis absorption spectrum of **DR100** in CH_2Cl_2 shows weak and broad absorptions in the 500−1000-nm region. During the oxidation, new absorption peaks at $\lambda_{max} = 360$, 530, and 710 nm were observed with isosbestic points. The strong signal at $\lambda_{max} = 710$ nm was assigned to the quinoidal structure of the cation of **156**. **DR100** has the character of a trimethylenemethane-type π-conjugation system. Thus, the nondisjoint diradical was expected to have a triplet ground state. A plot of $\chi_T - T$, to examine the effect of temperature on magnetic susceptibility, indeed showed a characteristic ferromagnetic curve, from which the exchange coupling (J/k_B) was determined to be greater than 300 K. The ESR spectrum in the solid state was found to be composed of two triplet species with similar $|D/hc|$ values of 0.00575 and 0.00570 cm^{-1} and an $|E/hc|$ value of 0.00055 cm^{-1} for one of the species. A spin-forbidden transition was clearly observed in the $g = 4$ region. These results suggested that one of the triplet diradicals had C_3-based symmetry, so the triplet diradical with $|E/hc| = 0$ was assigned to **DR100**. Trinitroxide **156** showed a spin-state change from the doublet species to the triplet species upon oxidation.

Yokoyama et al. reported the electronic structures for the polycationic states of a double-layered triphenylamine (TPA) linked by three *meta*-phenylenediamine pillars (Scheme 57).[338] The distance between the two central nitrogen atoms was found to be 5.8 Å according to X-ray crystallographic analysis. Although there is no direct through-space interaction between the two nitrogen atoms, it was clarified that the spin of the radical cation is delocalized over the whole molecular skeleton. The triplet ESR spectrum of the diradical dication was observed using 2 equiv of the oxidizing agent tris(4-bromophenyl)-aminium hexachloroantimonate ("Magic Blue"). The zfs *D* value was determined to be 4.9 mT, with a value of almost 0 for *E*. Thus, the average spin−spin distance was calculated to be 8.3 Å. This long spin−spin distance is due to the delocalization of the two spins in the molecule. From a plot of the intensity of the ESR signal as a function of temperature, a singlet ground state was found with an energy gap of 0.18 kcal mol^{-1}. In contrast to the experimentally determined singlet ground state, the triplet was calculated to be the ground-state spin multiplicity with a relatively large energy gap of 5.3 kcal mol^{-1}.

4. BIS(NITROXIDE)S

Nitroxides that can be easily prepared from nitroso compounds or from amines be oxidation are stable radicals and can easily be detected by ESR spectroscopy (Figure 85). The fundamental chemical and physical properties of stable nitroxides were invesitigated in pioneering studies by Rozantsev and Sholle[339] and Rassat and co-workers.[340,341] Stable nitroxides have

dx.doi.org/10.1021/cr400056a | *Chem. Rev.* 2013, 113, 7011−7088

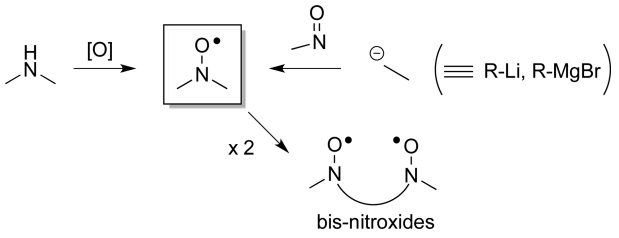

Figure 85. Preparation of nitroxides and bis(nitroxide)s.

provided many opportunities to investigate the chemistry, biochemistry, and materials science due to molecular magnetism. Intramolecular and intermolecular interactions of the nitroxide units are summarized in this section. Molecules with two nitroxide units are called bis(nitroxide)s.

4.1. Bis(nitroxide)s in Non-Kekulé Molecules

As mentioned in section 3.4, tetramethylmethane (TMM) and *meta*-quinodimethanes (*m*-QDM) are nondisjoint diradicals; thus, the parents TMM and *m*-QDM are triplet-ground-state molecules with large singlet−triplet energy gaps of ΔE_{ST} = 16.1 and 9.6 kcal mol^{-1}, respectively (Figure 86).[342−345] The triplet ground state of the *tert*-butyl-substituted *meta*-phenylene dinitroxide **DR102** (R = *tert*-Bu) was found in 1969.[346] A singlet−triplet energy spacing of $\Delta E_{ST} \approx$ 2.0 kcal mol^{-1}, much smaller than that of *m*-QDM, was calculated for the parent *meta*-phenylene bis(nitroxide) **DR102a** (R = H). The small singlet−triplet energy gap can be explained by the spin density on the benzylic positions. Thus, for bis(nitroxide)s, the spin density is delocalized on both the nitrogen and oxygen atoms. The lower the spin density on the benzylic positions, the smaller the energy gap in the diradical. However, the zfs $|D/hc|$ value of 0.012 cm^{-1} was found to be nearly the same as that of *m*-QDM, because the spin−spin distances in the two cases are almost the same.

The two nitroxide radicals interact intramolecularly with each other ferromagnetically to produce a triplet-ground-state molecule. However, magnetic susceptibility measurement of a crystal sample, namely, the α-phase crystal of **DR103** from CH_2Cl_2, showed practically diamagnetic behavior over the temperature range of 1.8−300 K (Figure 87).[347] The strong antiferromagnetic couplings are ascribed to the nature of the bonding between the two bis(nitroxide) molecules. Actually, the intermolecular N−O distance was found to be ∼2.3 Å, which is 24% shorter than the sum of the van der Waals radii between the nitrogen and oxygen atoms. The intramolecular N−O bond distance was found to be ∼1.3 Å, which was slightly longer than that in the monomeric bis(nitroxide) **DR103**. Similar intermolecular antiferromagnetic couplings have also been observed for other bis(nitroxide)s in which an intramolecular ferromagnetic interaction was observed. Interestingly, **DR103** was recrystallized from hexane in another type of crystal structure, the β phase, and this phase was found to show a different temperature dependency of the magnetic susceptibility. Thus, the magnetic susceptibility of the β-phase sample obeyed the Curie−Weiss low with a Curie constant of 1.00 cm^3 K mol^{-1} and a Weiss constant of −6.0 K. The value of the Curie constant coincides with the theoretical paramagnetic character of S = 1 (triplet state). More interestingly, a thermal phase transition from the α-phase crystal to the β-phase crystal was observed upon heating the sample at 350 K. The phase transition was found to be irreversible. Thus, bis(nitroxide)s such as **DR103** and **DR104** have potential utility as genuine organic write-once information-storage materials.[348,349]

Rajca et al. reported the isolation and magnetic characterization of diarylnitroxide diradical **DR105** (Scheme 58).[350] The dinitroxide was prepared by using dimethyldioxolane (DMDO) or *meta*-chloroperoxybenzoic acid (*m*-CPBA) as the oxidizing agent. Reduction of diradical **DR105** with iron/acetic acid cleanly gave diamine **157**. Structure **157** enforced a coplanar conformation for the nitroxide moieties and the *m*-phenylene coupling unit and, thus, was expected to provide a relatively large singlet−triplet energy gap. SQUID magnetometry of **DR105** clearly indicated that the ground state is the triplet with an energy gap of around 0.6 kcal mol^{-1}.[351]

The magnitude of the ferromagnetic coupling constant (J_{ab}) between the nitroxide radicals was found to be influenced by the noncovalent cation (Y^+)−anion(X^-) π interactions, which were computed at the M06-2X level of theory (Figure 88).[352] A large influence was observed for the Br^- ion, whereas the least influence was found for the Li^+ ion. Anions are prone to increase electron-exchange coupling, whereas positive ions decrease the magnitude of this coupling. The reason for the dramatic enhancement induced by the anions was found to be two-fold: First, there is an increase in the paratropic current density because of the small amount of charge transfer to the aromatic ring from the anion. Second, magnetization density accumulate on the external anion upon the occurrence of charge transfer.

Nitroxides are easily oxidized and reduced by appropriate compounds to generate anions and cations. Thus, the rapid reversible redox process of nitroxides has been used for materials chemistry applications such as radical batteries (Figure 89). In general, aromatic compounds such as anthracene are prone to emit light from electronically excited states. Such fluorescent labeling studies are currently utilized in many fields of chemistry, materials science, and biology. However, because of the redox properties of nitroxides, nitroxides bearing fluorescent chromophores do not emit any light with low quantum yields, because the electronically excited chromophore is rapidly quenched by the nitroxide. Fairfull-Smith et al. utilized this character to analyze the polymer

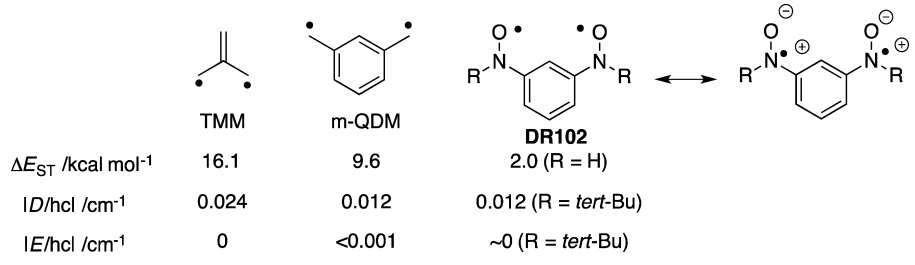

Figure 86. Singlet−triplet energy gap in **DR102** and its zero-field-splitting parameters D and E.

dx.doi.org/10.1021/cr400056a | *Chem. Rev.* 2013, 113, 7011−7088

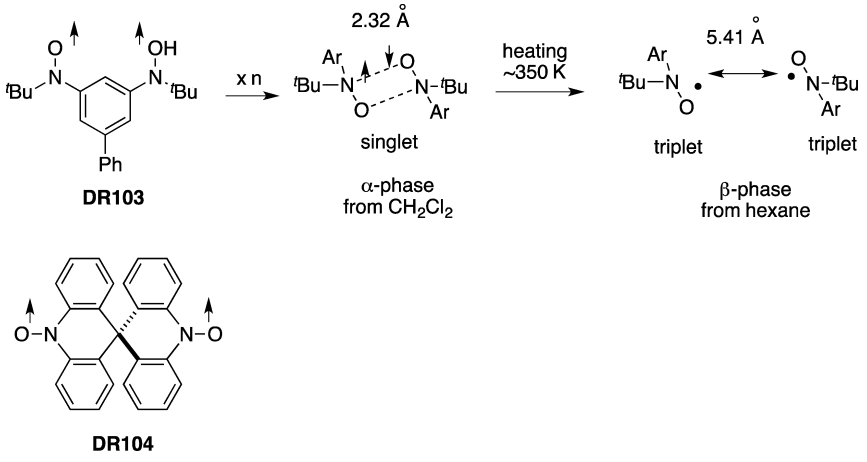

Figure 87. Intramolecular and intermolecular interactions in nitroxides **DR103** and **DR104**.

Scheme 58. Preparation of Planar Diradical DR105 from the Oxidation of 157

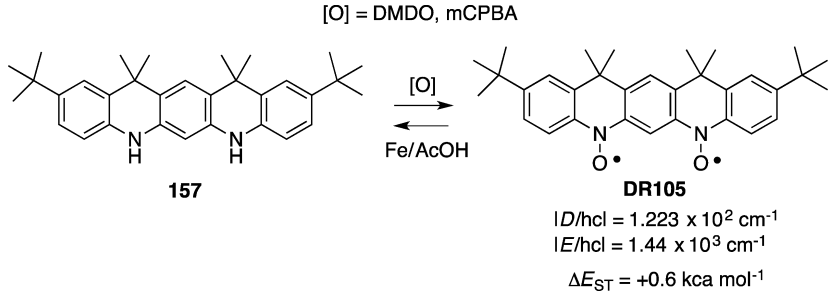

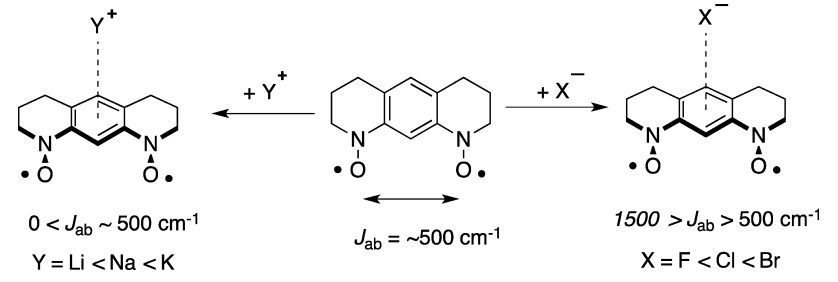

Figure 88. Effects of noncovalent interactions on the ferromagnetic coupling constant J_{ab}.

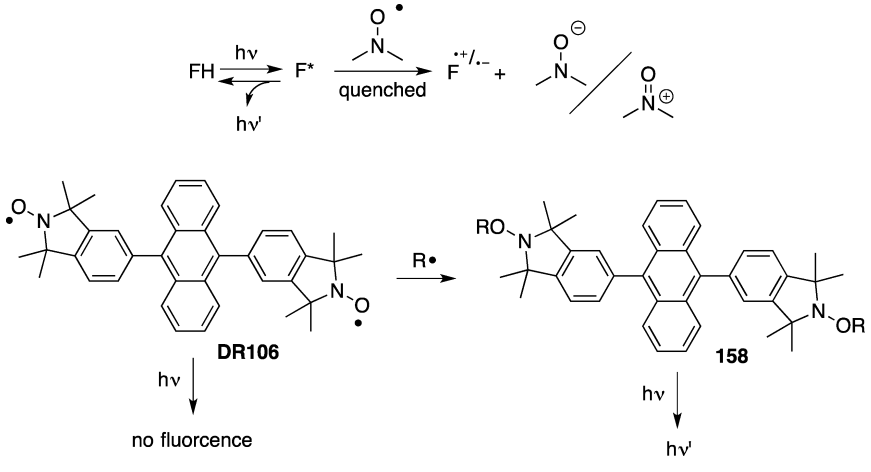

Figure 89. Redox and fluorescence properties of nitroxides.

dx.doi.org/10.1021/cr400056a | Chem. Rev. 2013, 113, 7011−7088

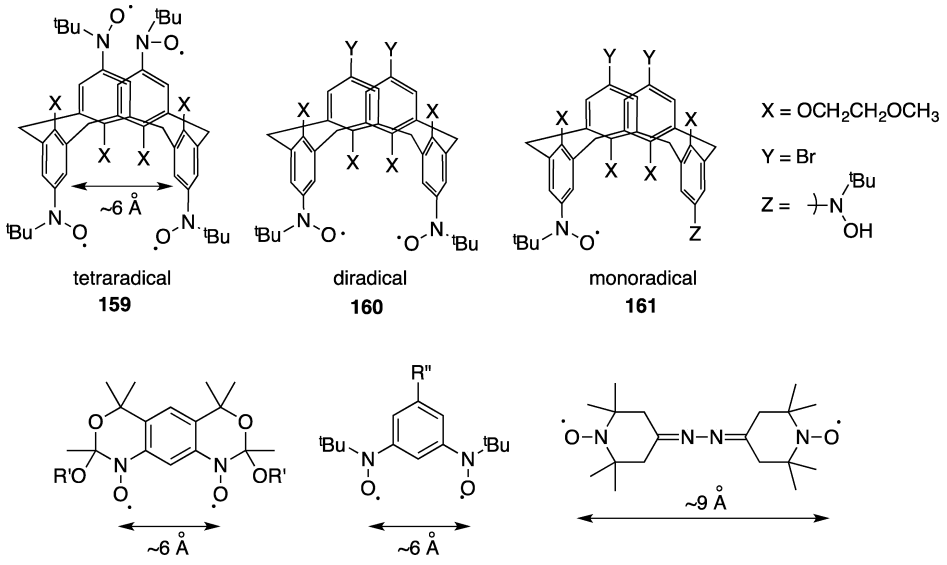

Figure 90. Relaxation enhancement by nitroxide−nitroxide interaction.

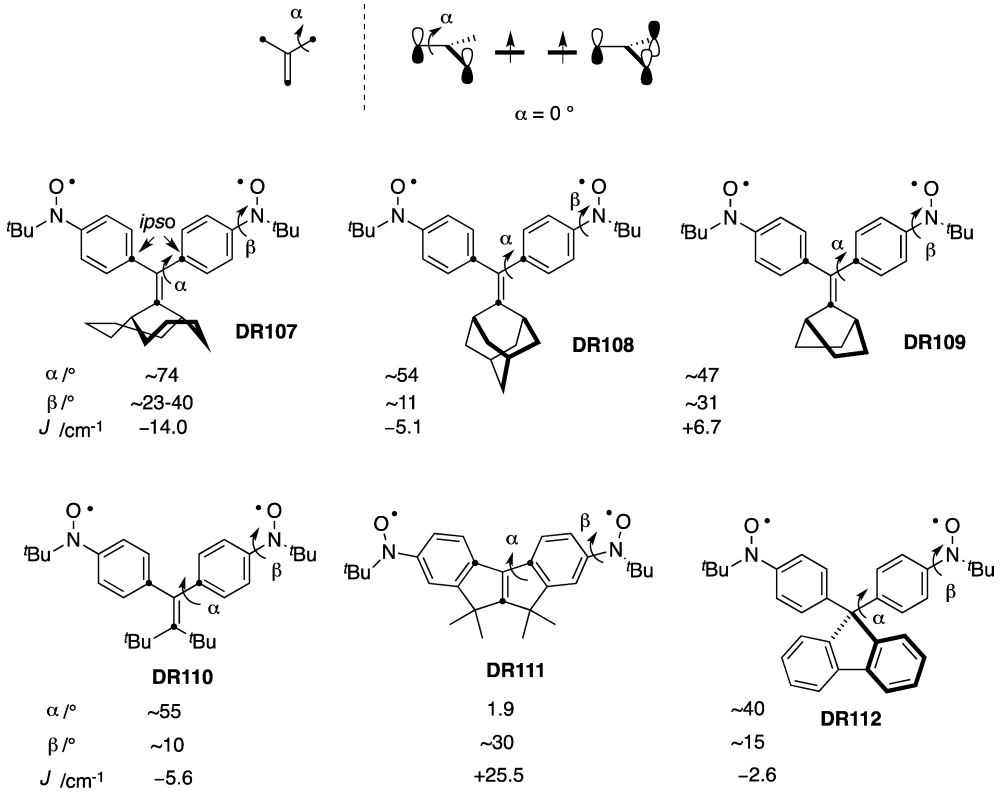

Figure 91. Conformational effect on the singlet−triplet energy gap in trimethylenemethane-based bis(nitroxide)s.

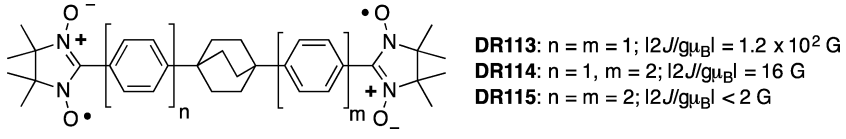

Figure 92. Effect of the distance between the two nitroxides on the exchange interaction.

degradation process.[353] After the radical-trapping reaction of nitroxide **DR106**, alkylated nitroxide **158** was found to start emitting light.

Electron spin relaxation rates $(1/T_1)$ are important parameters for spin-labeling experiments, dynamic nuclear polarization (DNP) studies, and spin−spin distance determinations. Recently, Sato et al. investigated the relaxation enhancement that arises from the nitroxide−nitroxide interaction using compounds **159**−**161** (Figure 90).[354] For diradical **159** with an interspin distance of 6 Å, the relaxation rate was

dx.doi.org/10.1021/cr400056a | Chem. Rev. 2013, 113, 7011−7088

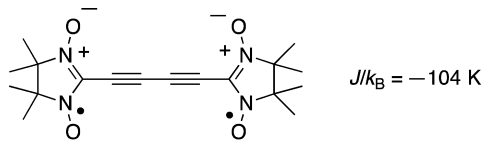

DR116

Figure 93. Magnetic property of **DR116**, in which two nitronyl nitroxide units are connected with a diacetylene bridge.

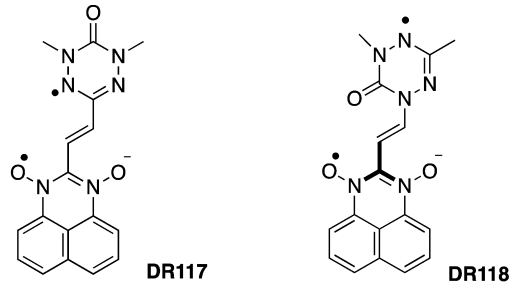

Figure 94. Intramolecular magnetic interaction (J) in diazaphenalenyl radicals **DR117** and **DR118**.

only slightly higher than that for monoradicals. The results indicate that the impact of the nitroxide−nitroxide interaction on electron spin relaxation extends to relatively short distances compared to the relaxation enhancement from rapidly relaxing metals, which extends to tens of angstroms. For interspin distances of ~6 Å, the relaxation rates in glassy solvents up to 300 K were found to increase in the order of monoradical **161** < diradical **160** < tetraradical **159**. These results suggest that modulation of the exchange interaction is not the main contribution to the relaxation. Thus, the trend is attributed to modulation of the dipolar interaction, which is greater for more flexible molecules and for less rigid glasses. Modulation of the dipolar couplings provides an effective spin relaxation pathway.[355]

Dougherty reported many examples of high-spin molecules with trimethylenemethane (TMM) as a triplet high-spin coupler.[40] The advantage of using TMM as a spin coupler is that the singlet−triplet energy spacing of TMM (ΔE_{ST} = 16.1 kcal mol^{-1}) is larger than that of *m*-QDM (ΔE_{ST} = 9.6 kcal mol^{-1}). Shultz and co-workers prepared the series of bis(nitroxide)s **DR107−DR112** in which the two nitroxide units are connected by trimethylenemethane (TMM) to understand the effect of conformation on the singlet−triplet energy gap (Figure 91).[356,357] As shown in the structures and singlet−triplet energy gaps, the conformations of the phenyl rings are important factors for the singlet preference of flexible diradicals.

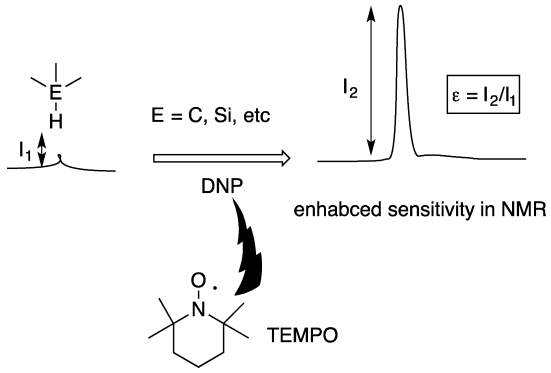

Figure 96. Nitroxide-induced dynamic nuclear polarization (DNP) enhancement in NMR signals.

As clearly shown in the structures **DR107−DR112**, the planarity of the TMM π face with the phenyl ring (phenyl torsion) significantly affects the singlet−triplet energy spacing. Thus, when the planarity is high (α value is low), the triplet was found to be the ground-state spin multiplicity, for example, for compounds **DR109** and **DR111**. The planarity effect can be explained by the triplet ground state of the parent TMM, which exhibits perfect planarity in the diradical structure. This perfect planarity produces degeneracy of the nonbonding molecular orbitals. When the torsional angle is high, reaching almost the twisted conformation of the phenyl ring, the singlet was found to be the ground-state spin multiplicity, as found for fluorenyl-based bis(nitroxide) **DR112**. In contrast to the sensitivity of torsional angle α, the dihedral angle, β, does not have much effect on the singlet−triplet energy spacing.

Higashiguchi et al. reported the evaluation of the decay constant of the conductive property of the molecular wire for the phenylene unit by probing the exchange interaction (J) between two nitroxides using ESR spectroscopic analyses of compounds **DR113−DR115** (Figure 92).[358] The exchange interaction was found to decrease with a decay constant of 0.51 ± 0.01 Å^{-1}.

Diradical **DR116**, in which two nitronyl nitroxides units are connected with a diacetylene bridge, was synthesized, and its magnetic properties were investigated (Figure 93).[359] The ESR spectrum in liquid solution consists of nine rather broad lines. The simulation of the spectrum revealed a hyperfine-coupling constant of 0.35 mT with four equivalent nitrogen atoms. The obtained coupling constant corresponds to approximately one-half the typical value of the hyperfine coupling constant (0.7 −0.75 mT) with two ^{14}N nuclei in nitronyl nitroxides. This indicates that the constant of the intramolecular exchange interaction between the unpaired electrons is substantially larger than that hyperfine coupling with the spins of the ^{14}N nuclei. The temperature-dependent change in the magnetic

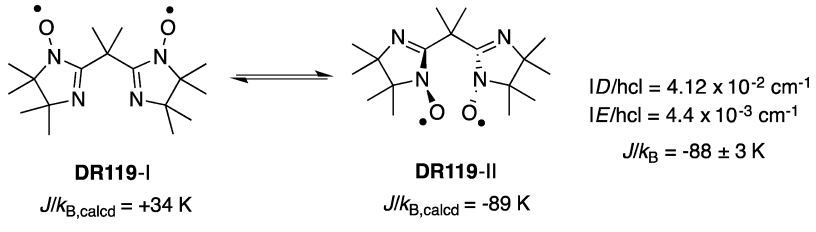

DR119-I
J/kB,calcd = +34 K

DR119-II
J/kB,calcd = -89 K

Figure 95. Conformation effect on the singlet−triplet energy gap in diradical **DR119**.

dx.doi.org/10.1021/cr400056a | *Chem. Rev.* 2013, 113, 7011−7088

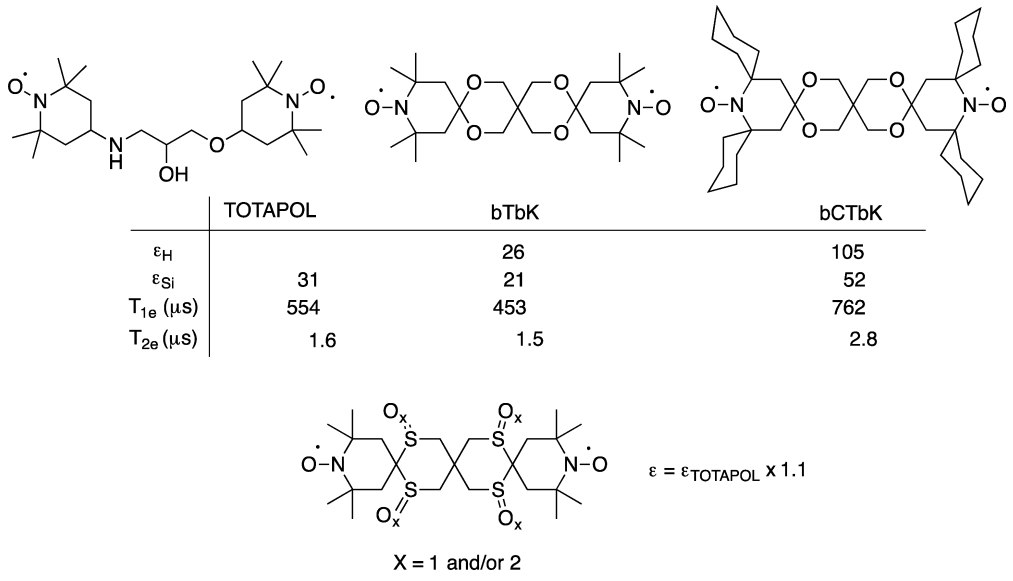

Figure 97. DNP effect induced by water-soluble bis(nitroxide)s.

Scheme 59. High Glycerol/Water-Soluble Bis(nitroxide)

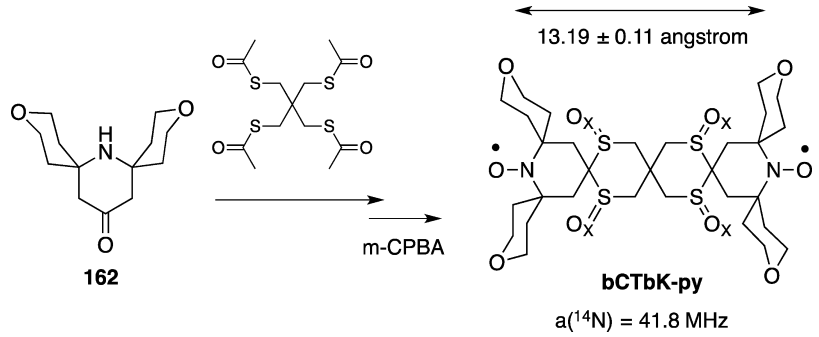

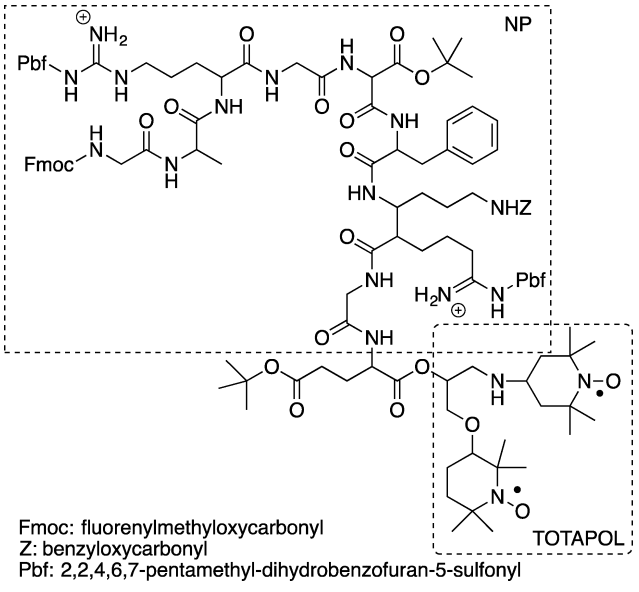

Figure 98. Solvent-free amorphous powder for DNP measurements.

properties revealed an antiferromagnetic interaction between the two spins with $J/k_B = -104$ K.

Ko et al. investigated the intramolecular magnetic interactions (J values) of diazaphenalenyl radicals **DR117** and **DR118** with a neutral radical to which they were connected by a conjugated unit at the UB3LYP level of theory (Figure 94).[360] Large magnetic interactions, $|J| > 400$ cm^{-1}, were computed for the combination of oxoverdazyl neutral radical with diazaphenalenyl radical connected by an ethylene unit.

The singlet ground state of diradical **DR119** was reported by Suzuki et al. (Figure 95).[361] Conformer I was predicted to be a triplet-ground-state molecule, whereas conformer II was computed to have a singlet ground state with $J/k_B = -89$ K. The X-ray crystal structure and temperature-dependent change in the intensity of the ESR spectrum of the prepared diradical **DR119** showed that diradical **DR119** exhibits conformer II and a singlet ground state with $J/k_B = -88 \pm 3$ K.

4.2. Dynamic Nuclear Polarization (DNP) by Bis(nitroxide) Diradicals

As indicated in the introduction of section 4, nitroxides are stable radicals. The distance-dependent change in the electron exchange interaction of two unpaired electrons can be estimated using the ESR spectroscopic analysis of stable bis(nitroxide)s. One of the recent topics of interest in bis(nitroxide) chemistry includes the enhancement of dynamic nuclear polarization (DNP) in nuclear magnetic resonance (NMR) spectroscopy.

NMR spectroscopy is one of the most powerful tools for obtaining structural and dynamic information on molecules and materials. However, an inherently poor sensitivity due to the

dx.doi.org/10.1021/cr400056a | Chem. Rev. 2013, 113, 7011−7088

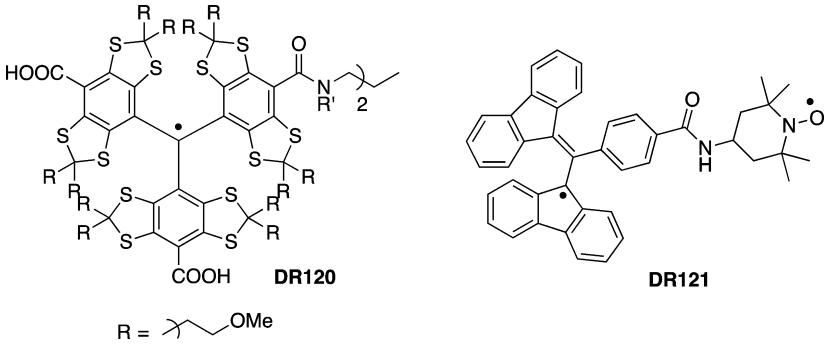

Figure 99. Weakly coupled ddiradials for DNP application.

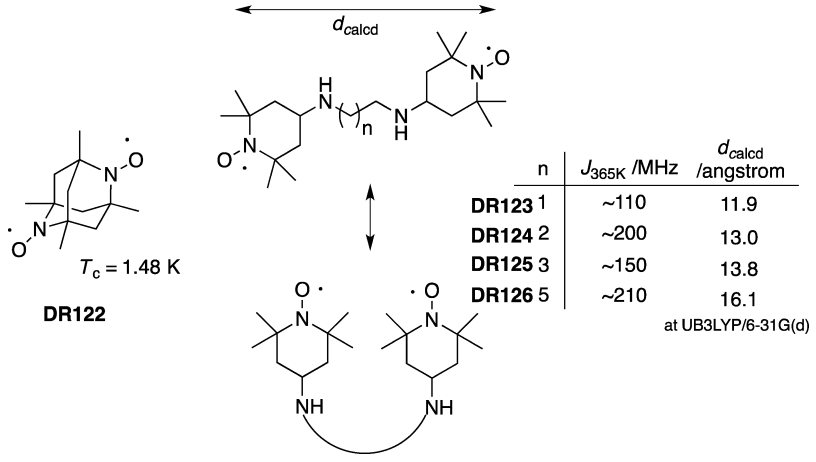

Figure 100. Bis(nitroxide)s with ferromagnetism.

Scheme 60. Spin Label Technique, Spin−Spin Interaction of the Two Nitroxides, Used to Detect the Dynamic Movement of α-Cyclodextrin (CD) in [2]Rotaxane

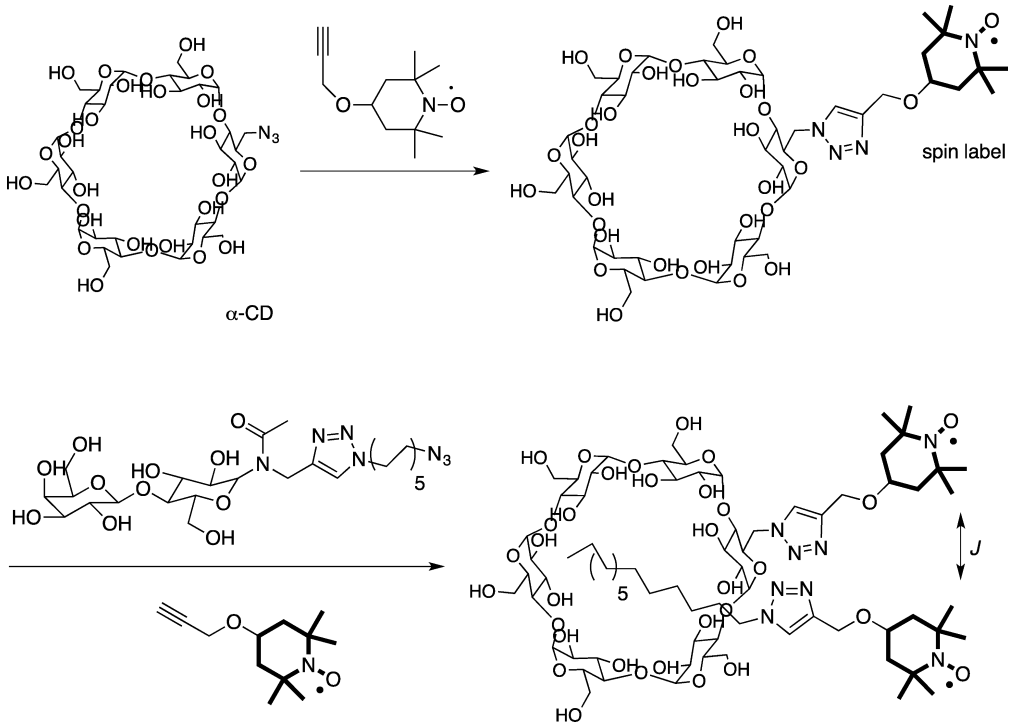

small spin momenta of nuclei does not allow this spectroscopic method to be used for the structural determination of low concentrations of compounds on material surfacees or for the monitoring of the reaction processes of functional molecules in

dx.doi.org/10.1021/cr400056a | Chem. Rev. 2013, 113, 7011−7088

Scheme 61. Photoswitching of Intramolecular Through-Space Magnetic Interaction in DR127

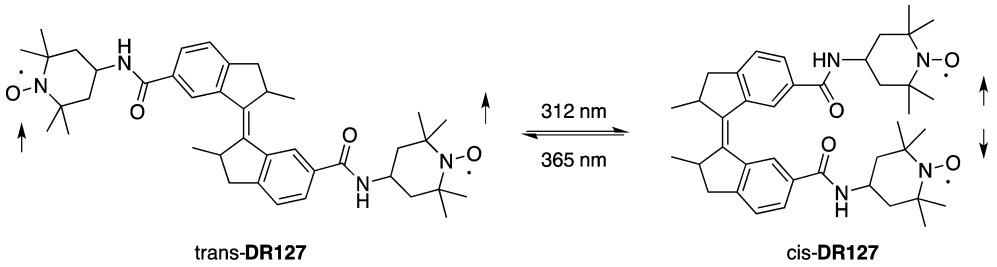

biology and materials science. Dynamic nuclear polarization (DNP) has the potential to increase NMR sensitivity by orders of magnitude by using the transfer of polarization from unpaired electrons to nuclei. This effect was first suggested in 1953 by Overhauser.[362] In the 1990s, DNP-enhanced NMR spectroscopy made great progress under the magic-angle-spinning conditions.[363] The DNP signal enhancement factor (ε) was found to be up to 250. The dramatic sensitivity increase allowed the elucidation of the bonding topologies at the surfaces of functionalized mesostructured materials.

The cross-effect mechanism is the most efficient for DNP at high fields. A cross-effect is strongly induced by the strong dipolar coupling of two unpaired couplings. Of course, the ESR frequencies must differ by the nuclear Larmor frequency. The first report on the cross-effect induced in DNP experiments was in the solution phase using a high concentration of monoradicals such as commercially available nitroxide radical (2,2,6,6-tetramethylpyperidine-1-yl)oxyl (TEMPO) (Figure 96). Matsuki et al. found that the water-soluble bis(nitroxide) TOTAPOL is a reagent for DNP, particularly for biological applications (Figure 96).[364] Thereafter, the rigid bis-TEMPO−bis-ketal (bTbK) and bis-cyclohexyl-TEMPO−bis-ketal (bCTbK) were reported for the detection of molecules on the surface of hybrid or inorganic materials. The enhancement factors for proton (ε_H) and silicon (ε_{Si}) were found to correlate with the electron spin−lattice relaxation time (T_{1e}) and the spin−spin relaxation time (T_{2e}). The longer relaxation time for bCTBK, compared to bTbK, was attributed to the rigidity of the structure around the nitroxide unit.[365]

Water-soluble bis(nitroxide)s are useful for determining the structure and dynamics of biologically active compounds such as enzymes. The water-soluble bis(nitroxide)s, which contain sulfoxide and sulfone units in the diradicals, have been prepared and tested for the DNP effect (see Figure 97). The DNP effect was found to be slightly larger than that found for TOTAPOL ($\varepsilon_{TOTAPOL}$).[366,367]

TOTAPOL is sparingly soluble in dimethyl sulfoxide (DMSO)/water mixtures and insoluble in glycerol/water mixtures. This limits the applicability of bTbK as a polarizing agent because glycerol/water serves as a cryoprotectant and is the solvent choice for the DNP of proteins. Kiesewetter et al. designed the TEMPO derivative bis-TEMPO−bis-thioketal-tetra-tetrahydropyran (bTbtk-py) with a high glycerol/water solubility.[368] The bis(nitroxide) was prepared from amine **162** and was found to exhibit excellent solubilities of 10.9 mM in the desired 60/40 glycerol/water mixture and 3.0 mM in D_2O (Scheme 59). The DNP-enhanced ^{13}C cross-polarization magic-angle-spinning (CP-MAS) NMR spectroscopy of ^{13}C-urea (1 M in 60/40 glycerol/water) showed ε = 230 versus thermal polarization. Under similar conditions, a lower enhancement, ε = 191, was found for TOTAPOL. The breadths and intensities of the enhancement field profiles of the two polarizing agents TOTAPOL and bTbtk-py suggest that the nitroxide moieties have different relative orientations and electron−electron couplings in the two diradicals. Thus, the NMR signal enhancement was shown to depend with extreme sensitivity on the modulation of the electron−electron distance and relative orientation of the NO moieties of the diradicals. The high sensitivity suggests that the structural fine-tuning should make it possible to obtain superior DNP polarizing agents.

Rossini et al. showed that DNP solid-state NMR spectroscopy can be applied to powdered microcrystalline solids to obtain sensitivity enhancements on the order of 100.[369] Bis-cyclohexyl-TEMPO−bis-ketal (bCTbK) was used for the DNP measurements. DNP enhancements on the order of 60 were obtained for microcrystalline glucose and sulfathiazole at 9.4 T at 105 K.

Methods enabling structural studies of membrane-integrated receptor systems without the necessity for purification provide an attractive perspective on membrane protein structure and molecular biology. DNP MAS NMR spectroscopy is a promising method for solving this problem. Linden et al. observed well-resolved solid-state NMR spectra of extensively ^{13}C-labled neurotoxin II bound to the nicotinic acetylcholine receptor in native membranes. TOTAPOL was used for the DNP study and was localized at the membrane and protein surfaces. Although weeks of measurement time were needed to obtain conventional MAS NMR data, they were able to reduce the measurement time by 6%.[370]

Many samples of biological origin such as membrane proteins and peptide fibrils cannot be dissolved or suspended at reasonable concentrations in any solvent. If solubility is limited, DNP enhancements of only small magnitudes are expected. Vitzthum et al. reported the development of a method using dry samples that do not require any solvents. The solvent-free amorphous powder in which TOTAPOL was covalently attached in the nonapeptide (NP) was prepared and used for DNP measurements. A modest enhancement of $\varepsilon < 4$ was detected after cross-polarization from ^1H to ^{13}C (Figure 98).[371]

As mentioned earlier, weakly exchange-coupled diradicals have attracted much attention in terms of their DNP applications in NMR spectroscopy. Recently, Ayabe et al. reported a quantitative evaluation of the weakly exchange-coupled interaction in diradicals using pulsed electron spin nutation (ESN) spectroscopy. Pulsed X-band ESN spectroscopy was found to provide accurately determined spin dipolar interaction measurements.[372] Diradicals **DR120**[373] and **DR121**[374] were also designed and synthesized for DNP (Figure 99).

dx.doi.org/10.1021/cr400056a | *Chem. Rev.* 2013, 113, 7011−7088

4.3. Spin Labeling Study

Probably, the most famous bis-nitroxide is compound **DR122**, which shows the transition temperature record (T_c = 1.48 K) in pure organic-nitroxide-based ferromagnetism (Figure 100).[375] This result indicates the existence of spontaneous magnetization below the critical temperature T_c. Each NO group has three close NO neighbors, suggesting a three-dimensional network of chains interconnected through inter- and intramolecular interactions. Both the intra- and intermolecular interactions were found to be ferromagnetic; thus, three-dimensional ferromagnetic order was observed at 1.48 K.

The through-space interaction was found to play a major role in determining the magnitude of the spin−spin exchange interaction, as confirmed by an ESR study of diradicals **DR123**−**DR126** in which the two TEMPO moieties are connected by the chains $-(CH_2)_n-$, n = 1−5.[376] The exchange interaction (J) was found to increase with increasing temperature and increasing leangth of the alkyl chain (i.e., distance d_{calcd} between the two nitroxide radicals). The distances were calculated for the linear conformer (most stable conformer) of the bis(nitroxide)s. The results clearly indicate that the exchange interaction is derived from the conformer in which the two radicals are located close each other.

Spin labels are generally used as tools for probing the local dynamics of proteins or biological membranes using ESR spectroscopy. The site-directed spin label technique allows one to monitor a specific region within a protein. Recently, a spin label technique based on the spin−spin interaction of two nitroxides was used to detect the rotaxanes and the dynamic movement of α-cyclodextrin (CD) in [2]rotaxane (Scheme 60).[377] Spin-labeled α-CD was prepared by a click reaction, namely, the Cu(I)-catalyzed azide−alkyne cycloaddition of azide derived from α-CD to the nitroxide. The bis-labeled rotaxane was prepared by a method based on formation and assembly by the click reaction of a pseudorotaxane composed of α-CD and C10 alkyl chain blocked at one end by a saccharidic stopper and carrying an azido group at the other end.

Wang et al. reported a photoswitchable intramolecular through-space magnetic interaction in diradical **DR127** (Scheme 61).[378] Irradiation of *trans*-**DR127** at 312 nm resulted in a decrease in the absorption band of *trans*-**DR127** at 297 nm with a concomitant increase of a new absorption band at 350 nm. An isosbestic point was maintained at 319 nm over the course of the irradiation. At the photostationary state, an 89% yield of *cis*-**DR127** was obtained. Upon irradiation of *trans*-**DR127** at 312 nm, the ESR spectrum showed substantial changes from a three- to a five-line spectrum. Irradiation at 365 nm drove the reverse *cis*-**DR127** to *trans*-**DR127** isomerization with a decrease in the intensity of the absorption band at 350 nm.

5. DIRADICALS IN METAL COMPLEXES

Molecular structure plays an important role in the design of magnetic materials and magnetic molecular devices.[379] The ground-state spin multiplicities of diradicals in metal complexes are largely dependent on the special orientation of the two radical parts. Copper(I) complexes **DR128**−**DR130** are examples of the spin−spin interaction. Iminonitroxide complex **DR128** has a triplet ground state and a pseudotetrahedral geometry at copper with a near-90° angle between the ligand planes,[380] whereas verdazyl complex **DR129** appears to have near-degenerate singlet and triplet states, and in the solid state, it shows a distorted structure in which the angle between the two ligand planes is 116°.[381] DFT calculations predict a perpendicular geometry minimum and a triplet ground state for both diradicals.

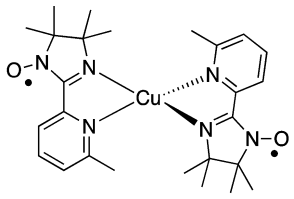

DR128

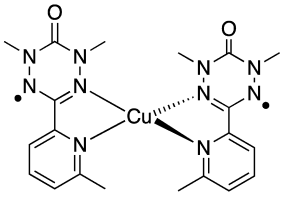

DR129

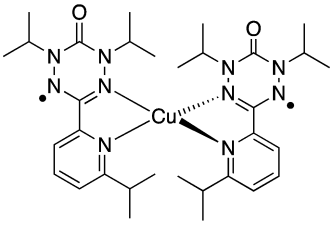

DR130

Brook et al. synthesized copper complex **DR130** with verdazyl units and characterized it by X-ray crystallography and magnetic susceptibility. The temperature-dependent change of the magnetic susceptibility indicated a triplet ground state of the diradical with J = 47 cm^{-1}.[382] The coordination geometry at copper was found to be distorted tetrahedral with the two ligand planes separated by 75°. Metal complexes with redox-active noninnocent ligands[383] might be important compounds for magnetic materials.[384] Related studies have been reported by Bachler et al., Herebian et al., and Patrenko et al.[385]

6. DIRADICALS IN MATERIALS

Organic-semiconductor-based devices, such as organic light-emitting diodes (OLEDs), organic field-effect transistors (OFETs), organic thin-film transistors (OTFTs), and solar cells, are current research interests because of their reduced fabrication costs compared to silicon-based materials. In general, the energy barrier between the Fermi level of the

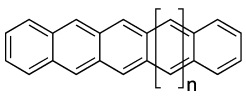

n	ground state
1	closed-shell singlet state
2	open-shell singlet state (-10.3, -0.8)*
3	open-shell singlet state (-7.1, -2.7)*
4	open-shell singlet state (-5.8, -5.2)*
5	open-shell singlet state (-5.5, -7.9)*
6	open-shell singlet state (-5.7, -10.4)*

* The energy gaps with (triplet, closed-shell singlet)

Figure 101. Polyacenes: polycyclic aromatic hydrocarbons consisting of linearly fused benzene rings.

dx.doi.org/10.1021/cr400056a | *Chem. Rev.* 2013, 113, 7011−7088

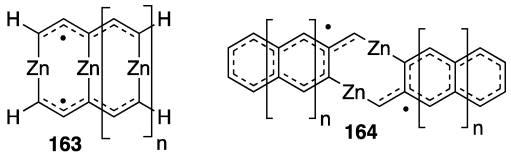

open-shell singlet gound state

n	energy gap with (triplet, closed-shell singlet)	
0	(-2.98, -10.67)*	(-2.98, -10.67)*
1	(-2.91, -7.87)*	(-2.08, -11.35)*
2	(-2.89, -6.33)	(-0.89, -13.54)
3	(-2.90, -5.33)	(-0.50, -15.23)
4	(-2.92, -4.65)	(-0.25, -17.11)

Figure 102. Multi-Zn-expanded oligoacenes **163** and **164** from benzene to pentacene and their open-shell character.

source electrode and the HOMO of the semiconductor is smaller than that between the Fermi level and the LUMO, for example, ~5.1 eV for Au and 4.5 eV for Cr. Thus, p-channel semiconductors are more common than n-channel ones. The most important point of the performance at the molecular level is the control of the energy levels of the HOMO and LUMO and their energy gaps. They determine the optical and electrochemical properties of organic compounds and the characteristics of the electronic devices. The band gap can be controlled by various factors including π-conjugation length, quinoidal contribution, and aromaticity. A strategy for obtaining good performance in n-channel conductance is to introduce an electron-withdrawing moiety in compounds. A small energy gap between the HOMO and LUMO provides a unique character for compounds with ambipolarity. Thus, diradicaloids are one of the most promising types of compounds that should exhibit small HOMO−LUMO energy spacings. A major problem with using diradicals and diradicaloids in materials is their inherent instability due to their open-shell character. So far, some strategies have been developed to stabilize the energy of and isolate these fascinating molecules. Some of the strategies were shown for delocalized Kekulé molecules.

Polyacenes are polycyclic aromatic hydrocarbons consisting of linearly fused benzene rings. Large polyacenes were predicted to behave as *n*-dimensional conductors with a zero band gap. Experimental and theoretical studies on oligoacenes to understand their fundamental electronic and geometric properties have attracted much attention. Organic electronic applications such as electrically pumped organic solid-state injection lasers, field-effect transistors, light-emitting diodes, organic conductors, and solar cells have stimulated interest in their fundamental properties. Pentacene (n = 1) is a closed-shell singlet-ground-state compound and has attracted much attention as the active semiconducting material in field-effect transistors because of its unusually high charge-carrier mobility (Figure 101). A smaller band gap would provide higher activity than obtained with pentancene. In 2004, Bendikov et al. theoretically investigated the open-shell diradical character of oligoacenes, namely, hexacene (n = 2), heptacene (n = 3), octacene (n = 4), nonacene (n = 5), and decacene (n = 6) (Figure 101).[386] At the B3LYP/6-31G(d) level of theory, the open-shell singlet state was calculated to be lower in energy than the triplet and closed-shell singlet states by −10.3 and −0.8 kcal mol^{-1}, respectively, for hexacene (n = 2). The singlet−triplet energy spacing was computed to decrease from hexacene to heptacene and octacene and then to become constant at approximately −5.5 kcal mol^{-1}. On the other hand, the energy gap with the closed-shell singlet state was computed to increase from 0.8 to 10.4 kcal mol^{-1} without showing any saturation. A small HOMO−LUMO energy gap of 1.80 eV was computed and found to be consistent with the experimental value of 1.84 eV. The calculated frontier orbitals clarified the disjoint character of the diradical. Thus, the singlet was found to be the ground-state spin multiplicity. Very recently, hexacene (n = 2) was isolated, and its crystal structure and charge-transport properties were investigated by Watanabe et al.[387]

Yang et al. computationally designed two classes of multi-Zn-expanded oligoacenes **163** and **164** from benzene to pentacene (Figure 102).[388] Combined density functional theory, CASSCF, and CCSD calculations predicted that all of these Zn-expanded oligoacenes have open-shell singlet-ground-state diradicals. The diradical character of the ground states of the molecules arises from the Zn-expansion-induced disjoint nature of the nonbonding molecular orbitals.

The size dependences of the diradical character and second hyperpolarizabilities in dicyclopenta-fused acenes (DPAs) **165** were investigated by Motomura et al. (Table 5).[389] The longitudinal second hyperporizability (γ), which is an indicator of nonlinear optical properties, of singlet DPAs was found to be significantly enhanced with increasing system size. This behavior is associated with an increase in the longitudinal spin polarization between the terminal five-membered rings of the DPAs, which is closely related to the diradical character of DPAs. The correlation of this property with the antiaromaticity of the terminal rings was also investigated.

Kono et al. prepared a series of benzobis(thiadiazole) (BBT) derivatives and investigated their semiconducting characteristics.[390] The benzobis(thiadiazole) unit is a heteroatom mimic of tetramethylenebenzene (TMB) and, thus, inherently has the character of a diradical (Figure 103). Although TMB is a non-Kekulé molecule, BBT can be categorized as a delocalized Kekulé diradical because of the hypervalency of the sulfur atom.

Table 5. Size-Dependent Changes in Diradical Character and Second Hyperpolarizabilities of Dicyclopenta-Fused Acenes

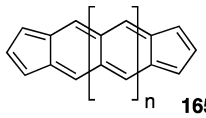

165

n	1	2	3	4	5	6	7	8	9	10	11
diradical character (occupation number in LUMO)	0.21	0.39	0.60	0.74	0.84	0.90	0.93	0.95	0.96	0.96	0.97
γ hyperpolarizability /10^5 a.u.	5.5	21.7	65.0	131	208	294	328	310	363	447	538
NICS(1) at terminal ring	109.6	9.9	0.6	-1.8	-2.7	-3.1	-2.8	-2.5			

dx.doi.org/10.1021/cr400056a | *Chem. Rev.* 2013, 113, 7011−7088

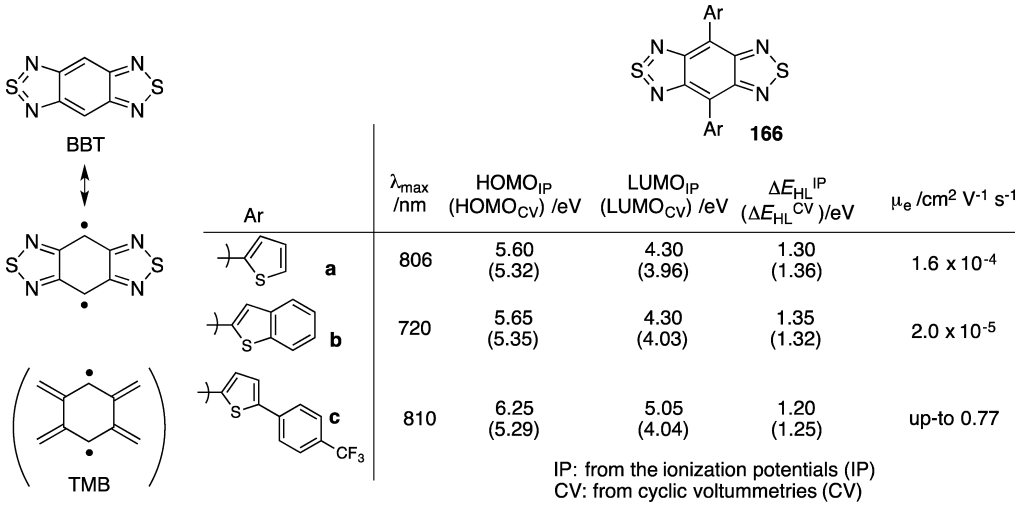

Ar	λ_{max} /nm	$HOMO_{IP}$ ($HOMO_{CV}$) /eV	$LUMO_{IP}$ ($LUMO_{CV}$) /eV	$\Delta E_{HL}{}^{IP}$ ($\Delta E_{HL}{}^{CV}$)/eV	μ_e /cm^2 V^{-1} s^{-1}
a	806	5.60 (5.32)	4.30 (3.96)	1.30 (1.36)	1.6 x 10^{-4}
b	720	5.65 (5.35)	4.30 (4.03)	1.35 (1.32)	2.0 x 10^{-5}
c	810	6.25 (5.29)	5.05 (4.04)	1.20 (1.25)	up-to 0.77

Figure 103. Series of benzobis(thiadiazole) (BBT) derivatives and their semiconducting characteristics.

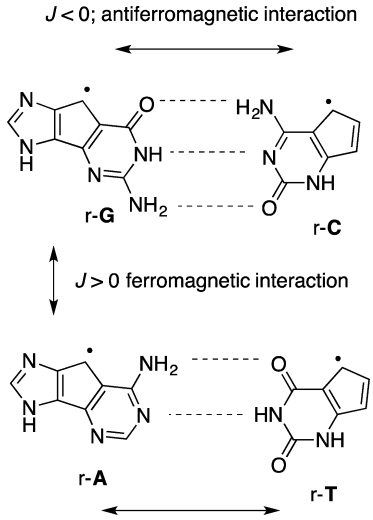

Figure 104. Radicalized DNA bases r-G, r-C, r-A, and r-T for novel electromagnetic properties.

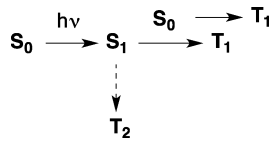

Figure 105. Singlet fission (SF): two triplet excited states (T_1) generated from the interaction of a singlet excited-state molecule (S_1) with a ground-state molecule (S_0)/.

In other words, the sulfur atom stabilizes the diradical. As expected, small HOMO−LUMO energy gaps (ΔE_{HL}) were found for compounds **166a−c** with low electronic excitation energies (λ_{max}). Compound **166c** exhibited a high electron mobility of up to 0.77 cm^2 V^{-1} s^{-1} at 130 °C. The introduction of the strong electron-withdrawing group and the inherent intermolecular interaction ability of the thiadiazole ring are responsible for the high performance.[391]

Radicalized DNA bases r-G, r-C, r-A, and r-T were designed for their novel electromagnetic properties (Figure 104).[392] The ionization potentials of the radicalized DNA bases were calculated to be 1.0 eV lower in energy than the corresponding standard DNA bases. Also, the electron affinities of the radicalized DNA bases were found to increase by about 2 eV compared to those of the four DNA bases. The radical−radical interactions between the two radicalized DNA bases, namely, r-G−r-C and r-A−r-T, were calculated at the BS-UB3LYP/6-311++G(d,p) level of theory. CASSCF calculations were also used for relative energy comparisons. An open-shell singlet ground state was found for the two possible hydrogen-bonded diradicals with small singlet−triplet energy spacings (J = −24.4 cm^{-1} for the r-G−r-C pair), because the pair of diradicals is categorized as disjoint diradicals. In the two-layer stacking model for a helix, a small ferromagnetic interaction was found for the 3′−5′ system.

Recent topics in research on organic photovoltaic cells focus on improvements in energy efficiency. Singlet fission (SF)[393] is a spin-allowed process in which two triplet excited states (T_1) are generated from the interaction of one singlet excited-state molecule (S_1) with a ground-state molecule (S_0). The efficient SF process of excitons improves the efficiency of energy conversion, because some excitons are deactivated before separating into electrons and holes. Efficient SF processes are assumed to be possible when the first excitation energy of the singlets (E_{S1}) is larger than the twice the triplet excitation energy (E_{T1}) and smaller than the second triplet excitation energy (E_{T2}): $E_{T2} > E_{S1} \geq 2E_{T1}$ (Figure 105).

Nakano and co-workers recently proposed that Kekulé hydrocarbons **167** and **168** with diradical character exhibit unique physicochemical properties that are applicable to singlet fission and optoelectronics (Figure 106).[394−396] The diradical and tetraradical characters were also found to play an important role in the feasibility of the SF processes, because the open-shell diradical character should significantly stabilize the open-shell triplet state rather than the singlet state. The authors proposed multiple diradical character y_0 and y_1 to predict the feasibility of the SF process. The diradical character y_0 is equal to the occupation number in the LUMO. The tetraradical character was evaluated by y_1, which is the occupation number in LUMO + 1. They found that the experimentally reported SF efficiencies for polyacenes were high when the y_0 value was around 0.2−0.4 and the y_1/y_0 ratio was less than 0.2. The intermediate character of the diradical and tetraradical is important for the SF efficiency. The parameters, y_0 and y_1/y_0, can be applied to antiaromatic hydrocarbons **167** and **168**. The singlet excited-state energies and the corresponding triplet

dx.doi.org/10.1021/cr400056a | Chem. Rev. 2013, 113, 7011−7088

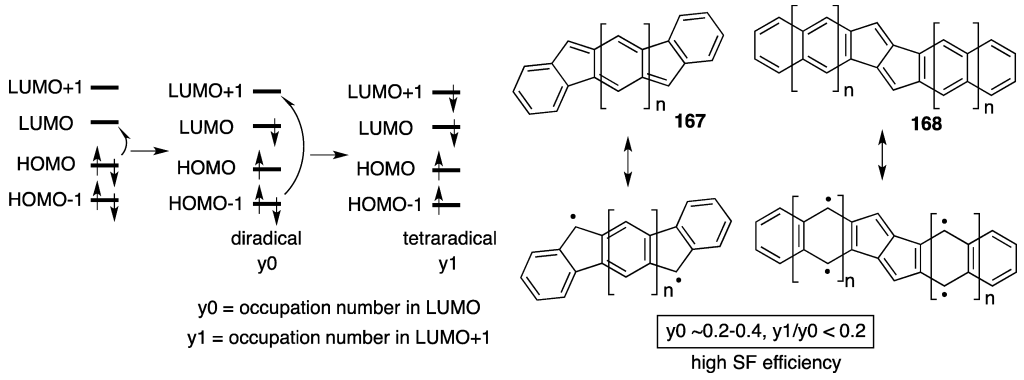

Figure 106. Kekulé hydrocarbons **167** and **168** with diradical character for OFETs and opto-electronics.

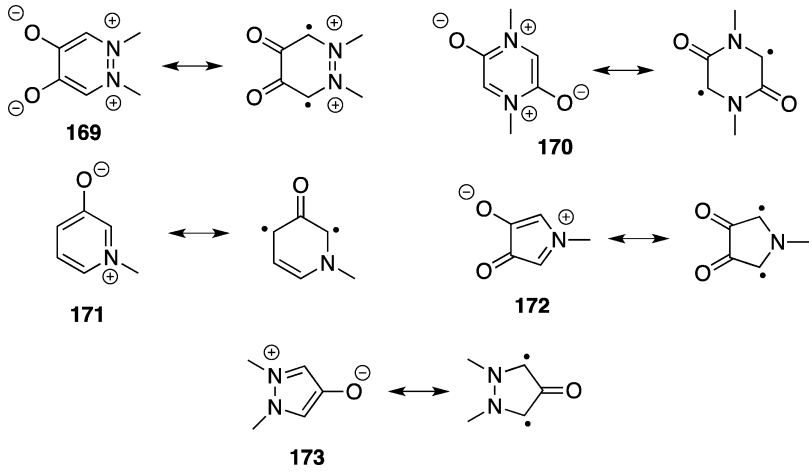

Figure 107. Candidate molecules for efficient process of singlet fission.

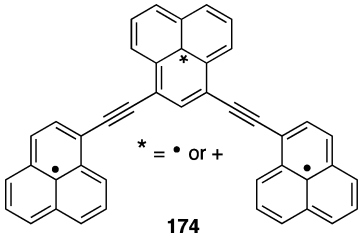

γ /a.u.	*
2.3 x 10^6	radical (•)
−8.0 x 10^7	cation (+)

Figure 108. High second hyperpolarizability (γ) of acetylene-linked phenalenyl radicals.

excited-state energies were computed using time-dependent (TD) DFT with the Tamm−Dancoff approximation (TDA). The energetic stabilization of the triplet excited state was found to be more sensitive to the number (n) of aromatic rings than that of the singlet excited states. Thus, for n = 2 and 3 in compound **167**, the singlet excitation energy was calculated to be larger than twice the triplet excitation energy. For compound **168**, efficient singlet fission was predicted for relatively small-size antiaromatic condensed-ring molecules, $y_0 \approx 0.4$ and $y_1/y_0 < 0.2$.

Akdag et al. designed candidate molecules for efficient singlet fission.[397] All of the excitation energies were calculated at the CASPT2 level of theory. The conditions $E_{T2} > E_{S1} \geq 2E_{T1}$ for

Scheme 62. Product Selectivity in the Solid-State Photochemical Cyclization of α-Adamantyl-*p*-methoxyacetophenone 176

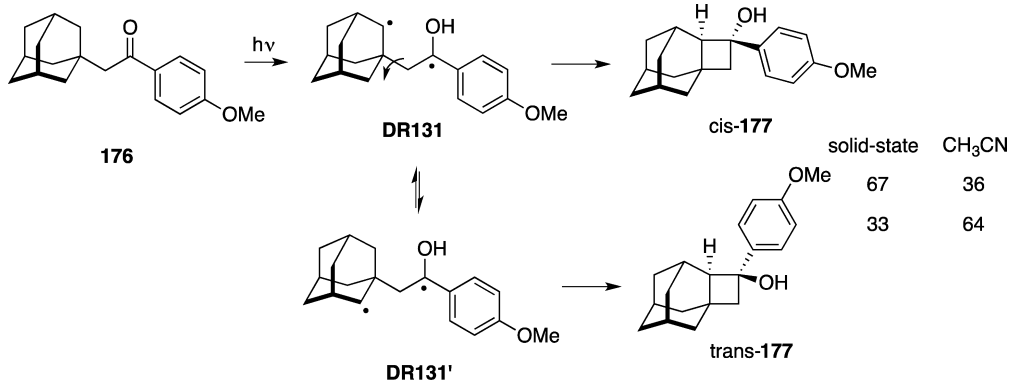

dx.doi.org/10.1021/cr400056a | Chem. Rev. 2013, 113, 7011−7088

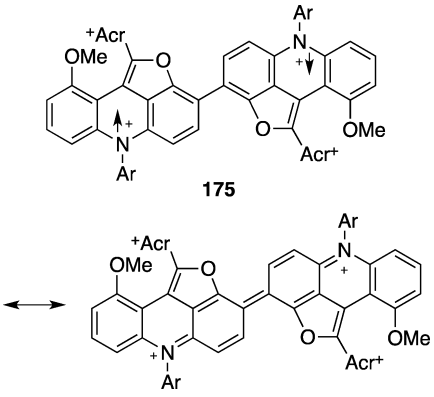

175

efficient singlet fission are fulfilled or nearly fulfilled for compounds **169**–**173**, which are the target molecules for experimental chemists to prepare singlet-fission materials (Figure 107).

Nakano and co-workers found the third-order optical properties at the molecular level and the second hyperpolarizability (γ), nonlinear optical properties, of open-shell singlet molecules with diradical characters have been theoretically predicted to exhibit a significant enhancement as compared to conventional closed-shell molecular systems.[398−401] In 2010 and 2011,[402,403] phenalenyl-based superethylene, superallyl, and superbutadiene in the singlet ground states were found to have diradical characters and exhibit larger γ values than the closed-shell pyrene-based superpolyethylene systems (Figure 108). In particular, the phenalenyl-based superallyl diradical with a positive charge was predicted to change the sign of γ and enhance its amplitude by a factor of 35 compared to that of the neutral superallyl diradical. Notable effects of an external electronic field and donor−acceptor substitution on increasing the second hyperpolarizability of the open-shell singlet diradicals were also reported by Nakano and co-workers.

In 2013, Kamada et al. found that the singlet diradical character actually increased the TPA cross section from <21 to 3600 GM in structure **175**.[404]

7. DIRADICAL INTERMEDIATES IN PHOTOCHEMICAL REACTIONS

Photoinduced reactions of ketones and azoalkanes often include triplet excited-state molecules. In many cases, diradical intermediates are involved in the photochemical reactions. Reports since 2009 are covered in this review article.

Scheme 64. Stereoselective Formation of Cyclopropane Derivative 178 in the Solid-State Photochemical Reaction of 179

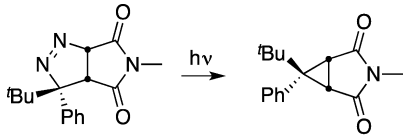

179 178

Kuzmanich et al. investigated product selectivity in the solid-state photochemical cyclization of α-adamantyl-*p*-methoxyacetophenone **176** (Scheme 62).[405] The cis-selective formation of the cyclobutanol product *cis*-**177** was found in the solid state, whereas the trans-selective formation of cyclobutanol occurred. The quantum yield (Φ = 0.39) in the solid state for the cyclobutanol formation reaction was determined to be 3 times greater than that in solution. The 1,4-diradical intermediate **DR131** in the successive Norrish type II and Yang cyclization reaction of crystalline α-adamantyl-*p*-methoxyacetophenone was directly analyzed in the crystalline sample. Excitation of **176** at 355 nm (10-ns pulse) in a nitrogen-degassed acetonitrile solution led to one transient absorbing between 350 and 440 nm with λ_{max} = 385 nm, which was assigned to the triplet excited state of **176**. The triplet excited species decayed in a clean first-order process with a lifetime of 80 ns. The transient

Scheme 63. Generation of Triplet *ortho*-Quinodimethane Diradicals DR132 in the Norrish Type-II Reaction of Acetophenone Derivatives

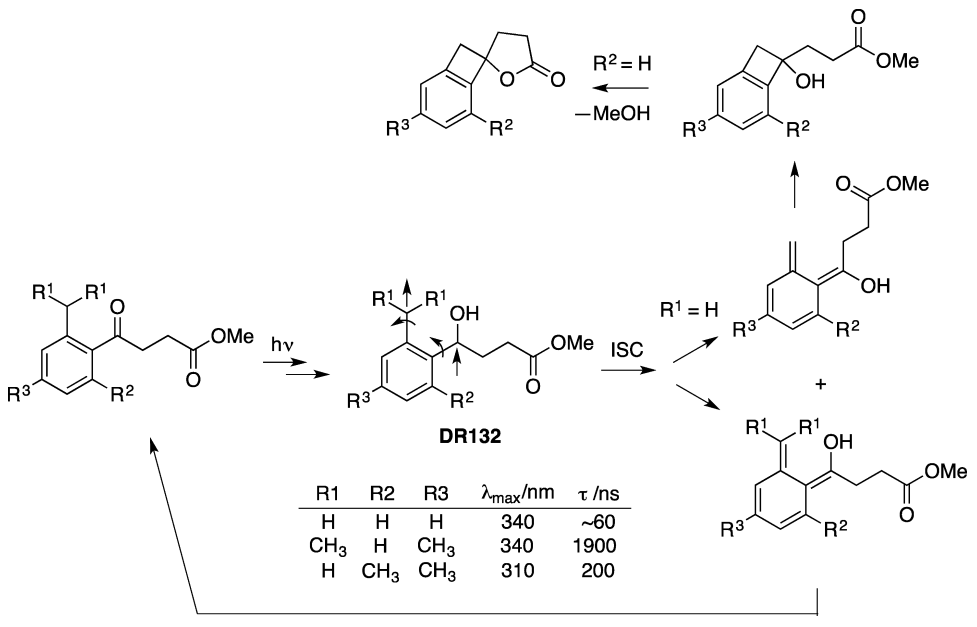

DR132

R1	R2	R3	λ_{max}/nm	τ /ns
H	H	H	340	~60
CH_3	H	CH_3	340	1900
H	CH_3	CH_3	310	200

dx.doi.org/10.1021/cr400056a | *Chem. Rev.* 2013, 113, 7011−7088

Scheme 65. Detection of Diradicals DR133 and DR134 in the Photochemical Reaction of Nanocrystalline

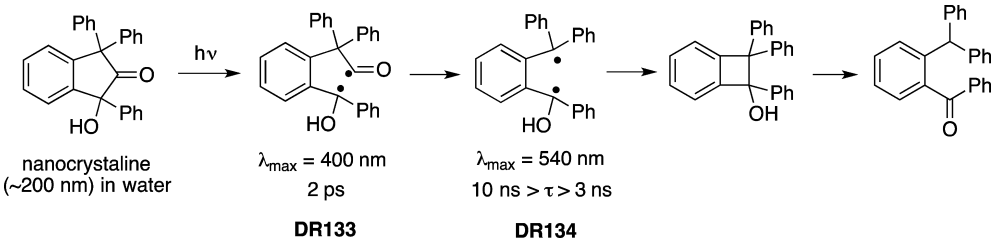

Scheme 66. Photoinduced Redox Reaction of Benzophenone Derivative 180

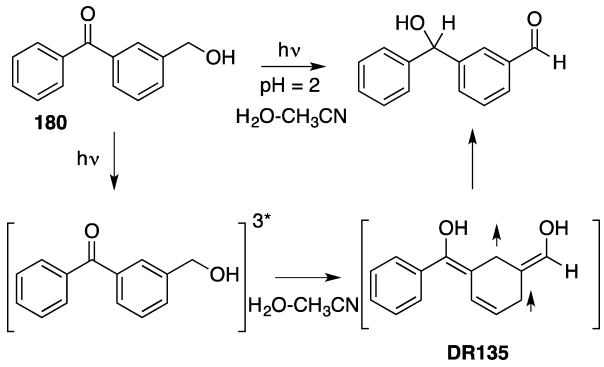

absorption spectroscopy of a nanocrystalline suspension (~200 nm in size) in water clarified the formation of the intermediary 1,4-triplet diradical **DR131** with a broad signal from 320 to 450 nm within 10 ns after laser excitation of **176**. The decay of the transients could be fit to a biexponential function with lifetimes of 10 and 103 ns. The former lifetime was assigned to the triplet excited state of the acetophenone derivative, and the latter was assigned to the 1,4-triplet diradical **DR131**. The Norrish type II hydrogen-transfer reaction was found to be 8 times faster in the solid than in solution.

Gudmundsdottir and co-workers reported the generation and reactivity of the triplet *ortho*-quinodimethane diradicals **DR132** in the Norrish type II reaction of acetophenone derivatives in which the ester group is attached (Scheme 63).[406] Photochemical reactions were utilized for the release of the alcohol moiety of the ester group. Methanol was released in the photochemical reaction. The triplet 1,4-diradicals with $\lambda_{max} \approx$ 350 nm were detected using the laser-flash-photolysis (LFP) method. The triplet diradical was confirmed by efficient quenching by molecular oxygen. The lifetime of the triplet diradicals was found to be strongly dependent on the substituent pattern on the phenyl ring. Thus, the twisted conformation and intramolecular hydrogen-bonded interaction were proposed to affect the rate constant of intersystem crossing.

The highly stereoselective formation of cyclopropane derivative **178** was found in the solid-state photochemical denitrogenation reaction of azoalkane **179**, although a mixture of the cis and trans isomers was found in the solution reaction in acetonitrile (Scheme 64).[407]

The two intermediary diradicals **DR133** and **DR134** were detected in the photochemical reaction of nanocrystals of 1,1,3-triphenyl-3-hydroxy-2-indanone (Scheme 65).[408] Diradical **DR133** was detected at 350−440 nm ($\lambda_{max} \approx$ 400 nm) with a lifetime of ca. 2 ps. A longer lifetime of diradical **DR134**, 3 ns < τ < 10 ns, was observed at 400−600 nm (λ_{max} = 540 nm). The intermediary diradicals were first detected in the decarbonylation reaction induced by photolysis.

Nanosecond time-resolved resonance Raman spectroscopic analysis was performed to investigate the photoinduced redox reaction of benzophenone derivative **180** (Scheme 66). Triplet diradical **DR135** was detected during the formation of the redox product. Density functional theory calculations were utilized to help the assignment of the intermediary Raman spectra.[409]

A hydrogen-bonding interaction in the exciplex intermediate and triplet 1,4-diradical intermediate was found for the stereoselective formation of oxetane derivative (Scheme 67).[410,411] A computational study on the triplet 1,4-diradical intermediates in the Paternó−Büchi reaction was recently performed by D'Auria and Racioppi at the UDFT level of theory.[412]

A laser-flash-photolysis study was performed to detect the intermediary triplet diradicals in the photochemical reactions of *o*-ethoxybenzophenone and *o*-2,2,2-trifluoroethoxybenzophenone in cyclohexane solution (Scheme 68).[413] The transient absorption spectra excited at 355 nm were observed for the photochemical reactions at 500−650 nm. The transient species were assigned to the intermediary triplet diradicals **DR136**. The lifetime of the trifluoro-substituted diradical was found to be 200 ns, which was longer than that of the derivative for the methyl-substituted diradical (25 ns). The lower stereoselectivity in the cyclization product for R = CF_3 than R = CH_3 was explained by the longer-lived diradical, because conformational changes are possible for the intersystem-crossing process.

Ayitou and Sivaguru found the enantiospecific photocyclization of axially chiral acrylanilides (Scheme 69).[414] The enantiomeric ratio in the photoproduct **181** during the 6π photocyclization was found to be dependent on the spin state

Scheme 67. Hydroxyl Group Effect on Stereoselectivity in the Paternó−Büchi Reaction

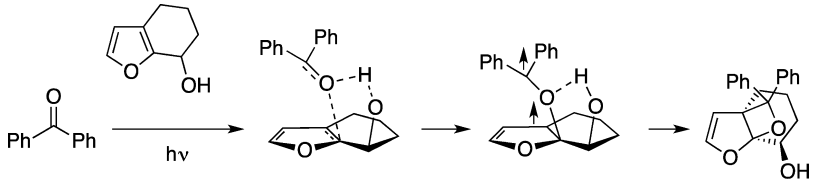

dx.doi.org/10.1021/cr400056a | Chem. Rev. 2013, 113, 7011−7088

Scheme 68. Generation of Triplet 1,5-Diradical in Photochemical Reactions of *o*-Ethoxybenzophenone and *o*-2,2,2-Trifluoroethoxybenzophenone

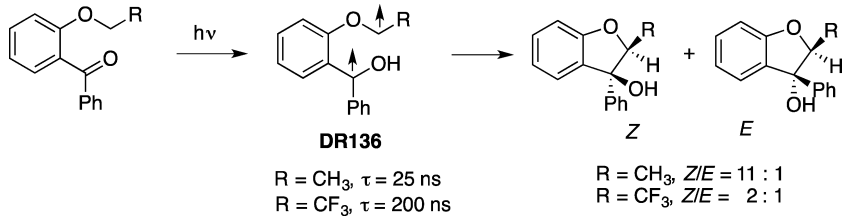

Scheme 69. Enatiospecific Photocyclization of Axially Chiral Acrylanilides

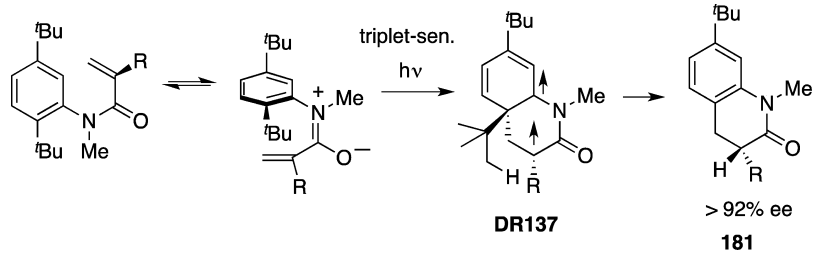

Scheme 70. Formation of the *aci*-Nitro Group from Ortho-Alkyl-Substituted Nitrobenzene

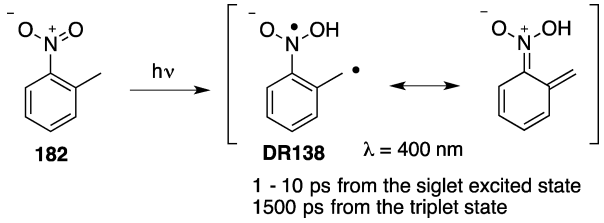

of the excited-state molecule, where the triplet state gave an enantiomeric ratio of >95: 5. The reaction mechanism was proposed to occur through the triplet diradical **DR137**.

The *ortho*-nitrobenzyl group is a well-known photolabile protecting group for carboxylic acids. It is commonly assumed that the transfer of a hydrogen atom from the ortho substituent to the triplet excited state of the nitro group is the primary step in the photoinduced deprotection process. Schmierrer et al. applied femtosecond spectroscopy to the photoreaction of *ortho*-nitrotoluene **182**. In the UV−vis transient absorption spectrum, a band peaking at 400 nm was assigned to *aci*-nitro form **DR138**. The formation of the *aci*-nitro group was found in both the singlet channel (1−10 ps) and the triplet channel (1500 ps)[415] (see Scheme 70).

Wang et al. found the photoinduced [4 + 4], [4 + 2], and [2 + 2] cycloaddition reactions of quinones with oxazoles (Scheme 71). The formation of the three possible cycloaddition

Scheme 71. Photoinduced [4 + 4], [4 + 2], and [2 + 2] Cycloaddition Reactions of Quinones with Oxazoles

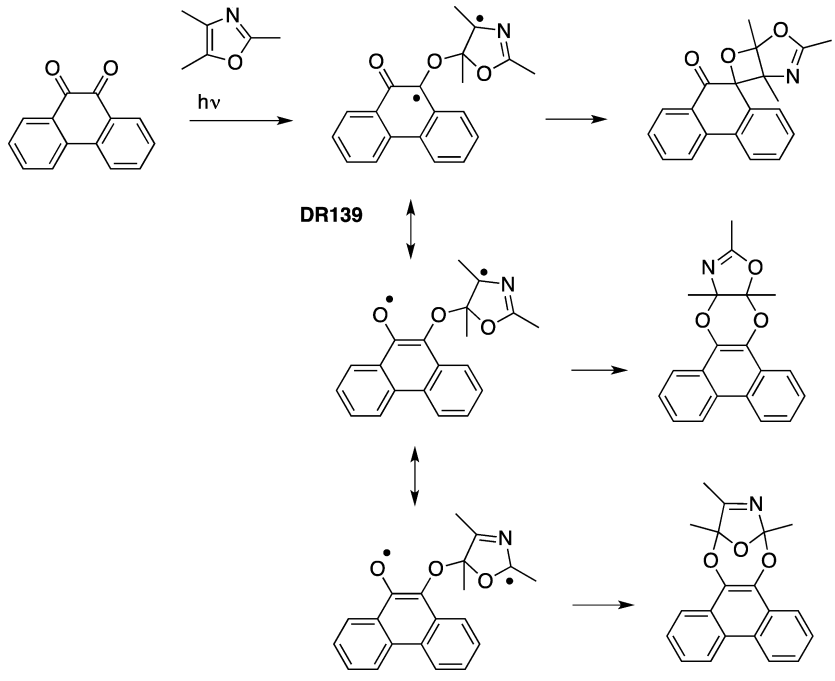

dx.doi.org/10.1021/cr400056a | *Chem. Rev.* 2013, 113, 7011−7088

Scheme 72. Stereoselective Cyclization Reaction through Diradical Intermediate DR140 in the Triplet-Sensitized Photoreaction of 183

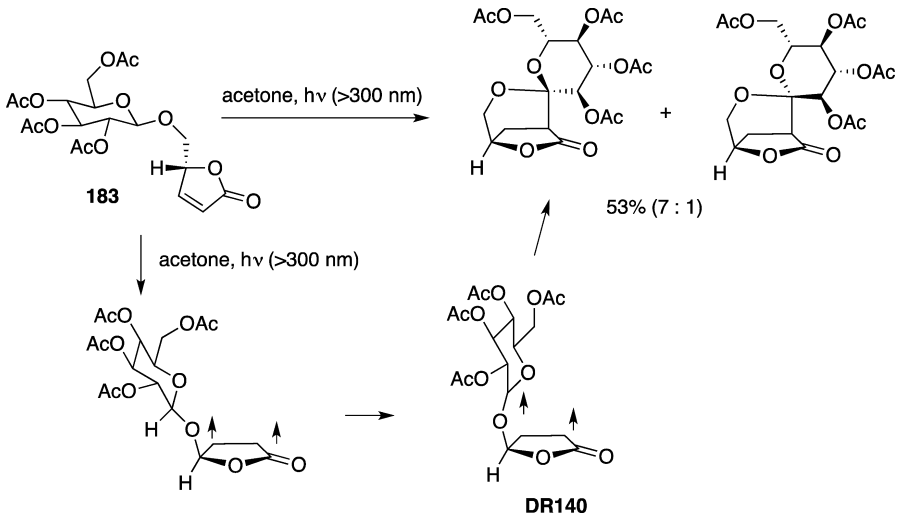

Scheme 73. Manipulation of Singlet−Triplet Equilibration of 1,4-Phenylenedinitrene Using a Strong Magnetic Field (up to 35 T)

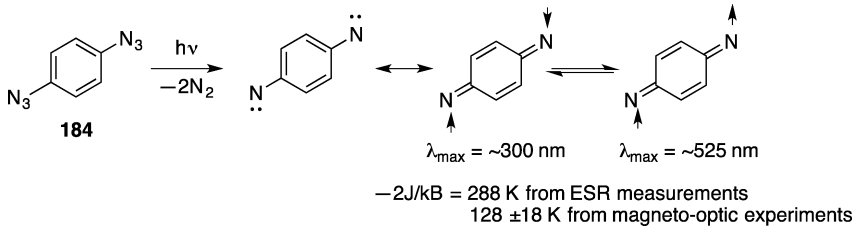

products can be explained by the intervention of the highly stabilized diradical **DR139**.[416]

Stereoselective cyclization reactions through diradical intermediate **DR140** were reported by Jahjah et al. in the triplet-sensitized photoreaction of **183** (Scheme 72).[417]

Manipulation of the singlet−triplet equilibrium of 1,4-phenylenedinitrene, which was generated by the photochemical denitrogenation of 1,4-diazidobenzene **184**, using a strong magnetic field (up to 35 T) was reported (Scheme 73).[418] The triplet state was the preferred spin state under high-magnetic-field conditions. Thus, the equilibrium was strongly affected by the magnetic field for molecules with small singlet−triplet energy spacings. Manipulation using an external magnetic field would be a useful method for determining the singlet−triplet energy spacing for diradicals that are thermally unstable, and thus, manipulation by temperature was not used to determine the energy gap.

8. SUMMARY

In this review article, recent development in diradical chemistry are summarized in detail. Diradicals are long-known chemical species, but they continue to be fascinating molecules because of their inherently high reactivity and their potential molecular functions, which are mainly derived from their small HOMO−LUMO energy gaps. Kinetic stabilization and thermodynamic stabilization have made it possible to isolate diradical species. Materials chemistry based on molecules with diradical character has just opened. The interplay between theory and experiments on diradical chemistry will assist in significant developments in this new field of chemistry.

AUTHOR INFORMATION

Corresponding Author

*E-mail: mabe@hiroshima-u.ac.jp.

Notes

The authors declare no competing financial interest.

Biography

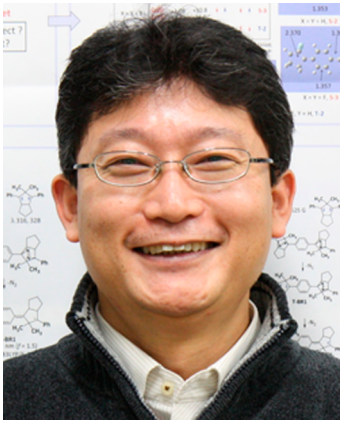

Manabu Abe was born in Sakai City, Osaka Prefecture, Japan. He received his Ph.D. in 1995 from the Kyoto Institute of Technology (KIT), under Professor Akira Oku, studying the oxidative ring-opening reaction of cyclopropanone acetals and its application to organic synthesis. In 1995, he became a faculty staff member at Osaka University (HANDAI, Professor Masatomo Nojima's group). From 1997 to 1998, he was an Alexander von Humboldt fellow with Professor Dr. Waldemar Adam at Universität Würzburg in Würzburg,

dx.doi.org/10.1021/cr400056a | Chem. Rev. 2013, 113, 7011−7088

Germany. He was also a visiting researcher at Ludwig-Maximilians-Universität München (Professor Dr. Herbert Mayr) in 2007. He moved to Hiroshima, Japan, and became a Full Professor in Organic Chemistry at the Department of Chemistry, Graduate School of Science, Hiroshima University (HIRODAI), in 2007. His research focuses on the chemistry of reactive intermediates, especially diradicals, organic photochemistry, and unusual molecules.

ACKNOWLEDGMENTS

The project on diradicals was supported by Grants-in-Aid for Science Research on Innovative Areas "Stimuli-Responsive Chemical Species" (No. 24109008) and "pi-Space" (No. 21108516) and Grant 19350021 from the Ministry of Education, Culture, Sports, Science and Technology, Japan, and by the Tokuyama Science Foundation. M.A. expresses his deep gratitude to Professor Masaaki Yoshifuji and the reviewers of this manuscript for their kind suggestions and comments on this article. This article is dedicated to Professor Dr. Waldemar Adam on the occasion of his 75th birthday and Professor Herbert Mayr on the occasion of his 65th birthday.

REFERENCES

(1) *Reactive Intermediate Chemistry*; Moss, R. A., Platz, M. S., Jones, M., Jr., Eds.; Wiley-Interscience: New York, 2004.
(2) In *Stable Radicals*; Hicks, R. G., Ed.; John Wiley & Sons: New York, 2010.
(3) Salem, L.; Rowland, C. *Angew. Chem., Int. Ed.* **1972**, *11*, 92.
(4) Borden, W. T. In *Diradicals*; Borden, W. T., Ed.; Wiley-Interscience: New York, 1982, 1.
(5) Bonacic-Koutecky, V.; Koutecky, J.; Michl, J. *Angew. Chem., Int. Ed.* **1987**, *26*, 170.
(6) *IUPAC Compendium of Chemical Terminology*, release 2.3.2; International Union of Pure and Applied Chemistry (IUPAC): Research Triangle Park, NC, 2012; p 168.
(7) *IUPAC Compendium of Chemical Terminology*, release 2.3.2; International Union of Pure and Applied Chemistry (IUPAC): Research Triangle Park, NC, 2012; p 427.
(8) Dupeyre, E. M.; Lemaire, H.; Rassat, A. *J. Am. Chem. Soc.* **1965**, *87*, 3771.
(9) Briére, R.; Dupeyre, R. M.; Lemaire, H.; Morat, C.; Rassat, A.; Rey, P. *Bull. Soc. Chim. Fr.* **1965**, 3290.
(10) Chandross, E. A. *J. Am. Chem. Soc.* **1964**, *86*, 1263.
(11) (a) von Eggers Doering, W.; Toscano, V. G.; Beasley, G. H. *Tetrahedron* **1971**, *27*, 5299. (b) Kolc, J.; Michl, J. *J. Am. Chem. Soc.* **1973**, *95*, 7391. (c) Dewar, M. J. S.; Wade, L. E. *J. Am. Chem. Soc.* **1977**, *99*, 4417. (d) Dewar, M. J. S.; Healy, E. F. *Chem. Phys. Lett.* **1987**, *141*, 521. (e) Michl, J.; Koutecký, B. *Tetrahedron* **1988**, *44*, 7559. (f) von Eggers Doering, W.; Wang, Y. *J. Am. Chem. Soc.* **1999**, *121*, 10112 . In their original article, "biradical and biradicaloid" were used instead of "diradical and diradicaloid"..
(12) Hund, F. *Z. Phys.* **1925**, *33*, 345.
(13) Dohnert, D.; Koutecky, J. *J. Am. Chem. Soc.* **1980**, *102*, 1789.
(14) Wenthold, P. G.; Squires, R. R.; Lineberger, W. C. *J. Am. Chem. Soc.* **1998**, *120*, 5279.
(15) Evangelista, F. A.; Allen, W. D.; Schaefer, H. F., III. *J. Chem. Phys.* **2007**, *127*, 024102.
(16) Carpenter, B. K.; Pittner, J.; Veis, L. *J. Phys. Chem. A* **2009**, *113*, 10557.
(17) Noodleman, L. *J. Chem. Phys.* **1981**, *74*, 5737. (b) Noodleman, L.; Baerends, E. J. *J. Am. Chem. Soc.* **1984**, *106*, 2316.
(18) (a) Yamaguchi, K.; Takahara, Y.; Fueno, T.; Nasu, K. *Jpn. J. Appl. Phys.* **1987**, *26*, L1362. (b) Yamaguchi, K.; Jensen, F.; Dorigo, A.; Houk, K. N. *Chem. Phys. Lett.* **1988**, *149*, 537.
(19) (a) Kitagawa, Y.; Saito, T.; Itoh, M.; Shoji, M.; Koizumi, K.; Yamanaka, S.; Kawakami, T.; Okumura, M.; Yamaguchi, K. *Chem. Phys. Lett.* **2007**, *442*, 445. (b) Saito, T.; Nishihara, S.; Kataoka, Y.; Nakanishi, Y.; Matsui, T.; Kitagawa, Y.; Kawakami, T.; Okumua, M.; Yamaguchi, K. *Chem. Phys. Lett.* **2009**, *483*, 168.
(20) Ess, D. H.; Johnson, E. R.; Hu, Z.; Yang, W. *J. Phys. Chem. A* **2011**, *115*, 76.
(21) (a) Scaiano, J. C. In *Reactive Intermediate Chemistry*; Moss, R. A., Platz, M. S., Jones, M., Jr., Eds.; John Wiley & Sons: New York, 2004; p 847. (b) Hilinski, E. F. In *Reactive Intermediate Chemistry*; Moss, R. A., Platz, M. S., Jones, M., Jr., Eds.; John Wiley & Sons: New York, 2004; p 873. (c) Baldwin, J. E. In *Reactive Intermediate Chemistry*; Moss, R. A., Platz, M. S., Jones, M., Jr., Eds.; John Wiley & Sons: New York, 2004; p 899.
(22) (a) Weil, J. A.; Bolton, J. R.; Wertz, J. E. *Electron Paramagnetic Resonce*; Wiley Interscience: New York, 1994. (b) Berson, J. A. In *The Chemistry of Quinoid Compounds*; Patai, S., Rappoport, Z., Eds.; Wiley: New York, 1988; Vol. *II*, pp 455−536. (c) Wasserman, E.; Hutton, R. S. *Acc. Chem. Res.* **1977**, *10*, 27.
(23) Eaton, S. S.; More, K. M.; Sawant, B. M.; Eaton, G. R. *J. Am. Chem. Soc.* **1983**, *105*, 6550.
(24) Bertrand, P.; More, C.; Guigliarelli, B.; Fournel, A.; Bennett, B.; Howes, B. *J. Am. Chem. Soc.* **1994**, *116*, 3078.
(25) Riplinger, C.; Kao, J. P. Y.; Rosen, G. M.; Kathiervelu, V.; Eaton, G. R.; Eaton, S. S.; Kutateladze, A.; Neese, F. *J. Am. Chem. Soc.* **2009**, *131*, 10092.
(26) See, for example: (a) Hirao, Y.; Ino, H.; Ito, A.; Tanaka, K.; Kato, T. *J. Phys. Chem. A* **2006**, *110*, 4866. (b) Sawai, T.; Sato, K.; Ise, T.; Shiomi, D.; Toyota, K.; Morita, Y.; Takui, T. *Angew. Chem., Int. Ed.* **2008**, *120*, 4052.
(27) Bleaney, B.; Bowers, K. D. *Proc. R. Soc. London A* **1952**, *214*, 451.
(28) Lineberger, W. C.; Borden, W. T. *Phys. Chem. Chem. Phys.* **2011**, *13*, 11792.
(29) Wenthold, P. G.; Lineberger, W. C. *Acc. Chem. Res.* **1999**, *32*, 597.
(30) Robinson, M. S.; Polak, M. L.; Bierbaum, V. M.; DePuy, C. H.; Lineberger, W. C. *J. Am. Chem. Soc.* **1995**, *117*, 6766.
(31) Caldwell, R. A. In *Kinetics and Spectroscopy of Carbenes and Biradicals*; Platz, M. S., Ed.; Plenum Press: New York, 1990; pp 77−116.
(32) Doubleday, C., Jr.; Turro, N. J.; Wang, J.-F. *Acc. Chem. Res.* **1989**, *22*, 199.
(33) Kita, F.; Adam, W.; Jordan, P.; Nau, W. M.; Wirz, J. *J. Am. Chem. Soc.* **1999**, *121*, 9265.
(34) Scaiano, J. C. *Tetrahedron* **1982**, *38*, 819.
(35) Adam, W.; Grabowski, S.; Wilson, R. M. *Acc. Chem. Res.* **1990**, *23*, 165.
(36) Griesbeck, A. G.; Mauder, H.; Stadtmueller, S. *Acc. Chem. Res.* **1994**, *27*, 70.
(37) Griesbeck, A. G.; Abe, M.; Bondock, S. *Acc. Chem. Res.* **2004**, *37*, 919.
(38) Johnston, L. J.; Scaiano, J. C. *Chem. Rev.* **1989**, *89*, 521.
(39) Johnston, L. J. *Chem. Rev.* **1993**, *93*, 251.
(40) Dougherty, D. A. *Acc. Chem. Res.* **1991**, *24*, 88.
(41) Coms, F. D.; Dougherty, D. A. *Tetrahedron Lett.* **1988**, *29*, 3753.
(42) Adam, W.; Harrer, H. M.; Kita, F.; Nau, W. M. *Pure Appl. Chem.* **1997**, *69*, 91.
(43) Arnold, D. R.; Evnin, A. B.; Kasai, P. H. *J. Am. Chem. Soc.* **1969**, *91*, 784.
(44) Buchwalter, S. L.; Closs, G. L. *J. Am. Chem. Soc.* **1975**, *97*, 3857.
(45) Buchwalter, S. L.; Closs, G. L. *J. Am. Chem. Soc.* **1979**, *101*, 4688.
(46) Jain, R.; Snyder, G. J.; Dougherty, D. A. *J. Am. Chem. Soc.* **1984**, *106*, 7294.
(47) Jain, R.; Sponsler, M. B.; Coms, F. D.; Dougherty, D. A. *J. Am. Chem. Soc.* **1988**, *110*, 1356.
(48) Adam, W.; Harrer, H. M.; Kita, F.; Nau, W. M. *Adv. Photochem.* **1998**, *24*, 205.
(49) For delocalized diradicals, see: Berson, J. A. *Acc. Chem. Res.* **1997**, *30*, 238.
(50) Abe, M.; Ishihara, C.; Nojima, M. *J. Org. Chem.* **2003**, *68*, 1618.

(51) Hoffmann, R. *J. Am. Chem. Soc.* **1968**, *90*, 1475.
(52) Hoffmann, R. *Acc. Chem. Res.* **1971**, *4*, 1.
(53) Abe, M.; Je, J.; Mishima, M. *Chem. Soc. Rev.* **2012**, *41*, 3808.
(54) Conrad, M. P.; Pitzer, R. M.; Schaefer, H. F., III. *J. Am. Chem. Soc.* **1979**, *101*, 2245.
(55) (a) Getty, S. J.; Hrovat, D. A.; Borden, W. T. *J. Am. Chem. Soc.* **1994**, *116*, 1521. (b) Lemal, D. M. *J. Org. Chem.* **2009**, *74*, 2413.
(56) (a) Abe, M.; Adam, W.; Nau, W. M. *J. Am. Chem. Soc.* **1998**, *120*, 11304. (b) Abe, M.; Adam, W.; Heidenfelder, T.; Nau, W. M.; Zhang, X. *J. Am. Chem. Soc.* **2000**, *122*, 2019.
(57) (a) Johnson, W. T. G.; Hrovat, D. A.; Skancke, A.; Borden, W. T. *Theor. Chem. Acc.* **1999**, *102*, 207. (b) Abe, M.; Kawanami, S.; Ishihara, C.; Nojima, M. *J. Org. Chem.* **2004**, *69*, 5622.
(58) Abe, M.; Ishihara, C.; Nojima, M. *J. Org. Chem.* **2003**, *68*, 1618.
(59) Abe, M.; Adam, W.; Borden, W. T.; Hattori, M.; Hrovat, D. A.; Nojima, M.; Nozaki, K.; Wirz, J. *J. Am. Chem. Soc.* **2004**, *126*, 574.
(60) Simmons, H. E.; Fukunaga, T. *J. Am. Chem. Soc.* **1967**, *89*, 5208.
(61) Ma, J.; Ding, Y.; Hattori, K.; Inagaki, S. *J. Org. Chem.* **2004**, *69*, 4245.
(62) Abe, M.; Ishihara, C.; Takegami, A. *J. Org. Chem.* **2004**, *69*, 7250.
(63) Giordan, J. C. *J. Am. Chem. Soc.* **1983**, *105*, 6544.
(64) (a) Abe, M.; Kubo, E.; Nozaki, K.; Matsuo, T.; Hayashi, T. *Angew. Chem., Int. Ed.* **2006**, *45*, 7828. (b) Abe, M.; Kubo, E.; Nozaki, K.; Matsuo, T.; Hayashi, T. *Angew. Chem., Int. Ed.* **2012**, *51*, 11911. (c) Manuscript in preparation.
(65) Nakamura, T.; Gagliardi, L.; Abe, M. *J. Phys. Org. Chem.* **2010**, *23*, 300.
(66) Adam, W.; Borden, W. T.; Burda, C.; Foster, H.; Heidenfelder, T.; Jeubes, M.; Hrovat, D. A.; Kita, F.; Lewis, S. B.; Scheutzow, D.; Wirz, J. *J. Am. Chem. Soc.* **1998**, *120*, 593.
(67) Zhang, D. Y.; Hrovat, D. A.; Abe, M.; Borden, W. T. *J. Am. Chem. Soc.* **2003**, *125*, 12823.
(68) Abe, M.; Adam, W.; Hara, M.; Hattori, M.; Majima, T.; Nojima, M.; Tachibana, K.; Tojo, S. *J. Am. Chem. Soc.* **2002**, *124*, 6540.
(69) Abe, M.; Hattori, M.; Takegami, A.; Masuyama, A.; Hayashi, T.; Seki, S.; Tagawa, S. *J. Am. Chem. Soc.* **2006**, *128*, 8008.
(70) Creary, X. *Acc. Chem. Res.* **2006**, *39*, 761.
(71) Abe, M.; Adam, W.; Borden, W. T.; Hattori, M.; Hrovat, D. A.; Nojima, M.; Nozaki, K.; Wirz, J. *J. Am. Chem. Soc.* **2004**, *126*, 574.
(72) Nakagaki, T.; Sakai, T.; Mizuta, T.; Fujiwara, Y.; Abe, M. *Chem.—Eur. J.*, published online Jun 20, 2013, 10.1002/chem.201300038.
(73) Mishima, M.; Fujiwara, Y.; Abe, M., manuscript in preparation.
(74) Nakamura, T.; Takegami, A.; Abe, M. *J. Org. Chem.* **2010**, *75*, 1956.
(75) (a) Mondal, K. C.; Roesky, H. W.; Schwarzer, M. C.; Frenking, G.; Tkach, I.; Wolf, H.; Kratzert, D.; Herbst-Irmer, R.; Niepötter, B.; Stalke, D. *Angew. Chem., Int. Ed.* **2013**, *52*, 1801. (b) Mondal, K. C.; Roesky, H. W.; Schwarzer, M. C.; Frenking, G.; Niepötter, B.; Wolf, H.; Herbst-Irmer, R.; Stalke, D. *Angew. Chem., Int. Ed.* **2013**, *52*, 2963. (c) Mondal, K. C.; Samuel, P. P.; Tretiakov, M.; Singh, A. P.; Roesky, H. W.; Stückl, A. C.; Niepötter, B.; Carl, E.; Wolf, H.; Herbst-Irmer, R.; Stalke, D. *Inorg. Chem.* **2013**, *52*, 4736.
(76) Abe, M.; Furunaga, H.; Ma, D.; Gagliardi, L.; Bodwell, G. J. *J. Org. Chem.* **2012**, *77*, 7612.
(77) Abe, M.; Kawanami, S.; Ishihara, C.; Nojima, M. *J. Org. Chem.* **2004**, *69*, 5622.
(78) Ashe, A. J., III. *J. Am. Chem. Soc.* **1973**, *95*, 818.
(79) Abe, M.; Ishihara, C.; Kwanami, S.; Masuyama, A. *J. Am. Chem. Soc.* **2005**, *127*, 10.
(80) Hamaguchi, M.; Nakaishi, M.; Nagai, T.; Nakamura, T.; Abe, M. *J. Am. Chem. Soc.* **2007**, *129*, 12981.
(81) Yagi, S.; Hiraga, Y.; Takagi, R.; Abe, M. *J. Phys. Org. Chem.* **2011**, *24*, 894.
(82) Ishihara, C.; Abe, M. *Aust. J. Chem.* **2010**, *63*, 1615.
(83) Hickenboth, C. R.; Moore, J. S.; White, S. R.; Sottos, N. R.; Baudry, J.; Wilson, S. R. *Nature* **2007**, *446*, 423.
(84) Lenhardt, J. M.; Ogle, J. W.; Ong, M. T.; Choe, R.; Martinez, T. J.; Craig, S. L. *J. Am. Chem. Soc.* **2011**, *133*, 3222.
(85) Kochhar, G.; Bailey, A.; Mosey, N. J. *Angew. Chem., Int. Ed.* **2010**, *49*, 7452.
(86) (a) Beyer, M. T.; Clausen-Schaumann, H. *Chem. Rev.* **2005**, *105*, 2921. (b) Ribas-Arino, J.; Marx, D. *Chem. Rev.* **2012**, *112*, 5414.
(87) Lenhardt, J. M.; Ong, M. T.; Choe, R.; Evenhuis, C. R.; Martinez, T. J.; Craig, S. *Science* **2010**, *329*, 1057.
(88) Soleilhavoup, M.; Bertrand, G. *Bull. Chem. Soc. Jpn.* **2007**, *80*, 1241.
(89) Scheschkewitz, D.; Amii, H.; Gornitzka, H.; Schoeller, W. W.; Bourissou, D.; Bertrand, G. *Science* **2002**, *295*, 1880.
(90) Amii, H.; Vranicar, L.; Gornitzka, H.; Bourissou, D.; Bertrand, G. *J. Am. Chem. Soc.* **2004**, *126*, 1344.
(91) Fuks, G.; Saffon, N.; Maron, L.; Bertrand, G.; Bourissou, D. *J. Am. Chem. Soc.* **2009**, *131*, 13681.
(92) Scheschkewitz, D.; Amii, H.; Gornitzizka, H.; Schoeller, W. W.; Bourissou, D.; Bertrand, G. *Angew Chem., Int. Ed.* **2004**, *43*, 585.
(93) Rodriguez, A.; Olsen, R. A.; Ghaderi, N.; Scheschkewitz, D.; Tham, F. S.; Mueller, L. J.; Bertrand, G. *Angew. Chem., Int. Ed.* **2004**, *43*, 4880.
(94) Rodriguez, A.; Tham, F. S.; Schoeller, W. W.; Bertrand, G. *Angew. Chem., Int. Ed.* **2004**, *43*, 4876.
(95) Rodriguez, A.; Fuks, G.; Bourg, J.-B.; Bourissou, D.; Tham, F. S.; Bertrand, G. *Dalton Trans.* **2008**, 4482.
(96) Bell, F.; Casanova, D.; Head-Gordon, M. *J. Am. Chem. Soc.* **2010**, *132*, 11314.
(97) Seiertstad, M.; Kinsinger, C. R.; Cramer, C. J. *Angew. Chem., Int. Ed.* **2002**, *41*, 3894.
(98) Cheng, M.-J.; Hu, C.-H. *Mol. Phys.* **2003**, *101*, 1319.
(99) Saettel, N.; Wiest, O. *J. Org. Chem.* **2003**, *68*, 4549.
(100) Schoeller, W. W.; Rozhenko, A.; Bourissou, D.; Bertrand, G. *Chem.—Eur. J.* **2003**, *9*, 3611.
(101) Jung, Y.; Head-Gordon, M. *J. Phys. Chem. A* **2003**, *107*, 7475.
(102) Henke, P.; Pankewitz, T.; Klopper, W.; Breher, F.; Schnöckel, H. *Angew. Chem., Int. Ed.* **2009**, *48*, 8141.
(103) Doddi, A.; Gemel, C.; Winter, M.; Fischer, R. A.; Goedecke, C.; Rzepa, H. S.; Frenking, G. *Angew. Chem., Int. Ed.* **2013**, *52*, 450.
(104) Jung, Y.; Heine, T.; Schleyer, P. v. R.; Head-Gordon, M. *J. Am. Chem. Soc.* **2004**, *126*, 3132.
(105) Tuononen, H. M.; Suontamo, R.; Valkonen, J.; Laitinen, R. S. *J. Phys. Chem. A* **2004**, *108*, 5670.
(106) Breher, F. *Coord. Chem. Rev.* **2007**, *251*, 1007.
(107) Niecke, E.; Fuchs, A.; Baumeister, F.; Nieger, M.; Schoeller, W. W. *Angew. Chem., Int. Ed.* **1995**, *34*, 555.
(108) Niecke, E.; Fuchs, A.; Nieger, M. *Angew. Chem., Int. Ed.* **1999**, *38*, 3028.
(109) Niecke, E.; Fuchs, A.; Nieger, M.; Schmidt, O.; Schoeller, W. W. *Angew. Chem., Int. Ed.* **1999**, *38*, 3031.
(110) Sebastian, M.; Nieger, M.; Szieberth, D.; Nyulaszi, L.; Niecke, E. *Angew. Chem., Int. Ed.* **2004**, *43*, 637.
(111) Sebastian, M.; Hoskin, A.; Nieger, M.; Nyulaszi, L.; Niecke, E. *Angew. Chem., Int. Ed.* **2005**, *44*, 1405.
(112) Schmidt, O.; Fuchs, A.; Gudat, D.; Nieger, M.; Hoffgauer, W.; Niecke, E.; Schoeller, W. W. *Angew. Chem., Int. Ed.* **1998**, *37*, 949.
(113) Schoeller, W. W.; Niecke, E. *Phys. Chem. Chem. Phys.* **2012**, *14*, 2015.
(114) Sugiyama, H.; Ito, S.; Yoshifuji, M. *Angew. Chem., Int. Ed.* **2003**, *42*, 3802.
(115) Sugiyama, H.; Ito, S.; Yoshifuji, M. *Chem.—Eur. J.* **2004**, *10*, 2700.
(116) Yoshifuji, M.; Arduengo, A. J., III; Konovalova, T. A.; Kispert, L. D.; Kikuchi, M.; Ito, S. *Chem. Lett.* **2006**, *35*, 1136.
(117) Yoshifuji, M.; Hirano, Y.; Schnakenburg, G.; Streubel, R.; Niecke, E.; Ito, S. *Helv. Chim. Acta* **2012**, *95*, 1723.
(118) Ito, S.; Kikuchi, M.; Sugiyama, H.; Yoshifuji, M. *J. Organomet. Chem.* **2007**, *692*, 2761.
(119) Ito, S.; Miura, J.; Morita, N.; Yoshifuji, M.; Arduengo, A. J., III. *Angew. Chem., Int. Ed.* **2008**, *47*, 6418.

(120) Ito, S.; Miura, J.; Morita, N.; Yoshifuji, M.; Arduengo, A. J., III. *Inorg. Chem.* **2009**, *48*, 8063.
(121) Ito, S.; Miura, J.; Morita, N.; Yoshifuji, M.; Arduengo, A. J., III. *Dalton Trans.* **2010**, *39*, 8281.
(122) Ito, S.; Miura, J.; Morita, N.; Yoshifuji, M.; Arduengo, A. J., III. *Heteroatom Chem.* **2010**, *21*, 404.
(123) Ito, S.; Kikuchi, M.; Miura, J.; Morita, N.; Yoshifuji, M. *J. Phys. Org. Chem.* **2012**, *25*, 733.
(124) Cui, C.; Brynda, M.; Olmstead, M. M.; Power, P. P. *J. Am. Chem. Soc.* **2004**, *126*, 6510.
(125) Wang, X.; Peng, Y.; Olmstead, M. M.; Fettinger, J. C.; Power, P. P. *J. Am. Chem. Soc.* **2009**, *131*, 14164.
(126) Cox, H.; Hitchcock, P. B.; Lappert, M. F.; Pirssens, L. J.-M. *Angew. Chem., Int. Ed.* **2004**, *43*, 4500.
(127) Dickie, D. A.; Lee, P. T. K.; Labeodan, O. A.; Schatte, G.; Weinberg, N.; Lewis, A. R.; Bernard, G. M.; Wasylishen, R. E.; Clyburne, J. A. C. *Dalton Trans.* **2007**, 2862.
(128) Beweries, T.; Kuzora, R.; Rosenthal, E.; Schulz, A.; Villinger, A. *Angew. Chem., Int. Ed.* **2011**, *50*, 8974.
(129) Demeshko, S.; Godemann, C.; Kuzora, R.; Schulz, A.; Villinger, A. *Angew. Chem., Int. Ed.* **2013**, *52*, 2105.
(130) Takeuchi, K.; Ichinohe, M.; Sekiguchi, A. *J. Am. Chem. Soc.* **2011**, *133*, 12478.
(131) Nied, D.; Köppe, R.; Klopper, W.; Schnöckel, H.; Breher, F. *J. Am. Chem. Soc.* **2010**, *132*, 10264.
(132) (a) Wiberg, K. B. *Chem. Rev.* **1989**, *89*, 975. (b) Levin, M. D.; Kaszynski, P.; Michl, J. *Chem. Rev.* **2000**, *100*, 169. (c) Messerschmidt, M.; Scheins, S.; Grubert, L.; Pätzel, M.; Szeimies, G.; Paulmann, C.; Luger, P. *Angew. Chem., Int. Ed.* **2005**, *44*, 3925. (d) Coppens, P. *Angew. Chem., Int. Ed.* **2005**, *44*, 6810. (e) Wu, W.; Gu, J.; Song, J.; Shaik, S.; Hiberty, P. C. *Angew. Chem., Int. Ed.* **2009**, *48*, 1407. (f) Wu, W.; Gu, J.; Song, J.; Shaik, S.; Hiberty, P. C. *Angew. Chem., Int. Ed.* **2009**, *48*, 1407. (g) Shaik, S.; Danovich, D.; Wu, W.; Hiberty, P. C. *Nat. Chem.* **2009**, *1*, 443.
(133) (a) Sita, L. R.; Bickerstaff, R. D. *J. Am. Chem. Soc.* **1989**, *111*, 6454. (b) Sita, L. R.; Kinoshita, I. *J. Am. Chem. Soc.* **1990**, *112*, 8839. (c) Sita, L. R.; Kinoshita, I. *J. Am. Chem. Soc.* **1991**, *113*, 5070.
(134) Drost, C.; Hildebrand, M.; Lönnecke, P. *Main Group Met. Chem.* **2002**, *25*, 93.
(135) Richards, A. F.; Brynda, M.; Power, P. P. *Organometallics* **2004**, *23*, 4009.
(136) (a) Nied, D.; Matern, E.; Berberich, H.; Neumaier, M.; Breher, F. *Organometallics* **2010**, *29*, 6028. (b) Nied, D.; Oña-Burgos, P.; Klopper, W.; Breher, F. *Organometallics* **2011**, *30*, 1419. (c) Nied, D.; Breher, F. *Chem. Soc. Rev.* **2011**, *40*, 3455.
(137) Ito, Y.; Lee, V. Y.; Gornitzka, H.; Goedecke, C.; Frenking, G.; Sekiguchi, A. *J. Am. Chem. Soc.* **2013**, *135*, 6770.
(138) Abersfelder, K.; White, A. J. P.; Berger, R. J. F.; Rzepa, H. S.; Schesschkewitz, D. *Angew. Chem., Int. Ed.* **2011**, *50*, 7936.
(139) Schrenk, C.; Kubas, A.; Fink, K.; Schnepf, A. *Angew Chem., Int. Ed.* **2011**, *50*, 7273.
(140) Rohmer, M.; Bénard, M. *Chem. Soc. Rev.* **2001**, *30*, 340.
(141) Konu, J.; Chivers, T.; Tuononen, H. M. *Chem.—Eur. J.* **2011**, *17*, 11844.
(142) Namai, H.; Ikeda, H.; Hoshi, Y.; Mizuno, K. *Angew. Chem., Int. Ed.* **2007**, *46*, 7396.
(143) Ikeda, H.; Matsuo, K.; Matsui, Y.; Matsuoka, M.; Mizuno, K. *Bull. Chem. Soc. Jpn.* **2011**, *84*, 537.
(144) Klukovich, H. M.; Kean, Z. S.; Iacono, S. T.; Craig, S. L. *J. Am. Chem. Soc.* **2011**, *133*, 17882.
(145) Yeong, H.-X.; Xi, H.-W.; Lim, K. H.; So, C.-W. *Chem.—Eur. J.* **2010**, *16*, 12956.
(146) Wang, X.; Peng, Y.; Zhu, Z.; Fettinger, J. C.; Power, P. P.; Guo, J.; Nagase, S. *Angew. Chem., Int. Ed.* **2010**, *49*, 4593.
(147) Power, P. P. *Nature* **2010**, *463*, 171.
(148) (a) Malcolm, N. O. J.; Gillespie, R. J.; Popelier, P. L. A. *J. Chem. Soc., Dalton Trans.* **2002**, 3333. (b) Jung, Y.; Brynda, M.; Power, P. P.; Head-Gordon, M. *J. Am. Chem. Soc.* **2006**, *128*, 7185. (c) Hardwick, J. A.; Baines, K. M. *Organometallics* **2010**, *29*, 1305. (d) Hurni, K. L.; Baines, K. M. *Chem. Commun.* **2011**, *47*, 8382.
(149) Lovitt, C. F.; Dong, H.; Hrovat, D. A.; Gleiter, R.; Borden, W. T. *J. Am. Chem. Soc.* **2010**, *132*, 14617.
(150) Myers, A. G.; Kuo, E. Y.; Finney, N. S. *J. Am. Chem. Soc.* **1989**, *111*, 8057.
(151) Nagata, R.; Hidenori, Y.; Murahashi, E.; Saito, I. *Tetrahedron Lett.* **1989**, *30*, 4995.
(152) Schmittel, M.; Strittmatter, M.; Kiau, S. *Tetrahedron Lett.* **1995**, *36*, 4975.
(153) Sakai, S.; Nishitani, M. *J. Phys. Chem. A* **2010**, *114*, 11807.
(154) Wenthold, P. G.; Wierschke, S. G.; Nash, J. J.; Squires, R. R. *J. Am. Chem. Soc.* **1994**, *116*, 7378.
(155) Neuhaus, P.; Henkel, S.; Sander, W. *Aust. J. Chem.* **2010**, *63*, 1634.
(156) Neuhaus, P.; Grote, D.; Sander, W. *J. Am. Chem. Soc.* **2008**, *130*, 2993.
(157) Wenthold, P. G.; Kim, J. B.; Lineberger, W. C. *J. Am. Chem. Soc.* **1998**, *120*, 5279.
(158) Wang, T.; Krylov, A. I. *J. Chem. Phys.* **2005**, *123*, 104304.
(159) Protti, S.; Ravelli, D.; Mannucci, B.; Albini, A.; Fagnoni, M. *Angew. Chem., Int. Ed.* **2012**, *51*, 8577.
(160) Cinar, M. E.; Vavilala, C.; Fan, V. J.; Schmittel, M. *Org. Biomol. Chem.* **2011**, *9*, 3776.
(161) Schmittel, M.; Vavilala, C.; Cinar, M. E. *J. Phys. Org. Chem.* **2012**, *25*, 182.
(162) Bücher, G.; Mahajan, A. A.; Schimittel, M. *J. Org. Chem.* **2009**, *75*, 5850.
(163) (a) Leopold, D. G.; Murray, K. K.; Lineberger, W. C. *J. Chem. Phys.* **1984**, *81*, 1048. (b) Leopold, D. G.; Murray, K. K.; Miller, A. E. S.; Lineberger, W. C. *J. Chem. Phys.* **1985**, *83*, 4849.
(164) Roth, H. D.; Hutton, R. S. *Tetrahedron* **1985**, *41*, 1567.
(165) Seburg, R. A.; DePinto, J. T.; Patterson, E. V.; McMahon, R. J. *J. Am. Chem. Soc.* **1995**, *117*, 835.
(166) Seburg, R. A.; Patterson, E. V.; Stanton, J. F.; McMahon, R. J. *J. Am. Chem. Soc.* **1997**, *119*, 5847.
(167) Seburg, R. A.; Patterson, E. V.; McMahon, R. J. *J. Am. Chem. Soc.* **2009**, *131*, 9442.
(168) Misochko, E. Y.; Akimov, A. V.; Korchagin, D. V.; Masitov, A. A.; Shavrin, K. N. *Phys. Chem. Chem. Phys.* **2012**, *14*, 2032.
(169) Wittig, G.; Pieper, G.; Fuhrmann, G. *Chem. Ber.* **1940**, *73*, 1193 . Before Wittig, *o*-benzyne as a reactive intermediate was proposed by two research groups; see refs 153 and 154.
(170) Stoermer, R.; Kahlert, B. *Chem. Ber.* **1902**, *35*, 1633.
(171) Bachmann, W. E.; Clarke, H. T. *J. Am. Chem. Soc.* **1927**, *49*, 2089.
(172) (a) Yoshida, H.; Ohshita, J.; Kunai, A. *Bull. Chem. Soc. Jpn.* **2010**, *83*, 199. (b) Yoshida, H.; Takaki, K. *Synlett* **2012**, *23*, 1725.
(173) Wentrup, C. *Aust. J. Chem.* **2010**, *63*, 979.
(174) Wenthold, P. G. *Aust. J. Chem.* **2010**, *63*, 1091.
(175) Winker, M.; Sander, W. *Aust. J. Chem.* **2010**, *63*, 1013.
(176) Sato, T.; Niino, H. *Aust. J. Chem.* **2010**, *63*, 1048.
(177) Wenthold, P. G.; Squires, R. R.; Lineberger, W. C. *J. Am. Chem. Soc.* **1998**, *120*, 5279.
(178) Rinkevicius, Z.; Agren, H. *Chem. Phys. Lett.* **2010**, *491*, 132.
(179) Darby, N.; Kim, C. U.; Salaum, J. A.; Shelton, K. W.; Takada, S.; Masamune, S. *Chem. Commun.* **1971**, 1516.
(180) (a) Jones, R. B.; Bergman, R. G. *J. Am. Chem. Soc.* **1972**, *94*, 660. (b) Bergman, R. G. *Acc. Chem. Res.* **1973**, *6*, 25. (c) Wenk, H. H.; Winker, M.; Sander, W. *Angew. Chem., Int. Ed.* **2003**, *42*, 502.
(181) (a) Roth, W. R.; Hopf, H.; Horn, C. *Chem. Ber.* **1994**, *127*, 1765. (b) Roth, W. R.; Hopf, H.; Wasser, T.; Zimmermann, H.; Werner, C. *Liebigs Ann.* **1996**, 1691.
(182) Perrin, C. L.; Reyes-Rodriguez, G. J. *J. Phys. Org. Chem.* **2013**, *26*, 206.
(183) Spence, J. D.; Rios, A. C.; Frost, M. A.; McCutcheon, C. M.; Cox, C. D.; Chavez, S.; Fernandez, R.; Gherman, B. F. *J. Org. Chem.* **2012**, *77*, 10329.

(184) Galm, U.; Hager, M. H.; Van Lanen, S. G.; Ju, J.; Thorson, J. S.; Shen, B. *Chem. Rev.* **2005**, *105*, 739.
(185) Joshi, M. C.; Rawat, D. S. *Chem. Biodiversity* **2012**, *9*, 459.
(186) Utsuki, T.; Kawai, M.; Nakanishi, K.; Ellestad, G. A. *Chem. Commun.* **2010**, *46*, 737.
(187) (a) Kagan, J.; Wang, X.; Chen, X.; Lau, K. Y.; Batac, I. V.; Tuveson, R. W.; Hudson, J. B. *J. Photochem. Photobiol. B* **1993**, *21*, 135. (b) Choy, N.; Blanco, B.; Wen, J.; Krishan, A.; Russell, K. C. *Org. Lett.* **2000**, *2*, 3761. (c) Evenzahav, A.; Turro, N. *J. Am. Chem. Soc.* **1998**, *120*, 1835. (d) Lewis, F. D.; Matzger, J. *J. Am. Chem. Soc.* **2005**, *127*, 9968. (e) Funk, R. L.; Young, E. R. R.; Williams, R. M.; Flanagan, M. F.; Cecil, T. L. *J. Am. Chem. Soc.* **1996**, *118*, 3291. (f) Kaneko, T.; Yakanashi, M.; Hirama, M. *Angew. Chem., Int. Ed.* **1999**, *38*, 1267. (g) Schmittel, M.; Viola, G.; Dall'Acqua, F.; Morbach, G. *Chem. Commun.* **2003**, 646. (h) Baroudi, A.; Mauldin, J.; Alabugin, I. V. *J. Am. Chem. Soc.* **2010**, *132*, 967. (i) Zhegalova, N. G.; Popik, V. V. *J. Phys. Org. Chem.* **2011**, *24*, 969.
(188) Nicolaou, K. C.; Zuccarello, G.; Riemer, C.; Estevez, V. A.; Dai, W.-M. *J. Am. Chem. Soc.* **1992**, *114*, 7360.
(189) Karpoc, G.; Kuzmin, A.; Popik, V. V. *J. Am. Chem. Soc.* **2008**, *130*, 11771.
(190) Kuzmin, A. V.; Popik, V. V. *Chem. Commun.* **2009**, 5707.
(191) Zhegalova, N. G.; Popik, V. V. *J. Phys. Org. Chem.* **2011**, *24*, 969.
(192) Breiner, B.; Kaya, K.; Roy, S.; Yang, W.-Y.; Alabugin, I. V. *Org. Biomol. Chem.* **2012**, *10*, 3974.
(193) Korovina, N. V.; Chang, M. L.; Nguyen, T. T.; Fernandez, R.; Walker, H. J.; Olmstead, M. M.; Gherman, B. F.; Spence, J. D. *Org. Lett.* **2011**, *13*, 3660.
(194) Roy, S.; Anoop, A.; Biradha, K.; Basak, A. *Angew Chem., Int. Ed.* **2011**, *50*, 8316.
(195) Nechab, M.; Campolo, D.; Maury, J.; Perfetti, P.; Vanthuyne, N.; Siri, D.; Bertrand, M. P. *J. Am. Chem. Soc.* **2010**, *132*, 14742.
(196) Gredicak, M.; Matanovic, I.; Zimmermann, B.; Jeric, I. *J. Org. Chem.* **2010**, *75*, 6219.
(197) Basak, A.; Das, S.; Mallick, D.; Jemmis, E. D. *J. Am. Chem. Soc.* **2009**, *131*, 15695.
(198) Pandithavidana, D. R.; Poloukhtine, A.; Popik, V. V. *J. Am. Chem. Soc.* **2009**, *131*, 351.
(199) Baroudi, A.; Mauldin, J.; Alabugin, I. V. *J. Am. Chem. Soc.* **2010**, *132*, 967.
(200) (a) O'Connor, J. M.; Lee, L. I.; Gantzel, P.; Rheingold, A. L.; Lam, K.-C. *J. Am. Chem. Soc.* **2000**, *122*, 12057. (b) O'Connor, J. M.; Friese, S. J.; Tichenor, M. *J. Am. Chem. Soc.* **2002**, *124*, 3506. (c) O'Connor, J. M.; Friese, S. J.; Rodgers, B. L. *J. Am. Chem. Soc.* **2005**, *127*, 16342. (d) O'Connor, J. M.; Friese, S. J. *Organometallics* **2008**, *27*, 4280.
(201) Ylijoki, K. E. O.; Lavy, S.; Fretzen, A.; Kundig, E. P.; Berclaz, T.; Bernardinelli, G.; Besnard, C. *Organometallics* **2012**, *31*, 5396.
(202) Clark, A. E.; Davidson, E. R. *J. Org. Chem.* **2003**, *68*, 3387.
(203) Siebert, M. R.; Osbourn, J. M.; Brummond, K. M.; Tantillo, D. J. *J. Am. Chem. Soc.* **2010**, *132*, 11952.
(204) Wang, S. R.; Qiu, Z.; Xie, Z. *J. Am. Chem. Soc.* **2011**, *133*, 5760.
(205) Cramer, C. J. *J. Am. Chem. Soc.* **1998**, *120*, 6261.
(206) Rau, N. J.; Wenthold, P. G. *J. Phys. Chem. A* **2011**, *115*, 10353.
(207) Goets, A. E.; Garg, N. K. *Nat. Chem.* **2013**, *5*, 54.
(208) Saito, T.; Thiel, W. *J. Phys. Chem. A.* **2012**, *116*, 10864.
(209) Ess, D. H.; Johnson, E. R.; Hu, Z.; Yang, W. *J. Phys. Chem. A* **2011**, *115*, 76.
(210) Breslow, R. *Acc. Chem. Res.* **1973**, *6*, 393.
(211) Baird, N. C. *J. Am. Chem. Soc.* **1972**, *94*, 4942.
(212) (a) Schleyer, P. v. R.; Maeker, C.; Drnsfelal, A.; Jiao, H.; van Eikema Homms, N. J. R. *J. Am. Chem. Soc.* **1996**, *118*, 6317. (b) Chen, Z.; Wannere, E. S.; Corminboeuf, C.; Puchta, E.; Schleyer, P. v. R. *Chem. Rev.* **2005**, *105*, 3842.
(213) Ogonea, V.; Schleyer, P. v. R.; Schreiner, P. R. *Angew. Chem., Int. Ed.* **1998**, *37*, 1945.
(214) (a) Möllerstedt, H.; Piqueras, M. C.; Crespo, R.; Ottosson, H. *J. Am. Chem. Soc.* **2004**, *126*, 13938. (b) Dahlstand, C.; Rosengerg, M.; Kilså, K.; Ottosson, H. *J. Phys. Chem. A* **2012**, *116*, 5008.
(215) Saito, T.; Nishihara, S.; Yamanaka, S.; Kitagawa, Y.; Kawakami, T.; Yamada, S.; Isobe, H.; Okumura, M.; Yamaguchi, K. *Theor. Chem. Acc.* **2011**, *130*, 749.
(216) Goroff, N. S. *Acc. Chem. Res.* **1996**, *29*, 77.
(217) Esselman, B.; McMahon, R. J. *J. Phys. Chem. A* **2012**, *116*, 483.
(218) Thompson, S. J.; Emmert, F. L., III; Slipchenko, L. V. *J. Phys. Chem. A* **2012**, *116*, 3194.
(219) Hopf, H. *Angew. Chem., Int. Ed.* **2012**, *51*, 11945.
(220) Bao, X.; Zhou, X.; Lovitt, C. F.; Venkatraman, A.; Hrovat, D. A.; Gleiter, R.; Hoffmann, R.; Borden, W. T. *J. Am. Chem. Soc.* **2012**, *134*, 10259.
(221) (a) Hirst, D. M.; Hopton, J. D.; Linnett, J. W. *Tetrahedron, Suppl.* **1963**, *2*, 15. (b) Gimarc, B. M. *J. Am. Chem. Soc.* **1970**, *92*, 266. (c) Bodor, N.; Dewar, M. J. S.; Harget, A.; Haselbach, E. *J. Am. Chem. Soc.* **1970**, *92*, 3854. (d) Haddon, R. C. *Tetrahedron Lett.* **1972**, *13*, 3897. (e) Fleischhauer, J.; Beckers, M.; Scharf, H.-D. *Tetrahedron Lett.* **1973**, *14*, 4275. (f) Beebe, N. H. F.; Sabin, J. R. *Chem. Phys. Lett.* **1974**, *24*, 389. (g) Haddon, R. C.; Poppinger, D.; Radom, L. *J. Am. Chem. Soc.* **1975**, *97*, 1645. (h) Raine, G. P.; Schaefer, H. F., III; Haddon, R. C. *J. Am. Chem. Soc.* **1983**, *105*, 194. (i) Frenking, G. *Angew. Chem., Int. Ed. Engl.* **1990**, *29*, 1410. (j) Janoschek, R. *J. Mol. Struct.* **1991**, *232*, 147. (k) Korkin, A. A.; Balkova, A.; Bartlett, R. J.; Boyd, R. J.; Schleyer, P. v. R. *J. Phys. Chem.* **1996**, *100*, 5702. (l) Schröder, D.; Heinemann, C.; Schwarz, H.; Harvey, J. N.; Dua, S.; Blanksby, S. J.; Bowie, J. H. *Chem.—Eur. J.* **1998**, *4*, 2550. (m) Talbi, D.; Chandler, G. S. *J. Phys. Chem. A* **2000**, *104*, 5872. (n) Wang, H.-Y.; Lu, X.; Huang, R.-B.; Zheng, L.-S. *J. Mol. Struct.* **2002**, *593*, 187. (o) Trindle, C. *Int. J. Quantum Chem.* **2003**, *93*, 286. (p) Maclagan, R. G. A. R. *J. Mol. Struct.* **2005**, *713*, 107. (q) Golovin, A. V.; Ponomarev, D. A.; Takhistov, V. V. *J. Comput. Methods Mol. Des.* **2011**, *1*, 14.
(222) (a) Guo, J.-C.; Hou, G.-L.; Li, S. D.; Wang, X.-B. *J. Phys. Chem. Lett.* **2012**, *3*, 304. (b) Gleiter, R.; Hyla-Kryspin, I.; Pfeifer, K.-H. *J. Org. Chem.* **1995**, *60*, 5878. (c) Jiao, H.; Frapper, G.; Halet, J.-F.; Saillard, J.-Y. *J. Phys. Chem. A* **2001**, *105*, 5945. (d) Zhou, X.; Hrovat, D. A.; Gleiter, R.; Borden, W. T. *Mol. Phys.* **2009**, *107*, 863.
(223) Bao, X.; Hrovat, D. A.; Borden, W. T.; Wang, X.-B. *J. Am. Chem. Soc.* **2013**, *135*, 4291.
(224) (a) Enoki, T.; Takai, K.; Kiguchi, M. *Bull. Chem. Soc. Jpn.* **2012**, *85*, 249. (b) Fujii, S.; Enoki, T. *Acc. Chem. Res.*, published online Nov 21, 2012, 10.1021/ar300120y.
(225) Konishi, A.; Hirao, Y.; Matsumoto, K.; Kurata, H.; Kishi, R.; Shigeta, Y.; Nakano, M.; Tokunaga, K.; Kamada, K.; Kubo, T. *J. Am. Chem. Soc.* **2013**, *135*, 1430.
(226) Quinkert, G.; Wiersdorff, W.-W.; Finke, M.; Opitz, K. *Tetrahedron Lett.* **1966**, *7*, 2193.
(227) Kolc, J.; Michl, J. *J. Am. Chem. Soc.* **1973**, *95*, 7391.
(228) (a) McMasters, D. R.; Wirz, J. *J. Am. Chem. Soc.* **2001**, *123*, 238. (b) McMasters, D. R.; Wirz, J. *J. Am. Chem. Soc.* **1997**, *119*, 8568.
(229) Snyder, G. J. *J. Phys. Chem. A* **2012**, *116*, 5272.
(230) Iwashita, S.; Ohta, E.; Higuchi, H.; Kawai, H.; Fujiwara, K.; Ono, K.; Takenaka, M.; Suzuki, T. *Chem. Commun.* **2004**, 2076.
(231) Ghereg, D.; Ech-Cherif El Kettani, S.; Lazraq, M.; Ranaivonjatovo, H.; Schoeller, W. W.; Excudié, J.; Gornitzka, H. *Chem. Commun.* **2009**, 4821.
(232) Shimizu, A.; Tobe, Y. *Angew. Chem., Int. Ed.* **2011**, *50*, 6906.
(233) Montgomery, L. K.; Huffman, J. C.; Jurczak, E. A.; Grendze, M. P. *J. Am. Chem. Soc.* **1986**, *108*, 6004.
(234) Kawase, T.; Ueno, N.; Osa, M. *Tetrahedron Lett.* **1992**, *33*, 5405.
(235) Takahashi, T.; Matsuoka, K.-I.; Takimiya, K.; Otsubo, T.; Aso, Y. *J. Am. Chem. Soc.* **2005**, *127*, 8928.
(236) Oritz, R. P.; Casado, J.; Rodriguez Gonzalez, S.; Hernandez, V.; Navarrete, J. T. L.; Viruela, P. M.; Oriti, E.; Takimiya, K.; Otsubo, T. *Chem.—Eur. J.* **2010**, *16*, 470.
(237) Handa, S.; Miyazaki, E.; Takimiya, K.; Kunugi, Y. *J. Am. Chem. Soc.* **2007**, *129*, 11684.

(238) Handa, S.; Miyazaki, E.; Takimiya, K. *Chem. Commun.* **2009**, 3919.
(239) Chesterfields, R. J.; Newman, C. R.; Pappenfus, T. M.; Ewbank, P. C.; Haukaas, M. H.; Mann, K. R.; Miller, L. L.; Frisbie, C. D. *Adv. Mater.* **2003**, *15*, 1278.
(240) (a) Suzuki, Y.; Miyazaki, E.; Takimiya, K. *J. Am. Chem. Soc.* **2010**, *132*, 10453. (b) Suzuki, Y.; Shimawaki, M.; Miyazaki, E.; Osaka, I.; Takimiya, K. *Chem. Mater.* **2011**, *23*, 795.
(241) Canesi, E. V.; Fazzi, D.; Colella, L.; Bertarelli, C.; Castiglioni, C. *J. Am. Chem. Soc.* **2012**, *134*, 19070.
(242) Wu, Q. H.; Li, R. J.; Hong, W.; Li, H. X.; Gao, X. K.; Zhu, D. B. *Chem. Mater.* **2011**, *23*, 3138.
(243) Qiao, Y.; Zhang, J.; Xu, W.; Zhu, D. B. *J. Mater. Chem.* **2012**, *22*, 5706.
(244) Qiao, Y.; Guo, Y.; Yu, C.; Zhang, F.; Zu, W.; Liu, Y.; Zhu, D. B. *J. Am. Chem. Soc.* **2012**, *134*, 4084.
(245) Motta, S. D.; Negri, F.; Fazzi, D.; Castiglioni, C.; Canesi, E. V. *J. Phys. Chem. Lett.* **2010**, *1*, 3334.
(246) Manner, V. W.; Markle, T. F.; Freudenthal, J. H.; Roth, J. P.; Mayer, J. M. *Chem. Commun.* **2008**, 256.
(247) Takahashi, K.; Suzuki, T. *J. Am. Chem. Soc.* **1989**, *111*, 5483.
(248) Rebmann, A.; Zhou, J.; Schuler, P.; Rieker, A.; Stegmann, H. B. *J. Chem. Soc., Perkin Trans. 2* **1997**, 1615.
(249) West, R.; Jorgenson, J. A.; Stearly, K. L.; Calabrese, J. C. *J. Chem. Soc., Chem. Commun.* **1991**, 1234.
(250) Ueda, A.; Nishida, S.; Fukui, K.; Ise, T.; Shiomi, D.; Kazunobu, S.; Takui, T.; Nakatsuji, K.; Morita, Y. *Angew. Chem., Int. Ed.* **2010**, *49*, 1678.
(251) Zhang, K.; Huang, K.-W.; Li, J.; Luo, J.; Chi, C.; Wu, J. *Org. Lett.* **2009**, *11*, 4854.
(252) Porter, W. W., III; Vaid, T. P.; Rheingold, A. L. *J. Am. Chem. Soc.* **2005**, *127*, 16559.
(253) Casado, J.; Patchkovskii, S.; Zgierski, M. Z.; Hermosilla, L.; Sieiro, C.; Oliva, M. M.; Navarrete, L. *Angew. Chem., Int. Ed.* **2008**, *47*, 1443.
(254) Casado, J.; Ortiz, R. P.; Navarrete, J. T. L. *Chem. Soc. Rev.* **2012**, *41*, 5672.
(255) Kikuchi, A.; Iwahori, F.; Abe, J. *J. Am. Chem. Soc.* **2004**, *126*, 6526.
(256) Haddon, R. C. *Nature* **1975**, *256*, 394.
(257) Nakatsuji, K.; Yoshida, K.; Murata, I. *J. Am. Chem. Soc.* **1982**, *104*, 1432.
(258) Goto, K.; Kubo, T.; Yamamoto, K.; Nakasuji, K.; Sato, K.; Shiomi, D.; Takui, T.; Kubota, M.; Kobayashi, T.; Yakusi, K.; Ouyang, J. *J. Am. Chem. Soc.* **1999**, *121*, 1619.
(259) Kubo, T.; Sakamoto, M.; Akabane, M.; Fujiwara, Y.; Yamamoto, K.; Akita, M.; Inoue, K.; Yakui, T.; Nakatsuji, K. *Angew. Chem., Int. Ed.* **2004**, *43*, 6474.
(260) Ohashi, K.; Kubo, T.; Masui, K.; Yamamoto, K.; Nakatsuji, K.; Takui, T.; Kai, Y.; Murata, I. *J. Am. Chem. Soc.* **1998**, *120*, 2018.
(261) Kubo, T.; Shimizu, A.; Sakamoto, M.; Uruichi, M.; Yakushi, M.; Nakano, M.; Shiomi, D.; Sato, K.; Takui, T.; Morita, Y.; Nakatsuji, K. *Angew. Chem., Int. Ed.* **2005**, *44*, 6564.
(262) Chikamatsu, M.; Mikami, T.; Chisaka, J.; Shimizu, A.; Kubo, T.; Morita, Y.; Nakatsuji, K.; Yoshida, J.; Azumi, R.; Yase, Y. *Appl. Phys. Lett.* **2007**, *91*, 043506-1.
(263) Kubo, T.; Shimizu, A.; Uruichi, M.; Yakushi, K.; Nakano, M.; Shiomi, D.; Sato, K.; Takui, T.; Morita, Y.; Nakatsuji, K. *Org. Lett.* **2007**, *9*, 81.
(264) Shimizu, A.; Uruichi, M.; Yakushi, K.; Matsuzaki, H.; Okamoto, H.; Nakano, M.; Hirao, Y.; Matsumoto, M.; Kurata, H.; Kubo, T. *Angew. Chem., Int. Ed.* **2009**, *48*, 5842.
(265) Shimizu, A.; Kubo, T.; Uruchi, M.; Yakushi, K.; Nakano, M.; Shiomi, D.; Sato, K.; Takui, T.; Hirao, Y.; Matsumoto, K.; Kurata, H.; Morita, Y.; Nakatsuji, K. *J. Am. Chem. Soc.* **2010**, *132*, 14421.
(266) Shimizu, A.; Hirao, Y.; Matsumoto, K.; Kurata, H.; Kubo, T.; Uruichi, M.; Yakushi, K. *Chem. Commun.* **2012**, *48*, 5629.
(267) Nagai, H.; Nakano, M.; Yoneda, K.; Kishi, R.; Takahashi, H.; Shimizu, A.; Kubo, T.; Kamada, K.; Ohta, K.; Botek, E.; Champagne, B. *Chem. Phys. Lett.* **2010**, *489*, 212.
(268) Smith, M. B.; Michl, J. *Chem. Rev.* **2010**, *110*, 6891.
(269) Kamada, K.; Ohta, K.; Shimizu, A.; Kubo, T.; Kishi, R.; Takahashi, H.; Botek, E.; Champagne, B.; Nakano, M. *J. Phys. Chem. Lett.* **2010**, *1*, 937.
(270) Lambert, C. *Angew. Chem., Int. Ed.* **2011**, *50*, 1756.
(271) Zimmerman, P. M.; Zhang, Z.; Musgrave, C. B. *Nat. Chem.* **2010**, *2*, 648.
(272) Sun, Z.; Huang, K.-W.; Wu, J. *Org. Lett.* **2010**, *12*, 4690.
(273) Sun, Z.; Huang, K.-W.; Wu, J. *J. Am. Chem. Soc.* **2011**, *133*, 11896.
(274) Li, Y.; Heng, E.-K.; Lee, B. S.; Aratani, N.; Zafra, J. L.; Bao, N.; Lee, R.; Sung, Y. M.; Sun, Z.; Huang, K.-W.; Webster, R. D.; Navarrete, J. T. L.; Kim, D.; Osuka, A.; Casado, J.; Ding, J.; Wu, J. *J. Am. Chem. Soc.* **2012**, *134*, 14913.
(275) Konishi, A.; Hirao, Y.; Nakano, M.; Shimizu, A.; Botek, E.; Champagne, B.; Shiomi, D.; Sato, K.; Takui, T.; Matsumoto, K.; Kurata, H.; Kubo, T. *J. Am. Chem. Soc.* **2010**, *132*, 11021.
(276) Zhang, K.; Huang, K.-W.; Li, J.; Luo, J.; Chi, C.; Wu, J. *Org. Lett.* **2009**, *11*, 4854.
(277) Zeng, Z.; Sung, Y. M.; Bao, N.; Tan, D.; Lee, R.; Zafra, J. L.; Lee, B. S.; Ishida, M.; Ding, J.; Navarrete, J. T. L.; Li, Y.; Zeng, W.; Kim, D.; Huang, K.-W.; Webster, R. D.; Casado, J.; Wu, J. *J. Am. Chem. Soc.* **2012**, *134*, 14513.
(278) Sun, Z.; Wu, J. *J. Mater. Chem.* **2012**, *22*, 4151.
(279) Zhu, X.; Tsuji, H.; Nakabayashi, K.; Ohkoshi, S.-I.; Nakamura, E. *J. Am. Chem. Soc.* **2011**, *133*, 16342.
(280) Chase, D. T.; Rose, B. D.; McClintock, S. P.; Zakharov, L. N.; Haley, M. M. *Angew. Chem., Int. Ed.* **2011**, *50*, 1127.
(281) Chase, D. T.; Fix, A. G.; Rose, B. D.; Weber, C. D.; Nobusue, S.; Stockwell, C. E.; Zakharov, L. N.; Lonergan, M. C.; Haley, M. M. *Angew. Chem., Int. Ed.* **2011**, *50*, 11103.
(282) Rose, B. D.; Vonnegut, C. L.; Zakharov, L. N.; Haley, M. M. *Org. Lett.* **2012**, *14*, 2426.
(283) Zeng, Z.; Ishida, M.; Zafra, J. L.; Zhu, X.; Sung, Y. M.; Bao, N.; Webster, R. D.; Lee, B. S.; Li, R.-W.; Zheng, W.; Li, Y.; Chi, C.; Navarrete, J. T. L.; Ding, J.; Casado, J.; Kim, D.; Wu, J. *J. Am. Chem. Soc.* **2013**, *135*, 6363.
(284) Nishinaga, T.; Tateno, M.; Fujii, M.; Fujita, W.; Takase, M.; Iyoda, M. *Org. Lett.* **2010**, *12*, 5374.
(285) Hiroto, S.; Furukawa, K.; Shinokubo, H.; Osuka, A. *J. Am. Chem. Soc.* **2006**, *128*, 12380.
(286) Cho, S.; Lim, J. M.; Hiroto, S.; Kim, P.; Shinokubo, H.; Osaka, A.; Kim, D. *J. Am. Chem. Soc.* **2009**, *131*, 6412.
(287) (a) Cameron, T. S.; Decken, A.; Grein, F.; Knapp, C.; Passmore, J.; Rautiainen, J. M.; Shuvaev, K.; Thompson, R. C.; Wood, D. J. *Inorg. Chem.* **2010**, *49*, 7861. (b) Shuvaev, K. V.; Passmore, J. *Coord. Chem. Rev.* **2013**, *257*, 1067. (c) Hicks, R. G. In *Stable Radicals*; Hicks, R. G., Ed.; John Wiley & Sons: New York, 2010; p 317.
(288) Lineberger, W. C.; Borden, W. T. *Phys. Chem. Chem. Phys.* **2011**, *13*, 11792.
(289) Berson, J. A. *Acc. Chem. Res.* **1997**, *30*, 238.
(290) Cramer, C. J. *J. Chem. Soc., Perkin Trans. 2* **1998**, 1007.
(291) (a) Davidson, E. R.; Borden, W. T. *J. Am. Chem. Soc.* **1977**, *99*, 2053. (b) Borden, W. T. In *Diradicals*; Borden, W. T., Ed.; Wiley-Interscience: New York, 1982; p 1.
(292) Neuhaus, P.; Grote, D.; Sander, W. *J. Am. Chem. Soc.* **2008**, *130*, 2993.
(293) Neuhaus, P.; Sander, W. *Angew. Chem., Int. Ed.* **2010**, *49*, 7277.
(294) Latif, I. A.; Hansda, S.; Datta, S. N. *J. Phys. Chem. A* **2012**, *116*, 8599.
(295) Matsumoto, K.; Inokuchi, D.; Hirao, Y.; Kurata, H.; Sato, K.; Takui, T.; Kubo, T. *Org. Lett.* **2010**, *12*, 836.
(296) Namai, H.; Ikeda, H.; Hoshi, Y.; Kato, N.; Morishita, Y.; Mizuno, K. *J. Am. Chem. Soc.* **2007**, *129*, 9032.
(297) Ikeda, H.; Matsui, Y.; Akimoto, I.; Kan'no, K.-i.; Mizuno, K. *Aust. J. Chem.* **2010**, *63*, 1342.

(298) Matsui, Y.; Namai, H.; Akimoto, I.; Kan'no, K.-I.; Mizuno, K. *Tetrahedron* **2011**, *67*, 7431.
(299) Ikeda, T.; Ikeda, H.; Takahashi, Y.; Yamada, M.; Mizuno, K.; Tero-Kubota, S.; Yamauchi, S. *J. Am. Chem. Soc.* **2008**, *130*, 2466.
(300) Kano, Y.; Mizuno, K.; Ikeda, H. *J. Phys. Org. Chem.* **2011**, *24*, 921.
(301) Ichino, T.; Villano, S. M.; Gianola, A. J.; Goebbert, D. J.; Velarde, L.; Sanov, A.; Blanksby, S. J.; Zhou, X.; Hrovat, D. A.; Borden, W. T.; Lineberger, W. C. *Angew. Chem., Int. Ed.* **2009**, *48*, 8509.
(302) Mozhayski, V.; Goebbert, D. J.; Velarde, L.; Sanov, A.; Krylov, A. I. *J. Phys. Chem. A* **2010**, *114*, 6935.
(303) Ichino, T.; Villano, S. M.; Gianola, A. J.; Goebbert, D. J.; Valarde, L.; Sanov, A.; Blanksby, S.; Zhou, X.; Hrovat, D. A.; Borden, W. T. *J. Phys. Chem. A* **2011**, *115*, 1634.
(304) Lopez, X.; Ruipérez, F.; Piris, M.; Matxain, J. M.; Ugalde, J. M. *ChemPhysChem* **2011**, *12*, 1061.
(305) Saito, T.; Nishihara, S.; Yamanaka, S.; Kitagawa, Y.; Kawakami, T.; Yamada, S.; Isobe, H.; Okumura, M.; Yamaguchi, K. *Theor. Chem. Acc.* **2011**, *130*, 739.
(306) Kuzmanich, G.; Sönig, F.; Tsai, C.-K.; Um, J. M.; Hoekstra, R. M.; Houk, K. N.; Guldi, D. M.; Garcia-Garibay, M. A. *J. Am. Chem. Soc.* **2011**, *133*, 2342.
(307) Kuzmanich, G.; Garcia-Garibay, M. A. *J. Phys. Org. Chem.* **2011**, *24*, 883.
(308) Koide, T.; Furukawa, K.; Shinokubo, H.; Shin, J.-Y.; Kim, K. S.; Kim, D.; Osuka, A. *J. Am. Chem. Soc.* **2010**, *132*, 7246.
(309) Martin, D.; Moore, C. E.; Rheingold, A.; Bertrand, G. *Angew. Chem. Int. Ed.* **2013**, *52*, 7014.
(310) Schulz, T.; Färber, C.; Leibold, M.; Bruhn, C.; Baumann, W.; Selent, D.; Porsch, T.; Holthausen, M. C.; Siemeling, U. *Chem. Commun.* **2013**, *49*, 6834.
(311) Ishida, M.; Shin, J.-Y.; Lim, J. M.; Lee, B. S.; Yoon, M.-C.; Koide, T.; Sessler, J. L.; Osaka, A.; Kim, D. *J. Am. Chem. Soc.* **2011**, *133*, 15533.
(312) Bos, R.; Tonkin, S. A.; Hanson, G. R.; Hindson, C. M.; Lim, K. F.; Barnett, N. W. *J. Am. Chem. Soc.* **2009**, *131*, 2770.
(313) Fu, Q.; Yang, J.; Wang, X.-B. *J. Phys. Chem. A* **2011**, *115*, 3201.
(314) Amiri, S.; Schreiner, P. R. *J. Phys. Chem. A* **2009**, *113*, 11750.
(315) Haider, K.; Soundararajan, N.; Shaffer, M.; Platz, M. *Tetrahedron Lett.* **1989**, *30*, 1225.
(316) Rajca, A.; Shiraishi, K.; Pink, M.; Rajca, S. *J. Am. Chem. Soc.* **2007**, *129*, 7232.
(317) Boratynski, P. J.; Pink, M.; Rajca, S.; Rajca, A. *Angew. Chem., Int. Ed.* **2010**, *49*, 5459.
(318) Rajca, A.; Olankitwanit, A.; Rajca, S. *J. Am. Chem. Soc.* **2011**, *133*, 4750.
(319) Nozawa, T.; Nagata, M.; Ichinohe, M.; Sekiguchi, A. *J. Am. Chem. Soc.* **2011**, *133*, 5773.
(320) Perrotta, R. R.; Winter, A. H.; Coldren, W. H.; Falvey, D. E. *J. Am. Chem. Soc.* **2011**, *133*, 15553.
(321) Perrotta, R. R.; Winter, A. H.; Falvey, D. E. *Org. Lett.* **2011**, *13*, 212.
(322) Hui, P.; Arif, K. M.; Chandrasekar, R. *Org. Biomol. Chem.* **2012**, *10*, 2439.
(323) Tretyakov, E. V.; Tolstikov, S. E.; Romanenko, G. V.; Bogomyakov, A. S.; Stass, D. V.; Maryasov, A. G.; Gritsan, N. P.; Ovcharenko, V. I. *Russ. Chem. Bull.* **2011**, *60*, 2608.
(324) Suzuki, S.; Furui, T.; Kuratsu, M.; Kozaki, M.; Shiomi, D.; Sato, K.; Takui, T.; Okada, K. *J. Am. Chem. Soc.* **2010**, *132*, 15908.
(325) Zhang, S.-H.; Xi, H.-W.; Lim, K. H.; Meng, Q.; Huang, M.-B.; So, C.-W. *Chem.—Eur. J.* **2012**, *18*, 4258.
(326) Stickley, K. R.; Blackstock, S. C. *J. Am. Chem. Soc.* **1994**, *116*, 11576.
(327) Sato, K.; Yano, M.; Furuichi, M.; Shiomi, D.; Takui, T.; Abe, K.; Itoh, K.; Higuchi, A.; Katsuma, K.; Shirota, Y. *J. Am. Chem. Soc.* **1997**, *119*, 6607.
(328) Bushby, R. J.; McGill, D. R.; Ng, K. M.; Taylor, N. *J. Chem. Soc., Perkin Trans. 2* **1997**, 1405.
(329) Okada, K.; Imakura, T.; Oda, M.; Baumgarten, M. *J. Am. Chem. Soc.* **1996**, *118*, 3047.
(330) (a) Dvolaitzky, M.; Chiarelli, R.; Rassat, A. *Angew. Chem., Int. Ed.* **1992**, *31*, 180. (b) Kanno, F.; Inoue, K.; Kago, N.; Iwamura, H. *J. Am. Chem. Soc.* **1993**, *115*, 847.
(331) Fang, S.; Lee, M.-S.; Hrovat, D. A.; Borden, W. T. *J. Am. Chem. Soc.* **1995**, *117*, 6727.
(332) (a) Nelsen, S. F.; Ismagilov, R. F.; Powell, D. R. *J. Am. Chem. Soc.* **1997**, *119*, 10213. (b) Nelsen, S. F.; Ismagilov, R. F.; Teki, Y. *J. Am. Chem. Soc.* **1998**, *120*, 2200.
(333) Sakurai, H.; Kumai, R.; Izuoka, A.; Sugawara, T. *Chem. Lett.* **1996**, 879.
(334) Rosspeintner, A.; Griesser, M.; Matsumoto, I.; Teki, Y.; Li, G.; Nelsen, S. F.; Gescheidt, G. *J. Phys. Chem. A* **2010**, *114*, 6487.
(335) (a) Kuratsu, M.; Kozaki, M.; Okada, K. *Angew. Chem., Int. Ed.* **2005**, *44*, 4056. (b) Kuratsu, M.; Kozaki, M.; Okada, K. *Chem. Lett.* **2004**, *33*, 1174. (c) Kuratsu, M.; Suzuki, S.; Kozaki, M.; Shiomi, D.; Sato, K.; Takui, T.; Okada, K. *Inorg. Chem.* **2007**, *46*, 10153.
(336) Kuratsu, M.; Suzuki, S.; Kozaki, M.; Shiomi, D.; Sato, K.; Takui, T.; Kanzawa, T.; Hosokoshi, Y.; Lan, X.-Z.; Miyazaki, Y.; Inaba, A.; Okada, K. *Chem.—Asian J.* **2012**, *7*, 1604.
(337) Suzuki, S.; Nagata, A.; Kuratsu, M.; Kozaki, M.; Tanaka, R.; Shiomi, D.; Sugisaki, K.; Toyota, K.; Sato, K.; Takui, T.; Okada, K. *Angew. Chem., Int. Ed.* **2012**, *51*, 3193.
(338) Yokoyama, Y.; Sakamaki, D.; Ito, A.; Tanaka, K.; Shiro, M. *Angew. Chem., Int. Ed.* **2012**, *51*, 9403.
(339) Rozantsev, E. G.; Sholle, V. D. *Synthesis* **1971**, 190.
(340) Brunel, Y.; Lemaire, H.; Rassat, A. *Bull. Soc. Chim. Fr.* **1964**, *8*, 1895.
(341) Dupeyre, R. M.; Rassat, A. *J. Am. Chem. Soc.* **1966**, *88*, 3180.
(342) Mukai, K.; Nagai, H.; Ishizu, K. *Bull. Chem. Soc. Jpn.* **1975**, *48*, 2381.
(343) Wenthold, P. G.; Hu, J.; Squires, R. R.; Lineberger, W. C. *J. Am. Soc. Mass Spectrom.* **1999**, *10*, 800.
(344) Wenthold, P. G.; Kim, J. B.; Lineberger, W. C. *J. Am. Chem. Soc.* **1997**, *119*, 1354.
(345) Wright, B. B.; Platz, M. S. *J. Am. Chem. Soc.* **1983**, *105*, 628.
(346) Calder, A.; Forrester, A. R.; James, P. G.; Luckhurst, G. R. *J. Am. Chem. Soc.* **1969**, *91*, 3724.
(347) Kurokawa, G.; Ishida, T.; Nogami, T. *Chem. Phys. Lett.* **2004**, *392*, 74.
(348) Nishimaki, H.; Mashiyama, S.; Yasui, M.; Nogami, T.; Ishida, T. *Chem. Mater.* **2006**, *18*, 3602.
(349) Ishida, T.; Ooishi, M.; Ishii, N.; Mori, H.; Nogami, T. *Polyhedron* **2007**, *26*, 1793.
(350) Rajca, A.; Shiraishi, K.; Rajca, S. *Chem. Commun.* **2009**, 4372.
(351) Rajca, A.; Shiraishi, K.; Boratynski, P. J.; Pink, M.; Miyasaka, M.; Rajca, S. *J. Org. Chem.* **2011**, *76*, 8447.
(352) Ali, M. E.; Oppeneer, P. M. *J. Phys. Chem. Lett.* **2011**, *2*, 939.
(353) Fairfull-Smith, K. E.; Blinco, J. P.; Keddie, D. J.; George, G. A.; Bottle, S. E. *Macromolecules* **2008**, *41*, 1577.
(354) Sato, H.; Kathirvelu, V.; Spagnol, G.; Rajca, S.; Rajca, A.; Eaton, S. S.; Eaton, G. R. *J. Phys. Chem. B* **2008**, *112*, 2818.
(355) Rajca, A.; Vale, M.; Rajca, S. *J. Am. Chem. Soc.* **2008**, *130*, 9099.
(356) Shultz, D. A.; Boal, A. K.; Lee, H.; Farmer, G. T. *J. Org. Chem.* **1999**, *64*, 4386.
(357) Shultz, D. A.; Fico, R. M.; Lee, H.; Kampf, J. W.; Kirschbaum, K.; Pinkerton, A. A.; Boyle, P. D. *J. Am. Chem. Soc.* **2003**, *125*, 15426.
(358) Higashiguchi, K.; Yumoto, K.; Matsuda, K. *Org. Lett.* **2010**, *12*, 5284.
(359) Tretyakov, E. V.; Tolstikov, S. E.; Romanenko, G. V.; Bogomyakov, A. S.; Stass, D. V.; Kadirov, M. K.; Holin, K. V.; Sinyashin, O. G.; Ovcharenko, V. I. *Polyhedron* **2011**, *30*, 2608.
(360) Ko, K. C.; Son, S. U.; Lee, J. Y. *J. Phys. Chem. B* **2011**, *115*, 8401.
(361) Suzuki, S.; Itoh, N.; Furuichi, K.; Kozaki, M.; Shiomi, D.; Sato, K.; Takui, T.; Ohi, H.; Itoh, S.; Okada, K. *Chem. Lett.* **2011**, *40*, 22.
(362) Overhauser, A. *Phys. Rev.* **1953**, *92*, 411.

(363) Hall, D. A.; Maus, D. C.; Grefen, G. J.; Inati, S.; Becerra, L. R.; Dahlquist, F. W.; Griffin, R. G. *Science* **1997**, *276*, 930.
(364) Matsuki, Y.; Maly, T.; Ouari, O.; Karoui, H.; Le Moigne, F.; Rizzato, E.; Lyubenova, S.; Herzfeld, J.; Prsner, T.; Tordo, P.; Griffin, R. G. *Angew. Chem., Int. Ed.* **2009**, *48*, 4996.
(365) Zagdoun, A.; Casano, G.; Ouari, O.; Lapadula, G.; Rossini, A. J.; Lelli, M.; Baffert, M.; Gajan, D.; Veyre, L.; Maas, W. E.; Rosey, M.; Weber, R. T.; Thieuleux, C.; Coperet, C.; Lesage, A.; Tordo, P.; Emsley, L. *J. Am. Chem. Soc.* **2012**, *134*, 2284.
(366) Dane, E. L.; Corzilius, B.; Rizzato, E.; Stocker, P.; Maly, T.; Smith, A. A.; Griffin, R. G.; Ouari, O.; Tordo, P.; Swager, T. M. *J. Org. Chem.* **2012**, *77*, 1789.
(367) Matsuzaki, Y.; Maly, T.; Ouari, O.; Karoui, H.; Moigne, F. L.; Rizzato, E.; Lyubenova, S.; Herzfeld, J.; Prisner, T.; Tordo, P.; Griffin, R. G. *Angew. Chem., Int. Ed.* **2009**, *48*, 4996.
(368) Kiesewetter, M. K.; Corzilius, B.; Smith, A. A.; Griffin, R. G.; Swager, T. M. *J. Am. Chem. Soc.* **2012**, *134*, 4537.
(369) Rossini, A.; Zagdoun, A.; Hegner, F.; Schwarzwälder, M.; Gajan, D.; Copéret, C.; Lesage, A.; Emsley, L. *J. Am. Chem. Soc.* **2012**, *134*, 16899.
(370) Linden, A. H.; Lange, S.; Franks, W. T.; Akbey, A.; Specker, E.; van Rossum, B.-J.; Oschkinat, H. *J. Am. Chem. Soc.* **2011**, *133*, 19266.
(371) Vitzthum, V.; Borcard, F.; Jannin, S.; Morin, M.; Miéville, P.; Caporini, M. A.; Sienkiewicz, A.; Gerber-Lemaire, S.; Bodenhausen, G. *ChemPhysChem* **2011**, *12*, 2929.
(372) Ayabe, K.; Sato, K.; Nishida, S.; Ise, T.; Nakazawa, S.; Sugisaki, K.; Morita, Y.; Toyota, K.; Shiomi, D.; Kitagawa, M.; Takui, T. *Phys. Chem. Chem. Phys.* **2012**, *14*, 9137.
(373) Macholl, S.; Johannesson, H.; Ardenkjaer, J. H. *Phys. Chem. Chem. Phys.* **2010**, *12*, 5804.
(374) (a) Dane, W. L.; Maly, T.; Debelouchina, G. T.; Griffin, R. G.; Swager, T. M. *Org. Lett.* **2009**, *11*, 1871. (b) Liu, Y.; Villamena, F. A.; Rockenbauer, A.; Song, Y.; Zweier, J. *J. Am. Chem. Soc.* **2013**, *135*, 2350.
(375) Chiarelli, R.; Novak, M. A.; Rassat, A.; Tholence, J. J. *Nature* **1993**, *363*, 147.
(376) Szydlowska, J.; Pietrasik, K.; Glaz, L.; Kaim, A. *Chem. Phys. Lett.* **2008**, *460*, 245.
(377) Casati, C.; Franchi, P.; Pievo, R.; Mezzina, E.; Lucarini, M. *J. Am. Chem. Soc.* **2012**, *134*, 19108.
(378) Wang, J.; Hou, L.; Browne, W. R.; Feringa, B. L. *J. Am. Chem. Soc.* **2011**, *133*, 8162.
(379) Kahn, O. *Molecular Magnetism*; VCH: New York, 1993.
(380) (a) Oshio, H.; Watanabe, T.; Ohto, A.; Ito, T.; Nagashima, U. *Angew. Chem., Int. Ed.* **1994**, *33*, 670. (b) Oshio, H.; Watanabe, T.; Ohta, A.; Ito, A.; Ikoma, T.; Tero-Kubota, S. *Mol. Cryst. Liq. Cryst.* **1995**, *283*, 47.
(381) Barclay, T. M.; Hicks, R. G.; Lemaire, M. T.; Thompson, L. K. *Inorg. Chem.* **2004**, *40*, 6521.
(382) Brook, D. J. R.; Yee, G. T.; Hundley, M.; Rogow, D.; Wong, J.; Van-Tu, K. *Inorg. Chem.* **2010**, *49*, 8573.
(383) (a) Kaim, W. *Inorg. Chem.* **2011**, *50*, 9752. (b) Luca, O. R.; Crabtree, R. H. *Chem. Soc. Rev.* **2013**, *42*, 1440.
(384) Gardiner, M. G.; Hanson, G. R.; Henderson, M. J.; Lee, F. C.; Raston, C. L. *Inorg. Chem.* **1994**, *33*, 2456.
(385) (a) Bachler, V.; Olbrich, G.; Neese, F.; Wieghardt, K. *Inorg. Chem.* **2002**, *41*, 4179. (b) Herebian, D.; Wieghardt, K. E.; Neese, F. *J. Am. Chem. Soc.* **2003**, *125*, 10997. (c) Patrenko, T.; Ray, K.; Wieghardt, K. E.; Neese, F. *J. Am. Chem. Soc.* **2006**, *128*, 4422.
(386) Bendikov, M.; Duong, H. M.; Starkey, K.; Houk, K. N.; Carter, E. A.; Wudl, F. *J. Am. Chem. Soc.* **2004**, *126*, 7416.
(387) Watanabe, M.; Chang, Y. J.; Liu, S.-W.; Chao, T.-H.; Goto, K.; Islam, M. M.; Yuan, C.-H.; Tao, Y.-T.; Shinmyozu, T.; Chow, T. J. *Nat. Chem.* **2012**, *4*, 574.
(388) Yang, H.; Song, Q.; Li, W.; Song, X.; Bu, Y. *J. Phys. Chem. C* **2012**, *116*, 5900.
(389) Motomura, S.; Nakano, M.; Fukui, H.; Yoneda, K.; Kubo, T.; Carion, R.; Champagne, B. *Phys. Chem. Chem. Phys.* **2011**, *13*, 20575.
(390) Kono, T.; Kumaki, D.; Nishida, J.-I.; Tokito, S.; Yamashita, Y. *Chem. Commun.* **2010**, *46*, 3265.
(391) Tomas, A.; Bhanuprakash, K. *ChemPhysChem* **2012**, *13*, 597.
(392) Han, L.; Zhao, Y. J.; Bu, Y. *J. Phys. Chem. C* **2012**, *116*, 23214.
(393) (a) Singh, S.; Jones, W. J.; Siebrand, W.; Stoicheff, B. P.; Schneider, W. G. *J. Chem. Phys.* **1965**, *42*, 330. (b) Geacintov, N.; Pope, M.; Vogel, F. *Phys. Rev. Lett.* **1969**, *22*, 593. (c) Smith, M. B.; Michl, J. *Chem. Rev.* **2010**, *110*, 6891. (d) Johnson, J. C.; Nozik, A. J.; Michl, J. *Acc. Chem. Res.* **2013**, *46*, 1290. (e) Lee, J.; Jadhav, P.; Reusswig, P. D.; Yost, S. R.; Thompson, N. J.; Congreve, D. N.; Hontz, E.; Voorhis, T. V.; Baldo, M. A. *Acc. Chem. Res.* **2013**, *46*, 1300. (f) Burdett, J. J.; Bardeen, C. J. *Acc. Chem. Res.* **2013**, *46*, 1312. (g) Chan, W.-L.; Berkelbach, T. C.; Provorse, M. R.; Monahan, N. R.; Tritsch, J. R.; Hybertsen, M. S.; Reichman, D. R.; Gao, J.; Zhu, X.-Y. *Acc. Chem. Res.* **2013**, *46*, 1321. (h) Wilson, M. W. B.; Rao, A.; Ehrler, B.; Friend, R. H. *Acc. Chem. Res.* **2013**, *46*, 1330. (i) Zimmerman, P. M.; Musgrave, C. B.; Head-Gordon, M. *Acc. Chem. Res.* **2013**, *46*, 1339.
(394) Minami, T.; Nakano, M. *J. Phys. Chem. Lett.* **2012**, *3*, 145.
(395) Ito, S.; Minami, T.; Nakano, M. *J. Phys. Chem. C* **2012**, *116*, 19729.
(396) Minami, T.; Ito, S.; Nakano, M. *J. Phys. Chem. A* **2013**, *117*, 2000.
(397) Akdag, A.; Havlas, Z.; Michl, J. *J. Am. Chem. Soc.* **2012**, *134*, 14624.
(398) Nakano, M.; Kishi, R.; Nitta, T.; Kubo, T.; Nakatsuji, K.; Kamada, K.; Ohta, K.; Champagne, B.; Botek, E.; Yamaguchi, K. *J. Phys. Chem. A* **2005**, *109*, 885.
(399) Kamada, K.; Ohta, K.; Kubo, T.; Shimizu, A.; Morita, Y.; Nakatsuji, K.; Kishi, R.; Ohta, S.; Furukawa, S.-i.; Takahashi, H.; Nakano, M. *Angew. Chem., Int. Ed.* **2007**, *46*, 3544.
(400) Kamada, K.; Ohta, K.; Shimizu, A.; Kubo, T.; Kishi, R.; Takahashi, H.; Botek, E.; Champagne, B.; Nakano, M. *J. Phys. Chem. Lett.* **2010**, *1*, 937.
(401) Nakano, M.; Kishi, R.; Ohta, S.; Takahashi, H.; Kubo, T.; Kamada, K.; Ohta, K.; Botek, F.; Champagne, B. *Phys. Rev. Lett.* **2007**, *99*, 033001.
(402) Nakano, M.; Kishi, R.; Yoneda, K.; Inoue, Y.; Inui, T.; Shigeta, Y. *J. Phys. Chem. A* **2011**, *115*, 8767.
(403) Nakano, M.; Minami, T.; Yoneda, K.; Muhammad, S.; Kishi, R.; Shigeta, Y.; Kubo, T.; Rougier, L.; Champagne, B.; Kamada, K.; Ohta, K. *J. Phys. Chem. Lett.* **2011**, *2*, 1094.
(404) Kamada, K.; Fuku-en, S.-i.; Minamide, S.; Ohta, K.; Kishi, R.; Nakano, M.; Matsuzaki, H.; Okamoto, H.; Higashibayashi, H.; Inoue, K.; Kojima, S.; Yamamoto, Y. *J. Am. Chem. Soc.* **2013**, *135*, 232.
(405) Kuzmanich, G.; Vogelsberg, C.; Maverick, E. F.; Netto-Ferreira, J. C.; Scaiano, J. C.; Garcia-Garibay, M. A. *J. Am. Chem. Soc.* **2012**, *134*, 1115.
(406) (a) Muthukrishnan, S.; Sankaranarayanan, J.; Pace, T. C. S.; Konosonoks, A.; DeMichiei, M. E.; Meese, M. J.; Bohne, C.; Gudmundsdottir, A. D. *J. Org. Chem.* **2010**, *75*, 1393. (b) Li, Q.; Sankaranarayanan, J.; Hawk, M.; Tran, V. T.; Brown, J. L.; Gudmundsdottir, A. *Photochem. Photobiol. Sci.* **2012**, *11*, 744.
(407) Shiraki, S.; Vogelsberg, C. S.; Garcia-Garibay, M. A. *Photochem. Photobiol. Sci.* **2012**, *11*, 1929.
(408) Kuzmanich, G.; Xue, J.; Netto-Ferreira, J.-C.; Scaiano, J. C.; Platz, M.; Garcia-Garibay, M. A. *Chem. Sci.* **2011**, *2*, 1497.
(409) Ma, J.; Li, M.-D.; Phillips, D. L.; Wan, P. *J. Org. Chem.* **2011**, *76*, 3710.
(410) (a) Adam, W.; Peters, K.; Peters, E. M.; Stegman, V. R. *J. Am. Chem. Soc.* **2000**, *122*, 2958. (b) Adam, W.; Stegmann, V. R. *Synthesis* **2001**, 1203. (c) D'Auria, M.; Racioppi, R.; Romaniello, G. *Eur. J. Org. Chem.* **2000**, 3265. (d) D'Auria, M.; Emanuele, L.; Poggi, G.; Racioppi, R.; Romaniello, G. *Tetrahedron* **2002**, *58*, 5045. (e) D'Auria, M.; Emanuele, L.; Racioppi, R. *Photochem. Photobiol. Sci.* **2004**, *3*, 927. (f) D'Auria, M.; Emanuele, L.; Racioppi, R.; Valente, A. *Photochem. Photobiol. Sci.* **2008**, *7*, 98.
(411) Yabuno, Y.; Hiraga, Y.; Takagi, R.; Abe, M. *J. Am. Chem. Soc.* **2011**, *133*, 2592.
(412) D'Auria, M.; Racioppi, R. *Eur. J. Org. Chem.* **2010**, 3831.

(413) Kim, H.; Park, B. S.; Jang, D.-J. *J. Photochem. Photobiol. A* **2011**, *218*, 174.
(414) Ayitou, A. J.-L.; Sivaguru, J. *Chem. Commun.* **2011**, *47*, 2568.
(415) Schmierrer, T.; Laimgruber, S.; Haiser, K.; Kiewisch, K.; Neugebauer, J.; Gilch, P. *Phys. Chem. Chem. Phys.* **2010**, *12*, 15653.
(416) Wang, L.; Huang, Y.-C.; Liu, Y.; Fun, H.-K.; Zhang, Y.; Xu, J.-H. *J. Org. Chem.* **2010**, *75*, 7757.
(417) Jahjah, R.; Gassama, A.; Bulach, V.; Suzuki, C.; Abe, M.; Hoffmann, N.; Martinez, A.; Nuzillard, J.-M. *Chem.—Eur. J.* **2010**, *16*, 3341.
(418) Günaydin-Sen, Ö.; Fosso-Tande, J.; Chen, P.; White, J. L.; Allen, T. L.; Cherian, J.; Tokumoto, T.; Lahti, P. M.; McGill, S.; Harrison, R. J.; Musfeldt, J. L. *J. Chem. Phys.* **2011**, *135*, 241101.

NOTE ADDED AFTER ASAP PUBLICATION

This paper was published ASAP on July 24, 2013. Figure 6 has been revised. The corrected version was reposted on July 29, 2013.